N72-26545

NASA CR-120930
(MCR-72-42)

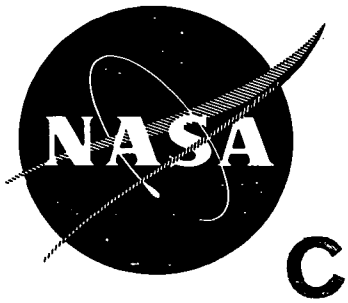

INSULATION SYSTEMS FOR LIQUID METHANE FUEL TANKS FOR SUPERSONIC CRUISE AIRCRAFT

by

H. F. Brady and D. Del Duca

MARTIN MARIETTA CORPORATION
P.O. Box 179
Denver, Colorado 80201

prepared for

NATIONAL AERONAUTICS AND SPACE ADMINISTRATION

NASA Lewis Research Center
Contract NAS3-12425
Joseph M. Ladd, Project Manager

NOTICE

This report was prepared as an account of Government-sponsored work. Neither the United States, nor the National Aeronautics and Space Administration (NASA), nor any person acting on behalf of NASA:

A.) Makes any warranty or representation, expressed or implied, with respect to the accuracy, completeness, or usefulness of the information contained in this report, or that the use of any information, apparatus, method, or process disclosed in this report may not infringe privately-owned rights; or

B.) Assumes any liabilities with respect to the use of, or for damages resulting from the use of, any information, apparatus, method or process disclosed in this report.

As used above, "person acting on behalf of NASA" includes any employee or contractor of NASA, or employee of such contractor, to the extent that such employee or contractor of NASA or employee of such contractor prepares, disseminates, or provides access to any information pursuant to his employment or contract with NASA, or his employment with such contractor.

Requests for copies of this report should be referred to

National Aeronautics and Space Administration
Scientific and Technical Information Facility
P.O. Box 33
College Park, Md. 20740

NASA CR-120930
(MCR-72-42)

FINAL REPORT

INSULATION SYSTEMS FOR LIQUID METHANE FUEL TANKS FOR SUPERSONIC CRUISE AIRCRAFT

by

H. F. Brady and D. Del Duca

MARTIN MARIETTA CORPORATION
P.O. Box 179
Denver, Colorado 80201

prepared for

NATIONAL AERONAUTICS AND SPACE ADMINISTRATION

June 1972

CONTRACT NAS3-12425

NASA Lewis Research Center
Cleveland, Ohio
Joseph M. Ladd, Project Manager
Air-Breathing Engines Division

Page Intentionally Left Blank

FOREWORD

The work described was accomplished at the Martin Marietta Corporation, Denver Division, under NASA Contract NAS3-12425 with Mr. Joseph M. Ladd, Air-Breathing Engines Division, NASA-Lewis Research Center, as Project Manager, and Mr. Rene Chambellan, Air-Breathing Engines Division, NASA-Lewis Research Center, as Research Advisor.

Page Intentionally Left Blank

ABSTRACT

Two insulation systems for tanks containing liquid methane in supersonic cruise-type aircraft were designed and tested after an extensive materials investigation. One system is an external insulation and the other is an internal wet-type insulation system. Tank volume was maximized by making the tank shape approach a rectangular parallelopiped. One tank was designed to use the external insulation and the other tank to use the internal insulation. Performance of the external insulation system was evaluated on a full-scale tank under the temperature environment of -320°F to 700°F (-196°C to 371°C) and ambient pressures of ground-level atmospheric to 1 psia (6.895 N/m^2). Problems with installing the internal insulation on the test tank prevented full-scale evaluation of performance; however, small-scale testing verified thermal conductivity, temperature capability, and installed density.

Page Intentionally Left Blank

CONTENTS

Figure

I. SUMMARY

The objective of this program was to develop insulation systems for liquid methane fuel tanks that could be used in supersonic cruise-type aircraft.

To accomplish this objective, a materials investigation program was completed that started with the selection of basic materials capable of withstanding the severe environmental conditions anticipated. These conditions included temperatures over the range of -259°F to +700°F (-162°C to +371°C) and pressures ranging from ground-level atmospheric to 1 psia (6.89 kN/m^2-a). After the selection of materials, insulation configurations were selected and a multiphased small-scale test program was undertaken. Insulation samples were exposed to pressure, temperature, vibration and combinations of the environments. A series of tests on the materials and insulation specimens included the following:

Thermal Conductivity and Heat Capacity

Specific Weight

Coefficient of Thermal Expansion

Water Absorption

High Temperature Compatibility

- Physical Appearance Tests
- Dimensional Stability
- Autoignition
- Chemical Stability

Mechanical Properties

- Shear Tests
- Fatigue (thermal shock) Tests
- Biaxial Cyclic Tests
- Vibration Tests
- Batting Compaction

At completion of the material test phase, two insulation configurations were selected for further testing. Full-scale tanks were designed and fabricated for installation of the insulations. One configuration was installed on the external skin of one tank while the other was installed on the internal surfaces of the other tank. After final installation of the internal insulation and during a checkout exposure to liquid nitrogen a number of cracks developed in the material face sheet. This tank was held for failure analysis while the externally insulated tank tests were conducted.

Failure analysis of the internally insulated tank prevented full-scale evaluation of insulation performance. Calorimeter test results of this insulation, however, did provide verification of anticipated operation. With hot- and cold-side temperatures of 100°F and -320°F (38°C and -195°C), respectively, the measured thermal conductivity was 0.024 Btu/hr-ft-°F (0.415 W/m-°C) for the 1/2-in. (1.27-cm.) thick internal insulation.

A full-scale thermal model of a wing section was fabricated for the test program. This fixture provided for the full range of temperature and pressure conditions anticipated for a supersonic cruise vehicle. The externally insulated tank was mounted in the wing and a test program was completed using liquid nitrogen as a test fluid. A series of 10 temperature cycles with wing skin temperature variations from room temperature to 700°F (371°C) were conducted along with 20 pressure cycles of ground-level ambient to 1 psia (6.89 kN/m^2-a). A baseline heat transfer test was made at the beginning and end of the test series to detect degradation. The effective thermal conductivity of the insulation before and after test was 0.0184 Btu/hr-ft-°F (0.318 W/m-°K) and 0.0144 Btu/hr-ft-°F (0.249 W/m-°K), respectively. Inspection of the insulation after test indicated no problems of any kind.

II. INTRODUCTION

The use of a cryogenic fuel in an aircraft, particularly a supersonic aircraft, introduces a number of problems not common to aircraft using conventional fuels. In general, fuel storage in an aircraft is in the wings in rectangular cross-section cavities formed by the wing structure. The primary problem in the storage of any type of fuel is to get the maximum quantity of fuel into a given volume with the least weight penalty and fuel loss due to boiloff.

The reference fuel used during the design phase was liquid methane although the test program used liquid nitrogen as the test fluid. Liquid methane, being a cryogen with a normal boiling point of -259°F (-162°C), requires a propellant tank insulated with a very high-performance insulation. In general, to determine the exact quantity of insulation to be used, a weight tradeoff analysis must be made that takes into account tank size and shape, insulation density and performance, and a number of factors pertaining to the particular aircraft and its purpose. Some of these factors are ground hold time, flight fuel use rate, wing skin heating rates, and flight pressure profiles. Because no specific purpose was established, a generalized case was considered. The objective of this program was to solve some of the insulation problems associated with a cryogenic tank of rectangular cross section. The goals we hoped to achieve in the insulation system design were--

1) a thermal insulation whose conductivity approaches that of air;

2) a design life of 30,000 hours (108 Ms) of flight and 30,000 temperature cycles;

3) satisfactory operation at a wing surface temperature of 700°F (371°C);

4) an installed density below 6 lb/ft^3 (96.12 kg/m^3).

The first portion of the program involved the selection of insulation configurations and materials. The final phase provided for installation of the insulation on large-scale tanks and testing under simulated aircraft flight conditions.

Page Intentionally Left Blank

III. DISCUSSION

A. THE CRYOGENIC FUEL STORAGE PROBLEM

The use of cryogenic fuel in an aircraft requires insulated tanks. The insulation must perform two functions: (1) it must maintain an acceptable fuel heating rate while the aircraft is on the ground, and (2) it must limit the fuel heat gain in flight to a level compatible with the total propellant feed system requirements. The problem could be considerably simplified if these two heating rates could be completely defined. An important difficulty is in defining what constitutes an acceptable or reasonable heat transfer level.

While sufficient insulation could be installed to achieve ground boiloff rates of very manageable values, the several inches of insulation required would not only cause a severe weight penalty, but also would present a volumetric efficiency problem. The fuel would probably be carried in wing cavities having rectangular cross sections and several inches of insulation could severely reduce the usable fuel volume. Because of methane's low density, the fuel volume must be efficiently used to realize its payload benefits. From a system viewpoint, the insulation must be minimized at the expense of higher ground hold heating rates.

As the insulation thickness is reduced, it naturally follows that while the aircraft is on the ground the wing temperature will be reduced. This reduction then increases the propensity for ice formation on the wing. Ice formation is the second tradeoff factor in defining the acceptable ground hold heating rate. However, it can readily be shown that for an air temperature below 40°F (4.4°C), an unreasonable amount of insulation [approximately 6 in. (15.2 cm)] would be required to prevent wing icing. This, then, dictates that the wing icing problem should be solved in a different manner (e.g., electrical heaters mounted in the wing) and this factor ought to be excluded from the ground heating design criteria.

We are now faced with a subjective tradeoff to a limited degree in that insulation weight and usable fuel volume must be balanced with ground handling and operational considerations.

The other consideration in the allowable heating rate (really insulation thickness) criteria is in-flight performance. Because the propellant feed system, and hence the required NPSH, is not completely specified at this time, an allowable energy gain or temperature rise in the liquid cannot be stated. This factor, plus the

allowable gas temperature rise when the tanks are nearly empty, forms the tradeoff in terms of the flight phase of operation. Again a specific heat transfer rate cannot be specified.

The governing factors are now evident, but to attack the insulation development problems, reasonable performance must be estimated. Although this performance level may be revised as the technology progresses, the major obstacles will have been identified and preliminary designs developed. Using the approximate thermal performance of polyurethane foam as a guide, first-order calculations indicated that an insulation thickness on the order of 1 in. (2.54 cm) would form a reasonable balance between the ground and flight requirements.

The most significant problems anticipated in developing the required insulation were associated with reliability of the insulation system. The required lifetime of the system, the severe cyclic temperature and pressure environment, the geometric constraints placed on the fuel tanks, the large number of small tanks required to store the total fuel load, and the impact of weight on cost and performance of the aircraft were considered. Figure 1 shows our conception of the interrelationships involved.

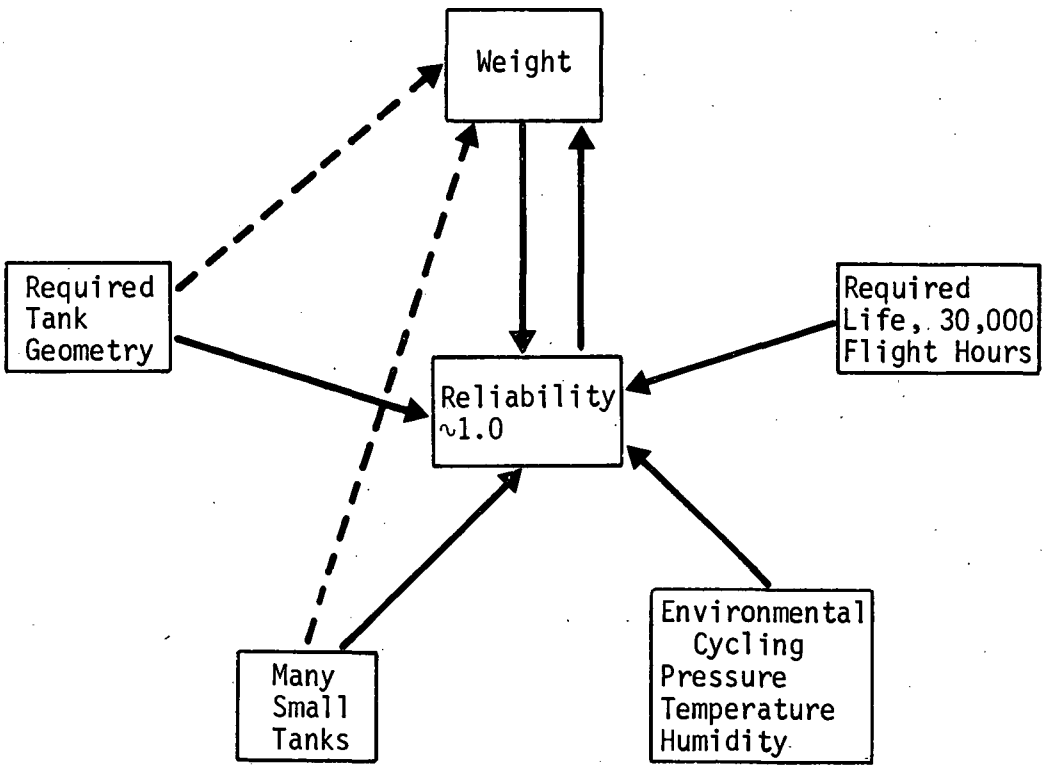

Figure 1. Relationship of insulation system reliability and the significant design considerations.

This figure indicates that the following four design conditions have an impact on the overall insulation system reliability, which must closely approach 1.0.

1) Life span of 30,000 flight hours (108 Ms);

2) Environmental cycling of temperature from liquid methane temperature to as high as 500°F (260°C) on the cold side, and from below room temperature to the hot wing condition on the hot side of the insulation. Environmental cycling of pressure from sea level ambient to 1 psia (6.89 kN/m^2) for external insulation and from something slightly greater than 1 psia (6.89 kN/m^2) to perhaps two or three atmospheres for internal insulation. Relative humidity up to 100% must be considered;

3) The tank must be configured to efficiently use the available wing void volume;

4) Many small tanks (if the entire fuel load is to be carried in wing tanks). The required tank geometry and many small tanks also result in a large exposed heat transfer area for the liquid volume stored, which directly affects the weight of insulation required.

The objective of this program was to obtain the required reliability with the four primary design considerations as fixed boundary conditions at a minimum total insulation system weight.

We recognize that many other factors must be kept in mind when selecting the final insulating system. These factors include cost, complexity, ground maintenance, compatibility with the electrical and hydraulic system, and consideration of the aeroelastic behavior of the wings. Rather major changes in the fuel system design and installation may be necessary to methane use as compared with kerosene fuel use. For example, if the use of methane requires several hundreds of tanks, a larger degree of paralleling of outflow lines with common sumps may be necessary to provide selective fuel control and crossfeed for center-of-gravity control of the aircraft. Connecting several hundreds of tanks in series would appear to introduce serious cause for concern about reliability.

B. THE INSULATION PROBLEM

1. Modes of Heat Transfer

To properly understand the characteristic thermal performance of an insulation under various conditions of temperature, pressure, gaseous constituents, and water content, the mechanism for flow of heat within the insulation must be examined. These mechanisms include conduction through the solid, conduction through the gas in the voids, convection, and radiation. It should also be noted that in the actual case all of these mechanisms interact and, from a theoretical standpoint, the insulation can generally be considered a complex system of nodes randomly interconnected by radiation, conduction, and convection. Under one set of conditions, one mode of heat transfer might predominate in a particular insulation, but under other conditions that same mode might not transport a significant fraction of the total heat flow. In designing an insulation system, it thus becomes important to analyze the modes of heat transport and then to design into the system the means that will most readily reduce heat flow in the most predominant modes. In the following paragraphs, we will examine the modes of heat flow associated with the aircraft operating conditions in the general types of materials applicable.

a. Radiation - The rather high, 550 to 700°F (288 to 371°C), temperatures encountered at the wing surface suggest that radiation might be an important mechanism of heat flow in the outer layers of insulation. This is readily confirmed by plotting the blackbody radiation (radiosity) as a function of temperature (fig. 2).

At the temperature of liquid methane, it is obvious that heat transfer by radiation cannot be very significant because the blackbody radiosity is on the order of 2.7 Btu/ft^2-hr (8.51 W/m^2) and, when the effective transmissivity of a typical porous insulation material is considered, the net radiated heat flow will be a small fraction of the design goal [on the order of 100 Btu/ft^2-hr (315 W/m^2)]. At room temperature, the radiosity is approximately equivalent to the design goal of 100 Btu/ft^2-hr (315 W/m^2). It might thus be reasonably judged that in a porous, gas-filled insulation system with reasonably low effective transmissivity, radiation is not the predominant mechanism for heat flow.

On the other hand, at the upper operating temperatures for the fuel tank insulation, the radiosity increases to 2000 to 3000 Btu/ft^2-hr (6.30 to 9.46 kW/m^2) and, even with low effective transmissivity, radiation constitutes a significant heat flow mechanism.

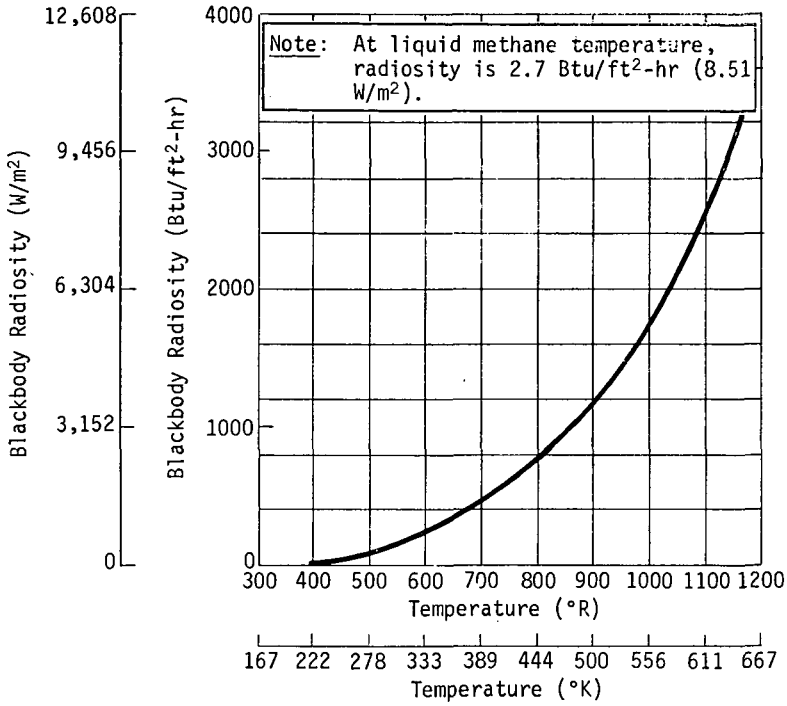

Figure 2. Blackbody radiosity as a function of emitting temperature.

b. Conduction - In a gas-filled (i.e., nonvacuum) system, gaseous conduction represents a lower limit for total heat flow. Conduction through the solid portions of the insulation media makes a contribution to total heat flow, but this can readily be maintained at a negligible level by use of a suitable porous or fibrous material.

The relatively low thermal conductivities of air and methane gas indicate that the use of either in a gas-filled insulation, where convection and radiation have been effectively eliminated, will readily accomplish the thermal requirements of the insulation system. In arriving at a specific system, however, care must be taken to account for the temperature effect on the thermal conductivity. Figure 3 illustrates the divergent effect of temperature on thermal conductivity between methane gas and air. This figure shows an increase of 50% or more in the 500°F (260°C) temperature range for methane gas over air. This suggests that an internal gas-filled insulation might be less efficient than an external air- or nitrogen-purged insulation. The effective conductivities of air-filled foam and air-filled fiberglass are also plotted.

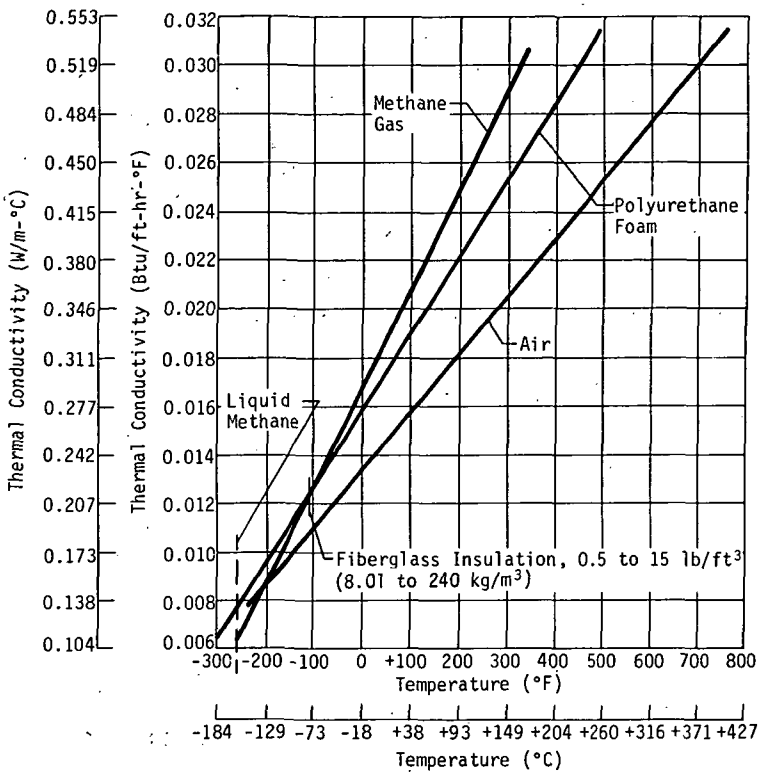

*Figure 3. Thermal conductivity as a function of temperature.**

To obtain a low thermal conductivity, the absorption of water vapor and carbon dioxide by, or the leakage of liquid methane into, the insulation must be prevented.

Thermal conduction through the tank supports must also be considered in the overall insulation system.

c. Convection - From the standpoint of insulation weight and thermal conduction through solids, it is desirable to reduce the quantity of solid matter in the insulation to a minimum. As the density of the porous material is reduced, the pore size generally increases thus permitting gas convection to develop in the pores. This effect, as well as radiation and transmissivity, has been studied as a part of the insulation development under contract to the Flight Dynamics Laboratory (HASP program). A 30-in. (76.2-cm)

*Christiansen, Hollingsworth, Marsh: "Low-Temperature Insulating Systems." *Advances in Cryogenic Engineering*, Vol 5, Plenum Press, New York, N.Y., 1959.

diameter, 6-in. (15.2-cm) thick sample of microquartz was tested in a guarded cold plate calorimeter using hot side temperatures to 1500°F (815°C) and liquid hydrogen as the heat sink. The sample was tested with and without Inconel radiation shields and filled with helium gas at ambient and 10 torr (1.33 kN/m^2) pressures. Figure 4 shows the data measured for these test conditions.

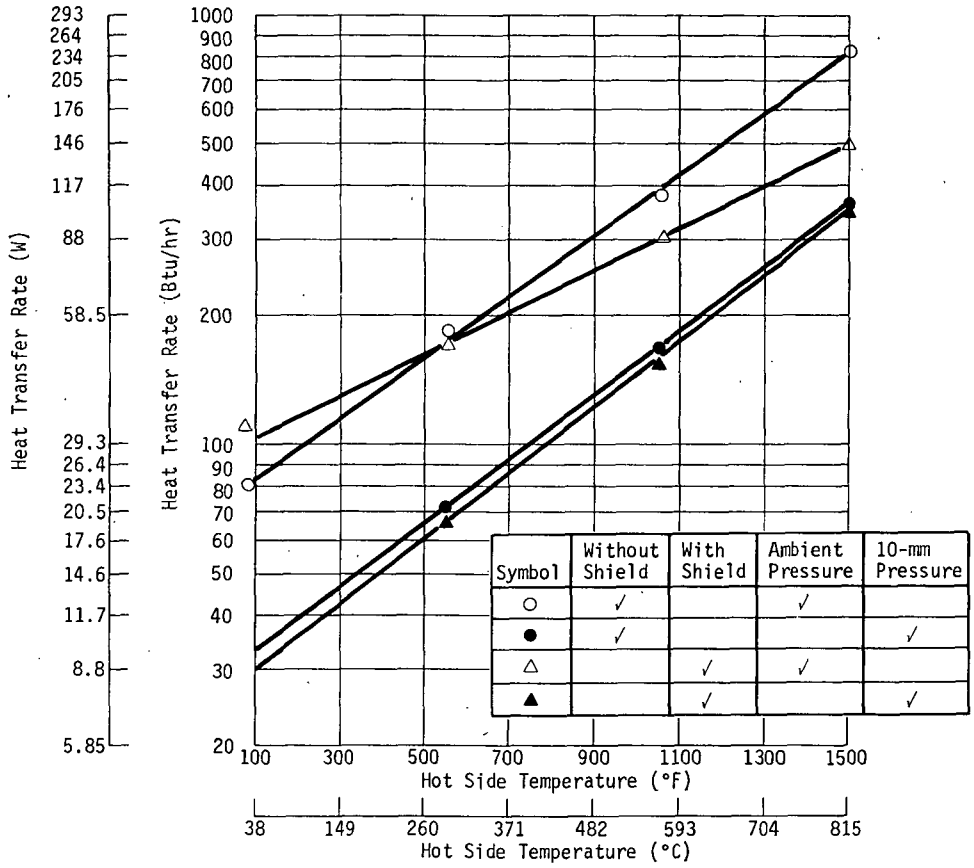

Figure 4. Heat transfer rate to LH_2 as a function of hot side temperature (HASP program).

Comparing the data taken at ambient pressure with the data taken at 10 torr (1.33 kN/m^2), we see a very large difference. These data are typical of most data we have obtained for a gas-purged insulation. The effect is explained in terms of convection. As gas is purged through the insulation, even at low rates, both free convection and forced convection occur and the effective conductance of the insulation is increased. This effect is very important with such large temperature differences as those studied in this program.

2. Factors Affecting Insulation Performance and Degradation

The most significant factors that tend to degrade the thermal performance of insulation are discussed in this subsection.

a. Water and Carbon Dioxide Absorption - An insulation external to the metal tank wall will cryopump water vapor and carbon dioxide from the atmosphere unless a complete seal or a purge are used. The tremendous difficulty of producing a complete seal can easily be overlooked. The proper perspective is obtained by careful examination of typical ground/ascent/cruise/descent environment conditions.

Under normal atmospheric conditions on the ground, the steady-state temperature profile through the insulation is approximately as shown in figure 5. The thermodynamic regions of solid/liquid/vapor are shown for representative atmospheric and insulation conditions, the water/vapor line being at the dewpoint. Under these conditions, the vapor pressure gradient results in a net migration of molecular water into the insulation where condensation or freezing occurs. Liquid water also moves in the direction of decreasing temperature because of capillary forces. Over a period of time, carbon dioxide absorption can be significant, even though its atmospheric content is only 0.03% at sea level. If no vapor barrier at all is used, the rate of condensation can be reasonably predicted by use of the convectional mass diffusion equations for either molecular or eddy diffusion of condensible gases. An impermeable seal placed over the insulation would eliminate the problem, but such a seal is almost impossible to achieve in practice. A purge of dry air can minimize the problem of moisture absorption, but a dry gas such as nitrogen may be needed to prevent carbon dioxide absorption.

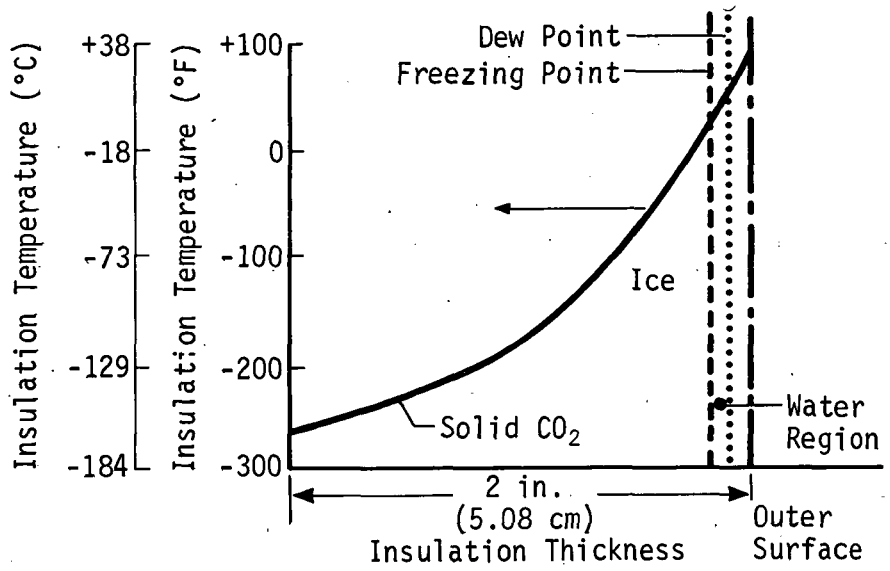

Figure 5. Typical insulation temperature profile.

b. Environmental Compatibility - The problems of thermal extremes, thermal shock, and long-term mechanical vibration are of major concern. Where temperature gradients across metal/nonmetal interfaces are in the range of 800 to 1000°F (371 to 538°C), differential expansion effects will damage most assemblies. The normal mechanical vibration of an aircraft wing can only hasten such destruction. A nonstructural insulation in the area of high thermal gradients is thus attractive.

The chemical environment of an external insulation is that of air (or perhaps an inert gas) at ambient pressure, 1 to 15 psia (6.89 to 103 kN/m^2). An external insulation should be noncombustible and should not be degraded by water, ice, or steam.

An internal insulation will operate in an environment of liquid or gaseous methane. It should be inert to solvent or swelling effects and should not generate oxidative radicals when at high temperature. Mechanically, an internal insulation should have high

integrity throughout the temperature extremes. For this reason, a designed geometry such as honeycomb is preferred to a random geometry (such as a foam). Mechanical durability over a long period of operation is imperative for a reliable internal insulation.

c. Seals and Purging - Long-term nonpurged cryogenic insulation requires absolutely impermeable seals. The only existing cryogenic hardware with a proven long-term cycling capability has metallic seals to provide vacuum insulation.

All organic materials have a finite permeability to air and water vapor and thus the long-term reliability of cryogenic insulation that depends on organic seals cannot be high.

A double-walled vacuumtight structure is conceivable for the liquid methane tanks of the SST. Such a structure might be made of welded elements, exterior shell over interior, with intermediate load-bearing insulation. Such tankage requires a weld temperature/weld design/insulation temperature compatibility and a tank geometry amenable to stresses from pneumatic pressures. Cylindrical tanks are easily built of such structures, but rectangular parallelepipeds are much more difficult.

Because a perfectly sealed insulation is either unreliable or impractical, two unsealed insulations that have the best prospects for high reliability performance and meet the design requirements were proposed. These involved--

1) multilayer, radiative insulation outside the tank with modest purge of dry gas;

2) Assembled honeycomb interior insulation with permeable membranes to maintain a thermal barrier of methane vapor.

3. Insulating Materials

Conductive/convective insulators are mostly voids separated by fibers or by cell walls (as in foams). Radiative insulators are merely surfaces of low emissivity and may be metal foil or a metal or nonmetal surface.

Foams, of either open or closed cells, are materials of random geometry with random variations of permeability, strength, and void volume. Foams are excellent insulators for cryogenic applications where an impermeable barrier can be provided; they are highly unreliable with permeable barriers.

Fibrous materials are excellent thermal insulators when convection through the material is inhibited. An open fibrous batting would be of no value inside a cryogenic tank because boiling would take place within the fibrous material. They can be of real value outside a tank if moisture and carbon dioxide condensation are inhibited.

Nonmetallic honeycombs are intermediate in thermal conductivity and are superior to both foams and fibrous materials in mechanical properties. For example, the Hexcel HRH327 honeycomb with a 1/4-inch (0.63-cm) cell and a 3.5 to 4.0 pcf (56.1 to 64.1 kg/m^3) density has a compressive strength of 340 psi (2.34 MN/m^2) and its tensile strength exceeds 10,000 psi (68.95 MN/m^2). A urethane foam of equal density has about a 75-psi (0.516-MN/m^2) compressive strength and only a 45-psi (0.31-MN/m^2) tensile strength.

To cover the temperature range for liquid methane on the aircraft, conductive, convective, and radiative transfer must all be minimized. This requires judicious combination of different materials. A combination implies reliable materials and fabrication techniques for joining or attaching insulating materials to each other and to the tank. A simple wrapping technique has been successfully used for nonstructural, multilayer superinsulation. The low weight, compressibility, and continuous assembly of wrapped insulation contribute to high reliability in very large dewars.

However, if the insulation is inside a tank and in contact with the cryogen, it must be mechanically bonded to the tank surface. Good adhesives are currently being used in cryogenic applications and at temperatures in the range of 500°F (260°C). However, few applications have a proven reliability of structural adhesives with thermal gradients and thermal shock for the wide temperature range anticipated with liquid methane in a supersonic cruise-type aircraft.

C. INSULATION SELECTION

During the program, two baseline insulation systems were selected for development. One system was to be applied to the external surface of a tank while the other was to be applied to the internal surface.

A number of investigations were initiated to help establish final configurations. These investigations, the details of which will be covered later, fell into the following general categories.

1) Material Studies - This effort involved the selection of materials capable of meeting the severe environmental requirements.

2) Thermal Conductivity - These tests were conducted using a guarded cylindrical calorimeter to measure the thermal conductivities and heat capacities of the insulation configurations using the materials selected in 1) above.

3) Specific Weight - Insulation system density was measured by weight and dimensional measurement of samples.

4) Coefficient of Thermal Expansion - A modified ASTM quartz dilatometer was used to measure sample dimensions at five temperatures to determine coefficient of thermal expansion.

5) High Temperature Compatibility Tests - Dimensional stability and autoignition tests were conducted over a wide temperature range and in both air and methane gas environments.

6) Mechanical Properties - Shear tests of bonded specimens, and thermal shock, temperature and pressure cycling, vibration, and batting compaction tests were conducted to verify acceptable mechanical properties of the materials and composite samples.

As a result of the various investigations and tests, configurations for both the external and internal insulations were established.

A cross section of the external insulation is shown in figure 6.

This insulation consists of layers of opacified fiberglass mat encapsulated by a metal foil cover. A fiberglass net over the foil holds the fiberglass mats and foil in place on the tank without significant compression of the fiberglass. A thin-wall perforated stainless steel tube provides a purge of dry gas to the fiberglass mat insulation to prevent moisture collection during temperature cycle breathing. The outer foil cover is also perforated allowing for venting of the purge gas.

The fiberglass mat material has a density of 0.6 lb/ft^3 (9.61 kg/m^3) and was opacified during manufacture by the addition of aluminum powder. The metal foil cover should be made of a rugged high temperature material such as Inconel for the actual aircraft installation.

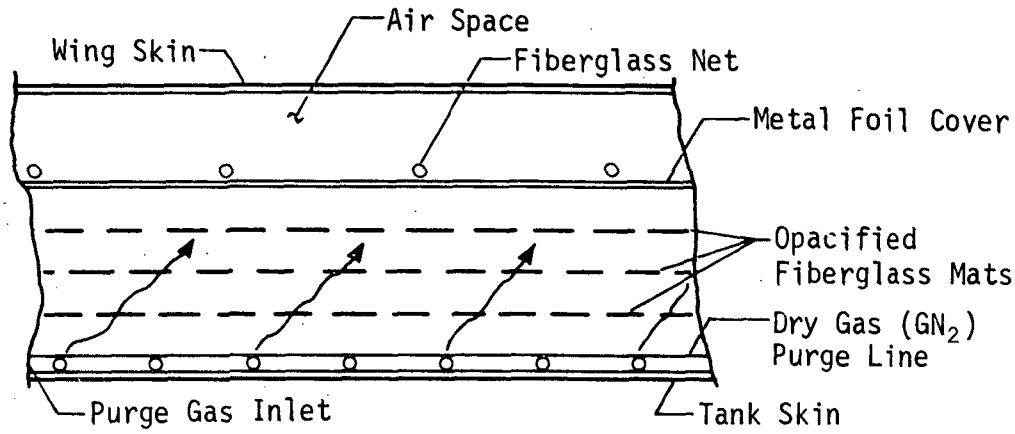

Figure 6. Cross section of external insulation.

A preliminary study was conducted of methods for obtaining "dry" purge gas to evaluate the feasibility of the gas-purged concept. Our conclusion is that several simple, reliable, low cost, and low weight methods for obtaining dry purge gas are available. We did not investigate these concepts further in this program but possible approaches are listed. It should be noted that one flight cycle requires approximately 2000 std cu ft (56.6 m^3) of dry gas, neglecting leaks in the system.

1) A liquid nitrogen system with a vaporizer coil. For one flight, 300 tanks and an insulation volume of 4.7 ft^3 (0.133 m^3), a total of approximately 21.8 gallons (0.082 m^3) of LN_2 will be required for the N_2 purge. This appears feasible;

2) Air will be dried by use of an airborne Freon refrigeration cycle dehumidifier. The dewpoint temperature requirements do not appear too difficult to obtain. A reduction in humidity to a vapor pressure of 0.13 mm Hg (17.3 N/m^2) is sufficient to reduce the total condensed water in 30,000 cycles to less than 1 lb (454 g);

3) Air could also be dried by cooling with methane boiloff or liquid methane;

4) A chemical desiccant might be used. Commercially available hygroscopic desiccants are adequate to reduce the partial pressure of water to adequate levels. A small compressor might be required with this system to maintain a slight positive gas pressure in the insulation. For ground operations, the compressors or refrigerators would be operated on ground power or a ground dry gas supply.

The internal insulation system selection is shown in cross section by figure 7.

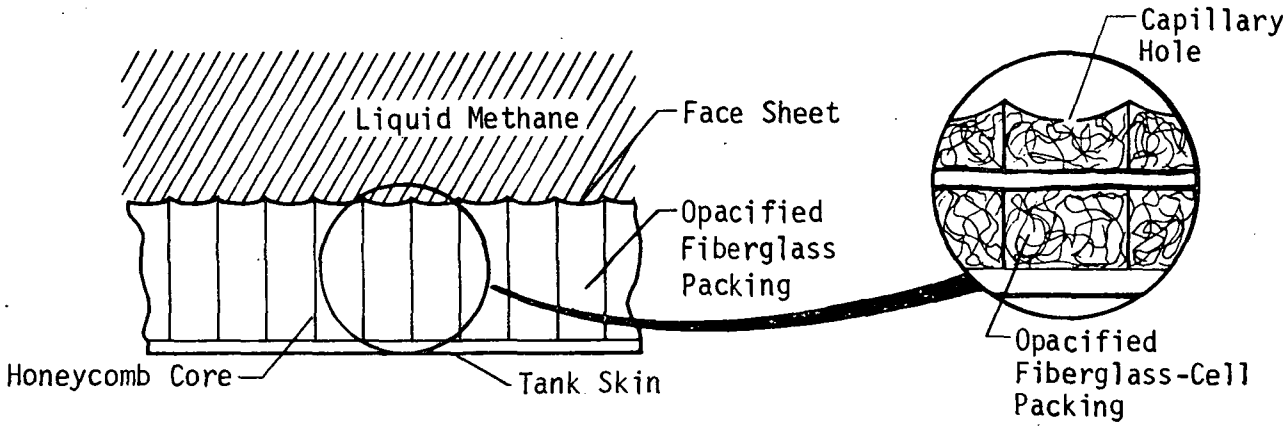

Figure 7. Internal insulation system configuration.

This insulation system consists of a honeycomb core of fiberglass cloth impregnated with polyimide resin. The core is bonded onto the metal tank wall using a polyimide adhesive. A fiberglass scrim cloth is used to hold the adhesive and fill any small voids or spaces between the tank wall and core. The core is filled with finely chopped opacified fiberglass to minimize both convection and radiation heat transmission through the core voids. A polyimide film face sheet is bonded to the core face on the inside of the tank using the same polyimide adhesive that was used to bond the core to the tank wall. After bonding, the face sheet is dimpled and a capillary hole is placed in the sheet over each honeycomb cell.

The insulation system is assembled in rectangular panels with the face sheet installed and the cells packed before bonding it to the tank wall. A detailed description of the assembly and installation of this system in a test tank is described in Chapter IV of this document.

Some of the problems with external insulation are overcome when the insulation is placed inside the tank wall. For example, the problem of cryopumping is eliminated and heat leaks through tank supports are greatly reduced. Also, the tank wall affords a high degree of protection against accidental mechanical damage. Some problems are to prevent liquid from entering the insulation, the possibility of engine contamination, and the finite probability of a catastrophic thermal failure as compared to the external system.

The greatest difficulties encountered in obtaining an internal lightweight, but still reliable, system are associated with structural problems. In the classic approach, some type of low-conductivity material is attached to the inner wall of the tank and a liner that prevents liquid from entering the insulation media is installed. Hydrostatic and gas pressure loads are transmitted by the liner through the insulation media to the tank wall. The induced compressive and shear loads in the insulation media and bondlines are greatly increased by the thermal stresses caused by the temperature differences across the insulation. Because materials possessing low thermal conductivities also possess low strengths, the stresses arising in the insulation commonly result in mechanical failure. Reinforcing the insulation with higher strength materials such as fiberglass filaments can overcome the problem of failure, but increases the weight and thermal conductivity.

The capillary system involves attaching a cellular material such as honeycomb core to the inside of the tank wall. To perform properly, the walls of the honeycomb material must be impervious to gas and must be attached to the wall so gas flow parallel to the tank wall is prevented. Material such as open-cell foam obviously will not meet this requirement. A perforated cover is then placed on the inside of the honeycomb material. The perforations or pores are sized so surface tension forces produce a stable curved "membranelike" liquid/gas interface that keeps liquid out of the cell. It is important to note that in the sense of static forces, the gas pressure in the cell is supporting the column of liquid above the cell. The membrane must, however, be mechanically stable or liquid will run into the cell and gas will run out. The liquid/vapor interface is maintained in a structurally stable shape by surface tension forces. It can be shown that when the ratio of liquid inertial forces to membrane surface forces is less than about 0.8, the membrane assumes a stable shape.* Simple computations show that, for this case, pores on the order of 1 millimeter are adequate. There is a small pressure difference across the membrane that is, again, due to surface tension effects.

---

*W. J. Masica, D. A. Petrash, and E. W. Otto: *Hydrostatic Stability of the Liquid-Vapor Interface in a Gravitational Field.* NASA TN D-2267. Lewis Research Center, Cleveland, Ohio, May 1964.

The pressure difference (ΔP) is given by

$$\Delta P = \gamma\left(\frac{1}{r_1} + \frac{1}{r_2}\right)$$

where γ is the coefficient of surface tension and r_1 and r_2 are the major and minor radii or curvature at any point on the static membrane.*

As a tank insulated with this material is filled, the gas in the cell cools and contracts and some liquid enters through the pore and then boils. The gas produced by this boiling pressurizes the cell and liquid is held out of the cell. Probably an excess of liquid intake occurs in the initial cooldown and gas bubbles flow from the cell until all the liquid is evaporated. Equilibrium is then established with a liquid/gas interface at the pore. If the tank were to be depressurized after equilibrium interfaces are established, gas would bubble from the insulation cells to obtain a new state of pressure equilibrium. Repressurization results in a sequence of events similar to the initial cooldown of the system.

The thermodynamic state of the liquid at the liquid/vapor (pore) interface is of considerable importance in system performance. It is necessary that a thermodynamic equilibrium exist across the phase boundary. The pressure is slightly greater in the gas than in the adjacent liquid because of the capillary pressure previously discussed, and the liquid must be saturated at the gas pressure.

The maximum pressure load introduced into the insulation system is limited to the capillary pressure, which is on the order of 1 psi (6.89 kN/m^2). Because the honeycomb core is essentially unrestrained at the dimpled line surface, it is very flexible in the plane of the tank wall, eliminating thermal stresses in the core and bondlines.

---

*L. M. Milne - Thompson: *Theoretical Hydrodynamics*. Macmillan Co., 196--

D. INSULATION MATERIAL STUDIES AND TESTS

This effort involved the selection of materials for insulation that could be expected to withstand the severe operating conditions. The range of operating temperatures were from a -320°F (-196°C) cold side temperature to a hot side temperature of +700°F (371°C). In the case of the internal insulation, the materials would also have to be compatible over the same temperature range in an atmosphere of methane.

1. Internal Insulation

A survey of plastic materials that could be used for the internal insulation was conducted. Only four candidate materials were found.

1) Polyimide

2) Polybenzimidazole

3) Polycarboranesiloxane

4) Polybenzimidazophyrrolone

The latter two meet the requirements, but were not considered for the project because of their embryonic stage of development. It is worthwhile to note that the polybenzimidazophyrrolone might be very promising for some future applications. There was very little test data on the material, but indications are that it loses very little weight when exposed to air at 1100°F (593°C).

Comparison of the two remaining candidates showed that polybenzimidazole had a higher lap shear strength than polyimide at all temperatures up to 800°F (427°C). However, thermal aging tests show that polyimide with an arsenic salt additive retains its strength very well during extended exposure to high temperatures; whereas, the polybenzimidazole rapidly loses its strength at elevated temperatures. The curing cycle for polybenzimidazole requires a pressure cure at 600°F (316°C), which is impractical for large items such as an LN_2 tank. The above factors led to the decision to use polyimide materials for the internal insulation system in the test program.

Polyimide is the resulting heterocyclic aromatic polymer from the reaction of a dianhydride and a diamine. It exhibits significant properties retention in air up to 500°F (260°C) for continuous service. The resin is usually cured in several temperature stages in a controlled atmosphere preferably in a vacuum. During the curing of the polyimide resin, water and other volatiles are found to leave small bubbles in the matrix. The vacuum process extracts most of these volatiles, so they would not be driven off during the high temperature service. Controlling the volatile liberation during curing, therefore, is important in controlling the void content of the resin, which means controlling the mechanical properties of the material. To properly cure the resin, the curing should be done in several temperature stages. The initial cure, around 200°F (93.2°C), sets the reaction under the necessary bonding pressure and extracts some of the volatiles. The next step, around 400°F (204°C), causes the reaction to complete and set the molecule. The final step, postcure, is accomplished at a temperature equal to or greater than the maximum service temperature. This cure completes the outgassing process and allows the material to be used without a substantial loss in properties.

Specific materials chosen for further testing were as follows.

1) Honeycomb - Hexcell polyimide honeycomb, which is a glass cloth base impregnated with a polyimide resin.

2) Face Sheet - Dupont Kapton film, fiberglass cloth, stainless steel dutch twill, and polyimide preimpregnated cloth.

3) Adhesives - American Cyanamid BR-34 and FM-34. The FM-34 is a fiberglass cloth impregnated with the basic BR-34 adhesive and partially cured.

a. Thermal Conductivity - A number of tests were conducted using a guarded calorimeter. The results of the individual tests are shown in table I along with the materials used for each calorimeter sample. Earlier tests (1 and 2) were run using a phenolic core material because the polyimide core material had not as yet been delivered from the manufacturer. The first test was run with liquid nitrogen to verify the basic insulation concept. The thermal conductivity measured was far above the calculated value expected of 0.02 Btu/hr-ft-°F (0.346 W/m-°C).

TABLE I. - INTERNAL INSULATION CALORIMETER TESTS

Test No.	Core	Packing	Face Sheet	Adhesive	Thermal Conductivity	Comments
1	3/8x1-in. (0.953x2.54-cm) thick Phenolic	None	No. 108 Fiberglass Scrim Cloth	Narmco 7343	0.33 Btu/hr-ft-°F (5.71 W/m-°C)	Test with LN_2 to prove basic concept
2	3/8x1-in. (0.953x2.54-cm) thick Phenolic	Fiberglass Batting	Stainless Steel Dutch Twill	Narmco 7343	0.02 Btu/hr-ft-°F (0.346 W/m-°C)	Test with LN_2 to check convection in cells
3	3/8x1-in. (0.953x2.54-cm) thick Polyimide	Opacified Fiberglass	Kapton 0.001-in. (0.025 mm)	American Cyanamid BR-34	0.033 Btu/hr-ft-°F (0.571 W/m-°C)	Configuration verification test
4	3/8x1-in. (0.953x2.54 cm) thick Polyimide	Opacified Fiberglass	Kapton 0.001-in. (0.025 mm)	American Cyanamid BR-34	0.065 Btu/hr-ft-°F (1.12 W/m-°C)	Configuration verification, tears in Kapton face sheet
5	3/8x1-in. (0.953x2.54 cm) thick Polyimide	Opacified Fiberglass	Kapton 0.001-in. (0.025 mm)	American Cyanamid BR-34	0.10 Btu/hr-ft-°F (1.73 W/m-°C)	Wet fiberglass packing
6	3/8x1-in. (0.953x2.54 cm) thick Polyimide	Opacified Fiberglass	Kapton 0.001-in. (0.025 mm)	American Cyanamid BR-34	0.024 Btu/hr-ft-°F (0.415 W/m-°C)	Oven-dried fiberglass packing

The results of this test indicated that the dominating mode of heat transfer inside the honeycomb cell at cryogenic temperatures is convection and not conduction. After the cryogenic test the sample tank was filled with water and it was noted that a number of cells were leaking, although there were no apparent failures of the capillary cloth.

The second test sample was similar to the first except that the cells were filled with fiberglass batting and the face sheet was changed to a woven stainless steel mesh. This sample was tested with liquid nitrogen in a horizontal position and yielded a thermal conductivity of 0.02 Btu/hr-ft-°F (0.346 W/m-°C), indicating that the gas convection problem had been solved and a value approaching gas conduction had been reached. It should be noted, however, that the cell leakage problem had not been solved. Further, single-cell tests indicated that a capillary breakdown was occurring in the cell face sheets due to the pore size.

The capillary pressure retention capability of a porous material is given by the equation on page 20, where γ is the surface tension of the fluid and r_1 and r_2 are the principal radii of curvature at any point on the gas/liquid interface. As the pore size increases, the r_1 and r_2 radii increase, resulting in a smaller (ΔP) pressure retention capability. With relatively large pores in the capillary cloth and stainless steel mesh, the pressure fluctuations in the tank liquid due to boiling, vibration, sloshing, etc, can easily exceed the pressure retention capability of the pores, resulting in breakdown of the capillary surface. As this occurs, tank liquid enters the cell, wetting the inside surface of the mesh face sheet.

With the cell in a horizontal position (i.e., face sheet horizontal), the liquid is dropped directly on the warm outer skin of the cell, flashing to vapor and rapidly pressurizing the cell to reestablish the stable capillary surface. If the cell is vertical (i.e., face sheet vertical), the liquid pours off the inside of the face sheet onto the cell side wall and finally contacts the outer skin. It is felt that considerably more liquid enters the cell in this latter position, resulting in larger volumes of vapor produced and a much higher overall thermal conductivity. To limit the amount of liquid ingested during each pressure fluctuation, a nonporous face sheet was considered and a decision was made to use 0.001-in. (0.025-mm) Kapton film. In this case, the sheet is dimpled after bonding and pierced with a single capillary hole per cell.

The third calorimeter was the first test of a sample using the selected materials of construction. This test was again run with a panel in a horizontal position. Results were not as good as expected with a thermal conductivity of 0.033 Btu/hr-ft-°F (0.571 W/m-°C) attained. It was later determined that the solid fraction of the polyimide-glass honeycomb was 10.3% for a core of 35 cells/ft. This solid fraction helps to explain this high conductivity because glass had a conductivity of about 0.45 Btu/hr-ft-°F (7.78 W/m-°C) and polyimide a conductivity of approximately 0.1 Btu/hr-ft-°F (1.73 W/m-°C).

Test 4 used similar materials, but was tested in a vertical position. The conductivity at 100°F (37.8°C) was determined at 0.065 Btu/hr-ft-°F (1.12 W/m-°C), which was about twice that measured in the previous calorimeter. Inspection of the calorimeter after the test showed several cracks in the Kapton face sheet that were caused by improper dimpling. With the calorimeter in a vertical position, the cracks permitted a pumping effect resulting in a higher conductivity. The fifth calorimeter test again utilized the same materials of construction and was conducted in a vertical position. The data indicated a conductivity of more than 0.1

Btu/ft-hr-°F (1.73 W/m-°C). A vacuum check was made on each cell to determine if there was leakage between cells. The results of these checks were negative. A retest in a horizontal position yielded the same value of conductivity. It was suspected at this time that the fiberglass cell filler might be wet. A final calorimeter was constructed using filler material dried in an oven at 600°F (316°C) overnight. Data results of this test are shown in figure 8. The value of slightly over 0.024 Btu/hr-ft-°F (0.415 W/m-°C) at 100°F (37.8°C) was considered to be a good conductivity value considering the more than 10% solid fraction of the core material.

b. Specific Weight - With the great number of test specimens of various kinds made during the material investigations, it was decided that a specific weight measurement would be made at the time the insulation was installed in the test tank. Samples of the 2½-in. (6.35-cm) and ½-in. (1.27-cm) tank insulation were measured and weighed, yielding densities of 3.38 lb/ft^3 (54.15 kg/m^3) and 4.85 lb/ft^3 (77.70 kg/m^3), respectively.

c. Coefficient of Thermal Expansion - As indicated in a previous section, the maximum pressure head introduced into the insulation system is in the order of 1 $lb/in.^2$ (6.89 kN/m^2). In addition, the honeycomb core is essentially unrestrained at the face sheet surface, thus eliminating thermal stresses in the core and in the face sheet-to-core bondlines. The materials are polyimide face sheet, polyimide/glass core and polyimide adhesive making the differential thermal movements minor if not nonexistent. A measurement of the thermal expansion of the Kapton polyimide film over six temperature spans covering the range of temperatures from -320°F (196°C) to 700°F (371°C) was made. The average coefficient of thermal expansion, which was very nearly constant, was 6.9×10^{-6} in./in.-°F (3.83×10^{-6} cm/cm-°C).

d. High Temperature Compatibility Tests - Resistance to heat and fuel (methane) exposure was determined by a series of tests of the insulation components. Two test setups were used; a steel bomb for the methane tests, and a high temperature oven for the open air tests. Additional data were obtained by thermogravimetric analysis (TGA) in an argon atmosphere.

Results of the test series indicated that at temperatures above 700°F (371°C) some material degradation occurred, however, all materials were able to withstand exposures for 24 hr (86.4 ks) up to 700°F (371°C) in any test atmosphere. Data on longer exposure times and at temperatures above 1000°F (538°C) were not obtained.

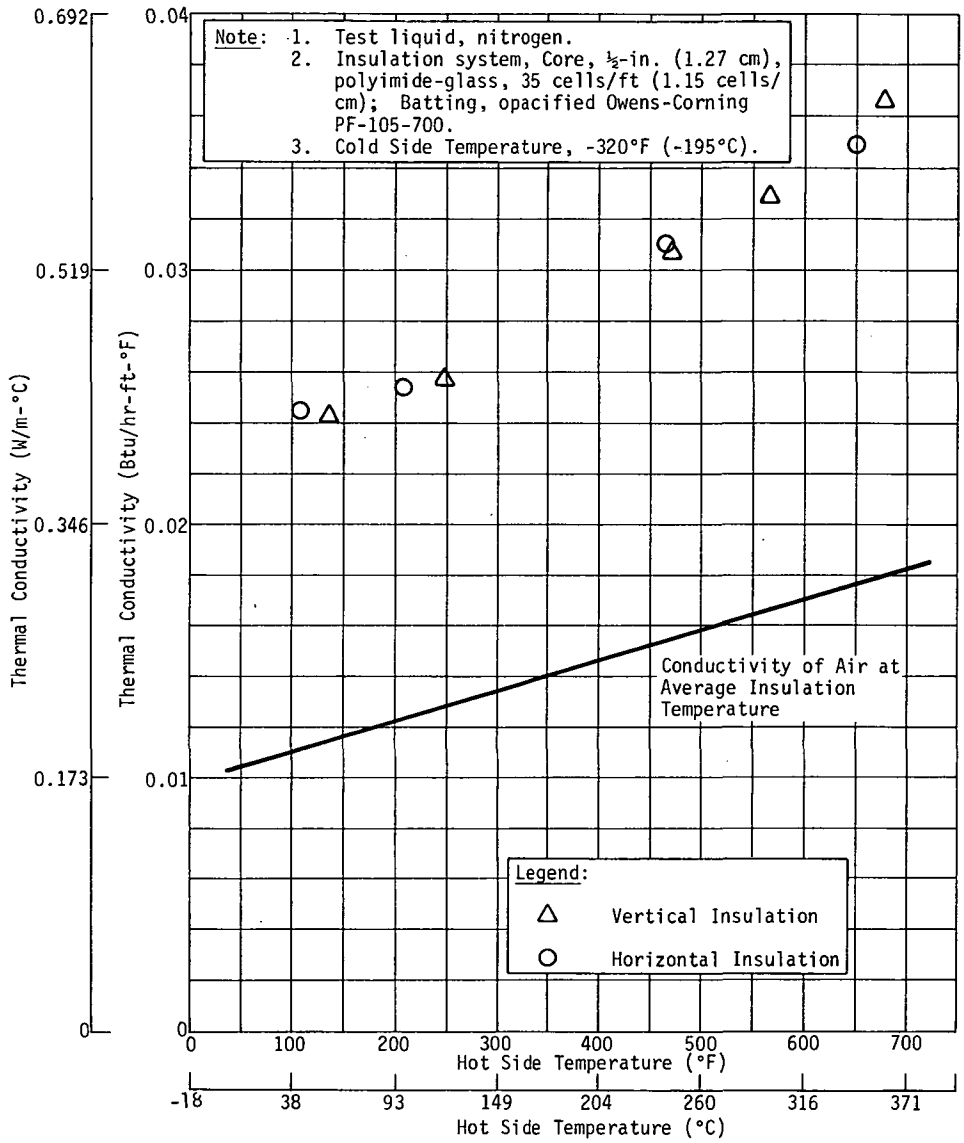

Figure 8. Thermal conductivity of internal insulation system.

The tests were divided into the following series:

1) Physical appearance changes,

2) Dimensional stability,

3) Autoignition,

4) Chemical stability.

The physical appearance changes were noted as a part of the temperature/atmosphere exposure tests. In all tests there was no evidence of charring, but some color changes were noted. Very little if any color change took place in the polyimide glass core samples, but there was considerable darkening of the polyimide film (Kapton). This material changed from a light to a very dark yellow as a result of temperature exposure. The fiberglass batting showed no physical changes nor did the adhesive (BR-34).

No dimensional changes were noted in any of the materials after temperature soak at 700°F (371°C). Slight dimensional changes were noted in the samples after exposure in the 900 to 1000°F (482 to 538°C) temperature range after the autoignition tests. These changes were more pronounced in those samples run in air than those run in methane. For a typical run made at 700°F (371°C) for 24 hr (86.4 ks), the polyimide film, the film adhesive, and the polyimide core were marked or scribed before test. The distance between the scribes, about 0.3 in. (0.76 cm), was measured with an optical comparator. After test, the samples were again measured and the two sets of measurements compared. The polyimide film and the film adhesive showed no dimensional changes. The polyimide core could not be measured accurately because of its springiness. All measurements taken were accurate to ±0.0001 in. (0.002 mm).

Test results were somewhat different in the range above 900°F (482°C). After these tests, deformation of all samples was obvious and measurements of the scribe marks could not be made. The autoignition tests were conducted in two bombs, one made of 300 series stainless steel and one of carbon steel. Four test series were run in each bomb with 100%, 10%, 6%, and 2% methane, by weight, mixed with air. No sample of insulation was found to cause a premature methane/air ignition nor was there any indication of a methane/insulation chemical reaction. The 2% methane/air mixture did not react significantly under any test condition.

Surprisingly, evidence of a methane/air reaction for other mixtures did not show up as a temperature spike even though very low heat capacity thermocouples were used. Instead, as a small quantity of chamber gas was leaked off after test, both odor and the presence of smoke was noted as evidence of a reaction. During the initial runs, an oil-like substance was found on the chamber walls and reaction occurred at relatively low temperatures in the 300 to 500°F (149 to 260°C) range. As the testing progressed, the reactions occurred less frequently and at increasingly higher temperatures. Apparently a passivation or aging process of the chamber walls was occurring with each test. A final run at 970°F (521°C) was completed with no evidence of reaction and little degradation of the test specimens noted.

A special 100% methane exposure test was run at 700°F (371°C) for 24 hr (86.4 ks). After this test, there was no evidence of reaction and the test specimens showed less dimensional change than similar samples heated in air.

Thermogravimetric analyses were run on each component of the insulation system. Both programmed temperature and isothermal modes were run. The programmed rate was a 6°C temperature rise per minute and the isothermal runs were made at 940°F (504°C) and at 700°F (371°C). All runs were conducted in an argon atmosphere. Results of these analyses show that none of the samples lost weight or were degraded at temperatures below 750°F (399°C) except for the FM-34 adhesive. Temperatures of the beginning of weight loss were as follows.

Polyimide film (Kapton)	870°F (465°C)
Polyimide honeycomb	750°F (399°C)
FM-34 film adhesive	570°F (299°C)

The FM-34 adhesive film continued to lose weight throughout the run starting at about 570°F (299°C). The maximum weight loss was about 19%. The TGA trace shows a flattening of the weight curve at 1470°F (799°C). This type of behavior is often indicative of incomplete cure. Isothermal runs at 700°F (371°C) showed no evidence of continued weight loss.

Isothermal runs of the polyimide film and honeycomb at 940°F (504°C) showed an almost negligible weight loss for the honeycomb; however, the polyimide film showed that a constant weight loss occurred. This would indicate that this temperature is too high for long-term service.

e. Mechanical Properties - A thermal shock machine (figure 9) was assembled for the simultaneous thermal cycling of four specimens. The specimens were lowered and raised by a double-acting air cylinder. Each specimen was attached to the rack by four rods, which in turn passed through enlarged holes in the specimen metal skin. In this way, as the rack was lowered, the samples could float in the liquid nitrogen rather than be completely submerged. As the temperature of the stainless steel skin reached 0°F (-18°C) the samples were raised and the heater strips turned on. The heater strips were mounted directly on the specimen skin. When the skin reached 700°F (371°C), the heaters were turned off and the specimens were lowered into the liquid nitrogen. One of the specimens with heater strips installed is shown in figure 10. A cycle time of approximately 7 min (420 sec) was attained with the system. Automatic operation was possible by using a set point recorder with microswitches to cycle the power and pneumatics. Automatic fill of the liquid nitrogen tank was accomplished by float switches that activated a solenoid operated fill valve.

The shock machine was then modified so the heaters would not be attached to the specimen. The heater assemblies were mounted on the machine structure so that, as the test specimen is raised, it contacts the heater and when lowered the heater remains in place. This change reduced the cycle time to approximately 3 min (180 sec).

Several sets of specimens were exposed to the thermal cycling test. The first set of specimens failed because of severe warpage of the steel skin. A second set of specimens was tested and after 1000 cycles the back plates were again severely warped. Three of the samples had no plastic failures, while one had a small crack in the Kapton face sheet along the honeycomb bondline in one cell. At 2300 cycles, tears in the Kapton face sheet had occurred in three samples. The fourth specimen was tested without a face sheet. Testing was continued to 3200 cycles at which time the three samples with face sheets had 4, 2 and 7 tears in the Kapton-to-honeycomb bond area.

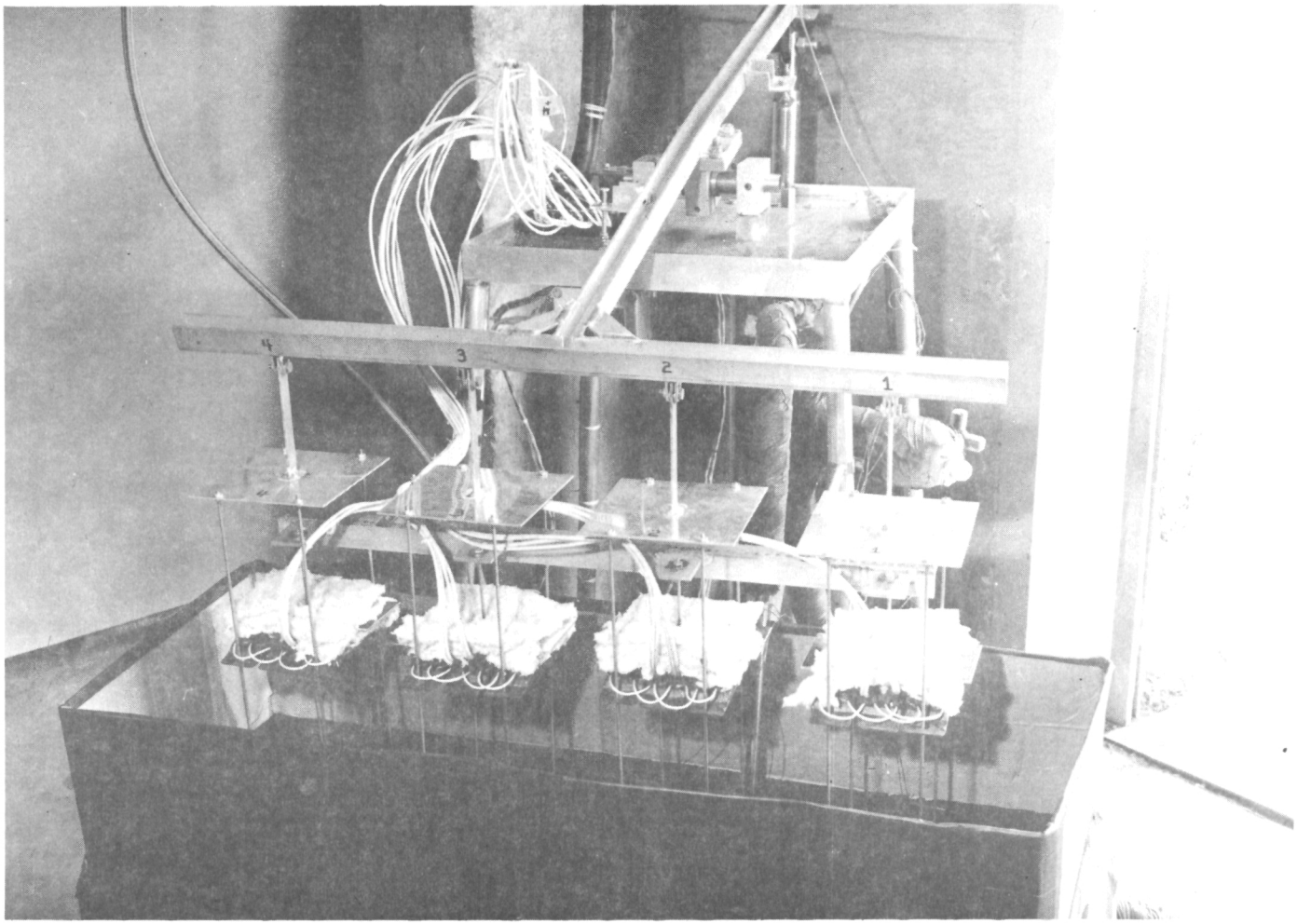

Figure 9. Thermal shock machine.

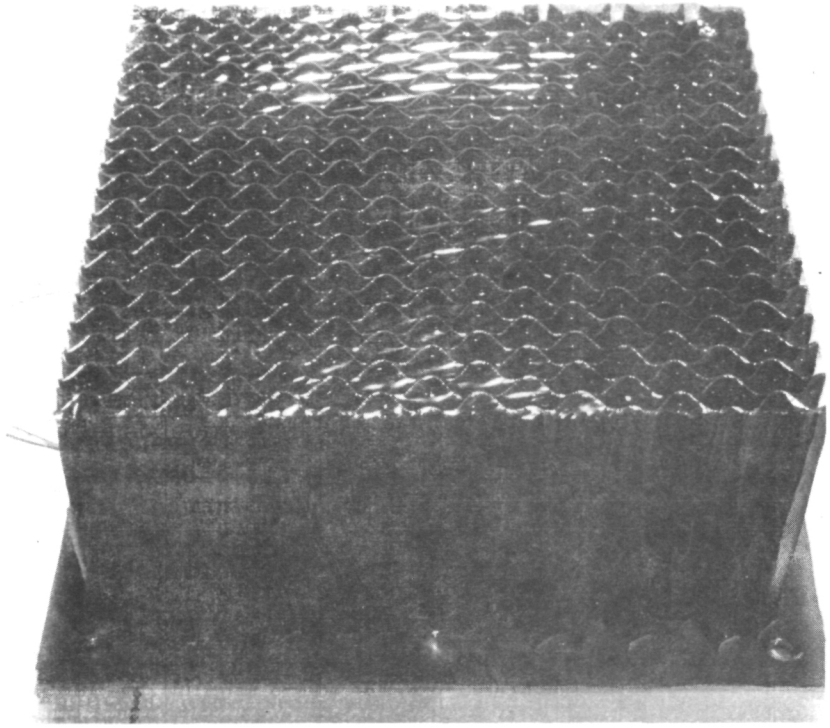

(a) Specimen before test, showing face sheet and capillary holes.

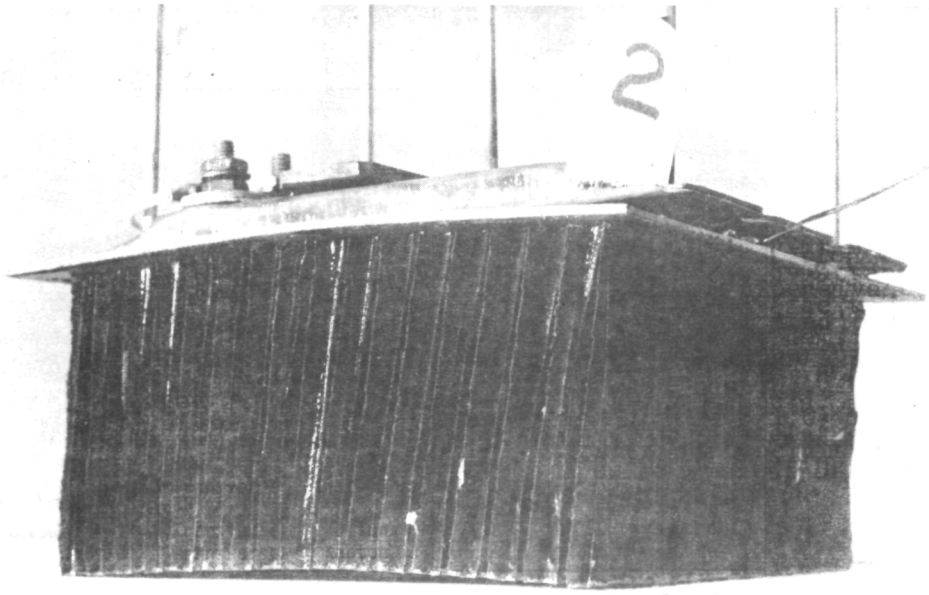

(b) Specimen before test with heater strips installed.

Figure 10. Sample specimens.

Two new specimens were fabricated and run for 4000 cycles. After which, one specimen had 23 failures and the other, 8 failures. In each case, the face sheet failures occurred at the bondline with the honeycomb core. In order to provide a significant life (30,000 cycles), the face sheet-to-honeycomb bond technique must be improved; however, it should be noted that the failures represent a small percentage of the number of cells under test. There were approximately 280 per specimen.

In addition to thermal or temperature shock, a pressure shock or pressure cycling test was completed to determine the effects of rapid pressure fluctuations on the insulation. A schematic of the test apparatus is shown in figure 11. The test specimens, one of which is shown in figure 12, were fabricated using a 1/8-in. (3.18-mm) thick stainless steel partial dome with a radius of curvature of 24 in. (61 cm) and a chord diameter of 19.5 in. (49.5 cm). Insulation specimens were then bonded onto the dome for testing.

The first specimen was subjected to outside skin temperatures up to 550°F (288°C) with liquid nitrogen in the container. With this thermal gradient across the insulation, the internal pressure was cycled between ambient and pressures up to 35 psid (241 kN/m^2). The maximum rate of pressure change was 45 psi/min (5.17 N/m^2-s). The thermal performance of the specimen did not change over the 10-cycle test sequence. Examination of the panel indicated that in about 15% of the cells, two small cracks radiated from the capillary holes in the face sheet. Examination of untested specimens also disclosed similar cracks and it was concluded that the cracks were introduced at the time the holes were made.

An improvement was made in the technique used to pierce the capillary holes. This consisted of allowing the heated needle to melt through the face sheet under its own weight, rather than forcing it through. Using the new method, a second specimen was tested. During this test, which was conducted with liquid nitrogen and a skin temperature of 700°F (371°C), no cracking was found. One hundred cycles were completed with no change in thermal performance noted.

A series of sheet strength tests were conducted to determine bonding strength of the insulation composite. Test specimens fabricated and tested are listed in table II. A schematic diagram of a typical test specimen is shown by figure 13, and figure 14 shows some of the fabricated specimens before test.

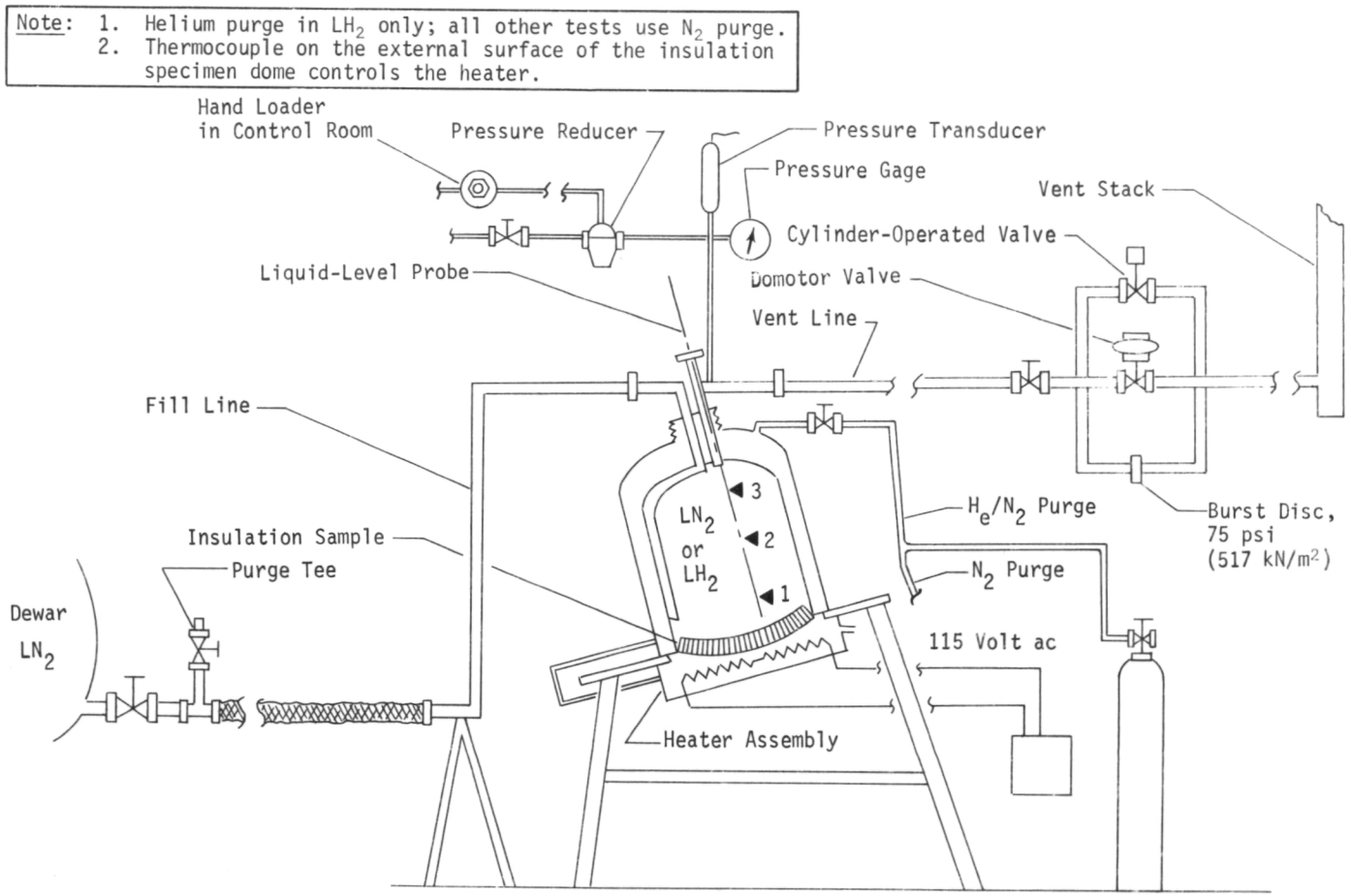

Figure 11. Biaxial test apparatus schematic.

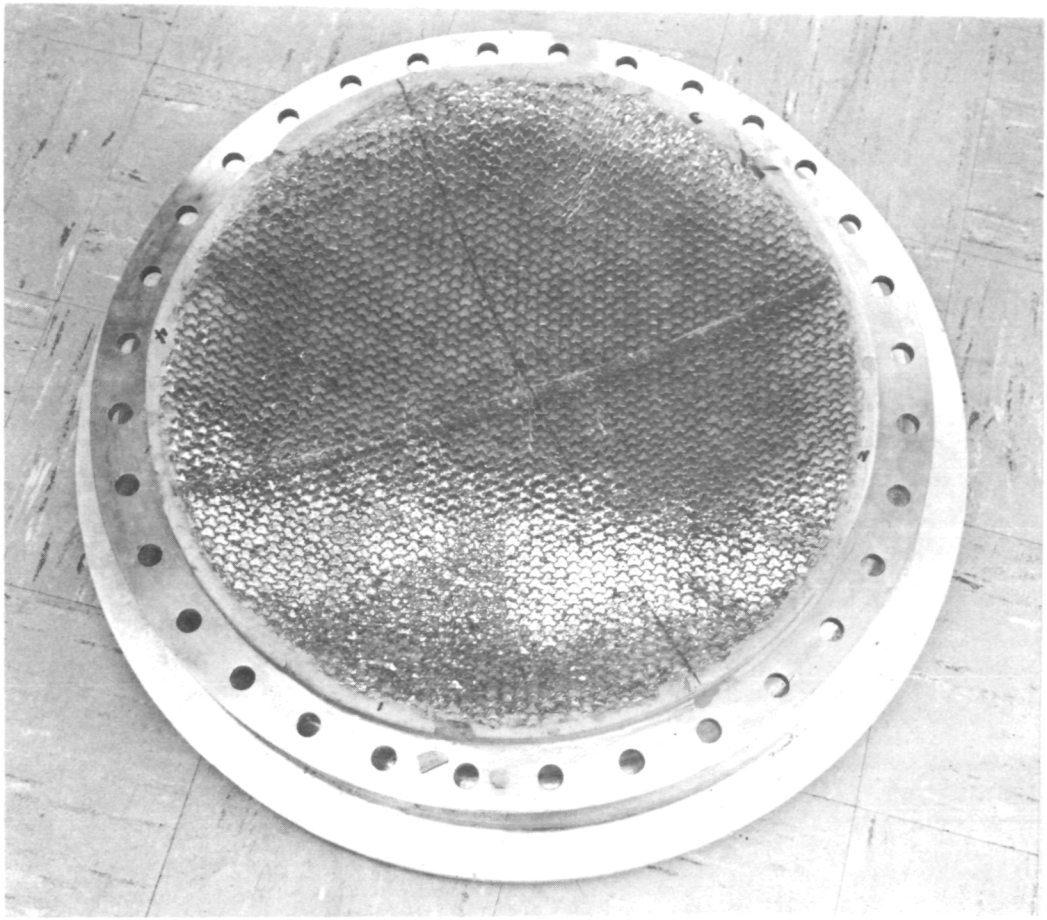

Figure 12. Dome pressure cycle specimen.

TABLE II - SPECIMENS FABRICATED AND TESTED

Test Temperature °F (°C)	Sample No.	Core Direction	Skins	Shear Strength, psi	Secant Modulus, psi	Failure
75 (24)	1-1	Longitudinal	Stainless	60	5750	Bond
	1-2	Longitudinal	Stainless	58	5300	Bond
	2-1	Transverse	Stainless	38	1900	Core
	2-2	Transverse	Stainless	36	1880	Core
	4-1	Longitudinal	Kapton	74	5500	Core
	4-2	Longitudinal	Kapton	67	4850	Core
75 (24)	10-1	Transverse	Kapton	42.7	3340	Core
	10-2	Transverse	Kapton	49.6	4770	Core
	5-1	Transverse	Kapton	44.5	3980	Core
	5-2	Transverse	Kapton	44.3	3360	Core
75 (24)	11-1	Transverse	Stainless	82.5	--	Adhesive
	11-2	Transverse	Stainless	90.3	--	Adhesive
	12-1	Longitudinal	Stainless	129	--	Adhesive
	12-2	Longitudinal	Stainless	137	--	Adhesive
75 (24)	13-1	Longitudinal	Stainless	127	3250	Core
	13-2	Longitudinal	Stainless	121	4385	Core
	14-1	Transverse	Stainless	63.4	2030	Core
	14-2	Transverse	Stainless	63.4	3375	Core
75 (24)	1'-1	Longitudinal	Stainless	120	6100	Core
	1'-2	Longitudinal	Stainless	110	7270	Core
	2'-1	Transverse	Stainless	55.8	2680	Core
	2'-2	Transverse	Stainless	61.6	2200	Core
75 (24)	4'-1	Longitudinal	Kapton	104	5640	Core
	4'-2	Longitudinal	Kapton	103	6950	Core
	5'-1	Transverse	Kapton	53.3	1480	Core
	5'-2	Transverse	Kapton	45.2	3330	Core
-320 (-196)	4'-1	Longitudinal	Kapton	128	8450	Core
	4'-2	Longitudinal	Kapton	120	7520	Core
	5'-1	Transverse	Kapton	72.4	3770	Core
	5'-2	Transverse	Kapton	71.0	3550	Core
-320 (-196)	1'-1	Longitudinal	Stainless	138	--	Core
	1'-2	Longitudinal	Stainless	156	1300	Core
	2'-1	Transverse	Stainless	74	1370	Core
	2'-2	Transverse	Stainless	72	950	Core
+700 (371)	2'-1	Transverse	Stainless	10.8	1060	Core
	2'-2	Transverse	Stainless	13.5	--	Core
	5'-1	Transverse	Kapton	7.1	890	Core
	5'-2	Transverse	Kapton	9.2	385	Core

Note: Shear strength and shear modulus at -320°F, 75°F and +700°F on polyimide-glass panels, ASTM C273, crosshead rate 0.025 in./min. Shear modulus calculated as slope to 50% of shear strength. Panels 2x6x1/2-in.

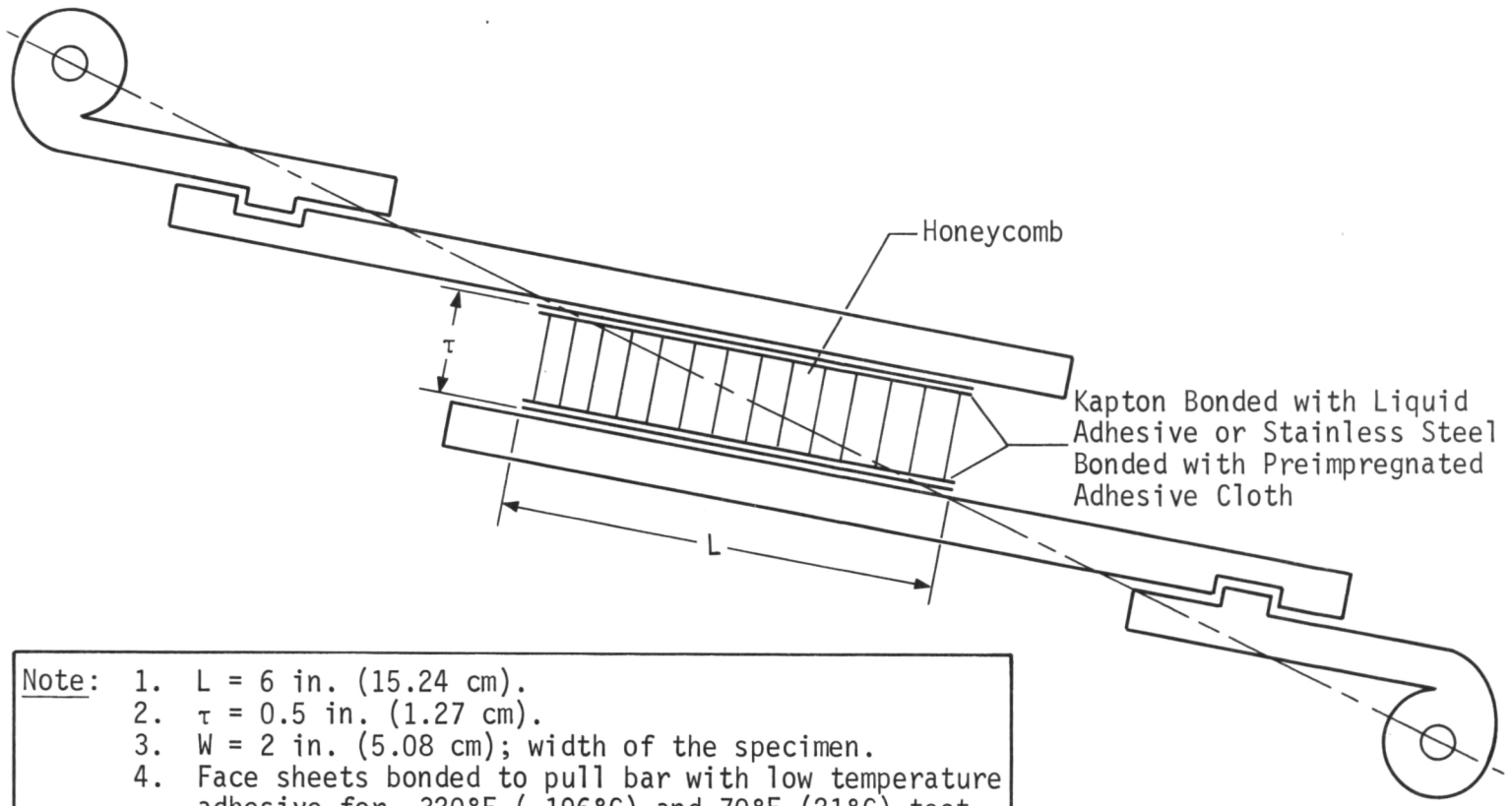

Note:
1. L = 6 in. (15.24 cm).
2. τ = 0.5 in. (1.27 cm).
3. W = 2 in. (5.08 cm); width of the specimen.
4. Face sheets bonded to pull bar with low temperature adhesive for -320°F (-196°C) and 70°F (21°C) test and with polyimide adhesive for 700°F (371°C) test.

Figure 13. Typical test specimen schematic.

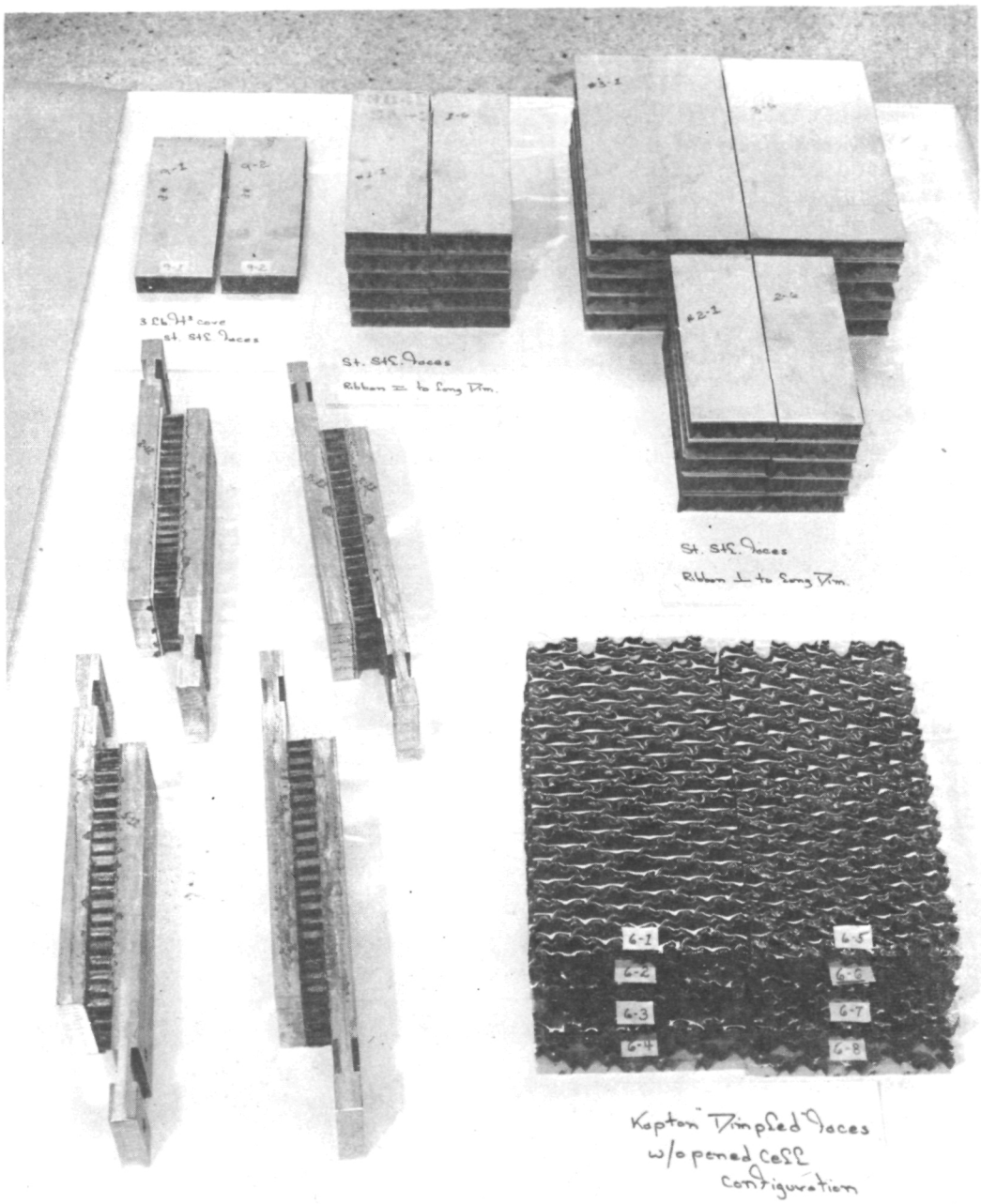

Figure 14. Some shear test specimens before test.

Acoustical tests were run on the insulated dome specimen. The dome, which had already been subjected to 100 pressure cycles from 0 to 30 psig (0 to 206 kN/m^2) with LN_2 on the insulation and 700°F (371°C) on the outside, was subjected to 140-db for 1 hr (3600 sec) directly on the Kapton capillary film. The dome was again pressure cycled (10 cycles) with LN_2 on the insulation and 700°F (371°C) on the outside of the dome. The power required to maintain 700°F (371°C) was the same as had been required prior to acoustical testing. The dome was removed and subjected to 110 db directly on the Kapton for 10 hr (36 ks). The dome was again pressure cycled in the -320 to 700°F (-196 to 371°C) environment. The power required to maintain 700° (371°C) was recorded and found to be the same as before all acoustical testing.

A second acoustical test was conducted on a dome specimen at cryogenic temperatures. The dome was positioned to obtain the 140 db at the Kapton face of the insulation. The insulation was precooled with liquid nitrogen and a liquid nitrogen spray maintained on the Kapton surface throughout the test. No degradation occurred during the test.

2. External Insulation

One of the major problems encountered in either insulation system is radiation heat transfer. Materials such as Johns-Manville Cerafelt and Babcock and Wilcox Kaowool are rather opaque to radiation, but the minimum weight is about 3 lb/ft^3 (48.1 kg/m^3). Owens-Corning has developed a high temperature fiberglass material bonded with a silicone resin, PF-105-700. The fiber diameter in the material is only 0.00004 in. (1.01 μm) resulting in an effective conductivity of 0.02 $Btu/hr\text{-}ft^2\text{-}°F$ (0.346 $W/m\text{-}°C$) at room temperature. The density of the PF-105-700 series is about 0.6 lb/ft^3 (9.61 kg/m^3). Owens-Corning was aware of the radiation transmissivity problem and, under Lewis Research Center and Martin Marietta Corporation impetus, has developed a material based on the PF-105-700 that is much more opaque. The new material, PF-105-700 TOR, is made with a binder that has aluminum powder added.

Materials selected for testing under the material testing program were as follows.

1) 3 lb/ft^3 (48.1 kg/m^3) Cerafelt in air

2) 3 lb/ft^3 (48.1 kg/m^3) Cerafelt, GN_2 purge

3) 0.6 lb/ft^3 (9.61 kg/m^3) Opacified PF-105-700, GN_2 purge.

a. Thermal Conductivity - One important aspect of the external insulation system is how much water can be tolerated in the insulation and its effect on thermal conductivity. A water absorption test was conducted to determine how rapidly water is accumulated. A cylinder 3-ft (91.5-cm) long and 4.5 in. (11.4 cm) in diameter was insulated with 1 in. (2.54-cm) of Cerafelt. The cylinder was then filled with LN_2 with the outside of the insulation exposed to ambient air. After a cold soak of a known time, the weight gain of the insulation was determined. These data are shown in table III. As can be seen, the weight gain varied from 120 to 152 grams in a 4 to 5 hour (14.4 to 18 ks) period. The difficulty in removing this moisture is also reflected in the table. After each cold soak, the test specimen was heated with infrared lamps to remove the moisture. In all cases, there was considerable moisture content after a 2-hr (7.2-ks) heat cycle.

Calorimeter tests were run on seven insulation configurations. The resulting conductivity as a function of temperature is shown in figure 15 and 16 for the 1/2-in. (1.27-cm) and 2½-in. (6.34-cm) laminates, respectively.

In the case of the 1/2-in. (1.27-cm) laminate tests the opacified material without radiation barriers is as good, and in some areas better than, the other configurations. With the 2½-in. (6.35-cm) laminates the opacified material with five radiation barriers and the straight opacified material are similar up to about 400°F (204°C) at which point the material with radiation barriers is better. The materials were subjected to 600°F (316°C) for 18 hr (64.8-ks) prior to test.

b. Specific Weight - The density of the opacified fiberglass is 0.6 lb/ft^3 (9.61 kg/m^3) while the density of the metal foil cover is 515 lb/ft^3 (8250 kg/m^3) if Inconel and 149 $lb/in.^3$ (2387 kg/m^3) if aluminum. If radiation barriers of aluminized polyimide are used the density of this material is 90.5 lb/ft^3 (1450 kg/m^3). For a laminate of 1/2-in. (1.27-cm) opacified fiberglass and an aluminum cover, the specific weight of the system would be 0.898 lb/ft^3 (14.4 kg/m^3); for a 2½-in. (6.35-cm) laminate with an aluminum cover and five radiation barriers, the specific weight is 0.841 lb/ft^3 (13.5 kg/m^3). The 2½-in. (6.35-cm) laminate without radiation barriers would have a specific weight of 0.660 lb/ft^3 (10.6 kg/m^3).

TABLE III. - WATER ABSORPTION IN CERAFELT INSULATION

Test No.	Initial Weight, g	LN_2 Soak Weight, g	Weight Gain, g	Heat Cycle Weight, g	Weight Removed, g	Weight Remaining, g	LN_2 Soak Time	Heat Cycle	ΔT LN_2, °F (°C)	ΔT Heat, °F (°C)	Relative Humidity, %
1	14,515	14,650	135	14,538	112	23	5 hr 16 min (18.96 ks)	1 hr 24 min (5.04 ks)	374 (190)	322 (161)	30.1
2	14,510	14,640	140	14,555	85	55	4 hr 14 min (15.24 ks)	2 hr (7.2 ks)	377 (192)	728 (387)	17
3	14,502	14,621	119	14,546	75	44	3 hr 56 min (14.16 ks)	2 hr (7.2 ks)	358 (181)	730 (388)	16
4	14,501	14,653	152	14,562	91	61	4 hr 28 min (16.08 ks)	2 hr (7.2 ks)	373 (189)	729 (388)	32
5	14,510	14,630	120	14,570	60	60	4 hr 40 min (16.80 ks)	2 hr (7.2 ks)	379 (193)	728 (387)	27

Tests 1, 2, 3 - tank was emptied before heating.
Tests 4, 5 - tank had LN_2 in it during heating.

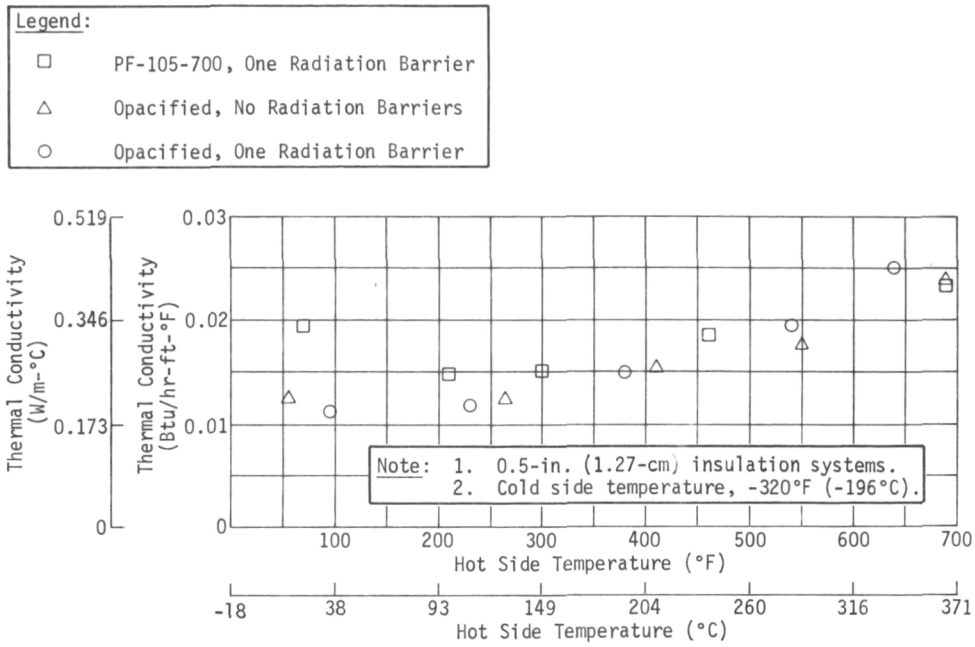

Figure 15. Insulation conductivity, 0.5-in (1.27-cm) insulation.

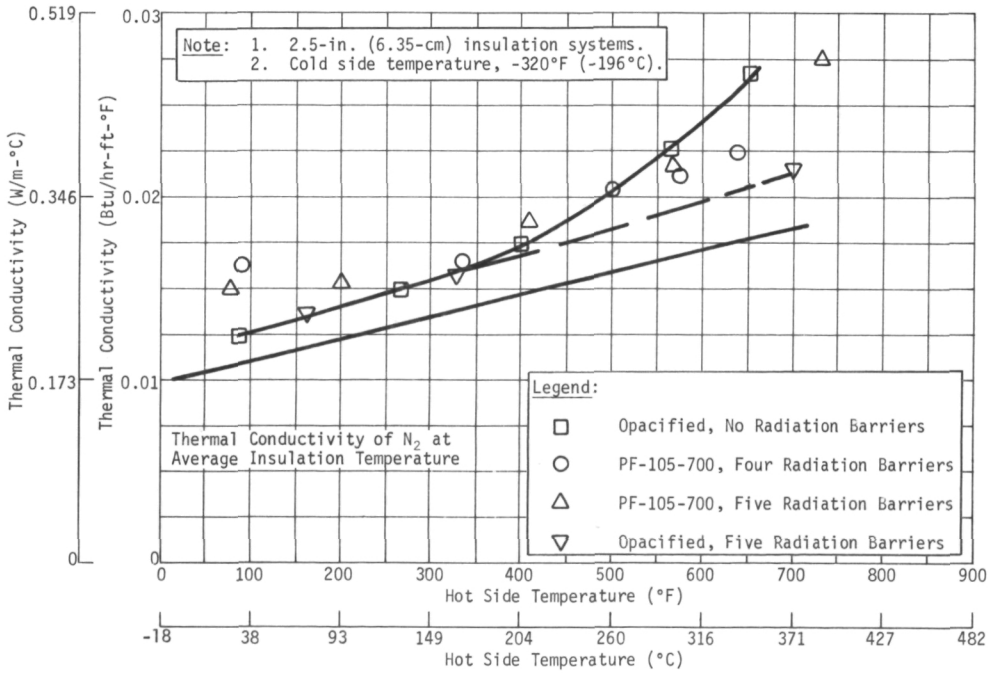

Figure 16. Insulation conductivity, 2.5-in. (6.35-cm) insulation.

c. Coefficient of Expansion - The fiberglass insulation material has a negligible coefficient of expansion in this application because it conforms to the tank skin in a flexible manner. Care must be taken, however, with the metal foil cover supports to allow for its expansion at the higher temperatures. When the tank skin is subjected to cryogenic temperatures it shrinks and, at the same time, the metal cover when subjected to the high wing skin temperatures, expands. This results in considerable differential movement between the tank skin and the metal cover.

d. High Temperature Compatibility - No problems are created at the higher temperatures with this insulation system because all materials are metals, glass, and polyimide and no adhesives are used.

e. Mechanical Properties - Again, due to the type of materials and their location on the outside of the tank, no problems were anticipated with temperature cycling. Because the system is essentially closed and purged with dry gas, external pressure variations could cause a problem. This must be eliminated during the system design by providing adequate gas venting to offset external pressure drops during climb to altitude and during cryogenic tank fill. In addition, a dry gas supply capability must be provided to offset external pressure increases during descent from altitude.

A series of fiberglass batting compaction tests were conducting using specimens 1/2 in. (1.27 cm) thick. Four pieces of batting 5-in. (12.7-cm) square were stacked for the compaction test. A thickness measurement of each batt was made, then the stack was loaded with a weight and held for 24 hr (86.4 ks), and a final thickness measurement was made. It was found that with a weight of 0.302 lb (137 g) the post compaction measurement indicated a 10% permanent set. As a result of these measurements, a value of 0.012 lb/in.^{2} (82.6 N/m^2) or 1.739 lb/ft^2 (12.0 kN/m^2) is the load under which a 10% permanent set will take place.

IV. TEST HARDWARE

After selecting the insulation configurations and at completion of the materials and sample test programs, a program was initiated to design large-scale tanks for a simulated flight test program. At the same time design work was started on a test fixture that would simulate the conditions expected in a supersonic aircraft wing during flight. In order to use the available volumes within a typical aircraft wing, a square or rectangular cross section tank was considered necessary.

A. TEST TANK DESIGN

A parametric analysis was made of "kick" loads, volumetric efficiency, and extreme fiber bending stress in the corner members of the square tanks. The parameters varied were tank width, height, and radius of curvature of the sides. The analysis indicates that a reasonable compromise between square corners and kick loads is a 24x24-in. (61x61-cm) tank with a 30-in. (76.2-cm) radius of curvature.

When considering volumetric efficiency both domes and flat end closures were considered. The results show that for tanks of the length considered, the type of end closure is a more important volumetric parameter than the radius of curvature of the sides. In general, 8 to 10% is gained in volumetric efficiency by using flat end closures. The kick load defines the cross sectional area of the tension members required to transmit the load to the wing structure. This cross sectional area and material must be consistent with the thermal heat leak considerations in the external insulation systems. For a given tank pressure the kick load increases rapidly with radius of curvature. Referring to figure 17(a) the two components of the kick load (lb/in.) can be calculated by the following equations:

$$Z_x = P[R_1^2 - (D_1/2)^2]^{\frac{1}{2}} - PD_2/2$$

$$Z_y = -PD_1/2 + P[R_2^2 - (D_2/2)^2]^{\frac{1}{2}}$$

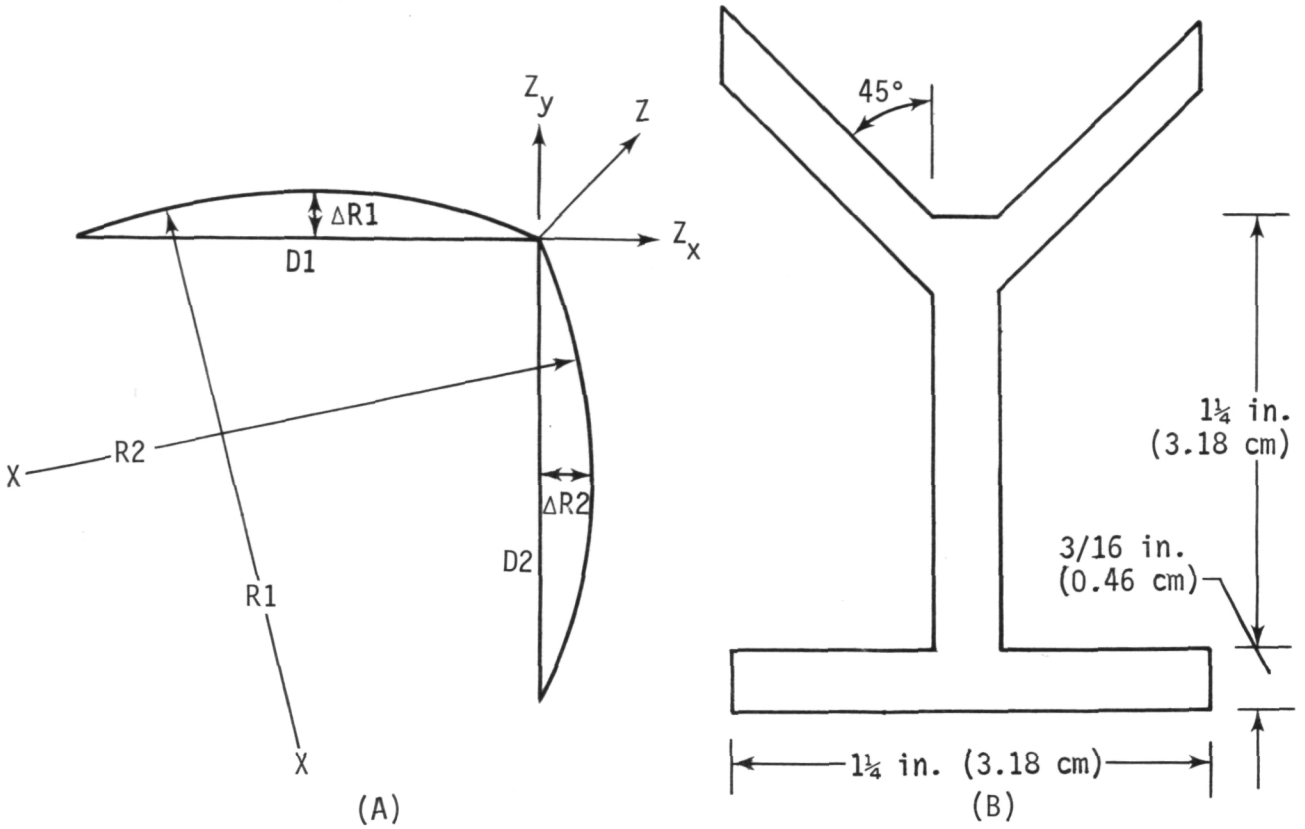

Figure 17. Square tank loads.

Table IV shows the kick load as a function of tank dimensions and radius of curvature of the sides. Also shown in Table IV is the extreme fiber stress in the corner beam of the tank divided by the square of the distance between tank supports that is calculated using the relationship:

$$\frac{\sigma}{\ell^2} = \frac{W}{8I/C}$$

where

σ = is the extreme fiber bending stress,

ℓ = is the distance between supports,

W = kick load,

I/C = section modulus of the corner member.

These stresses are based on a tank corner member with a configuration as shown in figure 17(b).

*TABLE IV. - SQUARE TANK KICK LOADS AND VOLUMETRIC EFFICIENCY**

D_2 (in.)	R_2 (in.)	D_1 (in.)	R_1 (in.)	Kick Loads X (lb/in.)	Kick Loads Y (lb/in.)	Kick Loads TOT (lb/in.)	ΔR_1 (in.)	ΔR_2 (in.)	σ/ℓ^2 (lb/in.^{4})	Volumetric Efficiency Flat	Volumetric Efficiency Dome
24	18	24	18	43	43	61	4.56	4.56	20	0.80	0.73
			24	264	43	268	3.19	4.56	91	0.82	0.75
			30	466	43	468	2.47	4.56	159	0.84	0.76
24	24	24	18	43	264	268	4.56	3.19	96	0.82	0.75
			24	264	264	374	3.19	3.19	133	0.85	0.77
			30	466	264	536	2.47	3.19	192	0.86	0.78
24	30	24	18	43	466	468	4.57	2.47	167	0.84	0.76
			24	264	466	536	3.19		192	0.86	0.78
			30	466	466	659	2.97	2.47	235	0.88	0.79

*Values based on ΔP of 30 psid.

As a result of the loads analysis, tanks were designed and built so the internal and external insulations could be tested. A stress analysis was completed to size the tank members. The following assumptions were used for this analysis.

1) Operating pressure = 30 psig (207 kN/m^2)

2) Factor of 2.0 for proof pressure

3) Factor of 2.5 for burst pressure

4) Maximum skin temperature (internal insulation) = 700°F (371°C)

5) Minimum skin temperature (external insulation) = -320°F (-196°C)

6) Insulation stiffness, to be neglected

This analysis resulted in the establishment of skin thickness, corner and end structural requirements and tank support sizes and locations. The material used for tank design was 21-6-9 stainless steel. This material was selected because of its good high- and low-temperature strengths along with good weldability.

Table V lists the material strength values used in the stress analysis.

TABLE V. - TEMPERATURE/STRENGTH OF 21-6-9 STAINLESS STEEL

Temperature, °F (°C)	Tensile Yield, psi (MN/m^2)	Tensile Ultimate, psi (MN/m^2)
+700 (371)	34,000 (234)	83,000 (572)
-265 (-165)	115,000 (792)	190,000 (1310)

The tanks were designed with equal internal volumes so that the internally insulated tank was structurally larger than the externally insulated tank by the thickness of the internal insulation. The tank designs are shown in figures 18 and 19 for the internal and external insulation configuration, respectively.

B. FABRICATION OF TEST TANKS

1. Structural Fabrication

Based on the designs established, two test tanks were fabricated; one for the external insulation and the other for internal insulation. The tanks were all-welded structures of stainless steel. Figure 20 shows the externally insulated tank in an early stage of fabrication. The primary structure, including corner angles and flat ends, was first assembled followed by installation of skin panels. In this case, the skin panels of 0.050-in. (1.27-mm) material were installed on the outside to provide a smooth external surface for insulation. Before installing the skin panels, a series of compression members were installed diagonally between the corner angles to offset kick loads. In addition, all internal instrumentation was installed in the tank with cabling routed through the fill and vent penetrations. This tank, with its internal structure, does not transmit pressure loads to the wing structure through the tank mount points. Mounting provisions required were only to support the weight of the tank and any loads created by wing movement (sloshing).

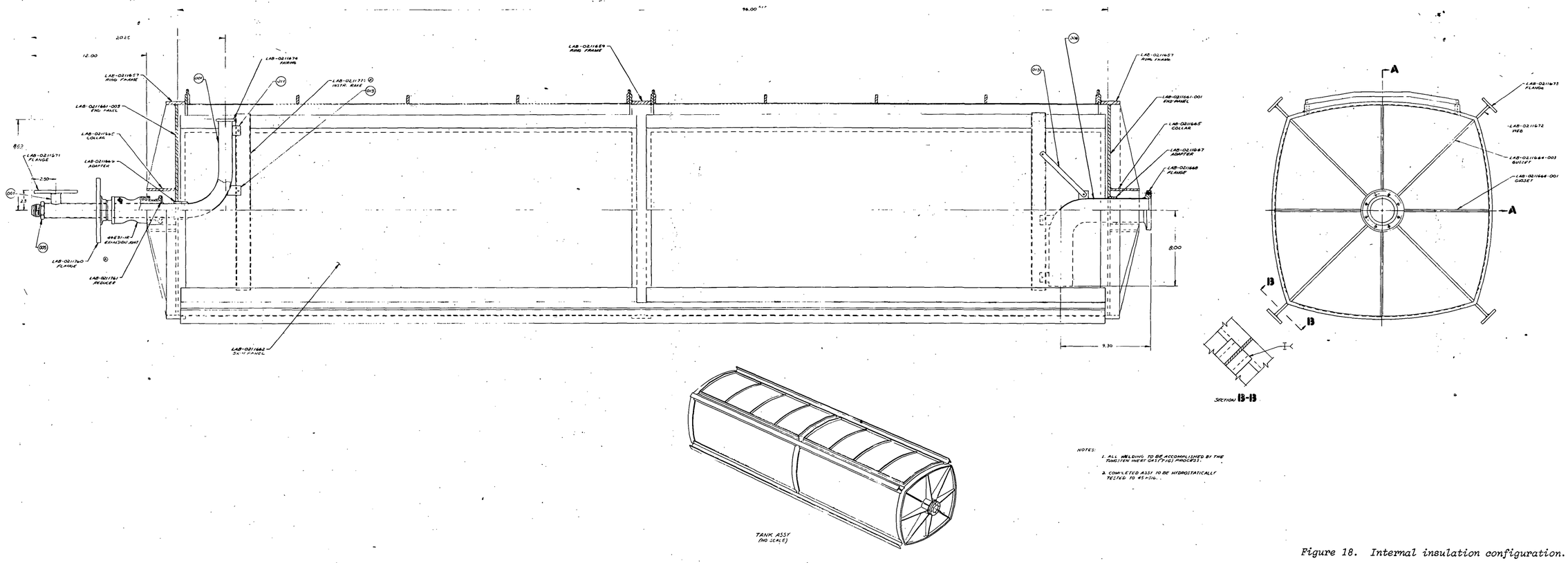

Figure 18. Internal insulation configuration.

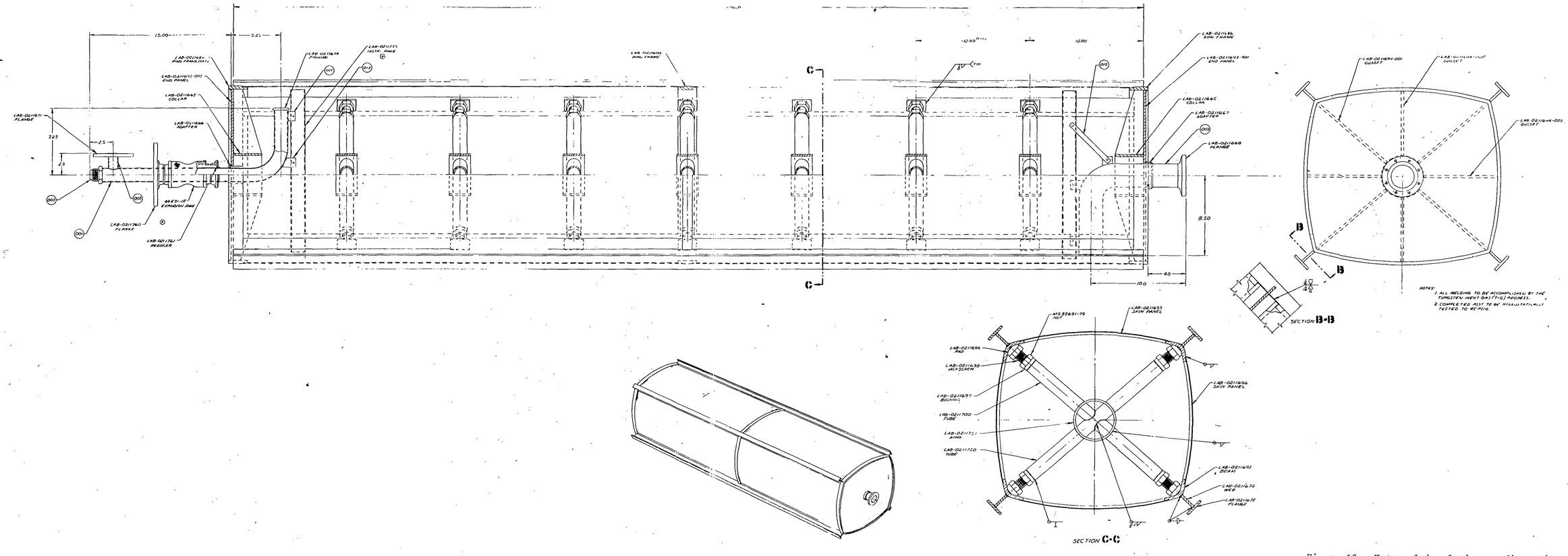

Figure 19. External insulation configuration.

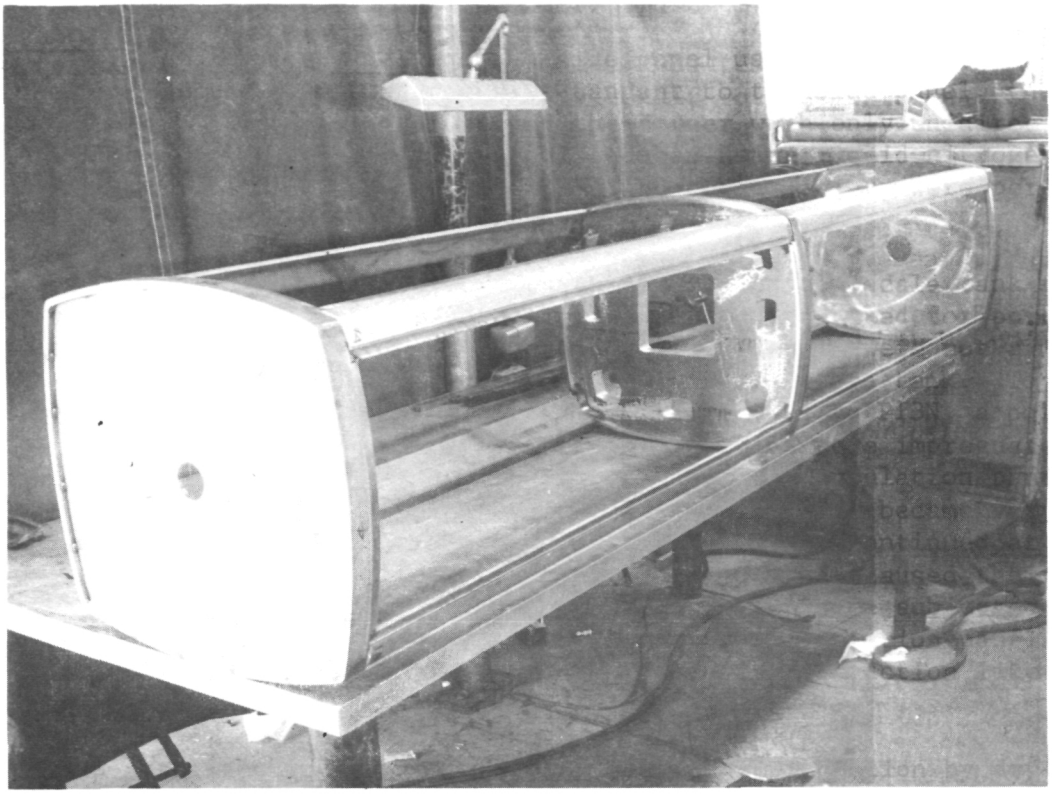

Figure 20. Externally insulated tank in early stage of fabrication.

Fabrication of the internally insulated tank was considerably different. In this case, the tank skins were mounted on the inside of the primary structure to provide a smooth internal surface for insulation bonding. Figure 21 shows this tank in an early stage of fabrication. Another major difference in this tank involves the structure required to offset kick loads. Because the insulation is installed internally and in order to avoid large heat losses to the external skin and structure the same type of compression members used in the externally insulated tank could not be used. Instead, the loads are taken out externally by attachments to the wing structure. This was accomplished by the use of turnbuckles between the corner angles of the tank and the simulated wing box trusses. Figure 22 shows the tank during a hydrostatic test mounted in the simulated wing basic structure. The turnbuckle arrangement allows the tank to grow in diameter and length during pressurization and heating without distorting the basic shape.

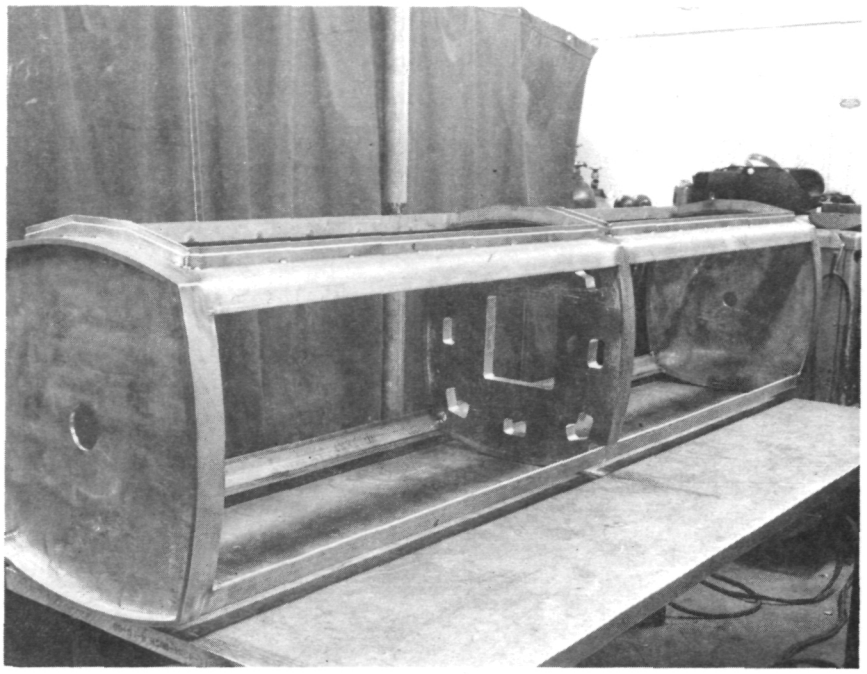

Figure 21. Internally insulated tank in early stage of fabrication.

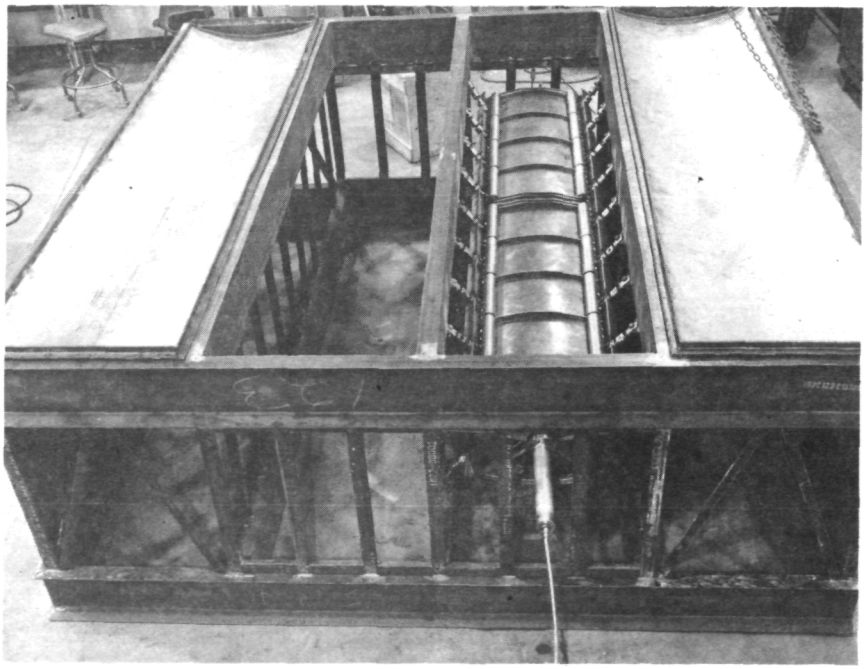

Figure 22. Internally insulated tank mounted in a simulated wing structure during hydrostatic test.

The tank was fabricated with two specially designed covers for installation of the internal insulation panels. After fabricating the tank and covers, the covers were welded in place for proof pressure testing with water. After hydrostatic testing, the cover welds were ground off and the covers removed for insulation installation. The reasoning behind these steps is that a cryogenic (liquid nitrogen) hydrostatic test is both hazardous and does not meet the basic needs of a tank structure that will operate at ambient to very high temperatures. The hazard involved lies in the use of a liquid that becomes saturated at an elevated pressure. If a rupture or partial rupture does occur, reducing the pressure rapidly, the liquid flashes to a vapor resulting in major damage to the tank. If water were used with the insulation installed, the cell packing would become wet as pressure forced the water into the cells and it would be extremely difficult if not impossible to remove this water.

Figure 23 shows the tank after fabrication and just before welding the covers for the hydrostatic test. Hydrostatic testing was completed on both tanks without a failure. During manufacture and due to the nature of the welded assembly, some wrinkles developed in the skins of both tanks. In the case of the externally insulated tank, this caused no problem with insulation installation. With the internally insulated tank, however, it was felt that a smooth contoured surface would be required to allow proper fit and bonding of the insulation panels. In an attempt to remove the wrinkles, the tank skins were hydraulically stretched by applying pressures above yield for the skins. While this effort did help to create a smooth surface, it did not entirely remove the wrinkles and did produce some out-of-contour bulging in the skin panels.

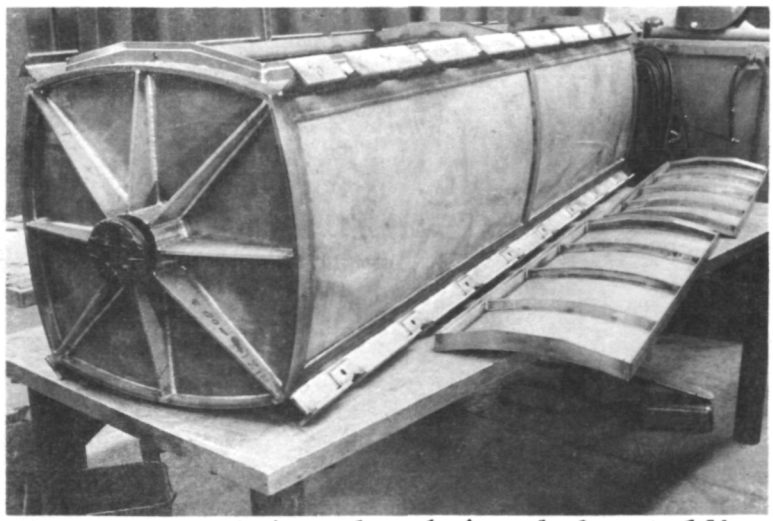

Figure 23. Fabricated tank just before welding on covers for hydrostatic test.

In addition to hydrostatic test on the internally insulated tank, a thermal expansion test was conducted before insulation installation. This test was intended to check out the tank mounting to see that no large stresses were created when the external surfaces were brought to 700°F (371°C). An infrared lamp cage was built around the tank in the hydrostat fixture and the external structure (wing) was insulated. The tank skin temperature was brought to 700°F (371°C) in approximately 2 min (120 s) and held at this temperature for 15 min (900 s) to allow the remainder of the tank to reach 700°F (371°C). Strain gages on the tank supports indicated low stress levels during this test; however, posttest examination indicated degradation of some of the gages and the results were not considered reliable. Examination of the tank revealed circumferential ripples in the removable panel skins.

After completing these tests, the removable panels were taken off to prepare for insulating the tank.

After hydrostatic testing of the externally insulated tank, the water was drained out and the tank dried using a hot gaseous nitrogen purge. Tank dryness was established by a dew point check of the effluent gas.

2. Installation of Insulation

After completing the tank structural fabrication and hydrostatic test, installation of the insulation was started.

a. Insulation of the Externally Insulated Tank - The externally insulated tank is shown in figure 24 after the insulation was installed. One-half in. (1.27 cm) of material was installed on the sides, top and ends of the tank, 2½ in. (6.35 cm) was installed on the bottom. The opacified fiberglass material was obtained in ½-in. (1.27-cm) thick batts so that one layer was applied to the top, sides, and ends and five layers were applied to the bottom. Thermocouples for measuring the tank skin temperatures were welded to the skin while those that were to measure temperature at various places in the insulation were welded to small aluminum foil disks as shown by figure 25.

All internal instrumentation such as level sensors and liquid temperature sensors was installed in the tank during tank fabrication.

Before installation, the insulation material was dried in an oven at 600°F (316°C) overnight and was sealed in a polyethylene bag that had been purged with dry nitrogen. The dry gas purge system was installed on the tank using fiberglass cord to hold it in place. The purge system consisted of perforated ¼-in. (6.35-mm) diameter tubes running the length of the tank at the corners and connected to a single manifold at one end of the tank.

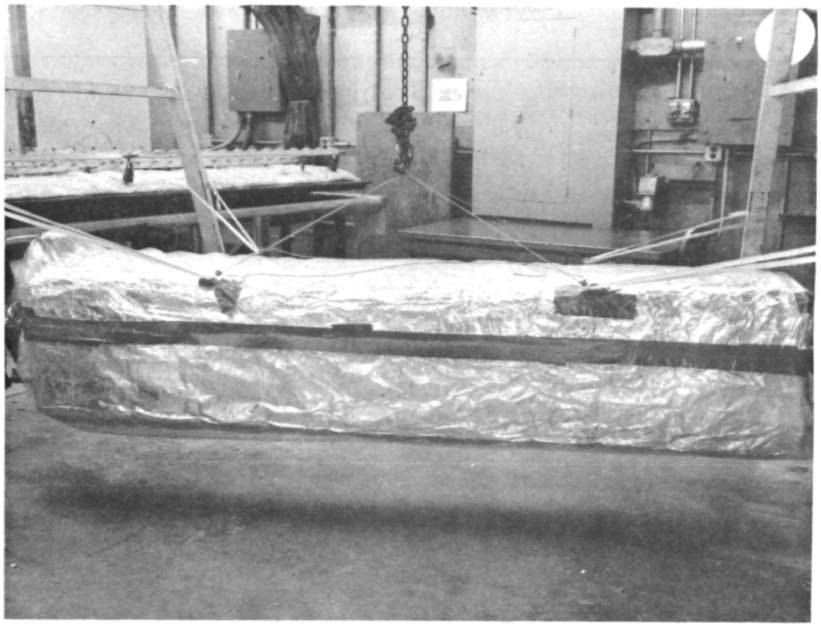

Figure 24. Externally insulated tank with insulation installed.

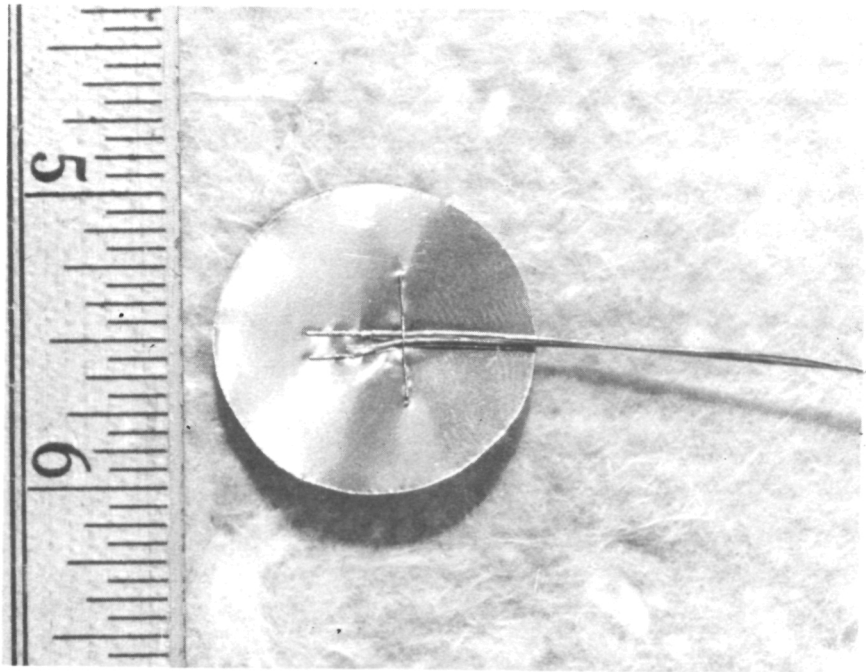

Figure 25. Thermocouple welded to aluminum foil disk.

Four layers of insulation were cut to fit the bottom of the tank and a single layer was cut to cover the entire circumference of the tank. Single pieces were cut and fit to the ends of the tank. The insulation was installed and held in place temporarily with tape and the dry nitrogen gas purge was started.

Radiation barriers were not used with the opacified fiberglass batting. During the calorimeter test program, the opacified fiberglass with 5 radiation barriers showed only slight improvement over the opacified material without barriers. This improvement was noted only at higher temperatures of 400°F (204°C) and above. On the other hand, the insulation density is increased significantly from 0.66 lb/ft^3 (10.57 kg/m^3) to 0.84 lb/ft^3 (13.46 kg/m^3) for a 2½-in. (6.35-cm) laminate when 5 radiation barriers are used.

An outer skin consisting of aluminum foil, 0.0015 in. (0.038-mm) thick with random perforations was installed over the fiberglass. Joints in the foil were overlapped and taped using a high-temperature reflective tape. The use of aluminum in place of Inconel created no problems because the cover carries no structural or significant pressure loads. As indicated, the installed density of this insulation was 0.66 lb/ft^3 (10.57 kg/m^3) for the 2½-in. (6.35-cm) thickness and 0.898 lb/ft^3 (14.39 kg/m^3) for the ½-in. (1.27-cm) thickness.

b. Insulation of the Internally Insulated Tank - Insulating the internally insulated tank was considerably more complex. This tank was designed and fabricated to provide a smooth internal surface to avoid any steps or discontinuities in the insulation core.

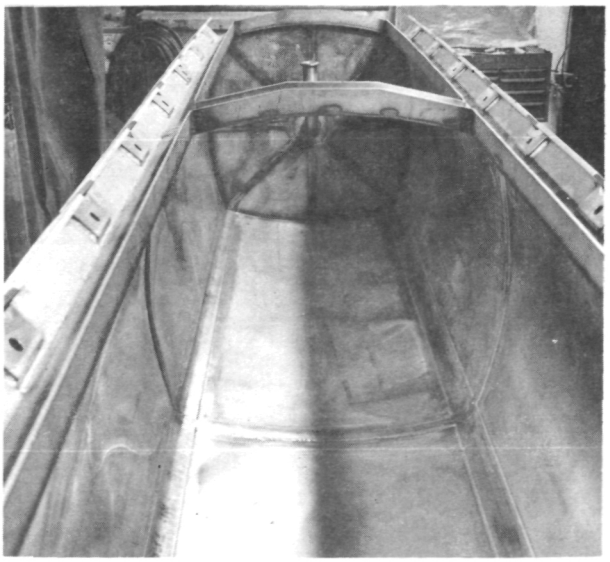

Figure 26. Inside of tank just before installing internal insulation.

Figure 26 shows the inside of the tank just before the insulation was installed. As can be seen, two large open panels on the top of the tank provided working space for installing the insulation panels.

To check out fabrication and installation procedures and to develop an adequate corner joint, a stainless steel box, 2x2x1 ft (61x61x 30.5 cm), was constructed. Polyimide core panels were fabricated and installed in the box. The panels were fabricated flat using procedures developed during the material tests. Bonding the Kapton face sheet to the honeycomb was accomplished by first thinning the BR-34 liquid polyimide adhesive to 60% solids with BR-34 thinner.

A short-napped or relatively smooth roller was used to apply the BR-34 to the honeycomb in the amount of about 4.25 g/ft^2. The adhesive was allowed to air dry 30 min (1.8 ks) at room temperature before applying the Kapton film. The Kapton film was applied and the composite bagged using 4-mil (0.10-mm) polyvinyl alcohol film. A suitable wooden frame was placed around the composite to support the side loads. An 8-psi (55.2-kN/m^2) vacuum was pulled and the following cure temperatures applied.

1) 70°F (21°C) to 220°F (104°C) in 20 min (1.2 ks)

2) 220°F (104°C) dwell for 15 min (0.9 ks)

3) 220°F (104°C) to 300°F (149°C) in 20 min (1.2 ks)

4) 300°F (149°C) dwell for 15 min (0.9 ks)

5) 300°F (149°C) to 350°F (177°C) in 20 min (1.2 ks)

6) 350°F (177°C) held for 2 hr (7.2 ks)

7) Cooled to 70°F (21°C) before release of pressure

An additional 5 psi (34.5 kN/m^2) was applied at the end of the 300°F (149°C) dwell time and held for the remaining cure time to produce the dimpling.

The panels were bonded into the box using FM-34 film adhesive. The refrigerated FM-34 adhesive cloth was allowed to warm to 70°F (21°C) before opening the vapor barrier shipping bag. The FM-34 was cut to size and applied to the stainless steel; then the honeycomb was laid on top of the adhesive cloth. The stainless steel to honeycomb bonding was performed at 12 psi (82.7 kN/m^2) using a vacuum bag. The cure cycle follows.

1) 70°F (21°C) to 550°F (288°C) in 30 min (1.8 ks)

2) 550°F (288°C) held for 90 min (5.4 ks)

All panels were put through the following postcure cycle.

1) 30 min (1.8 ks) at 350°F (177°C)

2) 1 hr (3.6 ks) at 350°F (177°C) to 550°F (288°C)

3) 2 hr (7.2 ks) at 550°F (288°C)

4) Slow cooling to 70°F (21°C)

The panel on the bottom of the stainless steel box was 2½-in. (6.35-cm) thick and the side panels were ½-in. (1.27-cm) thick. After several trial configurations the corner joint shown in figure 27 was selected.

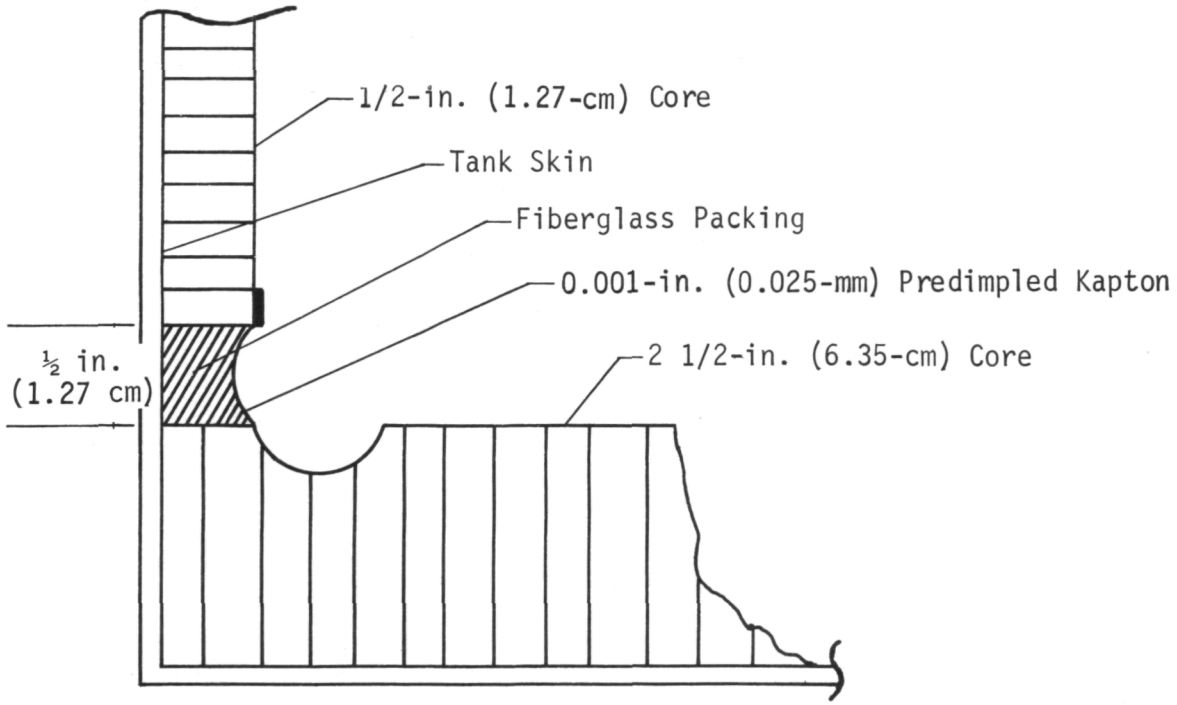

Figure 27. Corner joint configuration.

Following is the method used to construct the corner joint. The 2½-in. (6.35-cm) thick insulation on the base is grooved around the periphery leaving a ½-in. (1.27-cm) ridge around the periphery. The ½-in. (1.27-cm) side insulation sets on this ridge so that the side panel is tangent to the upper edge of the groove in the base. The side panel and base panel are separated by about ½ in. (1.27 cm) of fiberglass packing. The joint is then made between the

groove in the base panel and the side panel using predimpled Kapton. Because the side of the groove is tangent to the side panel, the Kapton splice piece can go around the corner with only unidirectional bending. Testing the insulated box using liquid nitrogen indicated that the insulation panels and corner joints were performing properly.

At about this time, and with insulation of the full-scale tank the next step, all polyimide insulation panels were checked for porosity. It was found that a large number of the cells were not airtight and had to be sealed before installation in the tank. To do this, the core was to be impregnated with Ciba Geigy P13N, a polyimide laminating varnish. Several small samples were impregnated and the porosity was eliminated. When the first insulation panel was placed in the P13N bath the solution immediately became very viscous and changed in color. Impregnation was discontinued at this point and an effort was made to determine what caused the reaction. Small quantities of a new batch of P13N were subjected to various contaminants that may have been on the insulation panels and it was determined that moisture could start a reaction like the one experienced.

At this point, the panels were prepared for impregnation by drying in an oven. All panels were already assembled to the point of having Kapton face sheets installed. To assure complete coating of the cell walls, the panels were submerged in a P13N bath, face sheet down, in a large vacuum chamber. Evacuation of the bath and panel removed all gas bubbles and allowed all surfaces to be wetted with the P13N varnish. After removal from the bath, the P13N was allowed to air dry and the face sheet capillary holes were repierced.

The next step involved insulating a portion of the full-scale tank to again check out the procedures and corner joint technique. A core material of glass cloth and phenolic was used to fabricate insulation panels for one end of the tank. This substitution was made to avoid the expense of the considerably more expensive polyimide core. A number of earlier material tests indicated that the phenolic core material provided essentially the same performance as the polyimide material under liquid nitrogen testing. Unfortunately, the phenolic cannot withstand the 700°F (371°C) temperatures anticipated at the tank skin during supersonic cruise.

A different fabrication method was used for the tank panels than for the box panels because the tank has curved skins. The 2½-in. (6.35-cm) bottom panel was mill cut on the inside for the corner radii. The panel was placed in a curved form, as shown in figure 28, that conformed to the tank skin curvature. The face sheet was bonded to the core and dimpled in the form to avoid wrinkles and stresses in the face sheet when the panel was bonded into the tank. The procedure used was the same as was used for the flat panels fabricated for the box test.

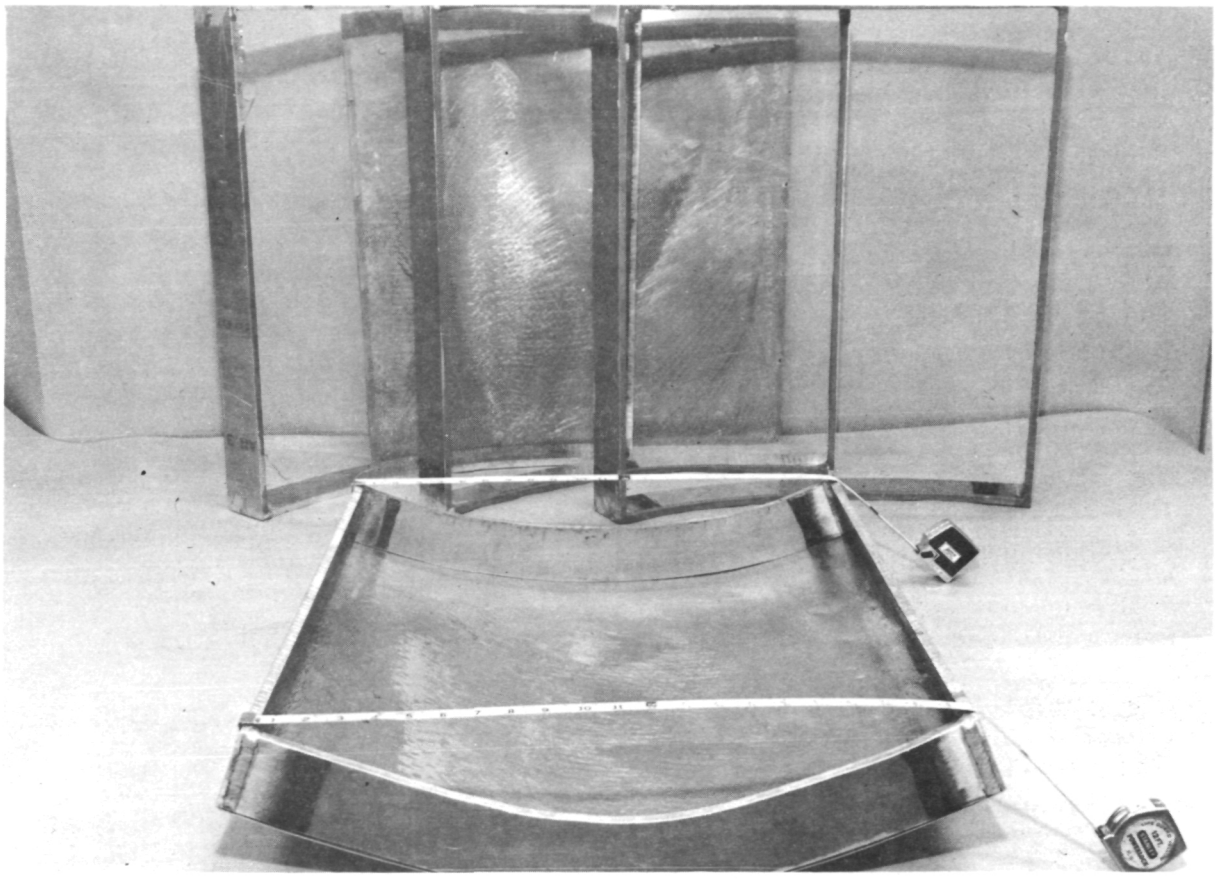

Figure 28. Forming tool for insulation fabrication.

The panels were bonded into the tank using FM-34 adhesive and the corner joints were made. A test with liquid nitrogen indicated the system was working properly and preparations were made to insulate the entire tank.

The phenolic panels were removed from the tank and the tank skin was cleaned using abrasive paper and buffed using green "scotch brite" scouring pads. The tank was primed with thinned BR-34 and the first polyimide panel was installed using the FM-34 adhesive.

Bonding temperatures were attained by suspending the tank over one of the heating panels fabricated for the thermal wing. In this way the skin of the tank was heated over the required temperature profile using a thermocouple on the skin as a control input to an ignitron power control system.

After bonding the second panel in the tank, it was noted that the first panel had debonded in several places. The tank had been maintained in an upright position during both panel bondings with a result that the skin temperature next to the first panel (bottom) during bonding of the second panel (side) had reached 650°F (343°C) in order to obtain 350°F (177°C) on the side. This temperature was below the allowable operating temperature of the bonding film and should not have caused a problem.

A check with the bonding film manufacturers indicated that the film we were using was probably not good. The film had been removed from the storage refrigerator several times and had not been resealed in an airtight bag after each use. This allows moisture to be absorbed in the film thus degrading the bonding properties. The film manufacturer had no film in stock and the delivery time for a new batch was about 45 days. A bonding program was initiated using the same liquid adhesive (BR-34) and glass cloth in order to produce a bonding film similar to the FM-34 previously used. Samples were made using varying amounts of BR-34 adhesive from 0.75 to 2.0 g/ft^2. Various styles of fiberglass cloth including 80, 100, 110, and 120 mesh were used with the adhesive. The glass was prewetted with the BR-34 and the remainder placed on the simulated tank skin and on the cloth after the cloth was installed on the skin. The core panels were installed on the adhesive and cured. Stainless steel skins both flat and curved were used to simulate the actual tank. Leak tests of the sample panels led to the decision to use 1.90 g/ft^2 of BR-34 along with the 120-mesh fiberglass cloth. This combination yielded the best bond with a minimum of leakage. Shear test specimens indicated this combination was as good as the original samples of FM-34 used during the material test program.

Before removing the debonded panels from the tank, a cell leak check was made in areas where the insulation remained bonded. This check used a new technique where each cell is pressurized to approximately 2 psig (13.8 kN/m^2). This is accomplished by placing a soft rubber tube on the face sheet over each cell and pressurizing the cell through the capillary hole. A flowmeter in the gas supply line indicates zero flow if the cell does not leak and flow at the leak rate if a leak does exist. It was found that a large number of the cells were leaking through the honeycomb cell walls.

Further core dip coating was considered but the idea was abandoned because the first dip coating obviously had not provided a lasting seal for the cell walls. At this point two outstanding problems were evident:

1) Most of the prepared polyimide insulation panels were porous and no clear plan for correcting the problems in the existing panels was available.

2) Some doubt still existed that the bonding problem caused by the bad batch of FM-34 had been solved.

A course of action was established which would solve or at least evaluate the significance of the problems. A series of special calorimeter tests were conducted to determine the effect of core porosity on insulation performance. The degree of degradation of thermal conductivity due to porosity was measured and showed what results could be anticipated in the test of the full-scale tank. Although this effort did not solve the porosity problem, it at least determined the magnitude and allowed continuation of the program. The details and results of this test series are reported in Appendix A of this document. In general, the results indicated a degradation of 19 to 56% in thermal conductivity due to porosity and degradation on the order of 12% due to moisture in the fiberglass cell filler.

A number of additional bonding specimens were prepared and tested to failure. In every case failure occurred in the core material rather than at the bondline.

To avoid further problems, which might be created by minor changes in materials or procedures, a process plan was developed for installing the insulation in the tank. This plan, which is attached as Appendix B, details each step and material used to finish insulating the tank. The plan was not intended to be a general insulation installation, but was tailored to this specific program for this specific tank. It was completed at the time when the two polyimide panels had been bonded into the tank with resultant debonding of the first panel.

The first attempts to remove the polyimide panels from the tank did not prove successful. It was not too difficult to cut the core away from the FM-34 adhesive sheet; however, removal of the adhesive was considerably more difficult. After conferring with the adhesive manufacturers, American Cyanamid, a high temperature bakeout procedure was attempted. This procedure involved placing

the tank in a high-temperature oven, bringing it up to 800°F (427°C), holding at that temperature for 2 hr (7.2 ks), and back to ambient. The only oven available that was large enough to hold the tank had a maximum temperature capability of only 775°F (413°C). To offset this lower temperature, the high-temperature hold period was extended to 3 hr (10.8 ks). This procedure was intended to cause the adhesive to overcure and turn to a powder by removal of all the volatiles.

Although the oven bake procedure did help, the adhesive was still not completely destroyed and considerable handscraping was required.

Following the Insulation Installation Process Plan, the tank was cleaned using a procedure that included degreasing, alkaline wash, pickle, and passivation with nitric/hydrofluoric acid and deoxidizing with nitric/dichromate solution. The inner surface was primed with thinned BR-34 and insulation installation progressed. No particular difficulty was experienced during panel installation. Bottom panels appeared to conform to the bottom wrinkles and bonding was solid. After all the panels were bonded in place, all splice joints were prepared. Tools had been fabricated to provide the predimpled longitudinal (single curvature) splice strips and the predimpled end (double curvature) splice strips. These tools are shown in figure 29. The gaps between panels were packed with strips of fiberglass and the predimpled Kapton strips were bonded in place using Whittaker Thermadite 17 adhesive.

A combined cure for the splice joints and a postcure for the entire tank including the insulated lids was planned. To provide bonding pressure for all splice joints, the entire inner surface of the tank was covered with fiberglass bleeder-cloth and vacuum bagged. The cover panels were bagged separately and the tank and covers were moved into a large heat treatment oven. The temperature cycle used for the combined cure/postcure is shown in figure 30. The vacuum bag pressure is also shown and, as indicated, the vacuum was maintained until the cure portion of the cycle was complete.

When the postcure was completed, the oven was cooled down and the tank and covers were examined. The tank internal surface and the covers are shown in figures 31 and 32.

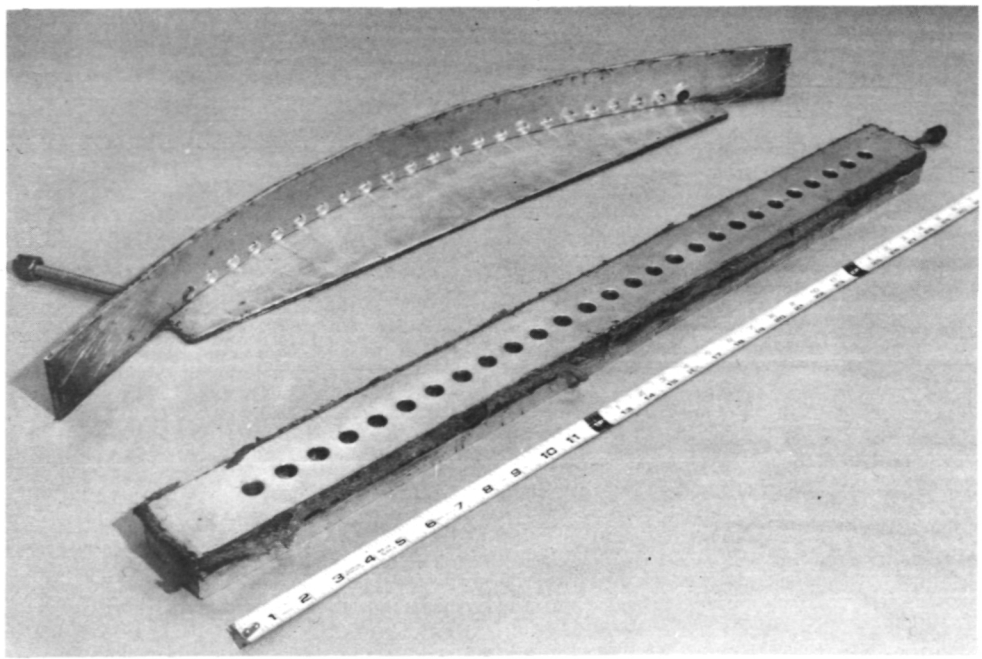

Figure 29. Tools used in fabricating splice strips.

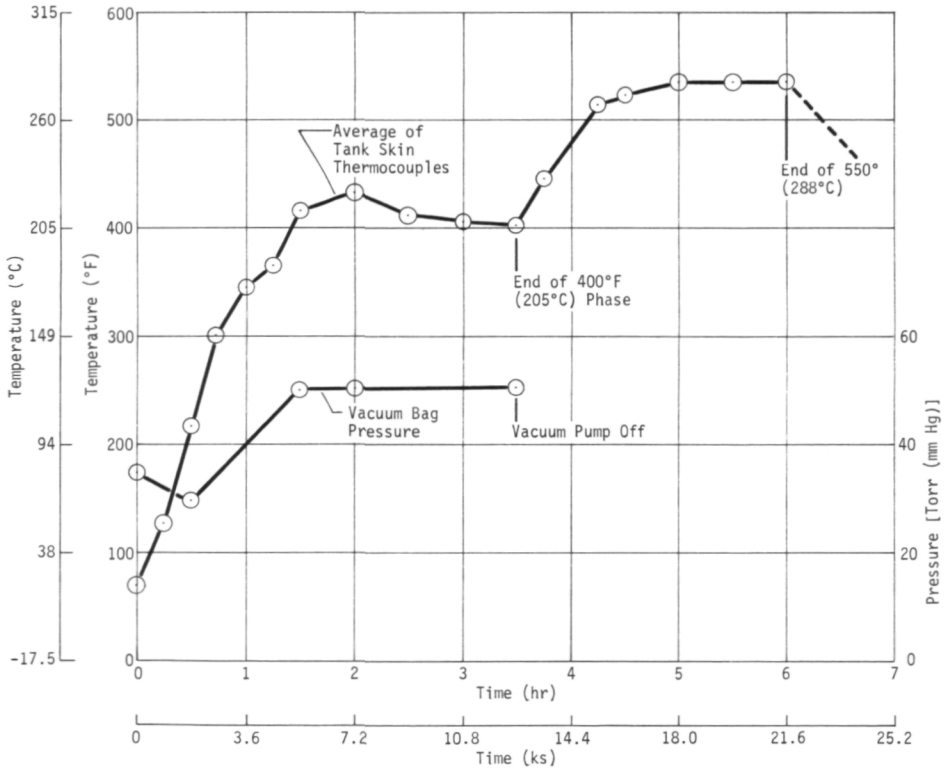

Figure 30. Combined cure posture temperature cycles for square methane tank.

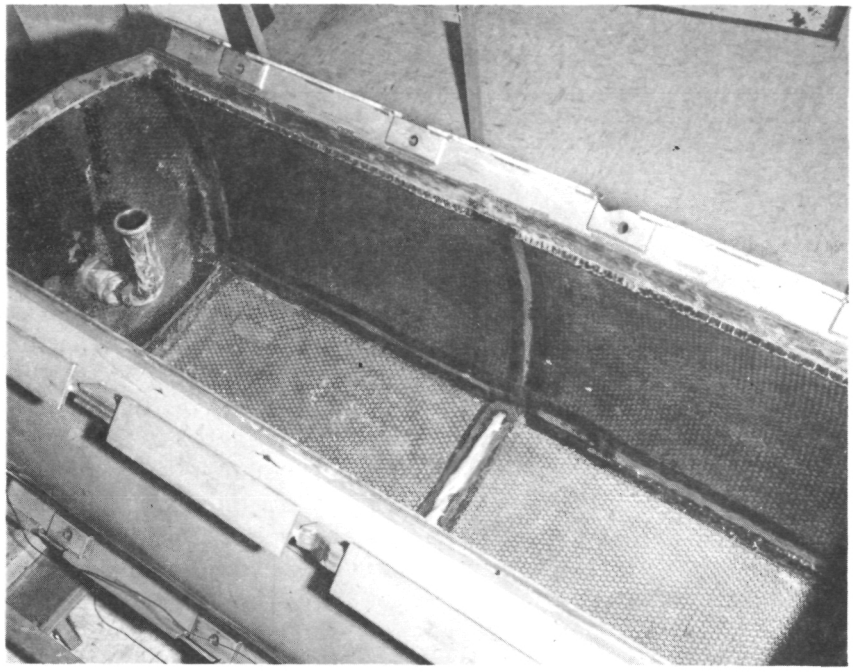

Figure 31. Tank internal surface after postcure.

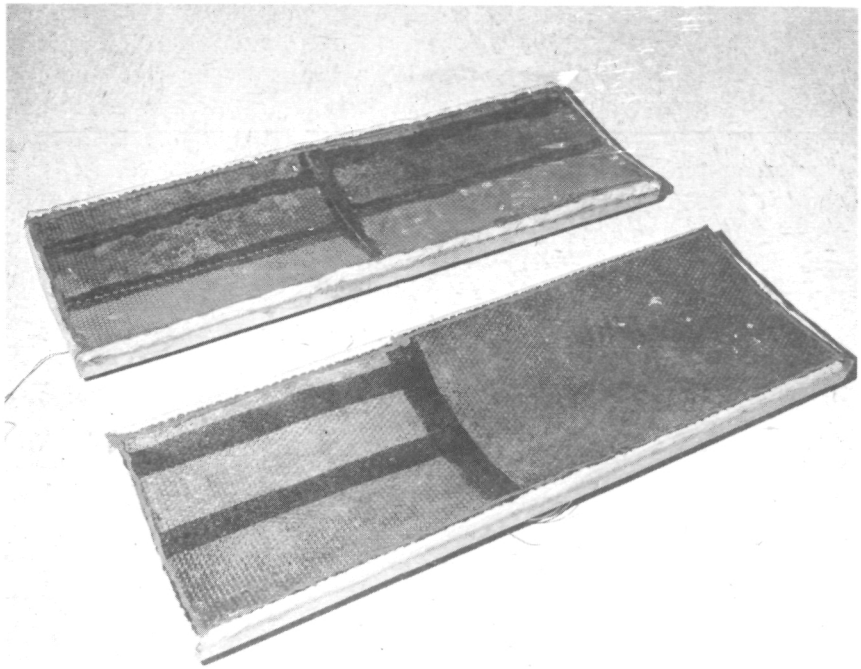

Figure 32. Tank covers after postcure.

Examination of the tank after the postcure indicated three problems:

1) A portion of the nylon vacuum bag had melted onto the Kapton face sheet. (See fig. 31 dark area on tank end.)

2) Much of the face sheet dimpling and splice dimpling had disappeared.

3) One section of the face sheet on the tank side had cracked for a distance of 6 to 8 in. (15.2 to 20.3 cm). The cracks were a series of single-cell face sheet failures that were not connected across the cell/face sheet bond line. The face sheet cracks were in an area of the tank where the metal skin had wrinkled during welding.

The tank was examined for further problems and each cell was checked to assure that the capillary hole was open. Because the tank bottom insulation appeared to be without a problem except for some loss of dimpling, it was exposed to several inches of liquid nitrogen. After 30 min (1.8 ks) at liquid nitrogen temperature, several cracks were found in the first two bottom panels on one end of the tank. One crack that was parallel to the tank centerline extended across a complete panel. Other cracks were about 6- to 8-in. (15.2- to 20.3-cm) long, branching from the panel edge or from the one long crack. The splice joint between the first two panels was also cracked.

On the following day liquid nitrogen was again put into the tank bottom to see if additional cracks would occur. Although one or two smaller cracks appeared, it was felt that the stresses caused by loss of dimpling had been relieved. A patching technique was developed to repair the cracks. This technique consisted of placing a rolled piece of fiberglass about the diameter of a pencil along the crack, then bonding a patch of Kapton film with RTV adhesive over the fiberglass. This technique is shown in figure 33 and provided a raised patch that allowed for thermal contraction of the patch film during cooldown. The RTV adhesive used is a high-temperature, ambient cure material that is compatible with the test conditions. After allowing sufficient time for the patch adhesive to set, the tank was again exposed to liquid nitrogen. Again, after a 30-min (1.8-ks) soak time, examination indicated a number of new cracks and some failures in the patch joints.

A second patching attempt was made using some improved techniques and followed by liquid nitrogen soak. This again proved fruitless and additional cracks developed.

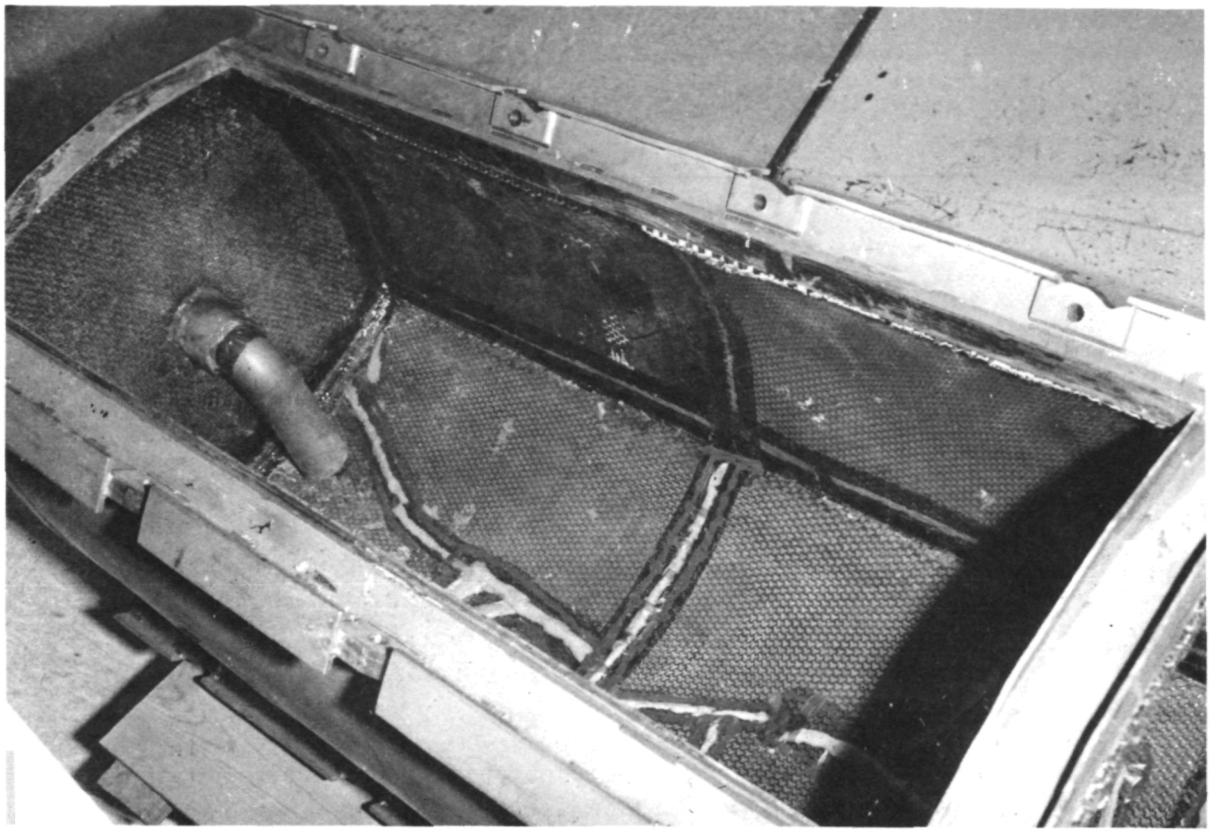

Figure 33. Patching technique.

In an attempt to determine what caused the failures in the insulation panels, a failure analysis plan was set up consisting of the following steps.

1) Trace the face sheet failures on the outer skin of the tank and attempt to correlate skin wrinkles and failures.

2) Measure movement of the tank skin (across wrinkles) before, during, and after filling the tank with liquid nitrogen.

3) Remove sections of the failed insulation for examination and failure mode determination.

Figure 34 shows the bottom of the tank with the insulation failure lines traced on the tank skin. In general, the failure traces follow the convex ridge lines of the wrinkled areas.

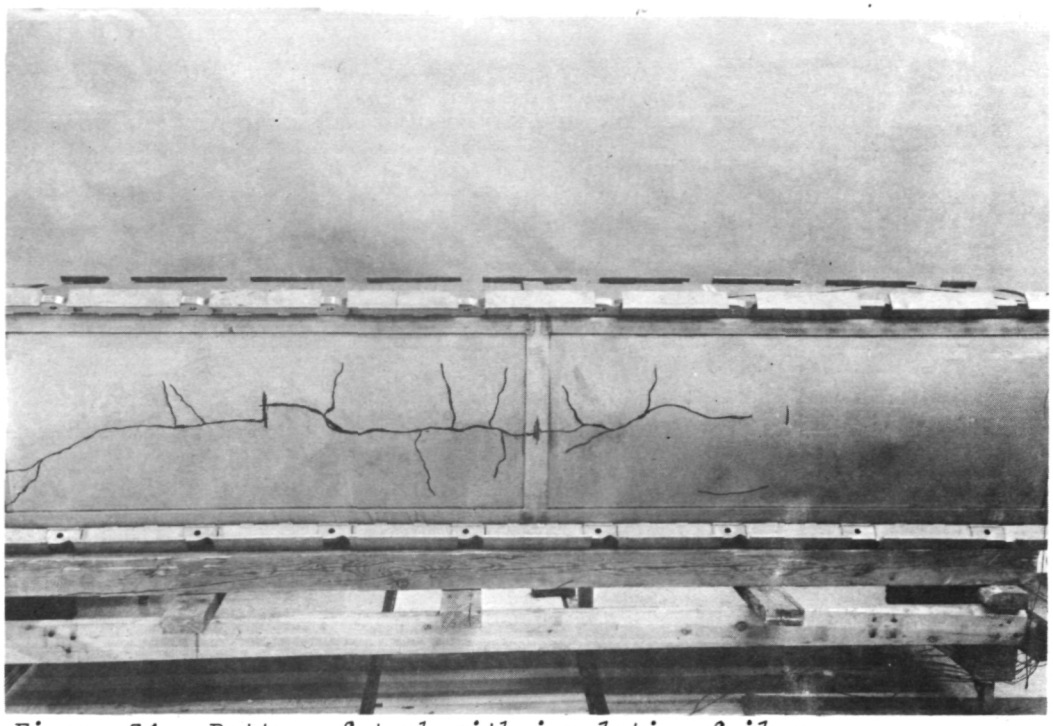

Figure 34. Bottom of tank with insulation failure lines traced on tank skin.

The tank was then supported at the ends and approximately 3 in. (7.62 cm) of liquid nitrogen was put into the tank. Three dial indicators were set up to measure deflections in the tank bottom across some of the major wrinkles during fill and cooldown. Figure 35 shows the indicator positions and the deflection measurements are tabulated. As indicated by the measurements, during the cooldown period following liquid nitrogen fill, the wrinkles tend to straighten out as the system cools. As the wrinkle straightens out, the face sheet on the inside of the tank over the wrinkle is put into tension; this tension is added to a tension created in the face sheet by thermal contraction during cooldown to liquid nitrogen temperature. After fill, the ridge of the wrinkle had moved up and the concave areas adjacent to the ridge had moved downward giving the ridge a net movement of 0.020-in. (0.51-mm) inward. As time increased, this movement increased to as much as 0.025 in. (0.64-mm) after 1 hr (3.6 ks) soak at liquid nitrogen temperature.

After the tank had warmed up, one of the bottom skin panels with the insulation attached was removed from the tank for examination. The insulation was sectioned through the area of one of the face sheet cracks to see how deep into the core the crack extended (fig. 36). It was found that the crack was only a rupture of the face sheet and the core was intact. The presence of liquid nitrogen at the skin during cold testing was apparently the result of individual cells under the cracked face sheet filling with liquid nitrogen.

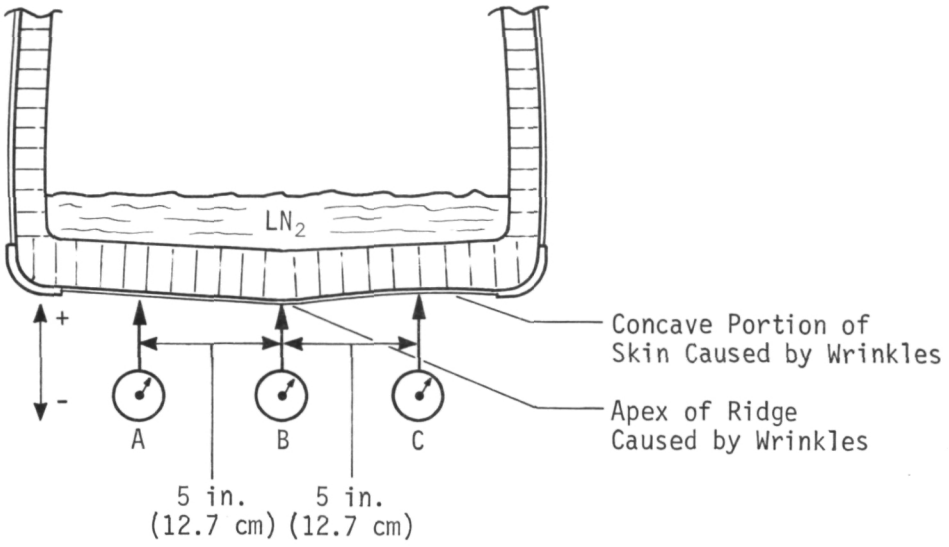

Time	A - in. (mm)	B- in. (mm)	C- in. (mm)
Before LN_2 Fill	0	0	0
After LN_2 Fill	-0.010(0.25)	+0.010(0.25)	-0.010(0.25)
30 min(1.8 ks)	0.006(0.15)	+0.014(0.36)	-0.010(0.25)
60 min(3.6 ks)	+0.001(0.02)	+0.026(0.66)	+0.005(0.13)

Figure 35. Measurement of tank skin deflections during cooldown.

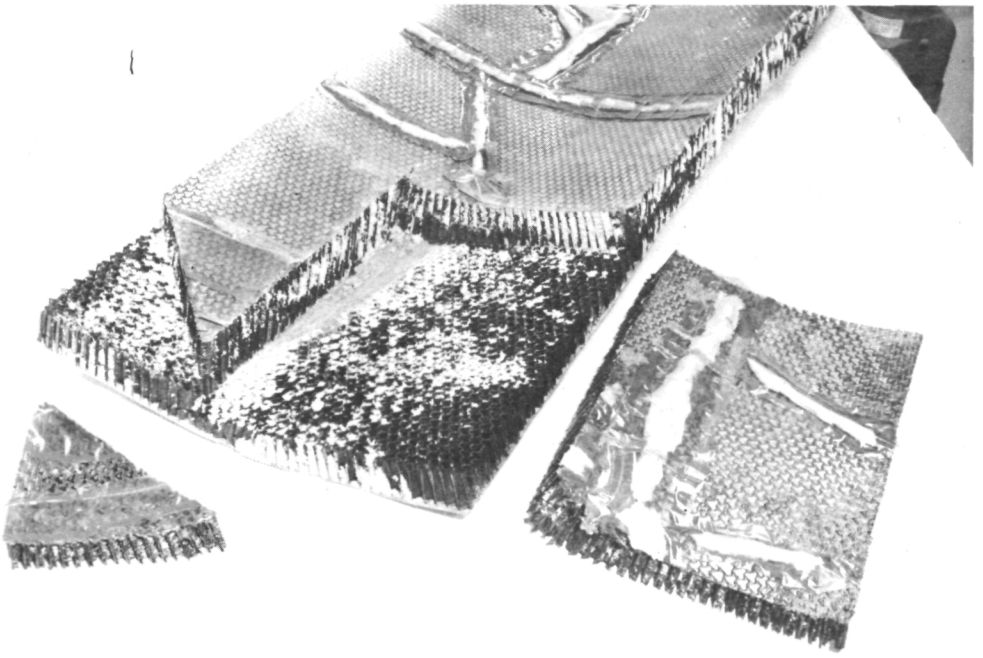

Figure 36. Sectioned insulation panel.

Examination of core bonding to the tank skin indicated some areas of voids as much as 1- to 2-in. (2.54- to 5.08-cm) in length in the vicinity of skin wrinkles. Some of the voids were between the fiberglass cloth and the core and others between the cloth and the tank skin. Under close examination the void areas were apparently the result of insufficient bonding force. In particular, the voids between the core and the bleeder cloth did not show a core imprint in the adhesive on the cloth indicating noncontact during adhesive cure.

A detailed analysis of the face sheet failures under magnification provided additional information. The ruptures were, in general, single cell failures. That is, the face sheet was torn in adjacent cells but the tears were not connected and therefore did not cross the face sheet to core bondlines. Each tear was through the capillary hole, which, under magnification, was not properly formed. The holes showed the effect of piercing with a hot needle by the permanently deformed material at the edge of each hole, however, the needle had apparently been forced through the sheet before it could completely melt. This was evidenced by the hole being partially torn out with the material from the hole itself pushed inside the cell as a flap. A large portion of the holes had two radiating cracks in the edge of the hole at about 90° from the flap. In those cells that were failed the face sheet rupture linked up with the cracks.

Comparing new pieces of Kapton material with that installed on the core did not indicate any thickness buildup from the P13N dip. Some concern had been felt that the dip might have coated the face sheet in an uneven manner causing thickness changes. This discontinuity would act as a stress riser in the sheet causing failure under stress. Analysis of the available data would indicate the reasons for failure were as follows.

1) Wrinkles in the tank skin created areas of stress concentration in the insulation core and face sheet after installation.

2) Postcure of the installed insulation caused a loss of dimpling in the face sheet and splice strips in some areas.

3) Improperly formed capillary holes provided cracks from which cell face sheet failures could originate at relatively low load conditions.

4) Cooldown of the insulation with liquid nitrogen as a postinstallation checkout increased the tensile stress levels in the face sheet. This came about through thermal contraction of the undimpled areas of the face sheet plus the overall tensile stress increase caused by straightening of the skin wrinkles during cooldown.

Combining the above effects created a stress level in a local area greater than the ultimate tensile strength of the insulation face sheet. In fact, in areas where capillary hole cracks exist, only a stress level necessary to propagate the crack was required. The tear strength in Kapton is only a fraction of the ultimate tensile strength of the material. The failure was then rapidly propagated through high stress fields in the face sheet from cell to cell due to the size of the initial failure and the toughness of the material.

C. DESIGN AND FABRICATION OF THE TEST FIXTURES

In order to apply the severe environmental requirements of this program to the test tanks, a sophisticated test apparatus was required. A thermal model of a portion of a wing was designed and fabricated. The wing section was to house four tanks with the two insulation test tanks in the two center bays. Tests requirements included simulated flight profiles for a supersonic cruise aircraft. This simulation called for wing skin temperatures of from ambient to 700°F (371°C) and air pressures in the wing bays from ambient down to 1 psia (6.89 kN/m^2-a).

The two outer tanks were to act as guard tanks to eliminate lateral heat transfer effects in the wing. The tanks used for this purpose were 150-gal (0.568 m^3) insulated tanks from a previous liquid methane program.

The basic wing structure and skins were fabricated from mild steel as shown in figure 37. Previous experience has shown that the design and operation of the infrared lamp heating systems is especially important. The problem is accentuated in this program by the high temperature at which the lamps must operate and by the corona problem at reduced pressures. It was decided that it would be necessary to water cool the lamps to maintain the lamp ends below the critical 600°F (316°C) level. For maximum reliability, the wiring inside the chamber should be kept to a minimum. Two prototype systems to accomplish these points were fabricated and tested. The first system (fig. 38) consisted of a half-round copper section, with lamp holders attached, mounted on the water cooling tube with a 1-mil (0.025-mm) Kapton film between them. The half round copper section served as the electrical conductor.

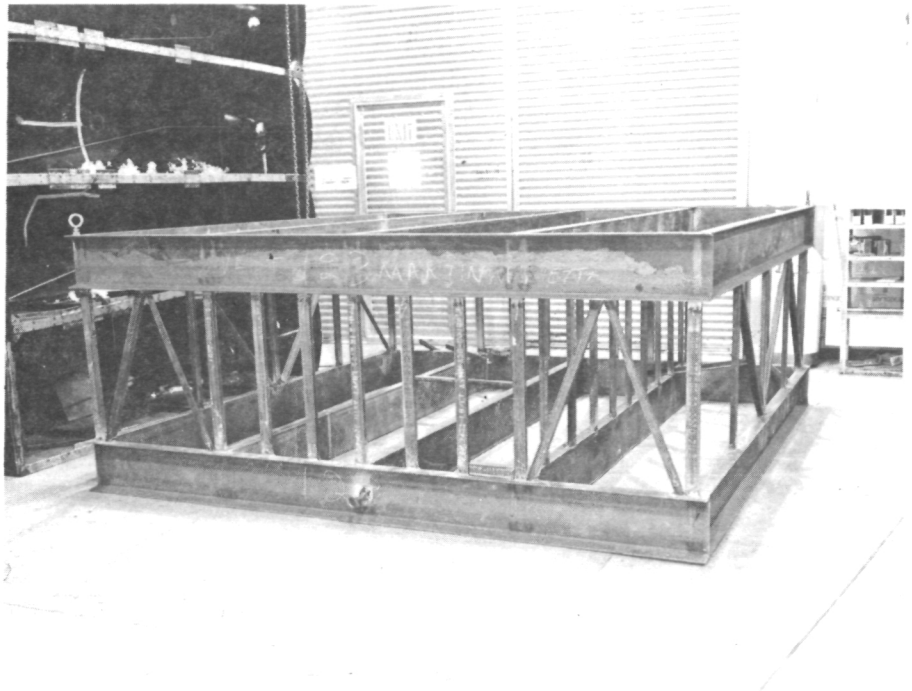

Figure 37. Construction of basic wing structure.

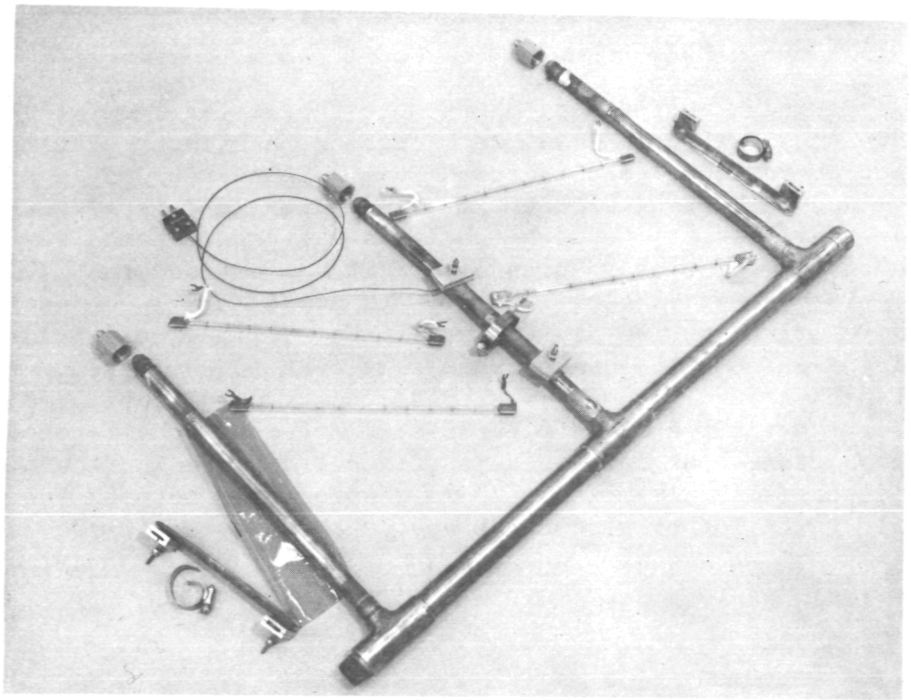

Figure 38. Round tube lamp cooler configuration.

Figure 39 shows the second system that was tested. It is similar to the first system except the copper half-round section has been replaced by a square aluminum tube. The water cooling tube is centered in the square tube by nonconducting screws. The annulus between the round and square tube is filled with MgO to give a good thermal, but poor electrical, path between the square tube and the cooling tube. Both systems were tested in the apparatus shown in figure 40. The lamps were turned on and the temperature of the box was brought up to 700°F (371°C) and held for 6 hr (21.6 ks). As a worst case the lamp ends were insulated with Cerafelt to simulate the lower connection in the high-altitude chamber. Both systems performed satisfactorily in maintaining lamp end temperature. With no insulation on the lamp ends, the lamp end temperature was held to 550°F (288°C) or less during the transient and steady-state periods. With insulation on the ends, the lamp end temperature went to 635°F (335°C) for a short time during the transient and then fell back to 495°F (257°C) during the steady-state portion of the test. The lamp ends were insulated and tested only in the square tube configuration. In general, the half-round copper configuration ran slightly cooler than the square tube configuration. Of the two configurations, the square tube was felt to be more reliable. This was primarily because of the possibility of puncturing the Kapton film due to burrs or rough spots on the cooling tube or half round. The two center bays were isolated from the remainder of the wing by a vacuum box to provide for simulated altitude variations. Figure 41 shows the wing structure with the outer bay covers installed. The infrared heat lamp system was installed on the inside of the covers, one of which is shown in figure 42. A simulated skin was installed in the bays between the infrared heat system and the tank insulation. This skin was heated and temperature controlled to provide a thermal simulation of a supersonic cruise vehicle wing skin during flight.

Figure 43 shows the systems that were used to provide fluids to the tank for test. Liquid nitrogen was used to simulate liquid methane fuel for tank loading. Gaseous nitrogen was supplied for tank pressurization and to purge the tank insulation. A large vacuum pumping system was connected to the center cavity to provide pressure variations that simulate aircraft altitude changes.

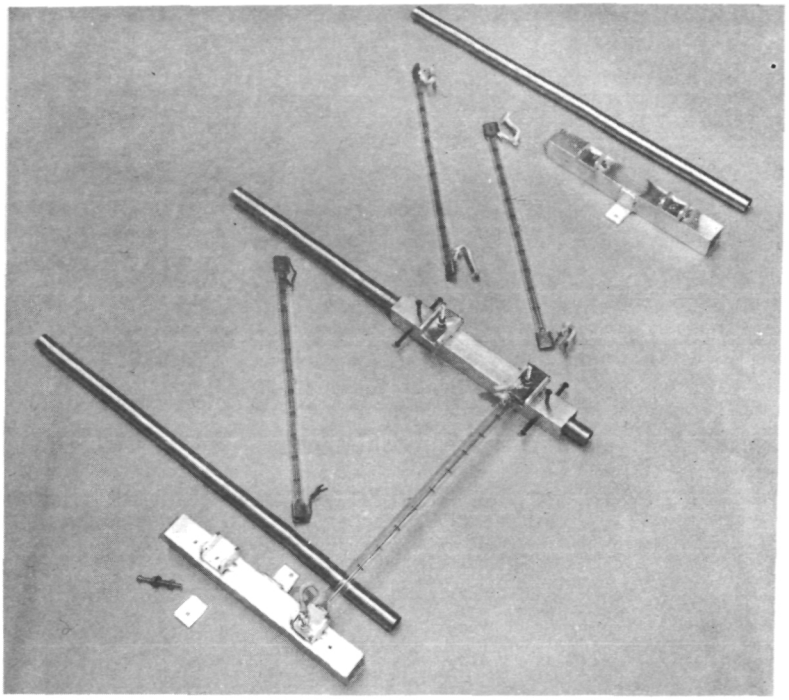

Figure 39. Square tube lamp cooler configuration.

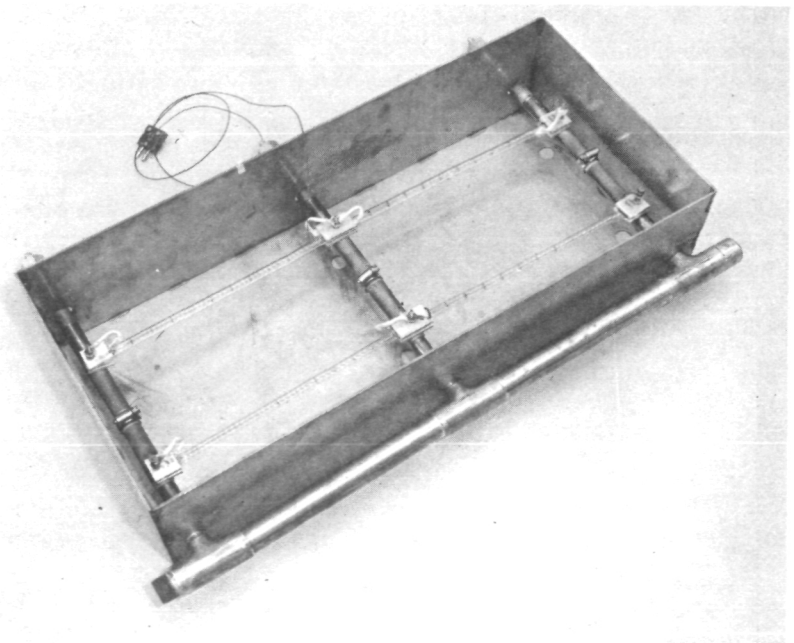

Figure 40. Lamp cooler test fixture.

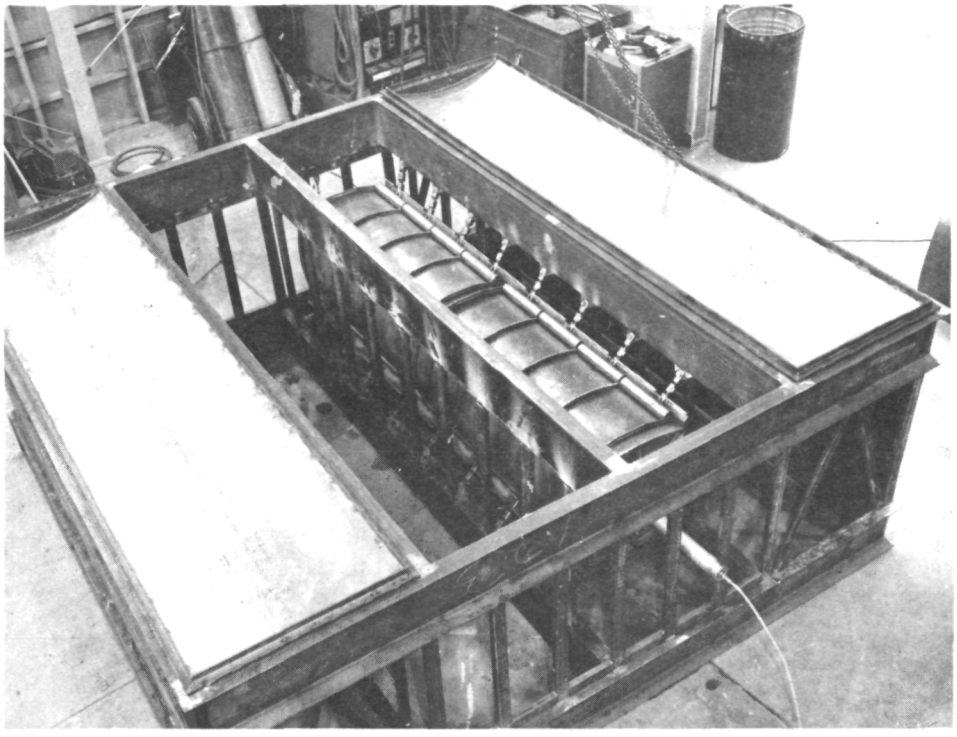

Figure 41. Wing structure with outer bay covers installed.

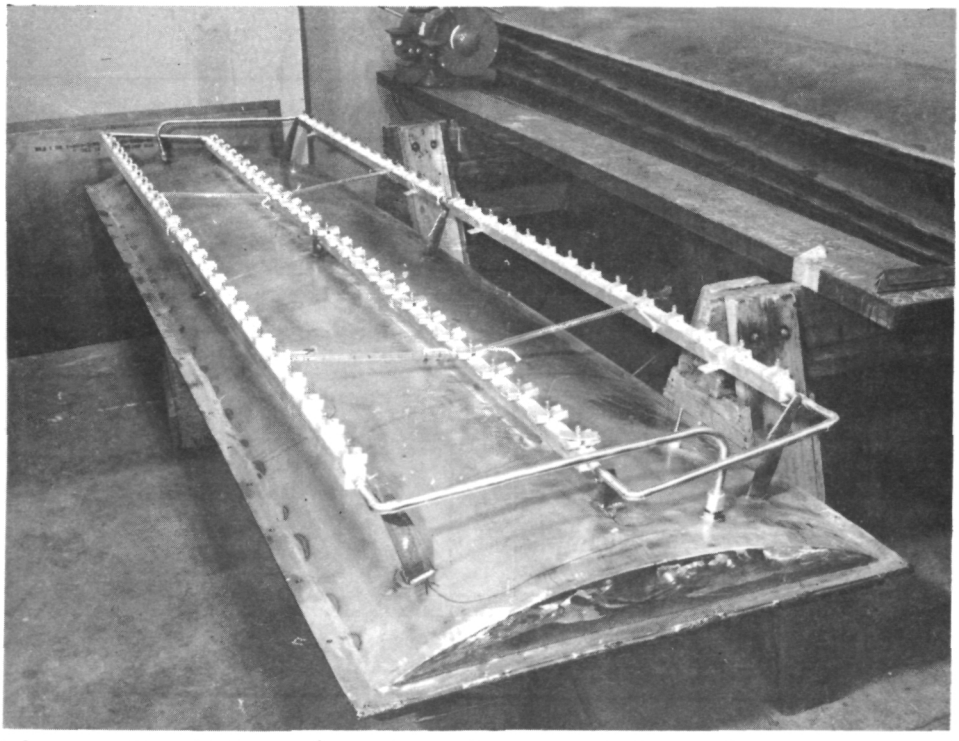

Figure 42. Infrared heat system mounted on wing cover panel.

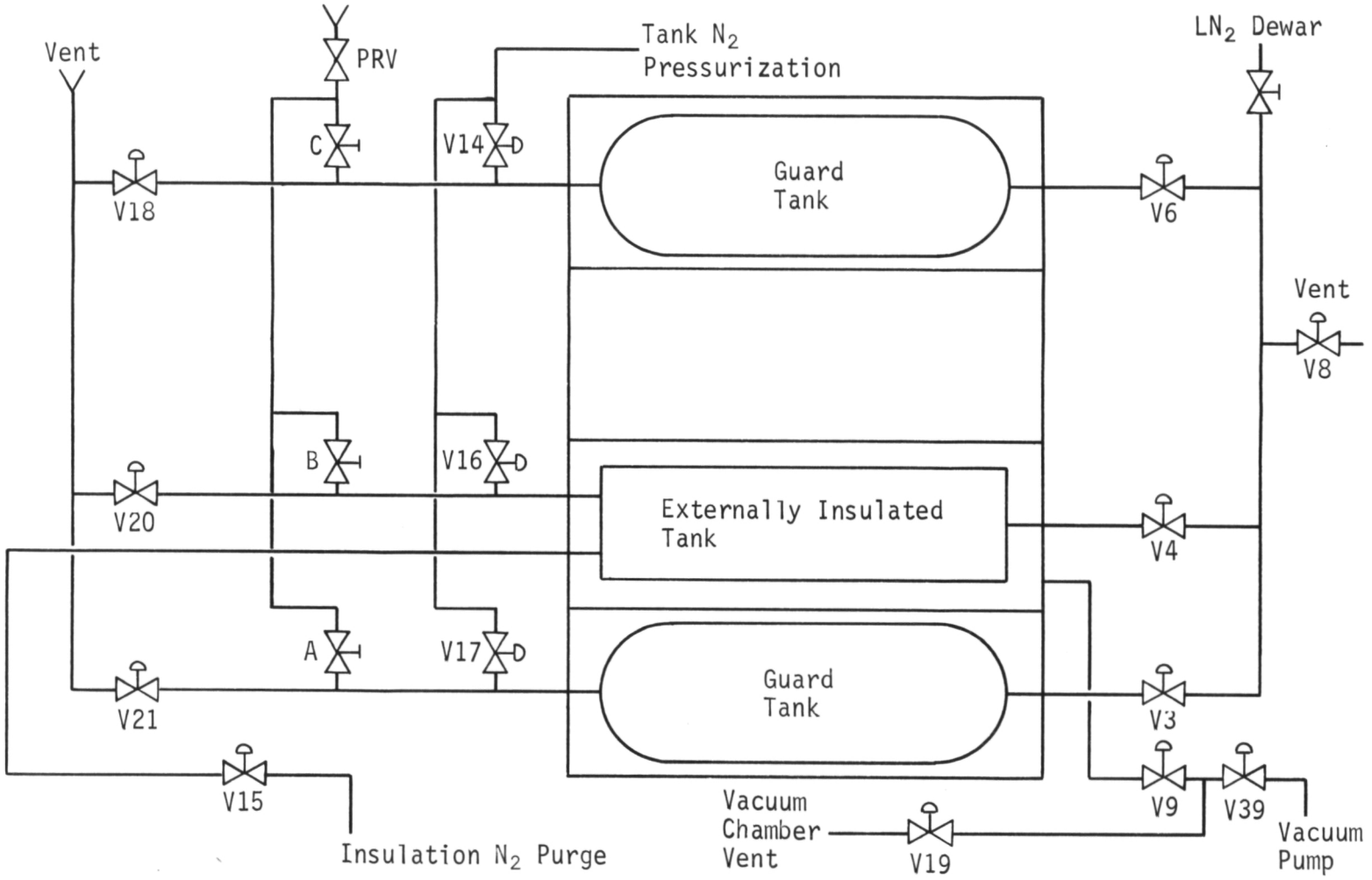

Figure 43. Thermal wing fluid system schematic.

D. INSTRUMENTATION AND DATA COLLECTION

As a final verification of insulation performance the test program was intended to provide a considerable quantity of data. The test tank was instrumented during fabrication as shown by figure 44. A list and general location of the instrumentation used on both the tank and thermal wing is found in table VI. Sensors located internally were installed before closing the tank and were mounted on the diagonal tension members used to offset kick loads. External sensors were installed as the tank was insulated. In general, the sensors were intended to provide measurements of the condition of the liquid and gas in the tank. This included temperatures, pressures and liquid level. The external sensors were to measure temperature of the skin and at various points in the insulation. Sensors not directly a part of the tank provided both vent gas and pressurization gas flowrates.

Through a variety of standard amplifiers and power supplies, the signals from the sensors were conditioned to provide an analog voltage in the range of ±64 mV. These signals were then input to an IEC Subscriber Station (fig. 45 and table VII), which had a 100-channel, low-level analog input capability, a PCM output of 312 20-bit words, and a multiplexing and transmitting capability. This low-level, analog-to-digital acquisition system is transportable to permit the input of data in remote locations.

A permanent hard-wired link was used to transmit the data from the IEC 501 unit to a central data recording station. At the station, the signal was input to a Lear-Seigler 670A telemetry processor (fig. 46 and 47, and table VIII), which had a data rate capability of 1 channel at 0.8 to 1,250,000 bits per second of serial PCM data, or 14 channels at a maximum rate equal to 1.25/N (N = number of data channels) of parallel data. The main frame has 4096 36-bit words of core memory, and the formatter has 1024 18-bit words of core memory. After the PCM signal was decoded and conditioned to provide a binary digital output from the 670A unit, the output was recorded on a 7-track tape unit. These tapes were input to a CDC 6500 computer along with a plot computer program. The computer program:

1) Averages the data samples for each data channel over any specified time increment;

2) Skips any specified time increment between averages;

3) Compares each individual data point with the average and omits any point that differs from the average by more than a preselected amount. If a point is omitted, the remaining points are again averaged. This portion of the program is used to eliminate extraneous noise on the data signal whenever the noise affects less than half the data samples;

4) Converts each of the averaged data points (in mV) to a temperature, pressure, liquid level, or flowrate of gas or liquid;

5) Plots as many as five channels per plot against a preselected time scale on a continuous roll of photosensitive paper. Plot titles, data point identification, annotations, and ordinate and abscissa nomenclature are printed on each plot. In addition, each plot is placed on microfilm;

6) Stores the averaged data points of item 3) above on magnetic tape.

Data points may be replotted at any time with changes of scale, if required. This allows any section of the plot to be expanded for closer investigation.

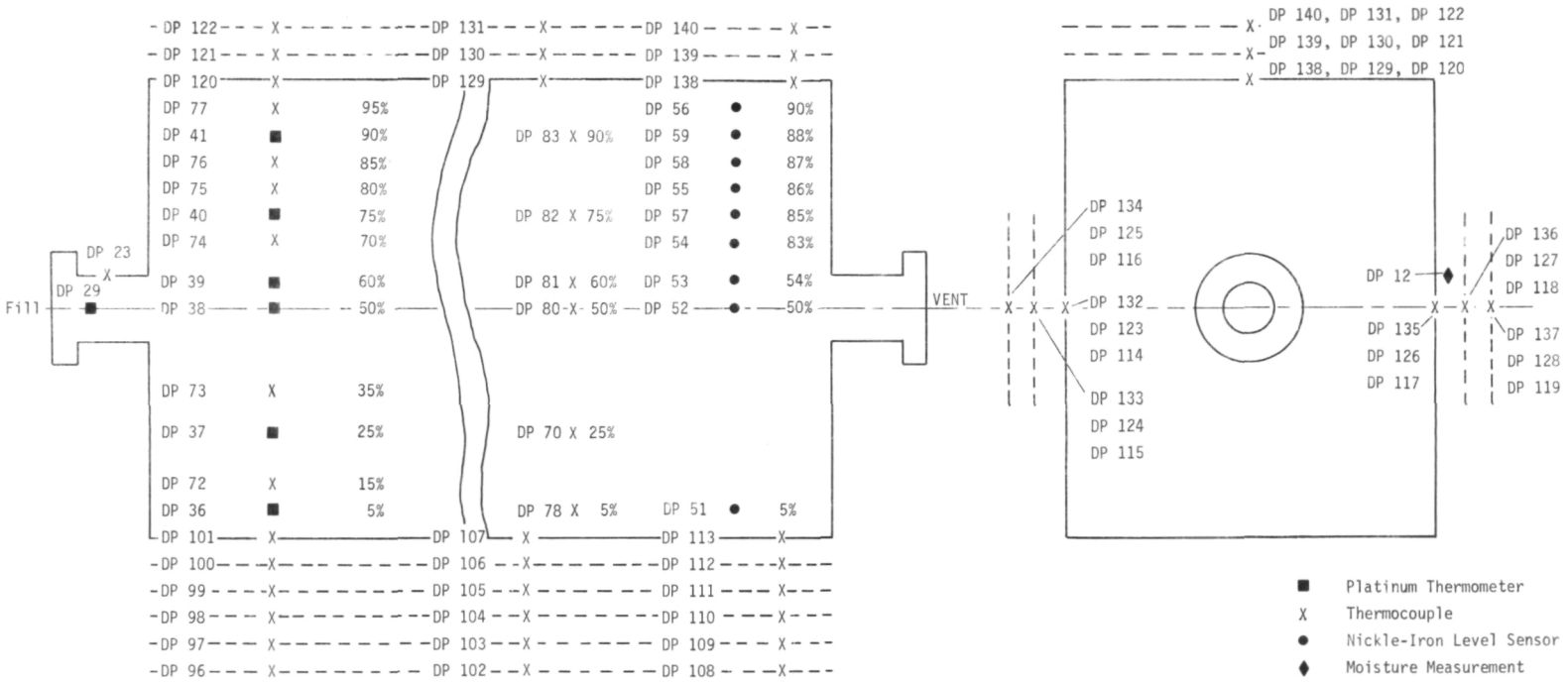

Figure 44. Externally insulated tank sensors.

TABLE VI. - TANK AND WING INSTRUMENTATION SENSORS

Type of sensor	Location	Purpose
Thermocouple chromel/ constantan	On two vertical probes at 12 locations in the tank.	To measure the temperature of the gas and of the liquid in the tank.
	12 on the tank skin, three on each side.	To measure the temperature of the skin on the tank.
	15 placed between each half-inch layer of insulation on the bottom side of tank, 12 placed every quarter inch of insulation on top and sides of tank.	To obtain the temperature distribution across the insulation in order to calculate the heat loss.
6 pl	6 placed on wing skins, 2 bottom, one each side.	To obtain and control wing skin temperature as desired.
	2 on wing root structure between vacuum chamber and guard bays.	To obtain main structure temperature.
	One each, placed in the fill and vent lines of the tank.	To obtain and monitor fill and vent temperature.
Platinum thermomenter	On a vertical probe at 6 levels inside the tank.	To accurately measure the temperature of the liquid in the tank.
	In the fill line just outside the tank.	To accurately measure the temperature of the liquid at the inlet of tank.
Hot Wire liquid level sensors	On a vertical probe inside the tank at 8 locations.	To determine liquid level in the tank and monitor boil-off rate.
Pressure transducers	2 on the vent line between tank and tank vent valve	To obtain tank ullage pressure.
	2 each on the tank vent flow-meter venturi.	To obtain inlet and delta pressure for flow determination.
	Pressure tap on the vacuum chamber	To obtain reading of chamber pressure.

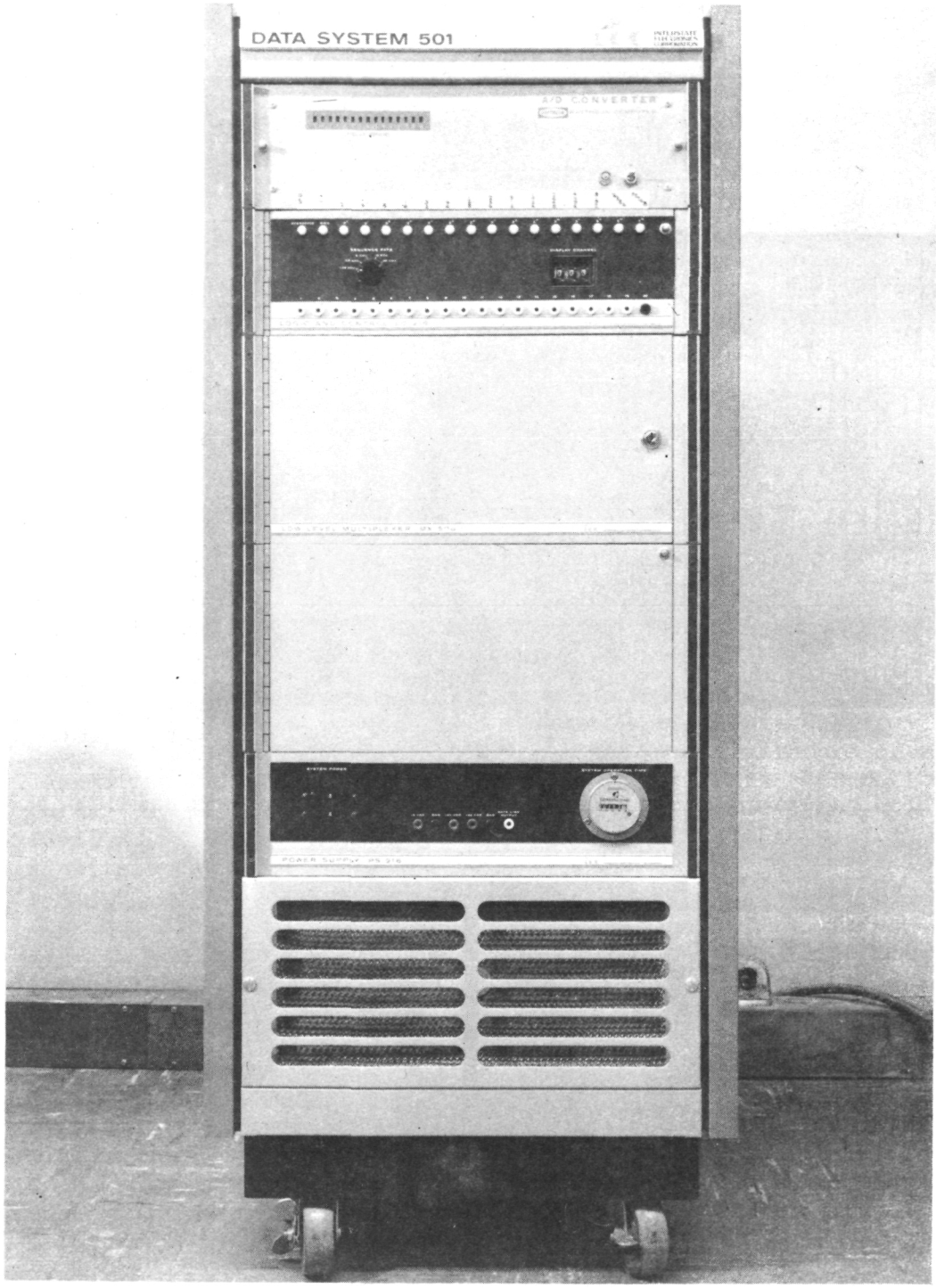

Figure 45. IEC 501 data system.

TABLE VII. - TECHNICAL SPECIFICATIONS FOR 501 DATA SYSTEM

Data input characteristics	
Type of inputs	Analog, differential shielded
Input amplitude	4, 8, 16, 32, 64 mV, full-scale
Number of inputs	100, expandable to 250
Common-mode input	10 V peak, dc to 60 Hz
Source impedance	Less than 1000 ohm
Common-mode rejection	100 dB, dc through 60 Hz
Sampling rate	1.25, 2.5, 5, 10, or 20 kHz steady-state
Output characteristics	
Type of output	PCM format, biphase-M (Manchester 1)
Amplitude out of data link line driver	Approximately 16 V, peak-to-peak
Amplitude out of data link receiver	1 V, rms
Frame length	312 words
Frame content	Frame synchronization word, information word, 10 calibration words, and 300 data words
Word length	20 bits
Environmental characteristics	
Temperature	0 to 50°C
Pressure altitude	Up to 10 000 ft
Humidity	0 to 90% without condensation
Power requirements	115 V ac ± 10%, 60 ± 2 Hz 5A
Size	
Main cabinet	22-1/16 in. wide × 25-1/2 in. deep × 54-7/6 in. high
Receiver enclosure	8 in. wide × 8 in. high × 4 in. deep
Multiplexer subsystem characteristics	
Accuracy	±0.05% of full scale
Crosstalk	±0.02%
Manual gain selection	2000, 1000, 500, 250, 125
Programmable gain selection	2000, 500, 125 by groups of 10 channels
Automatic gain selection	2000, 500, 125
Gain stability	0.05% in 200 hr
Analog-to-digital converter characteristics	
Input range	±8.192 V, full-scale
Bit weighting	4 mV per bit
Input impedance	100 megohm, minimum
Resolution	12 bits (11 bits and sign)
Output code	Negative number (two's complement)
Digital input and output	"1" = 4.5 ± 0.5, "0" = 0 ± 0.5 V
Digitizing accuracy	±0.05% of full scale ± 1/2 LSB

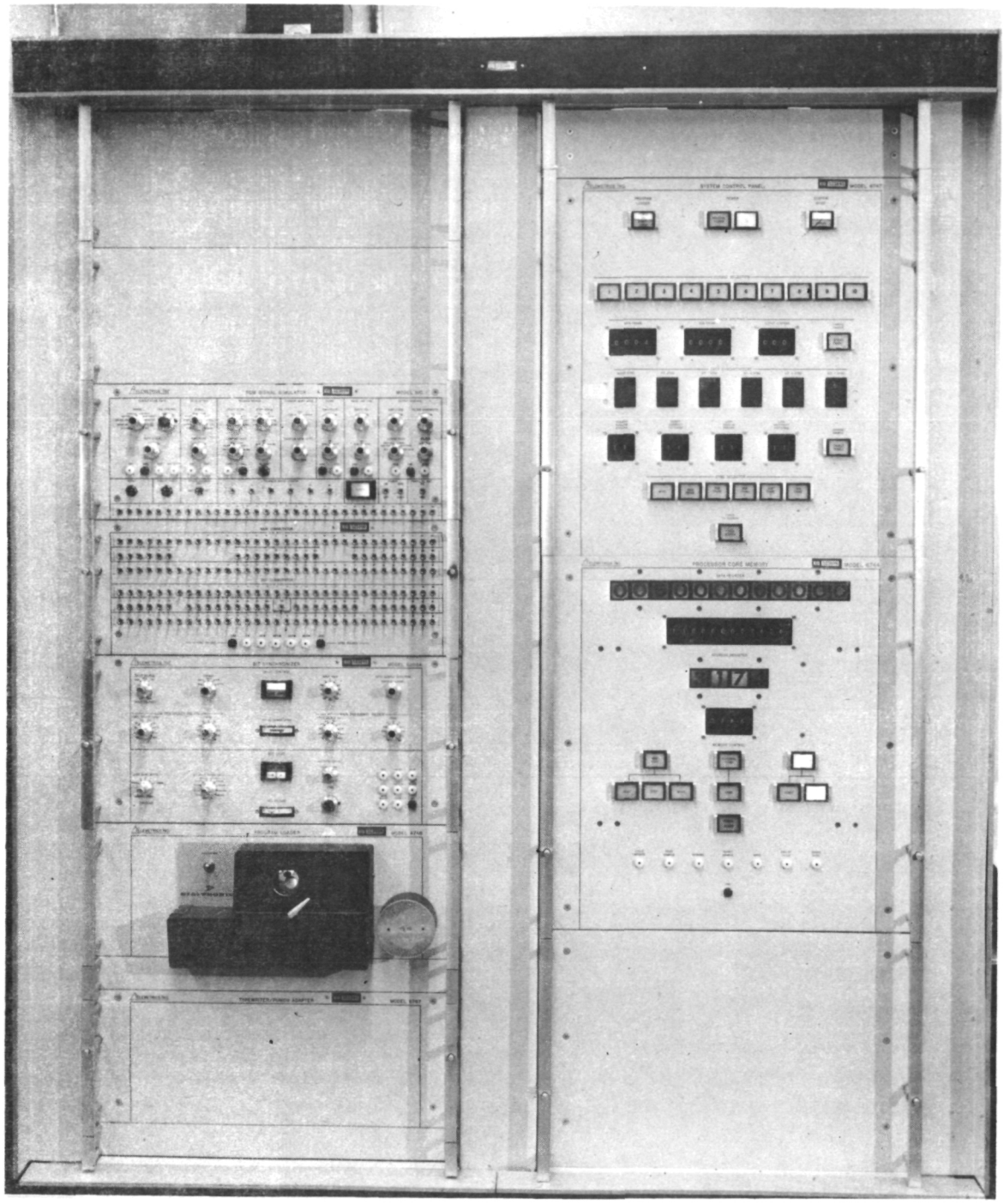

Figure 46. Lear-Seigler 670A telemetry processor.

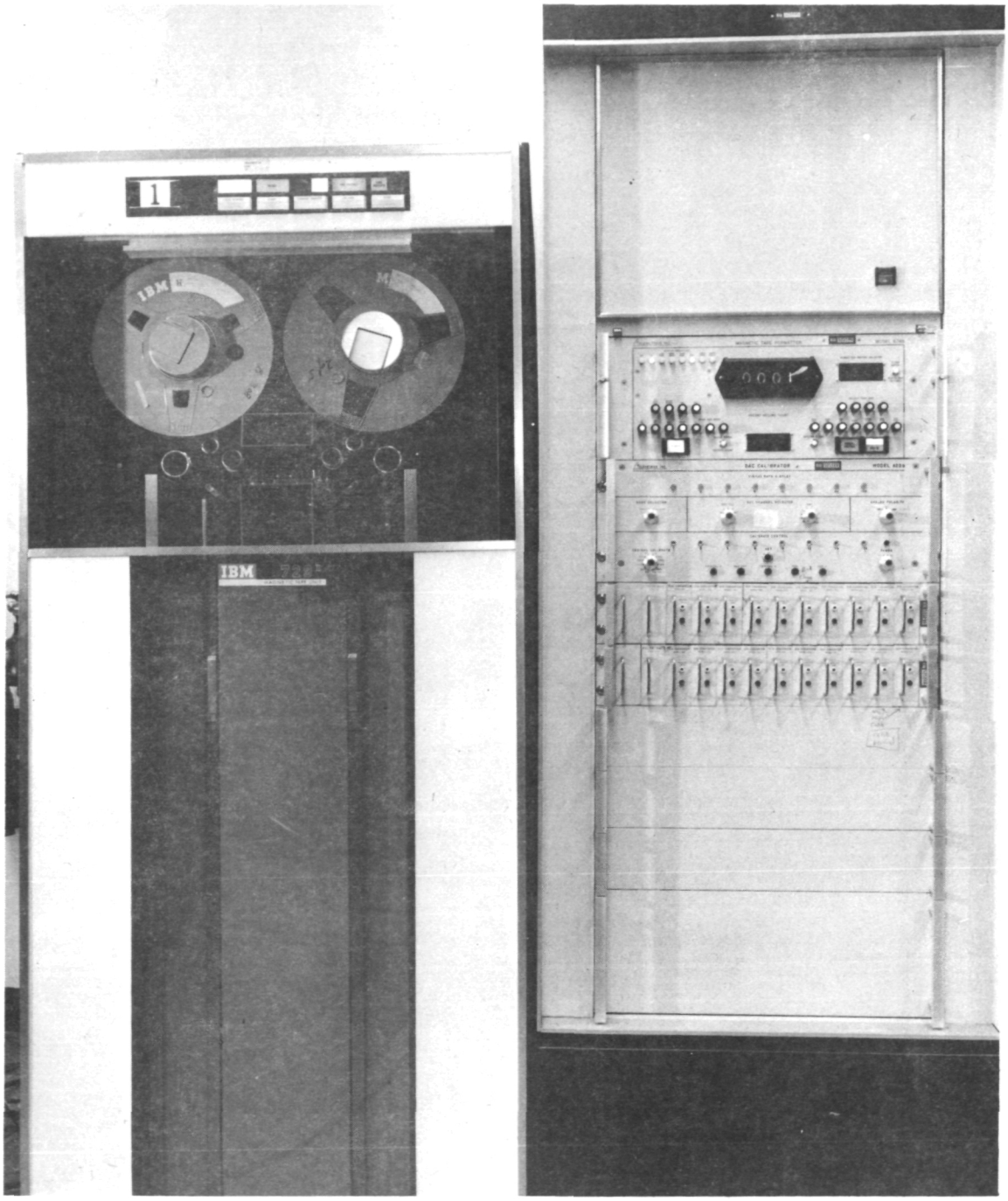

Figure 47. 6748 magnetic tape formatter and 729 Mod II tape drive.

TABLE VIII. - TECHNICAL SPECIFICATIONS FOR LEAR-SIEGLER 670A TELEMETRY PROCESSOR

Input power	115 V ± 10% at 45 to 400 cps single phase, 50 A
Power consumption	4 KW
Data input characteristics	
Types of input	Serial or parallel
Serial data	PCM NRZ-S data accompanied data input clock
Data rate	1 channel at 0.8 to 1 250 000 bits per sec.
Word length	From 1 to 64 bits, variable from word to word
Data alignment	MSB or LSB, or mixed MSB and LSB words
Parallel data	PCM NRZ-S data accompanied by data transfer pulse
Data rate	14 data channels at a maximum rate equal to 1.25/N, where N = number of data channels
Word length	From 1 to 64 bits, variable from word to word
Data alignment	MSB or LSB
Data output characteristics	
Type of output	Parallel
Data rate	500 000 words per sec, maximum
Word length	From 1 to 64 bits, variable from word to word
Data identification	A unique 11-bit I.D. code for each main frame and subframe word
Data use code	Provides for addressing up to 63 (511 optional) output peripheral devices. Any data channel may be addressed to any one of the 63 output devices
Core memory characteristics	Coincident-current storage element
Capacity	4096 36-bit words. Each word has three 12-bit addressable fields
Function modes	Operate (automatic), manual, or external
Access modes	Random or sequential address
Address modes	Direct-address, indirect-address, relative address, or no-address
Operating modes	Full cycle (clear/write and read/restore). Modify cycle (read/modify and restore)
Cycle times	Full cycle, 2 μsec Read only, 1.2 μsec Modify and restore, variable Data access, 0.85 μsec

TABLE VIII. - TECHNICAL SPECIFICATIONS FOR LEAR-SIEGLER 670A TELEMETRY PROCESSOR - Concluded

Operation times (minimum including access)	
Add/subtract	2 μsec
Multiply	17 μsec
Logical (OR, AND, exclusive OR)	2 μsec
Data transfer	2 + 0.2 N μsec, where N = bits/word
Environmental characteristics	
Temperature	
Operating	50 to 100°F (operating time above 100°F limited to 4 hr)
Nonoperating	40 to 150°F
Relative humidity	95% maximum
Air conditioning	Refrigeration, 1 ton
Dimensions	76 in. high × 48 in. wide × 32 in. deep
Input/output unit characteristics	
High-speed paper tape reader, 8-level	300 characters per sec
Paper tape punch (optional)	50 characters per sec
Typewriter (optional)	15.5 characters per sec
Bit synchronizer (optional)	1 250 000 bits per sec
Paper tape reader (optional)	
PCM simulators (optional)	
Digital-to-analog converter (optional)	8- or 10-bit conversion
PAM/PDM-to-PCM converter (optional)	
Magnetic tape formatters	Systems presently operating with IBM, such as Mod II, IBM Mod IV Ampex TM3, and Ampex TM7
General-purpose computers	Systems presently operating with CDC 160A, IBM 1800, and SDS Sigma 11

V. TEST PROGRAM

A comprehensive test program was carried out to evaluate the full-scale insulated tank. This program was designed to expose the insulation to the environments expected for a supersonic cruise aircraft. The testing was conducted in four phases as follows.

1) Initial Baseline - An evaluation of insulation performance at the beginning of testing.

2) Temperature Cycling - Exposure of the insulation to the anticipated flight temperature range.

3) Pressure Cycling - Exposure of the insulation to the anticipated flight ambient pressure range.

4) Final Baseline - A posttest evaluation of insulation performance to determine if testing degraded the material.

The following paragraphs provide a description of each test series along with a presentation of the data obtained. The results are discussed and observations summarized. The final subsection provides the results of the posttest examination of the tank and insulation.

A. TEST DESCRIPTIONS AND DATA

1. Baseline Tests

Two baseline tests were conducted during the test series. The initial baseline test was the first of the test series conducted with the externally insulated tank, and the final baseline test was the last test conducted. The purpose of these tests was to determine an average apparent thermal conductivity based on liquid level measurements, temperature differences across the insulation, and boiloff rates. Some indication of insulation degradation or improvement could also be noted from the results of these tests.

Table IX provides a summary of the two baseline test runs.

TABLE IX. - SUMMARY OF TWO BASELINE TESTS

	Preheat conditions			Event times, sec		
	Temperature, °F(C°)	Pressure, psia (N/cm^2)	Dew point, °F(°C)	Fill to 10%	Time to 700°F	Time to boil to 50%
First baseline	48.4 (9.1)	11.8 (8.14)	16 (-8.9)	3800	2900	13,280
Second baseline	28 (-2.2)	11.68 (8.05)	-37 (-38.3)	1020	2100	15,520

It should be noted that during a pretest checkout the lamp cooling water system was leaking. This could have created an almost 100% humidity in the chamber during heat up. As indicated by the first baseline dew point measurement, the purge gas in the insulation was not as dry as had been anticipated. A dew point of -30°F (-34.4°C) to -90°F (-67.8°C) is the range usually experienced with the nitrogen gas used.

Figures 48 and 49 show the test tank pressure from start of fill through test completion for both the initial and final baseline tests. One effect that appears to be present during the initial baseline test is that the tank was quite warm. This is evident in both the pressure rise and the amount of time it takes to fill the test tank. During the heatup periods both curves are nearly the same shape, showing a drop in tank pressure. They then both increase during final topping, 3.5 psia (2.42 N/cm^2) during the initial baseline and 3.3 psia (2.28 N/cm^2) during final test. This would imply that the condition of the run tank for this operation was similar. During the boiloff period the average tank pressures are nearly equal; however, the elapsed time from initiation of boiloff to 50% ullage is 13,280 sec for the initial test to 15,520 sec for the final test with 700°F (371.5°C) at the outside skin. This would indicate that the insulation is becoming more efficient. This was probably caused by the insulation drying out as indicated by the dew point improvement.

The next two figures, figures 50 and 51, show temperatures measured by platinum thermometers located at varying levels in the test tank. These are located at approximately the 60, 75, and 90% levels. Note the sensitivity of the liquid temperature to the tank gas pressure at these levels. This would indicate that the liquid was saturated as would be expected. Another point worth noting is the decrease in temperature experienced by each transducer during the time the liquid vapor interface is passing. The drop is approximately 0.5°F (0.28°C).

Figures 52 and 53 show the temperature of the liquid at greater depths in the tank. These measurements also track tank gas pressure with a one-to-one correspondence. The drop in temperature as the gas-vapor interface passes the transducer is also noted. Figures 54 through 61 can also be used to detect any stratification of the LN_2 in the tank. The area selected to analyze is the point in time when 700°F (371.5°C) is reached, approximately 7350 sec for the initial baseline test, and 2580 sec for the final baseline test. As these data show, there is at most less than a 0.2°F (0.11°C) stratification at this point. This level of stratification stays nearly the same throughout the initial baseline test; however, the final baseline test does show signs of more extensive stratification during the boiloff portion of this test. This can be seen on figures 52 and 53 as 0.75°F (0.42°C).

Figures 54 through 57 show the temperature distribution in the tank bottom insulation during the two baseline tests. These figures also show, as was noted earlier in this discussion, that the insulation appears to get more efficient with time. For example the insulation closest to the wing bottom exceeded 500°F (260°C) during the initial baseline test, but only reached 479.3°F (248.5°C) during the final baseline test. This effect is also evident on figures 56 and 57 where the insulation 2.5 in. (6.35 cm) in from the wing bottom is 121.8°F (67.7°C) cooler during the final test than during the initial baseline test.

In figures 58 and 59, the temperature distribution through the insulation on a side of the tank shows the same improvement with age, but to a lesser extent. For example, the temperature of the insulation 0.25 in. (0.635 cm) from the tank skin is -5°F (-21°C) during the latter portion of the initial baseline test and is -16.8°F (-27.2°C) during a similar time period of the final baseline test, a change of 11.8°F (6.6°C).

The insulation on the wing top was nearly equal for both tests, as figures 60 and 61 show. It should be noted that the temperatures in the insulation during the final baseline test appear to be in a more transient state than those during the initial baseline test.

The flow rate was determined from level sensor data and venturi flowmeter installed in the vent line. During the initial baseline test the average flowrate was determined to be 121.2 lb/hr (15.3 g/sec), and during the final baseline test was determined to be 96.7 lb/hr (12.19 g/sec). The use of this parameter is shown in Appendix C where the apparent thermal conductivity is derived.

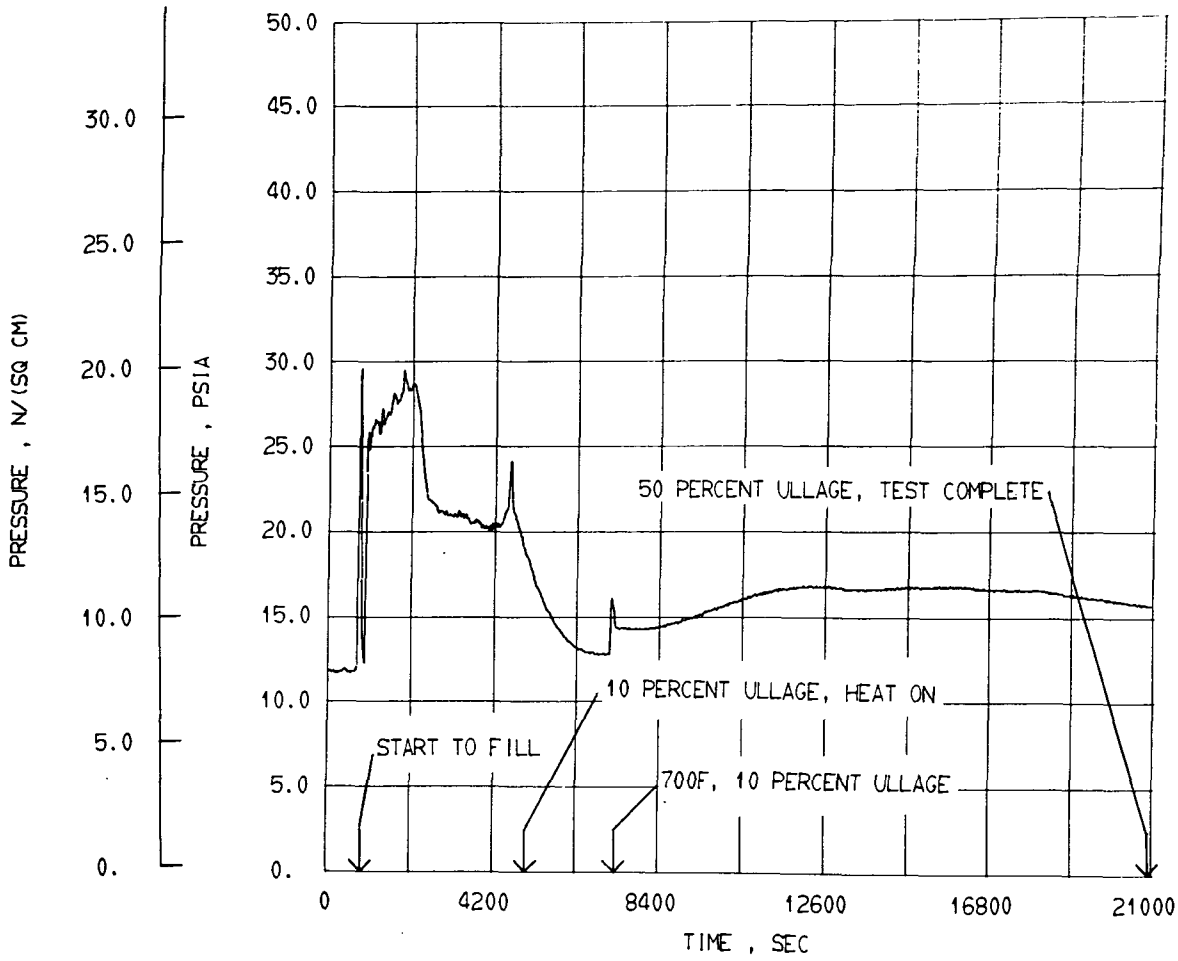

Figure 48. Square tank exterior insulation, initial baseline test, test tank pressure.

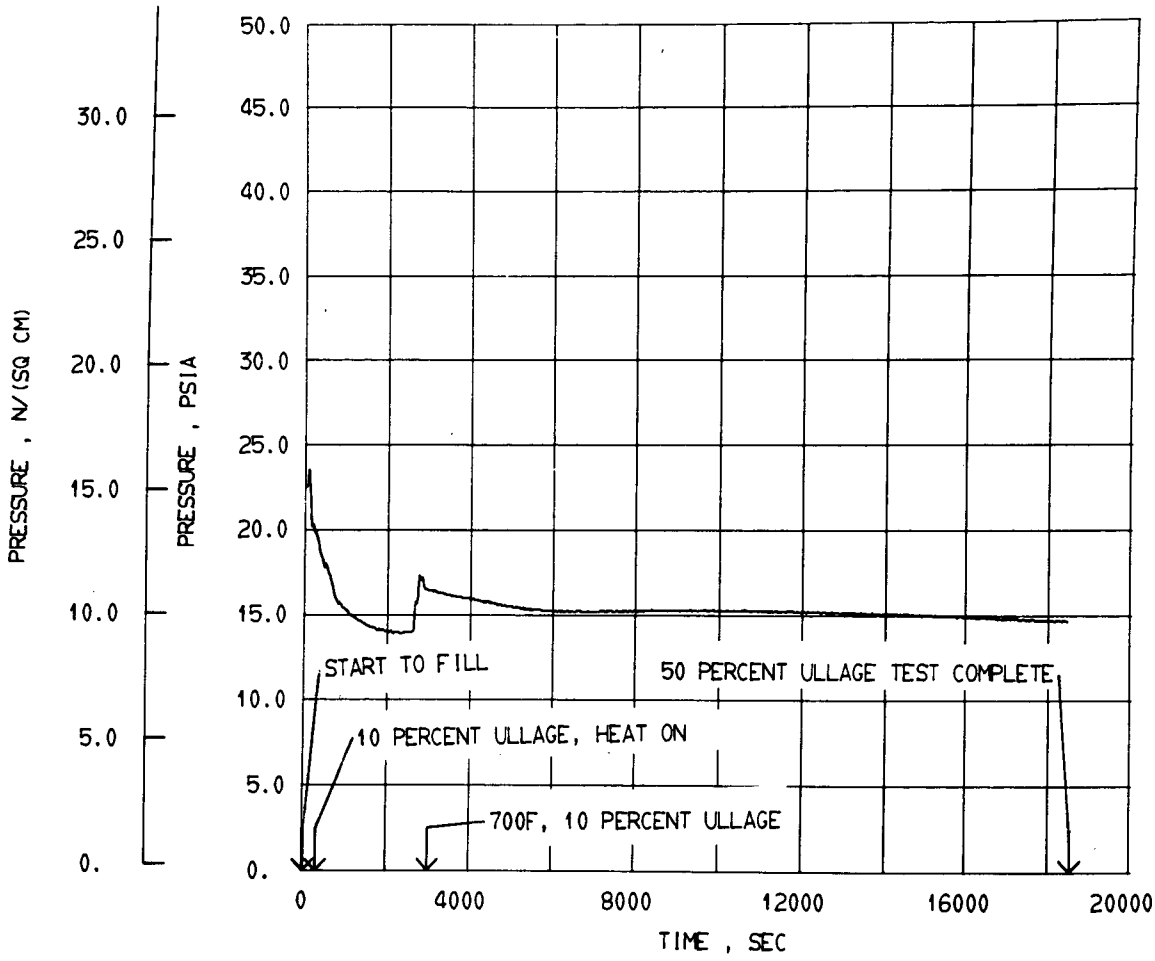

Figure 49. Square tank exterior insulation, final baseline test, test tank pressure.

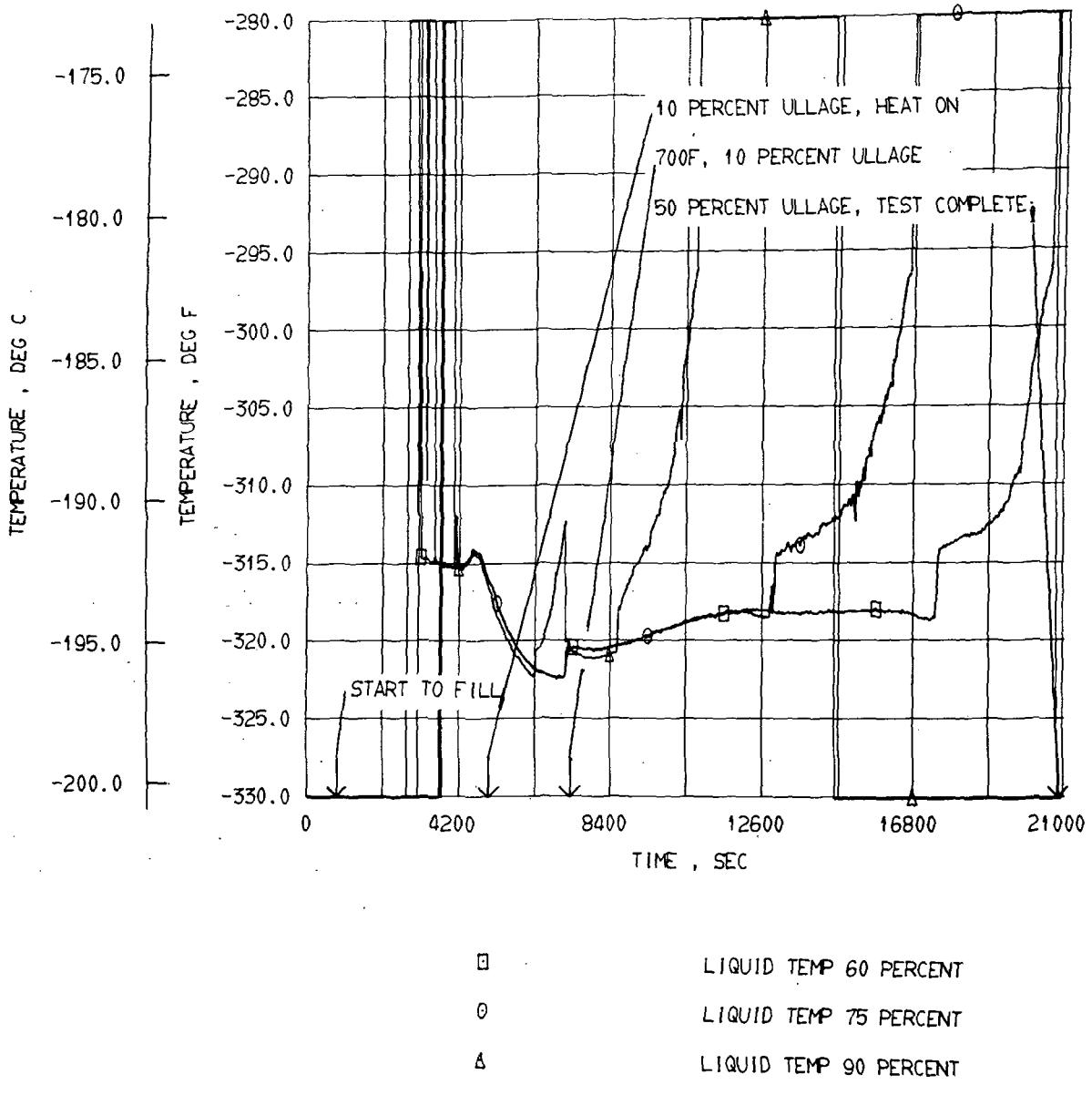

Figure 50. Square tank exterior insulation, initial baseline test, liquid temperature, 60,75 and 90% levels.

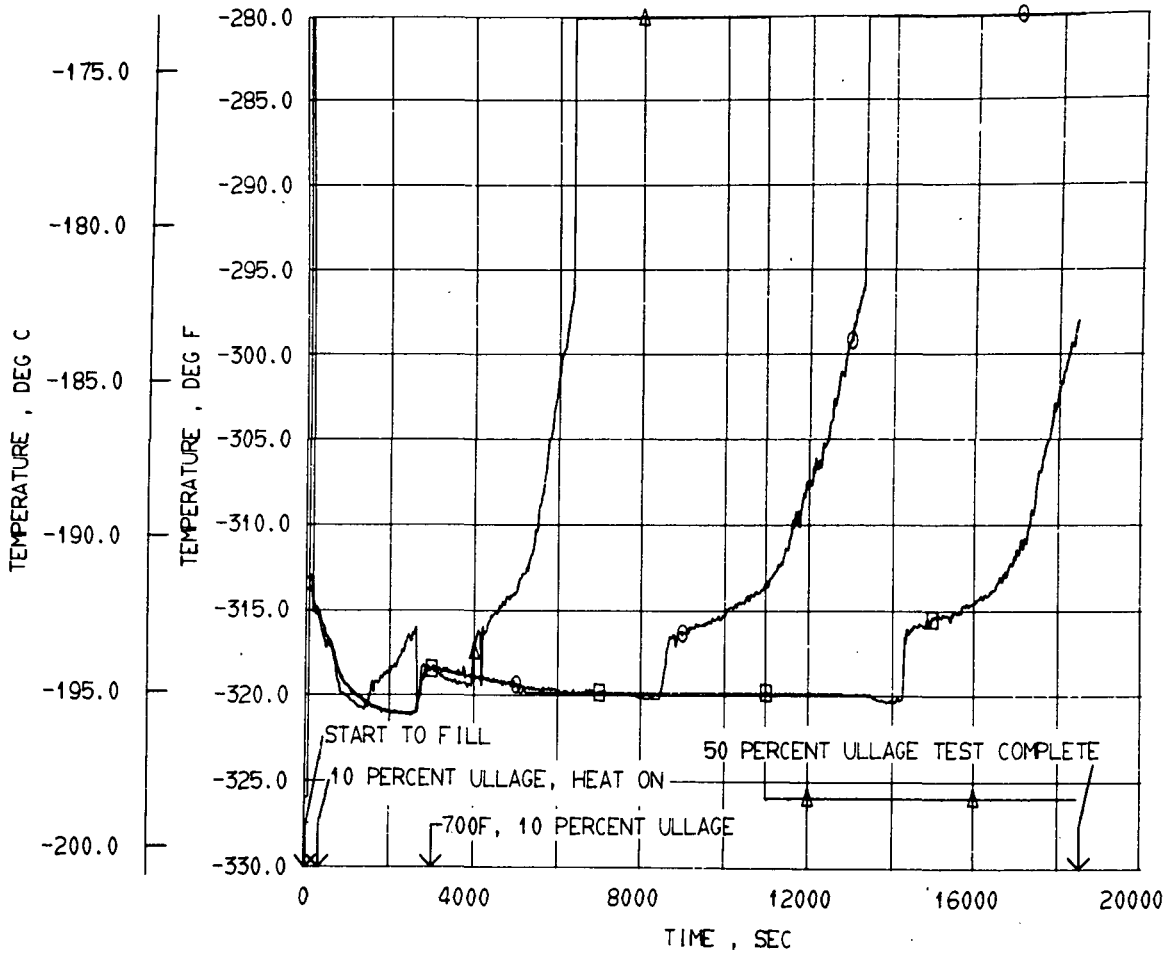

Figure 51. Square tank exterior insulation, final baseline test, liquid temperature, 60,75 and 90% levels.

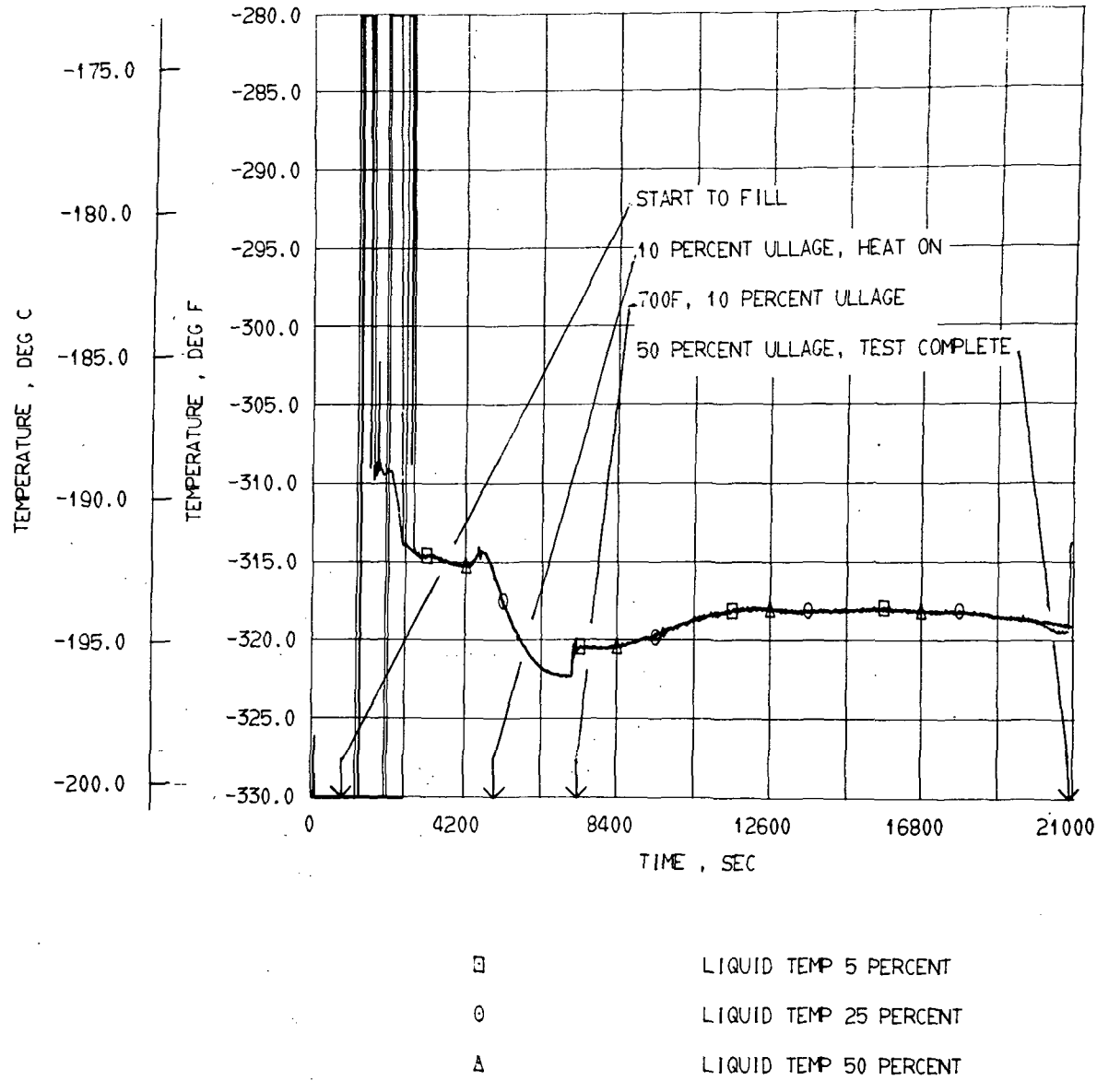

Figure 52. Square tank exterior insulation, initial baseline test, liquid temperature, 5,25 and 50% levels.

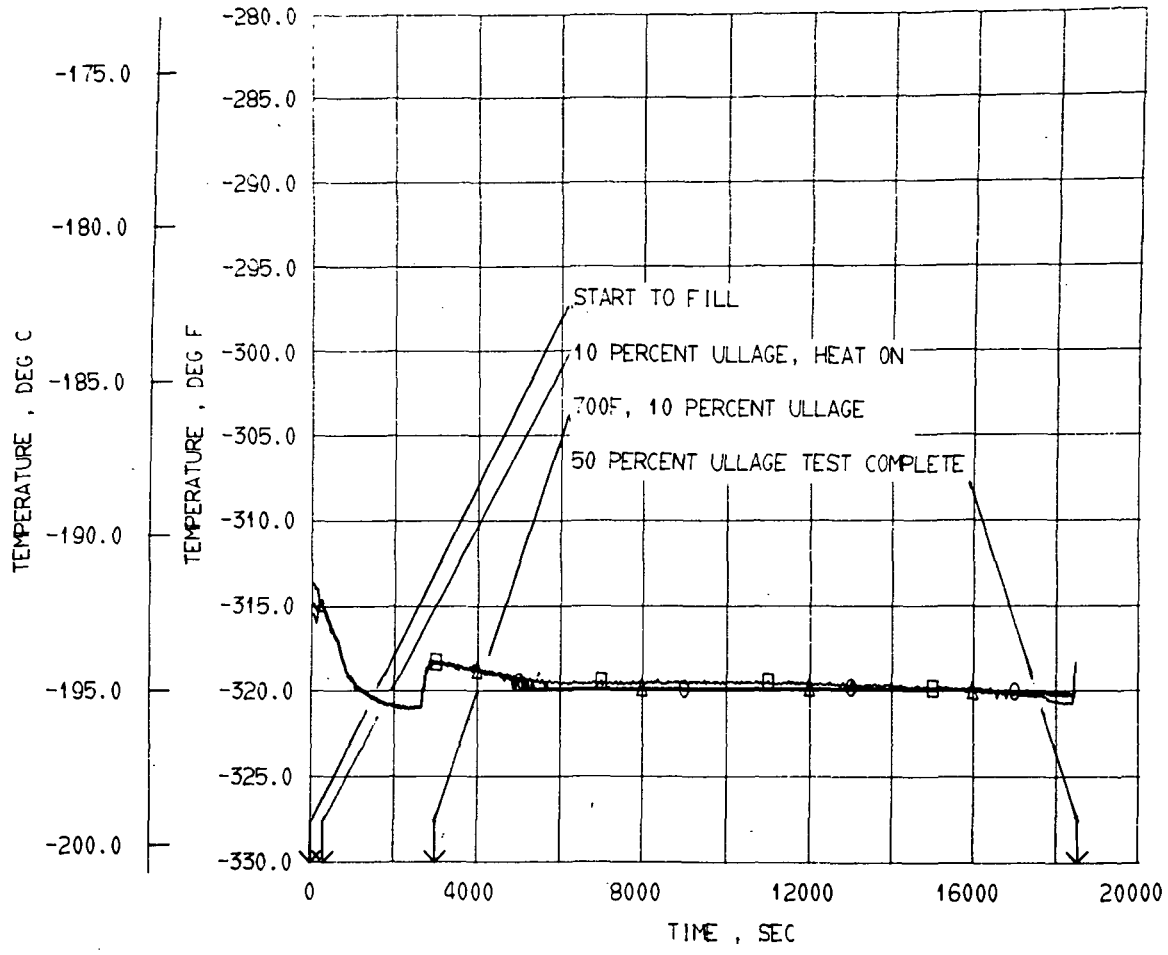

Figure 53. Square tank exterior insulation, final baseline test, liquid temperature, 5,25 and 50% levels.

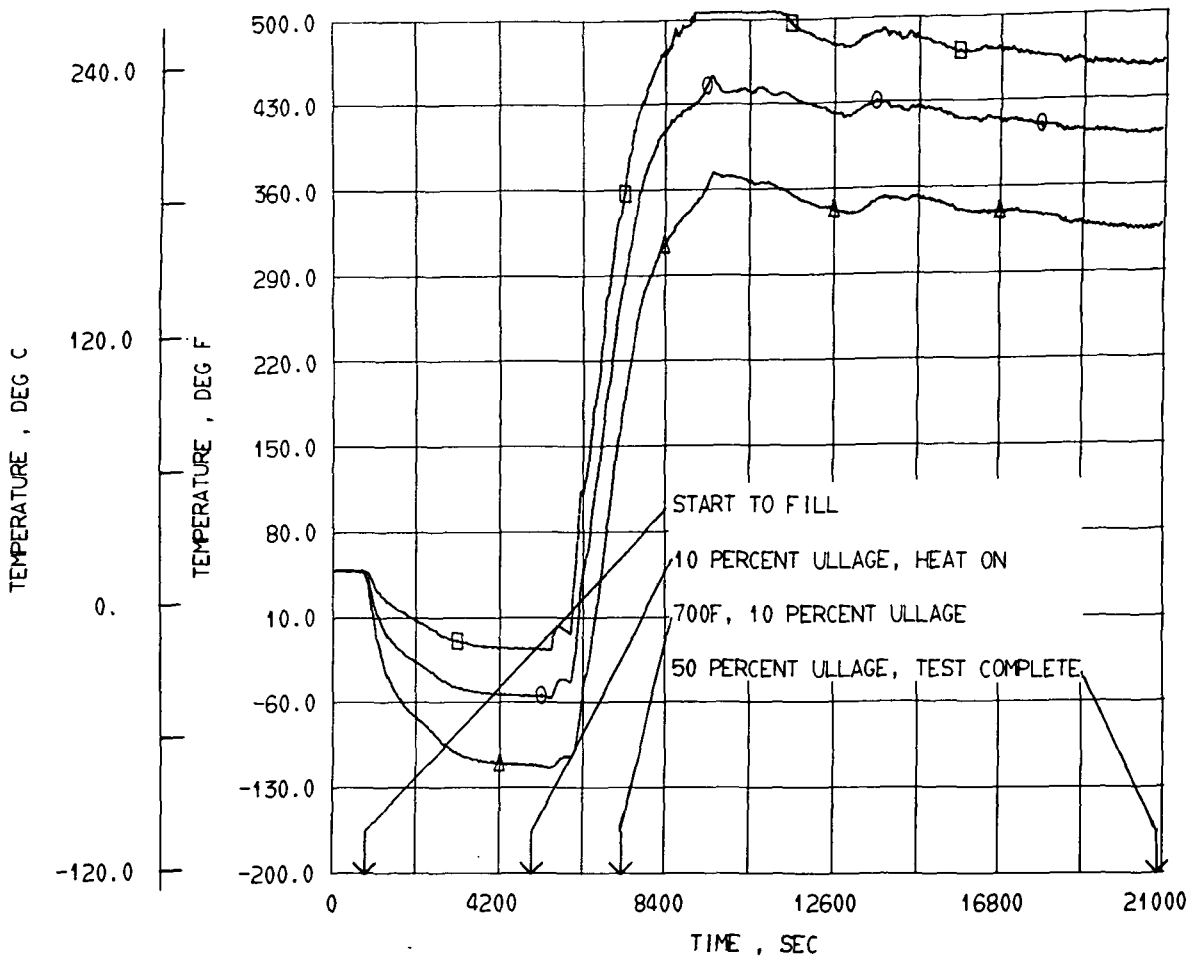

Figure 54. Square tank exterior insulation, initial baseline test, insulation temperatures on wing bottom.

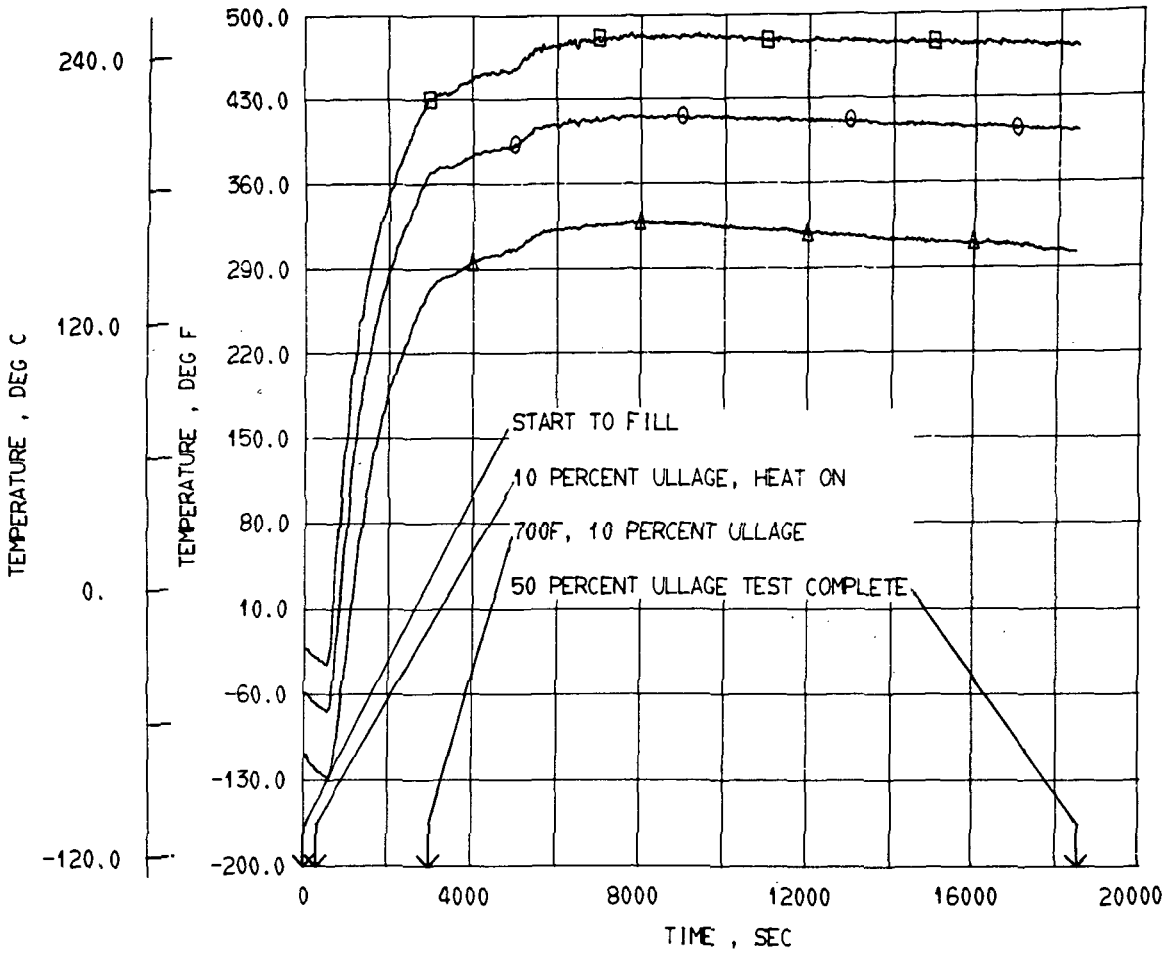

Figure 55. Square tank exterior insulation, final baseline test, insulation temperatures on wing bottom.

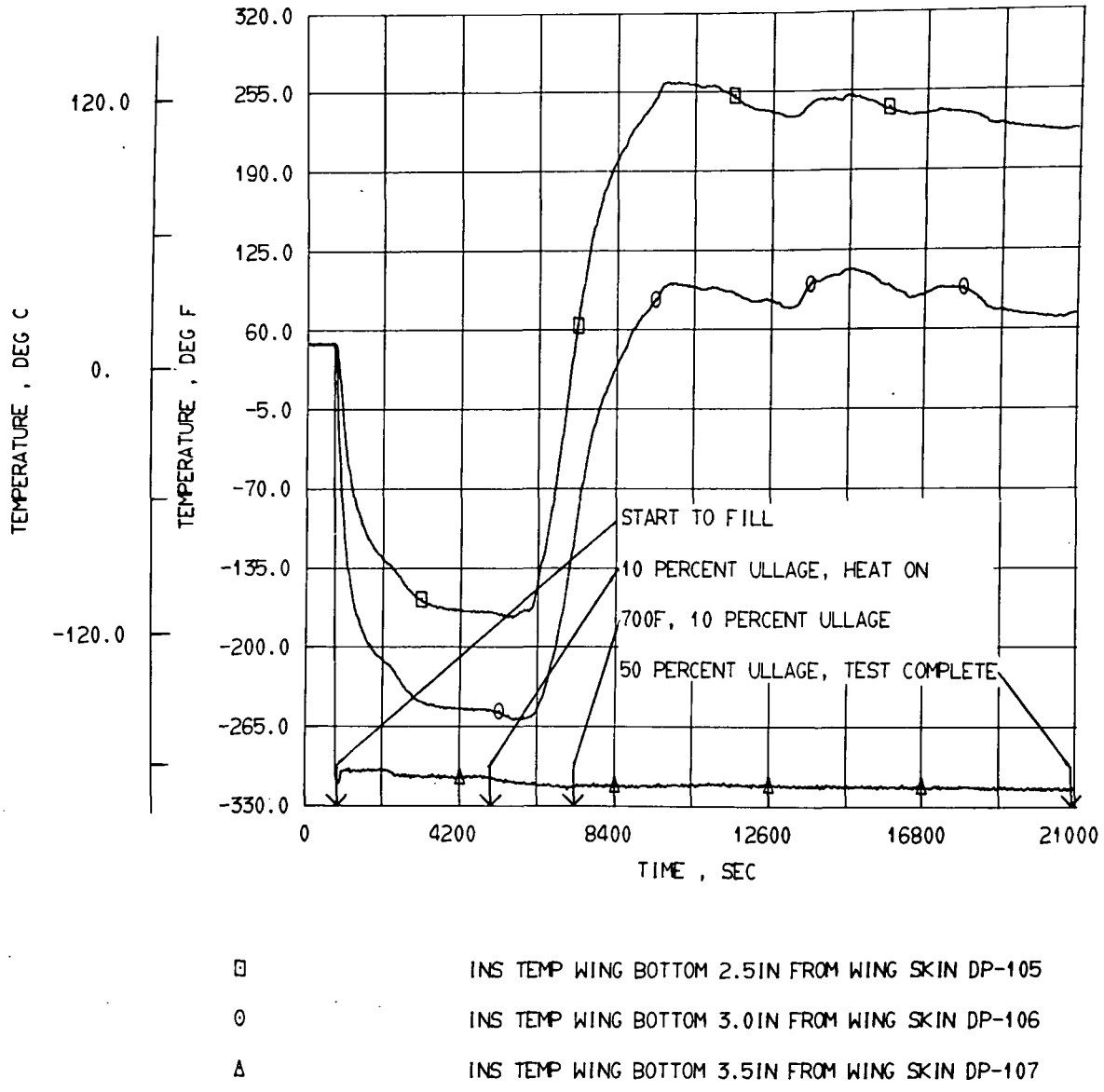

Figure 56. Square tank exterior insulation, initial baseline test, insulation temperatures on wing bottom.

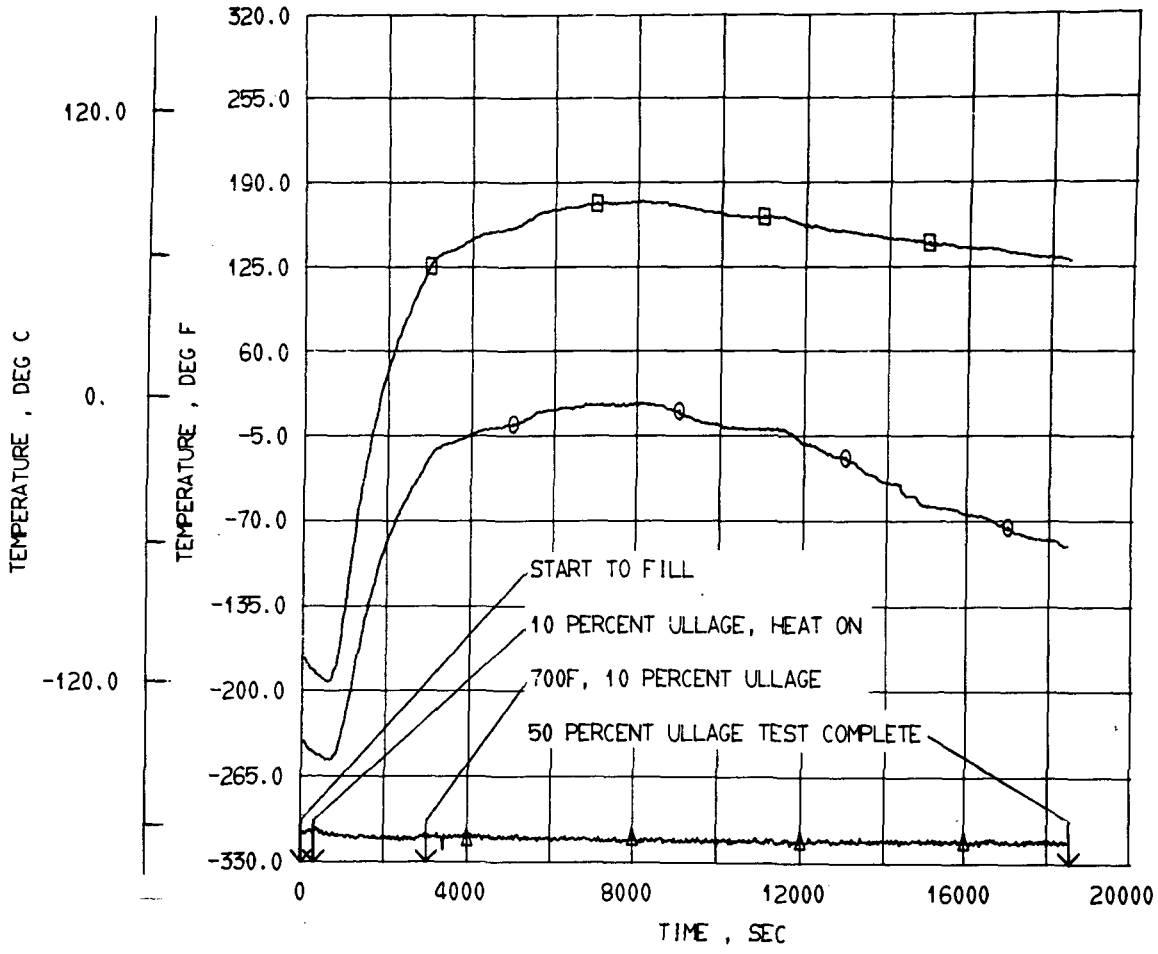

Figure 57. Square tank exterior insulation, final baseline test, insulation temperatures on wing bottom.

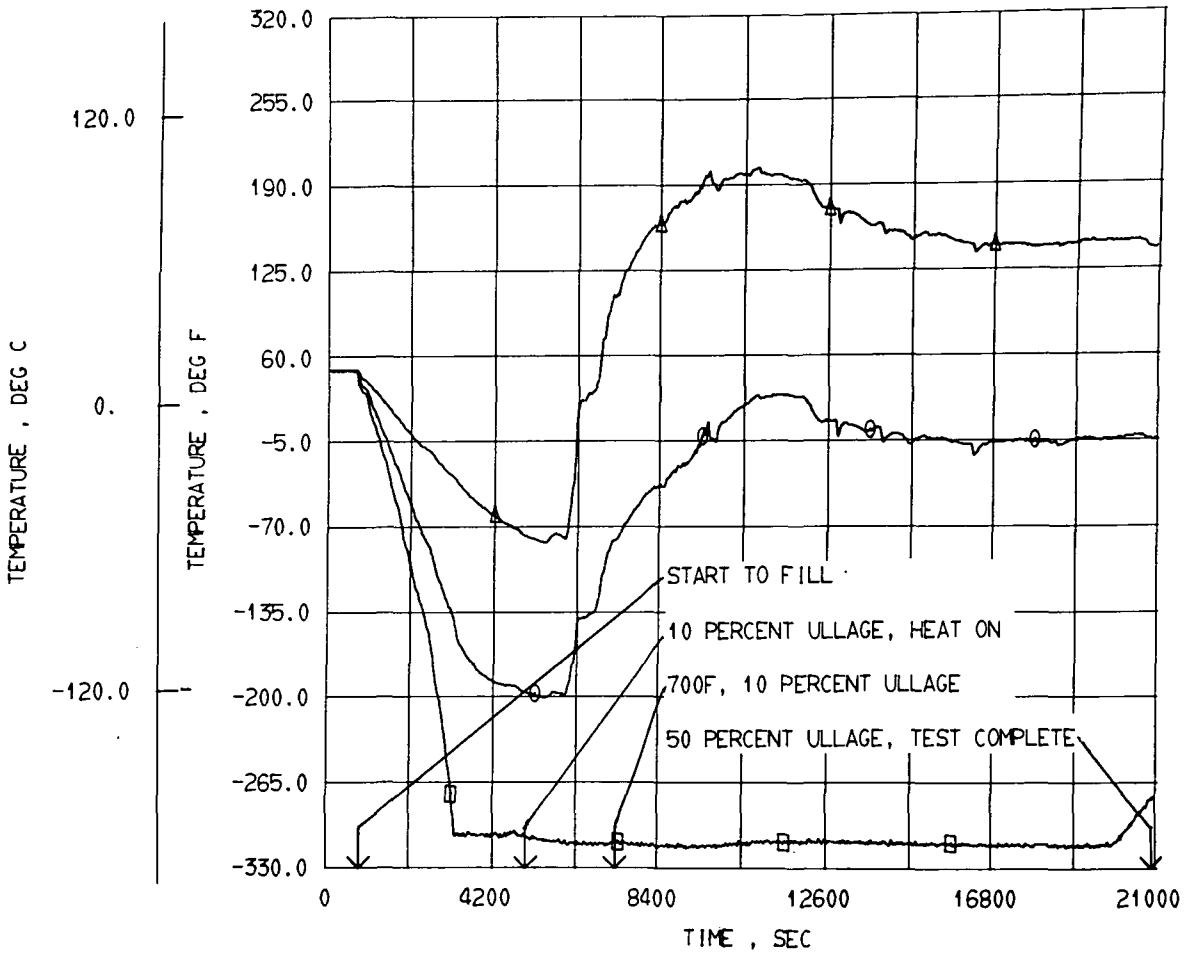

Figure 58. Square tank exterior insulation, initial baseline test, insulation temperature on side.

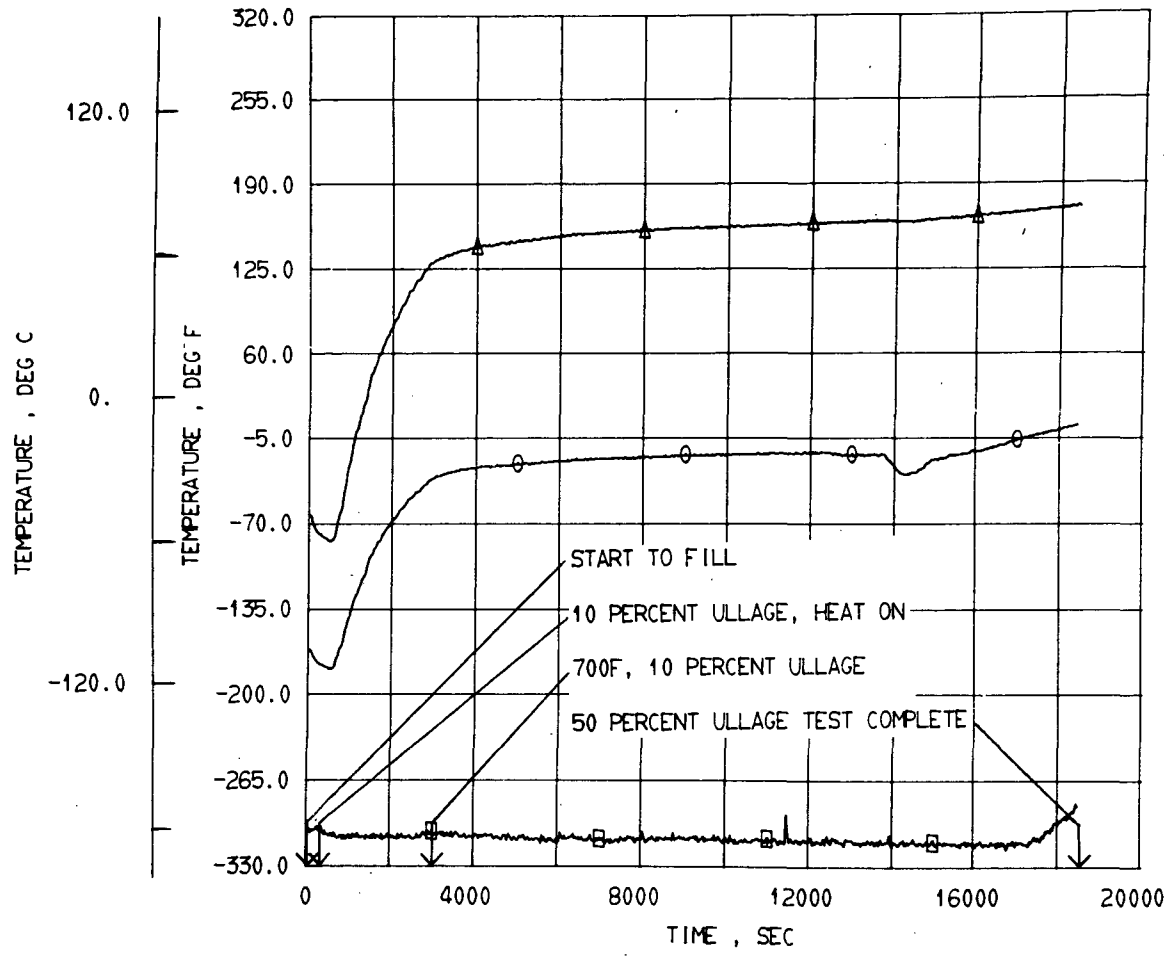

Figure 59. Square tank exterior insulation, final baseline test, insulation temperature on side.

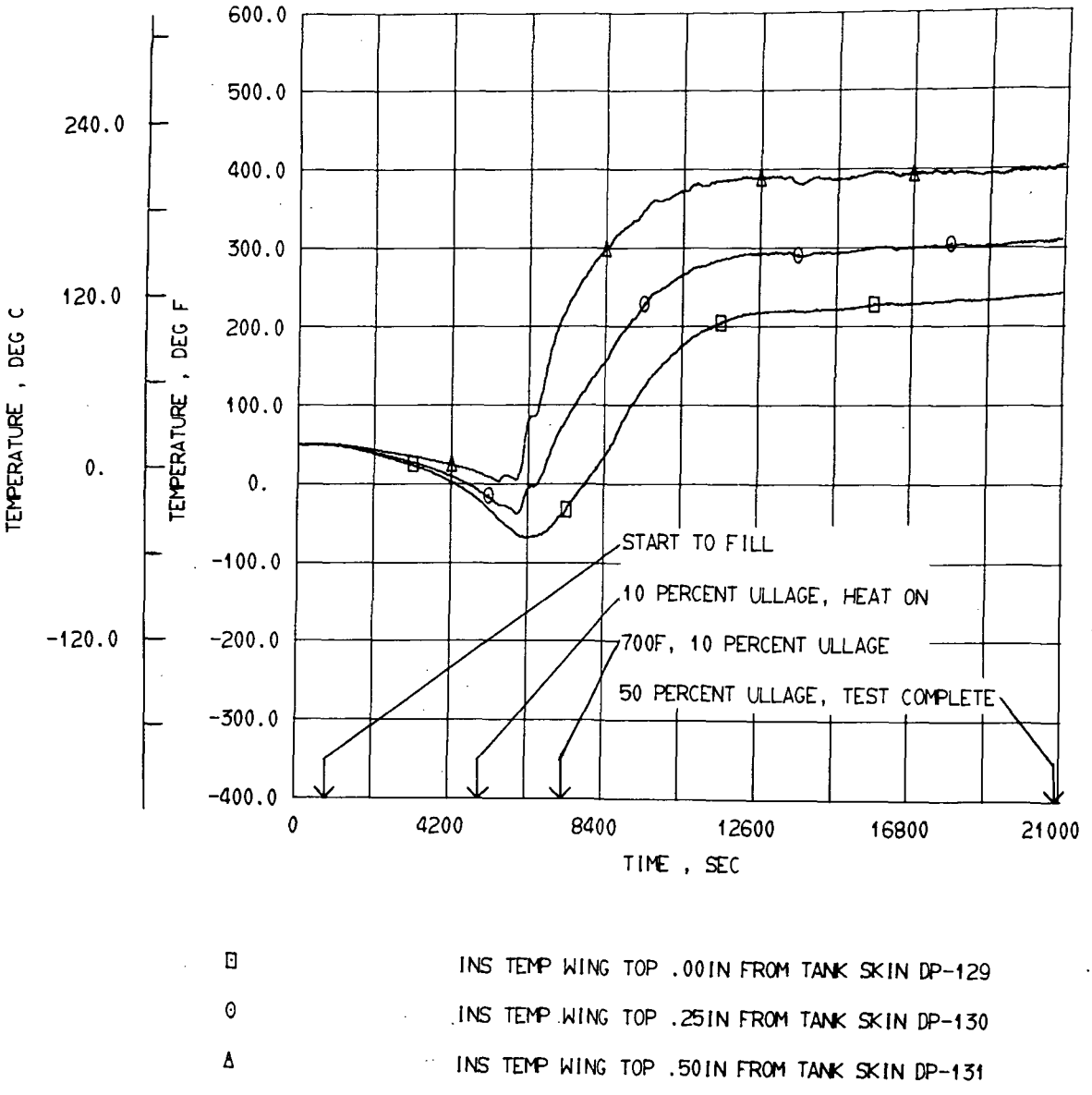

Figure 60. Square tank exterior insulation, initial baseline test, insulation temperatures on wing top.

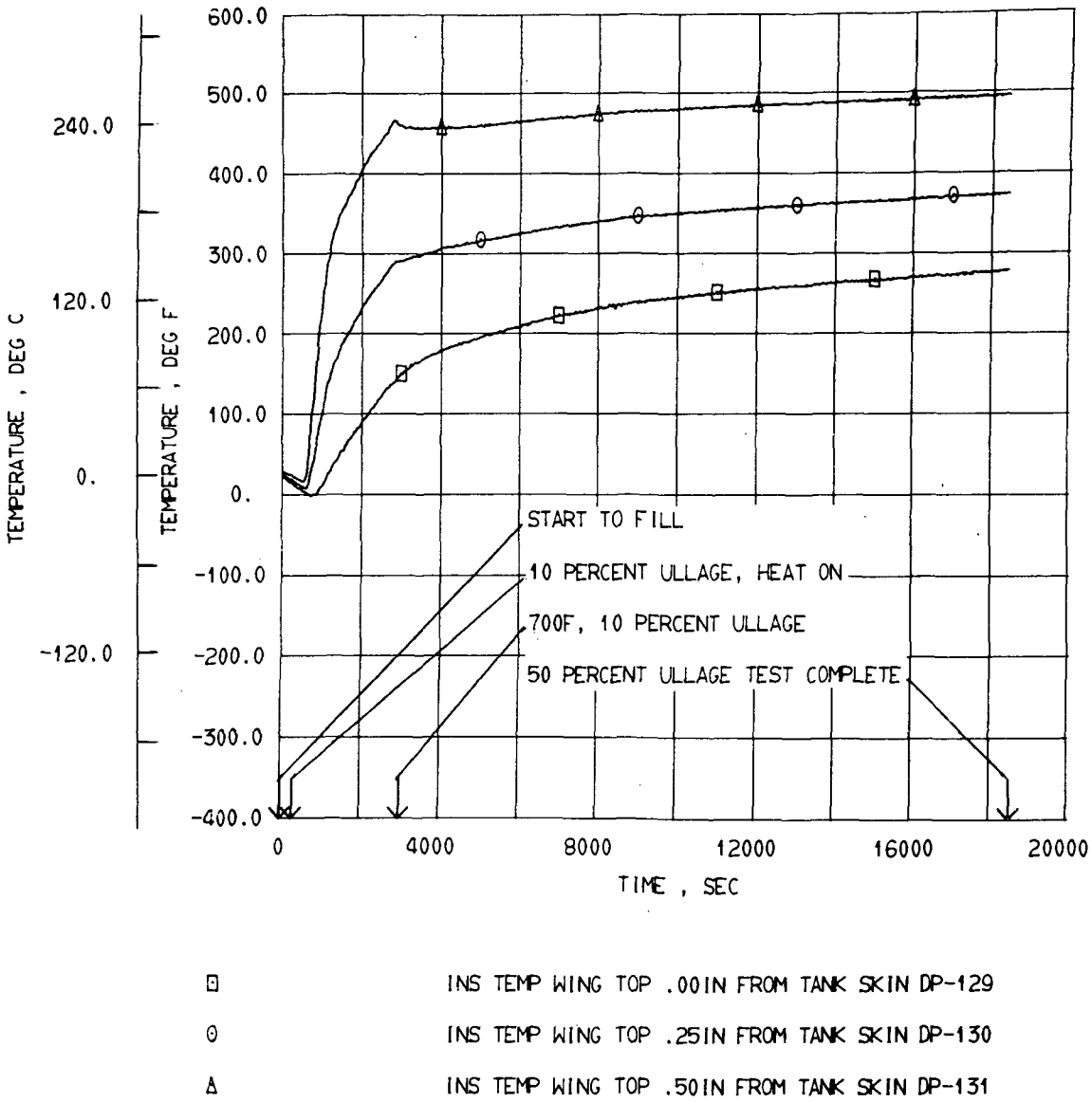

Figure 61. Square tank exterior insulation, final baseline test, insulation temperatures on wing top.

2. Temperature Cycling Tests

After the first baseline test of the tank, a series of 10 temperature cycles were completed. During these tests the simulated wing skin was temperature controlled to a profile shown by figure 62. These cycles provided data for evaluating the insulation during tank fill, simulated ascent, cruise/expulsion, and descent.

A cycle consisted of filling the tank with liquid nitrogen to 10% ullage, holding for 15 min (900s), heating the wing skin to 700°F (371°C), holding the filled tank for 30 min (1.8 ks), draining, holding the empty tank for 30 min (1.8 ks), and then cooling the skin to ambient. A minimum cooling time of 30 min (1.8 ks) between cycles was used.

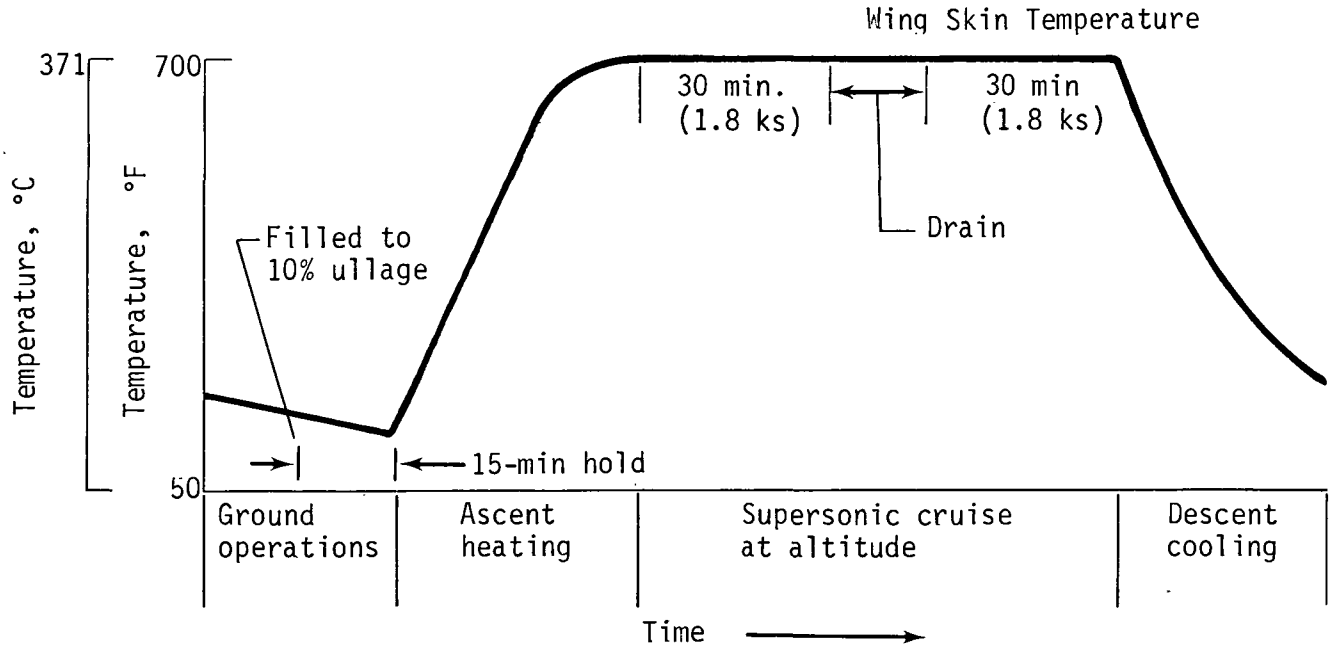

Figure 62. Temperature Cycling.

Figures 63 through 66 give a chronological history of the tank gas pressure, temperatures of the liquid in the tank, the simulated wing structure temperatures, and temperatures of the insulation on the bottom, sides, and top of the tank for temperature cycles 1, 4, 7, and 10. These cycles were considered to be representative of the performance of the insulation during the temperature cycling.

The tank gas pressures during temperature cycling are shown in figures 63 through 66. The only significant item noted on these curves is the temperature/pressure relationship that is brought out quite dramatically. Figure 63 shows Cycle 1 tank pressure and figure 67 Cycle 1 liquid temperatures at the 5, 25, and 50% level and the effects of tank pressure on liquid temperature are noted. At about 8000 sec a 4-psia (2.76 N/cm^2) increase in tank pressure causes a 2.7°F (1.5°C) increase in the liquid temperature. There were some vent rate control problems during Cycle 1 along with a momentary loss of heater power, which accounts for the roughness of the cycle. These were corrected on subsequent tests.

Figures 67 through 74 show the temperature of the liquid at various levels in the tank. The platinum thermometer at the 90% level is the most interesting because it demonstrates the effect of decreasing pressure on temperature at the liquid surface. This effect can be seen when the temperature drops from 0.5°F (0.27°C) to 0.7°F (0.39°C) lower for this probe than for those located deeper in the liquid.

The wing skin temperatures, figures 75 through 78, show the thermal load placed on the insulated tank during each test. As would be expected the top wing skin temperature is 700°F (371.5°C). The bottom skin temperature peaks out at around 530°F (277°C) for Cycles 4, 7, and 10. Cycle 1 shows the effects of the high humidity in the wing chamber plus the momentary loss of power to the heating elements. The bottom wing temperatures are 560°F (294°C) for Cycle 1 and remain at 490°F (255°C) after the heat is removed. The side wing temperatures are 482.5°F (250°C) or 462.9°F (239°C) on Cycle 1 and for 4, 7, and 10 they all peak out at about 583.4°F (306°C). The high humidity is suspect for this phenomena because the dew point for the respective cycles was +32°F (0°C) for Cycle 1, -2°F (-18.9°C) for Cycle 4, -10°F (-23.3°C) for Cycle 7, and -35°F (-37.2°C) for Cycle 10.

The insulation temperatures during the temperature cycles are shown in figures 79 through 94. Figures 79 through 86 show the temperature gradient through the bottom insulation. Again the effect of the high dew point can be seen in Cycle 1. The gradient is not as distinct as it is for Cycles 4, 7, and 10. It should also be noted that there does not appear to be any degradation of the insulation with time. For example, the insulation temperature 2.0 in. (5.07 cm) in from the wing skin and 3.0 in. (7.61 cm) in

from the wing skin reaches 290°F (143°C) and -5°F (-20.5°C), respectively, during Cycles 4, 7, and 10. This is repeatable for each of these cycles.

Figures 87 through 94 show the insulation temperatures at the side of the tank and at the tank top. It can again be seen that there is no insulation degradation due to the temperature cycles, and as the dew point gets lower in the wing the data is more repeatable.

As the data show and inspection confirmed, there was no damage to the insulation due to temperature cycling.

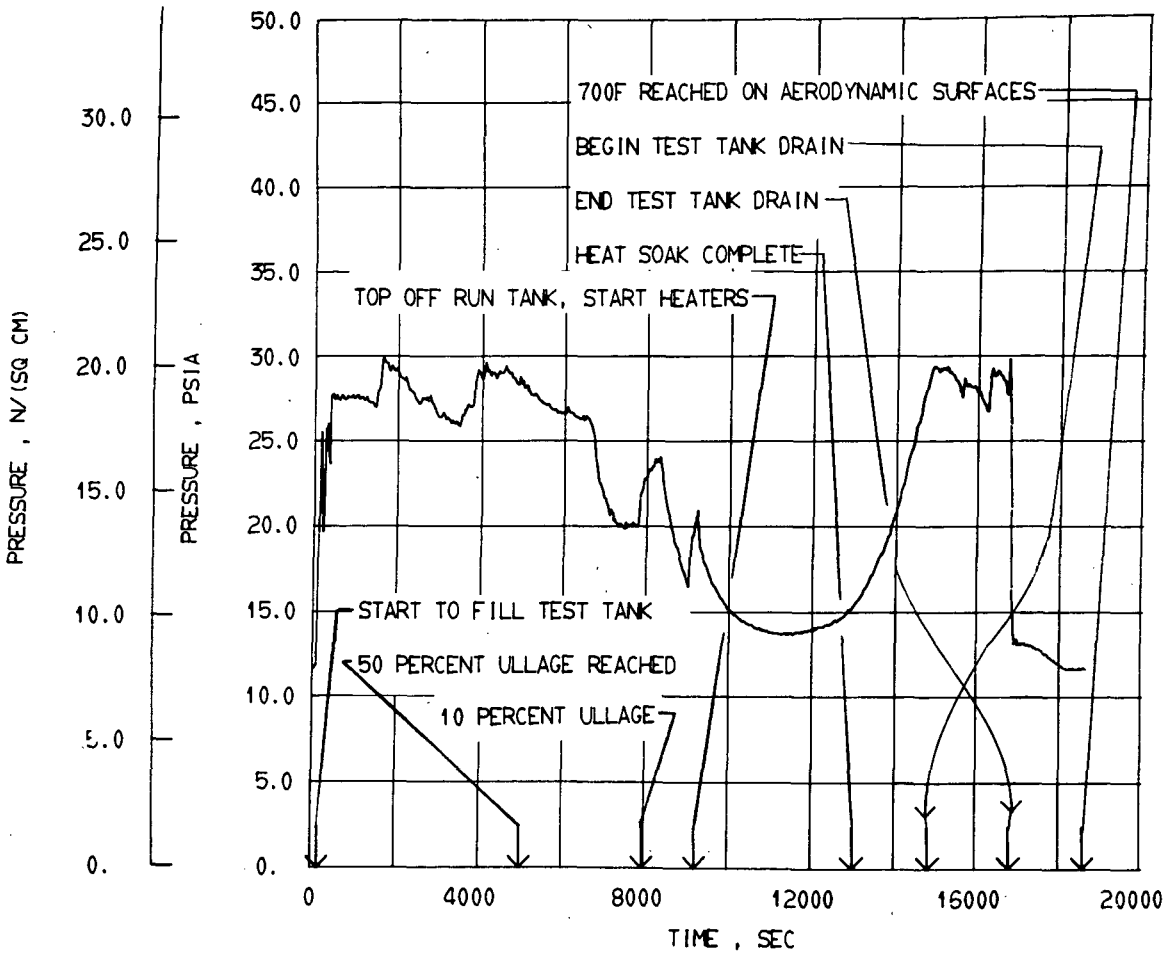

Figure 63. Square tank exterior insulation, temperature cycle 1, test tank pressure.

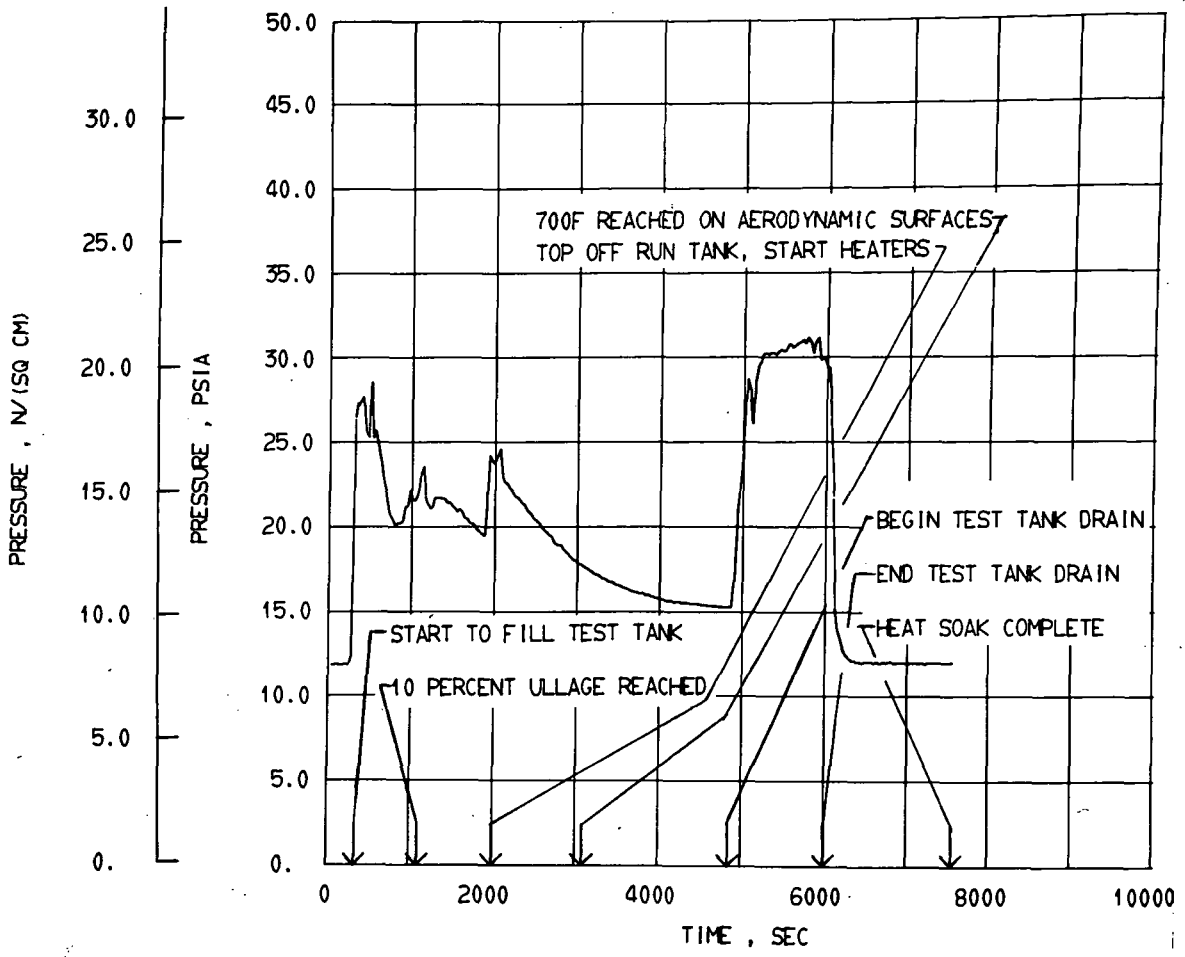

Figure 64. Square tank exterior insulation, temperature cycle 4, test tank pressure.

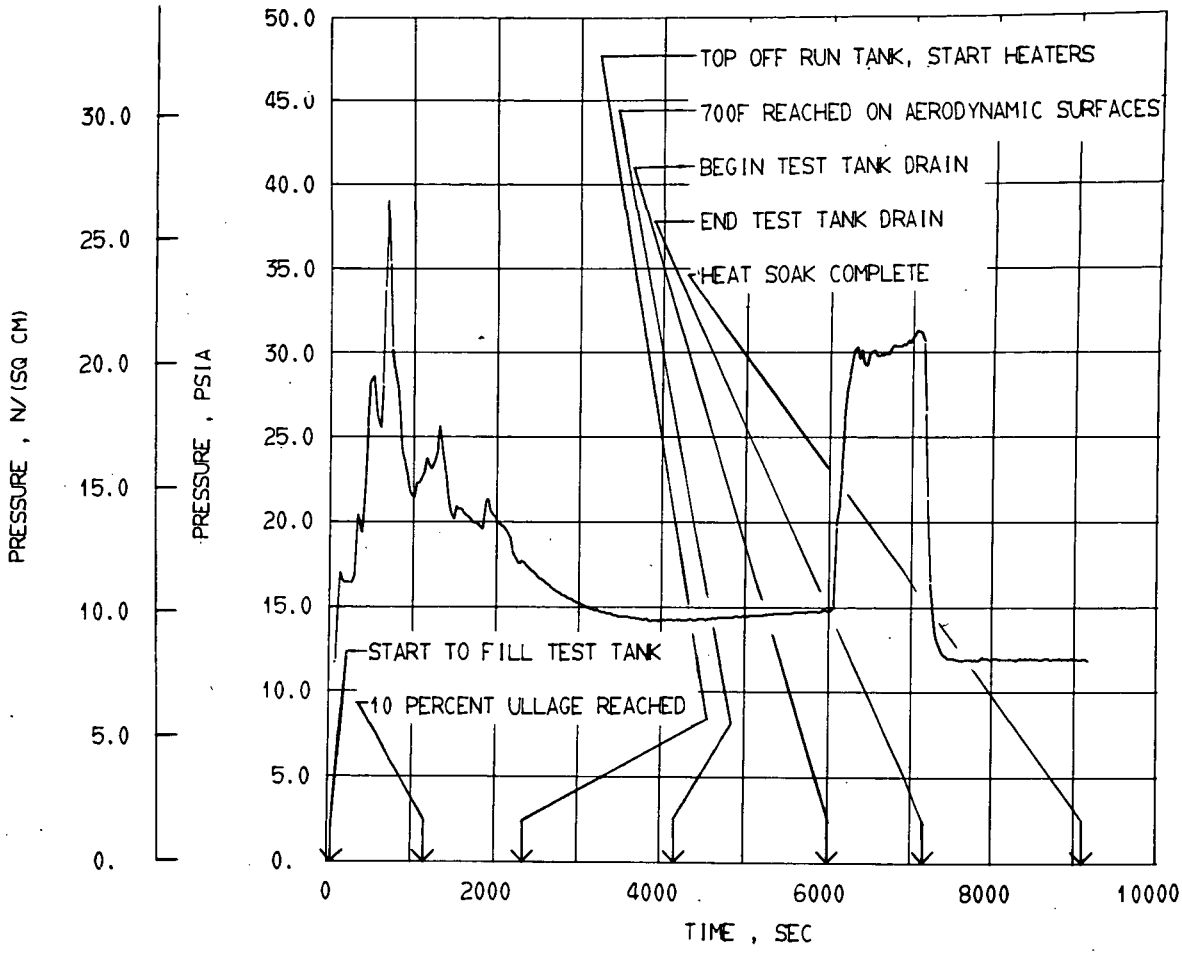

Figure 65. Square tank exterior insulation, temperature cycle 7, test tank pressure.

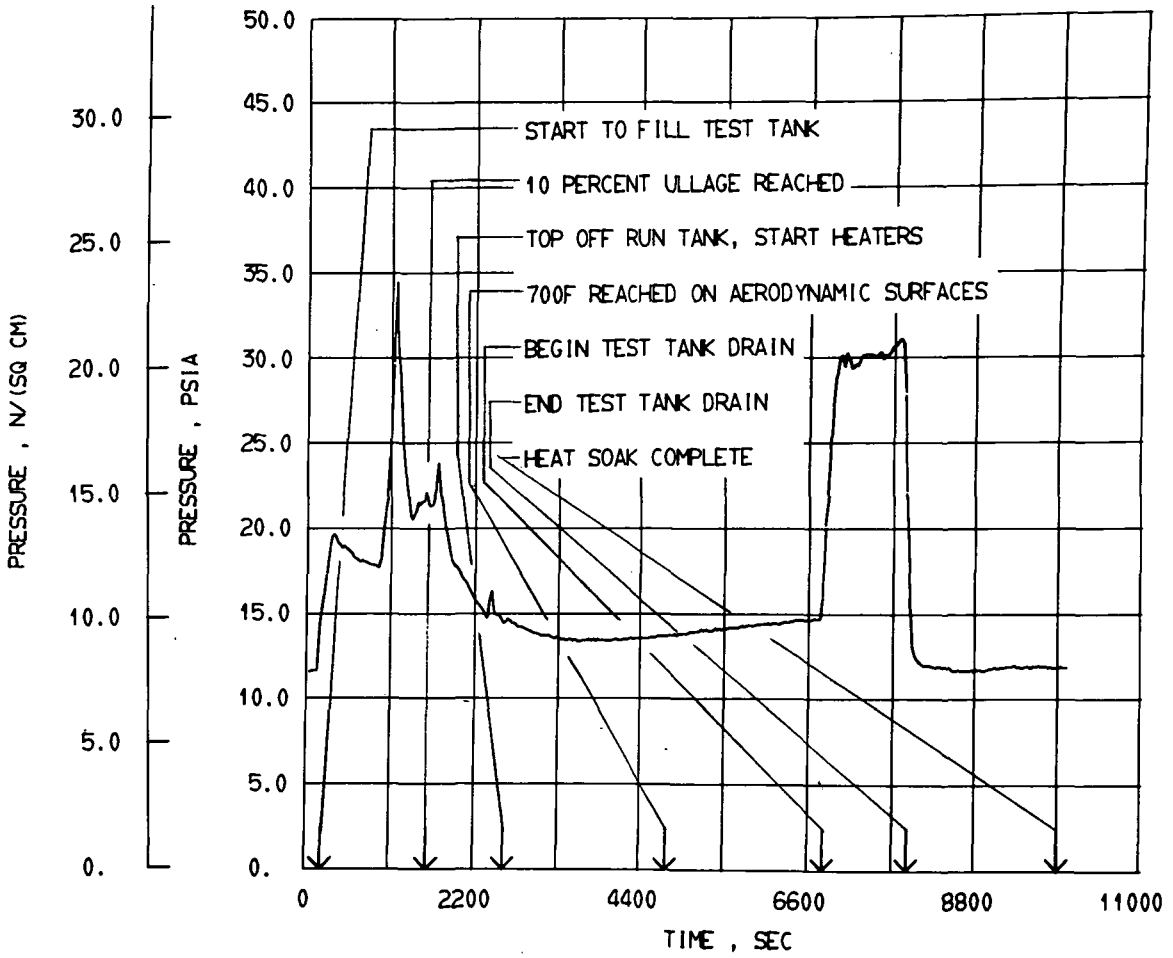

Figure 66. Square tank exterior insulation, temperature cycle 10, test tank pressure.

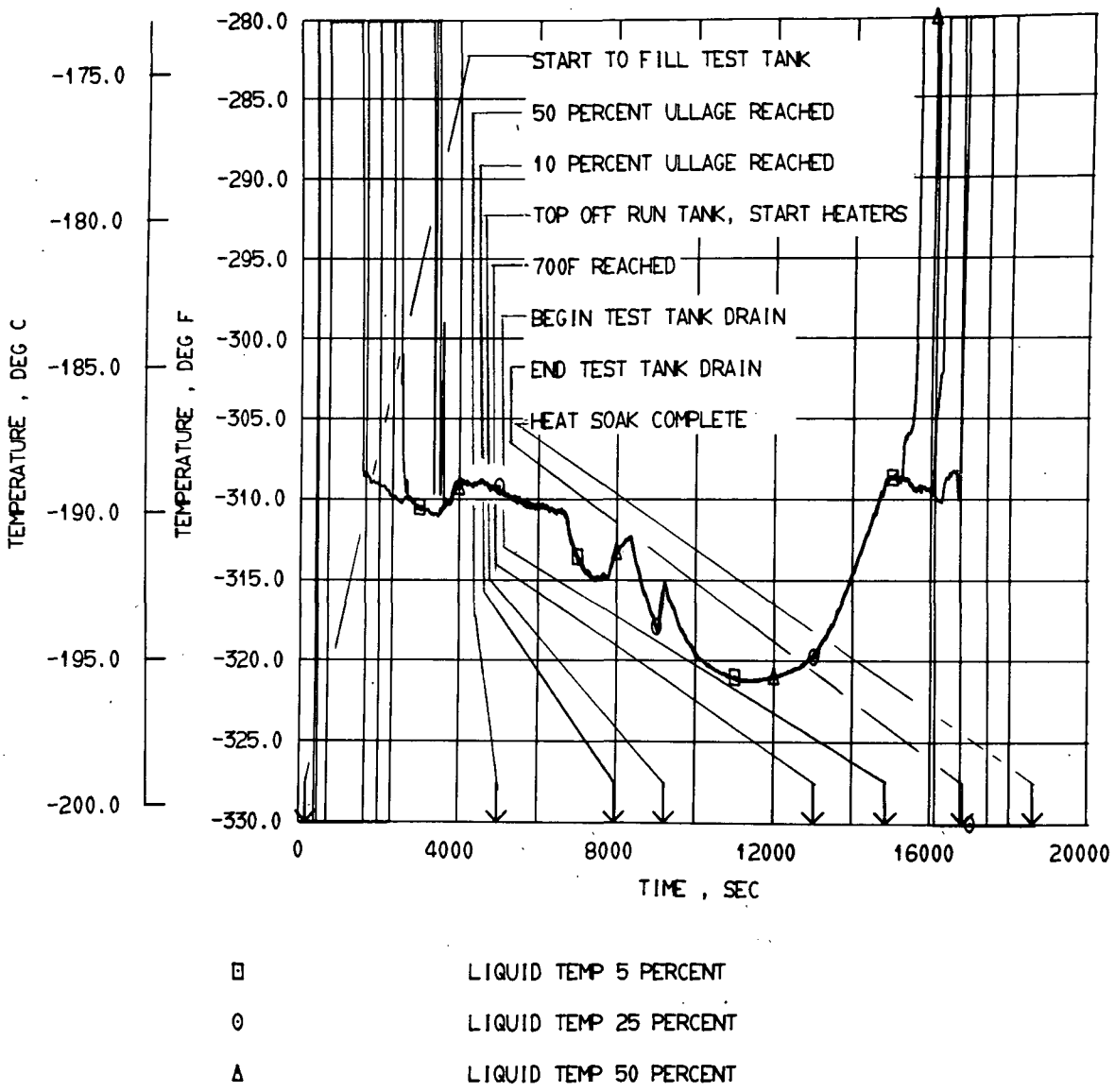

Figure 67. Square tank exterior insulation, temperature cycle 1, liquid temperatures at 5,25 and 50% levels.

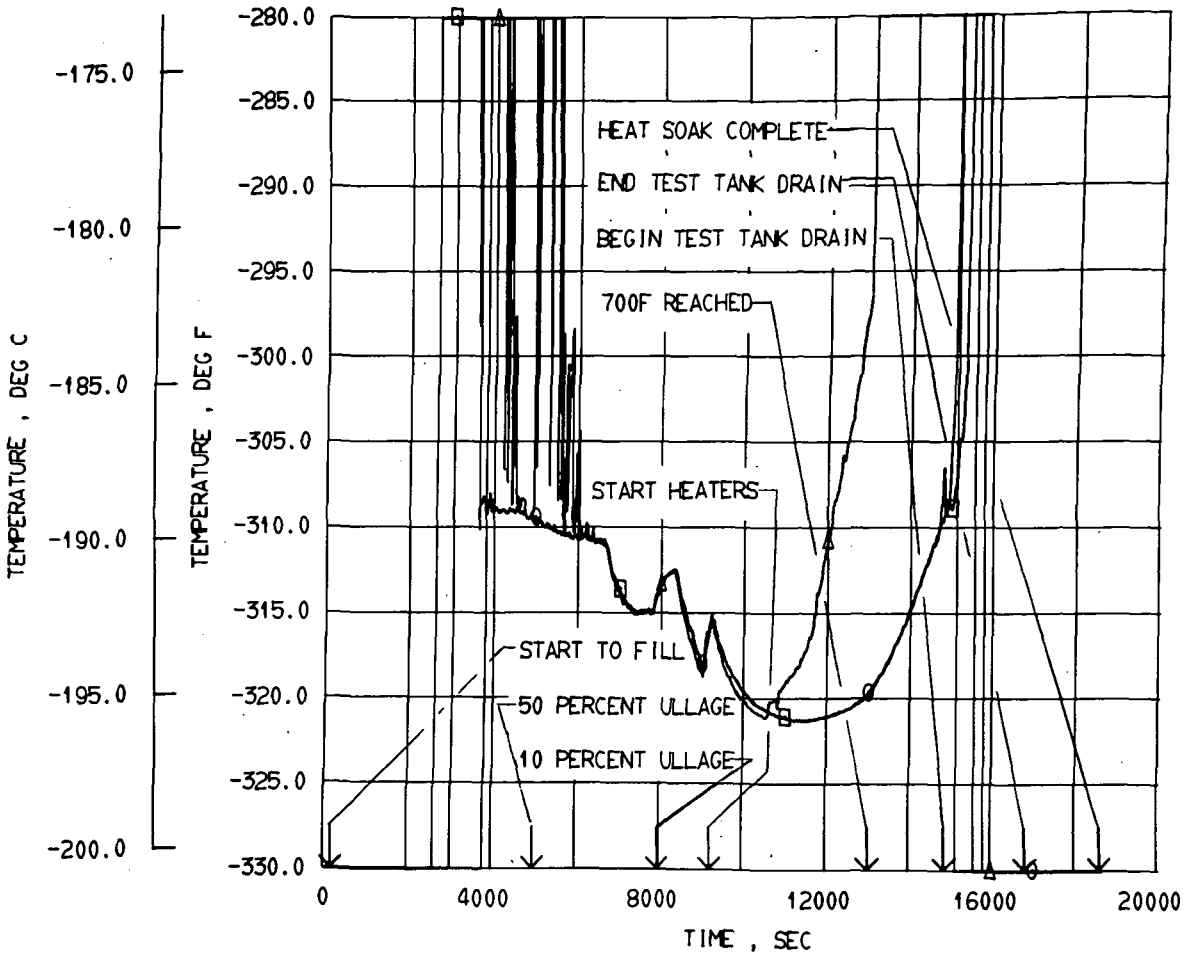

Figure 68. Square tank exterior insulation, temperature cycle 1, liquid temperatures at 60,75 and 90% levels.

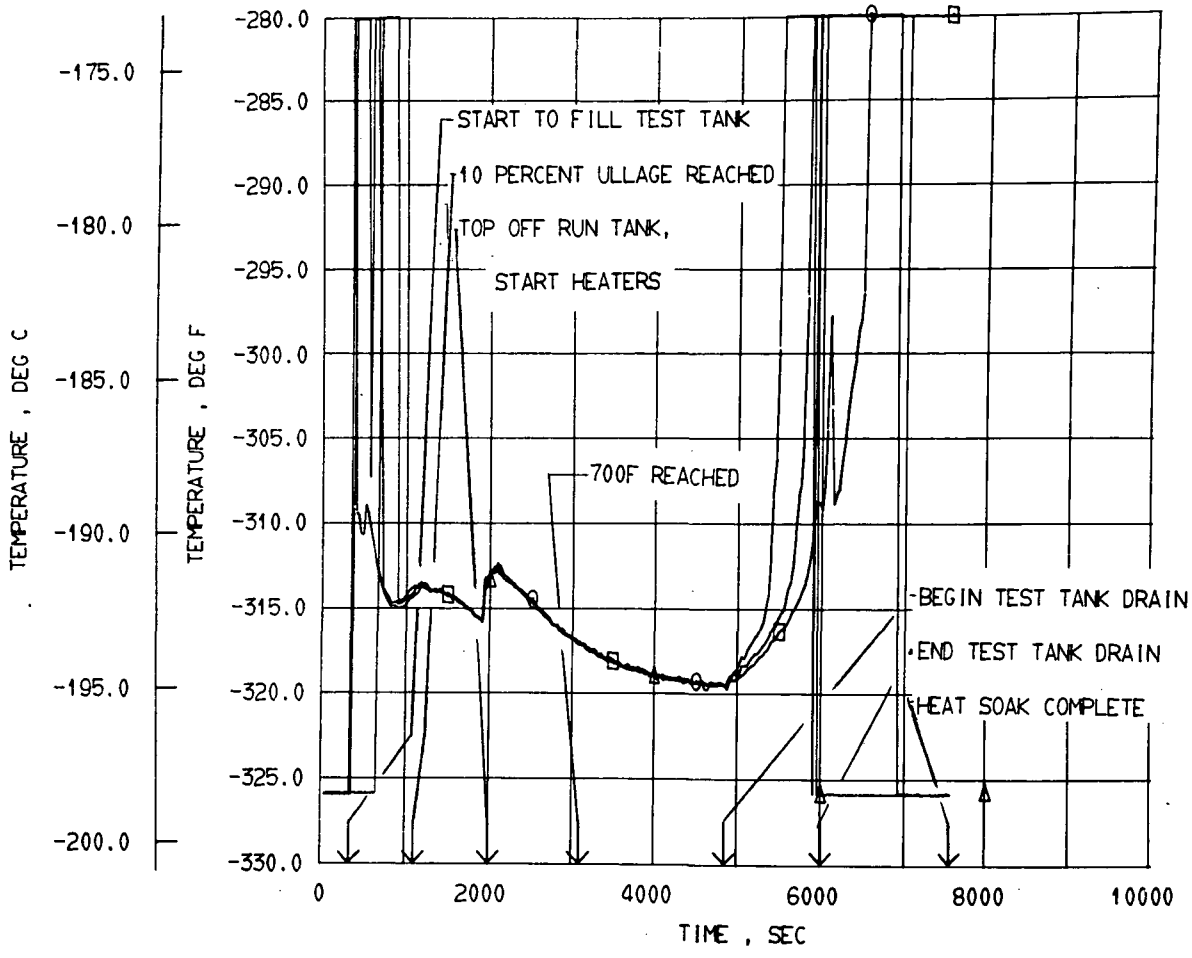

Figure 69. Square tank exterior insulation, temperature cycle 4, liquid temperatures at 5,25 and 50% levels.

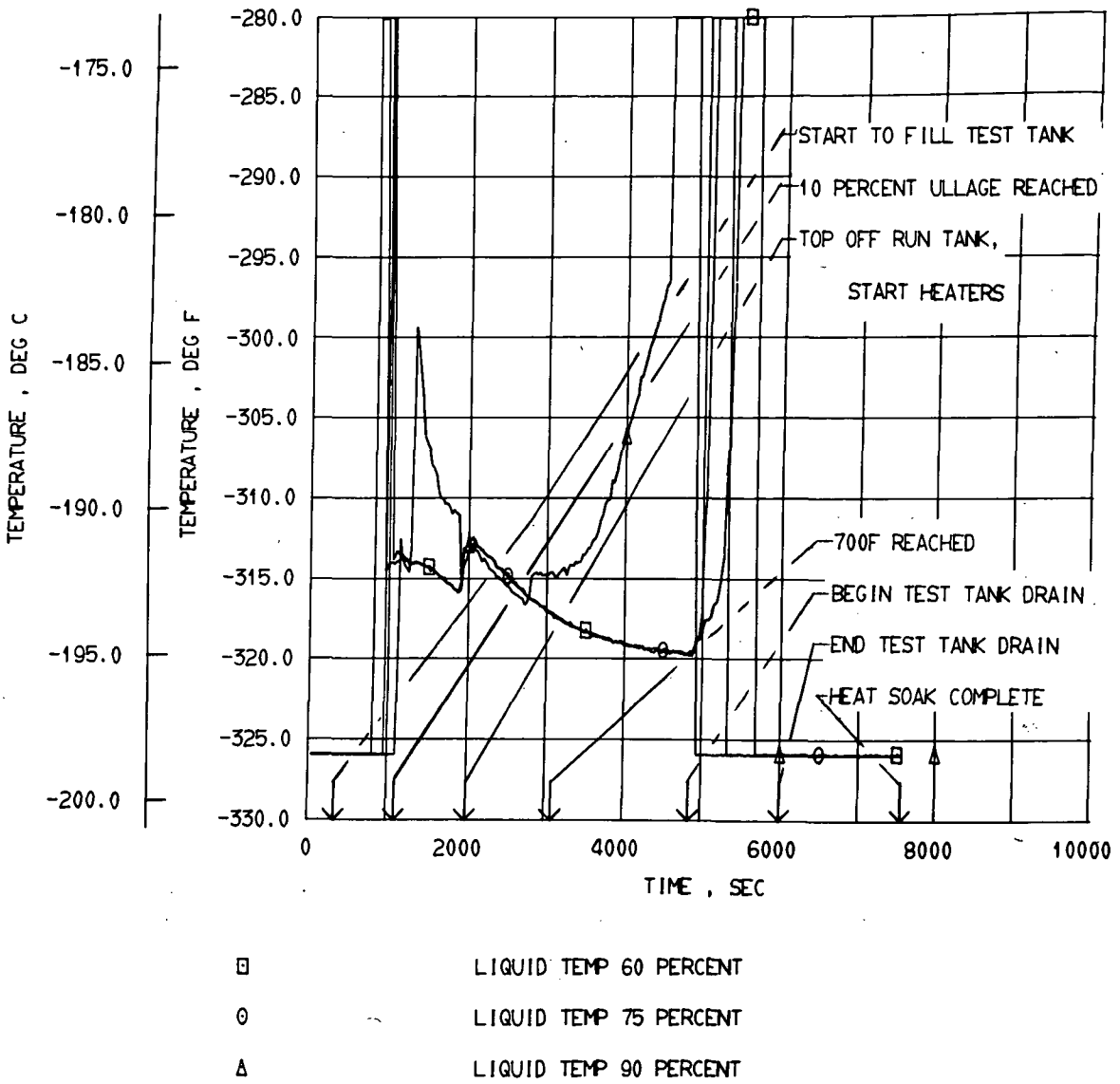

Figure 70. Square tank exterior insulation, temperature cycle 4, liquid temperatures at 60,75 and 90% levels.

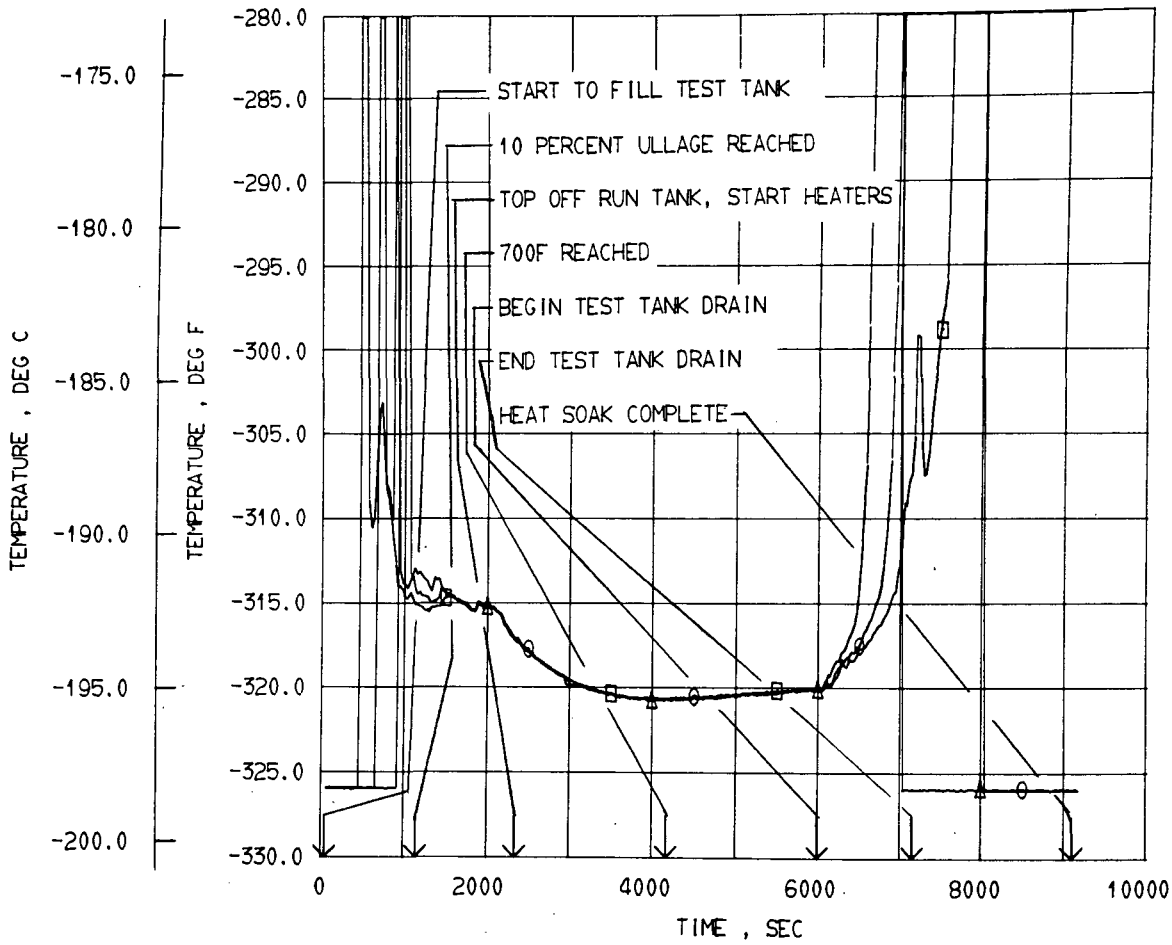

Figure 71. Square tank exterior insulation, temperature cycle 7, liquid temperatures at 5,25 and 50% levels.

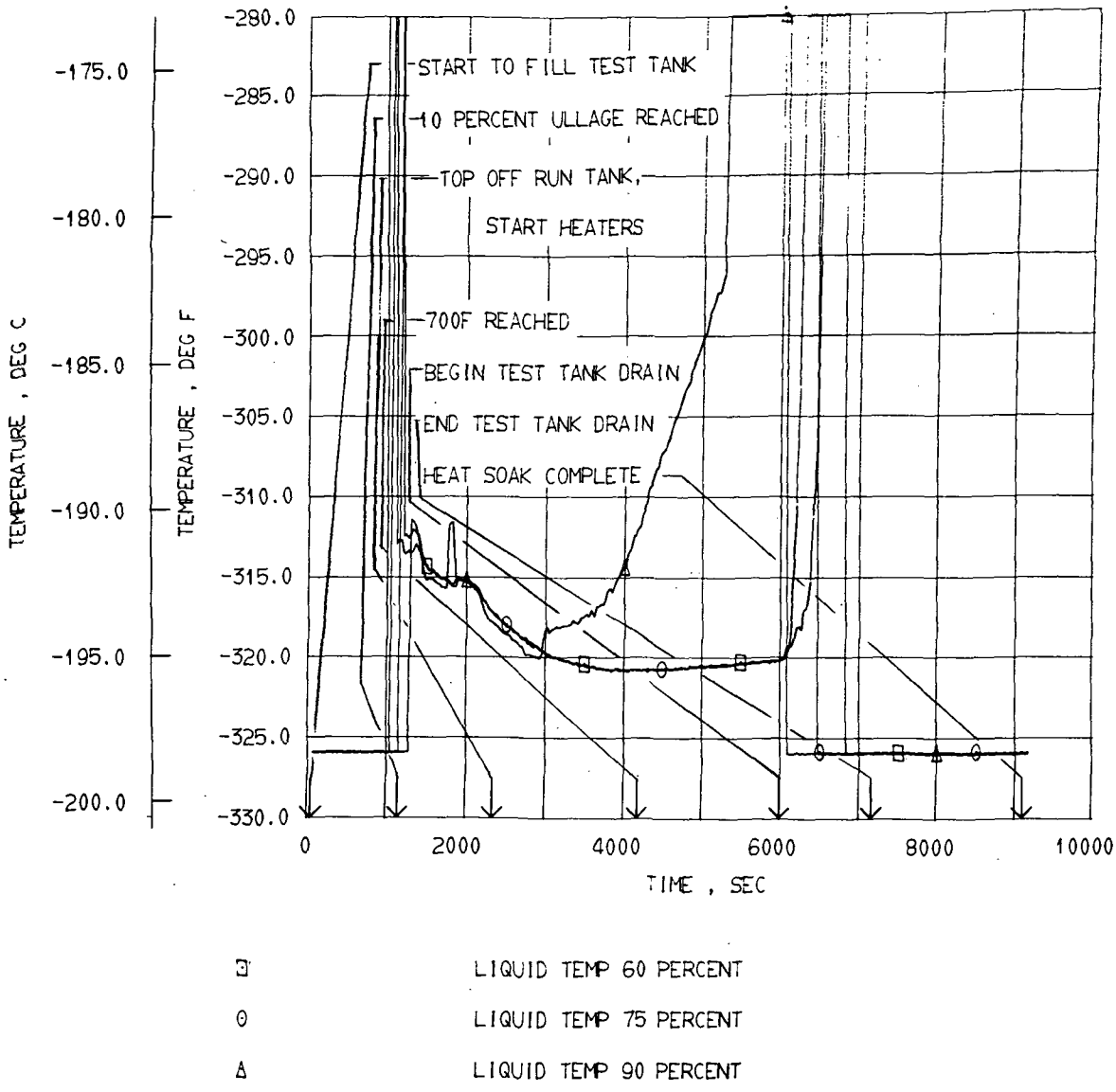

Figure 72. Square tank exterior insulation, temperature cycle 7, liquid temperatures at 60,75 and 90% levels.

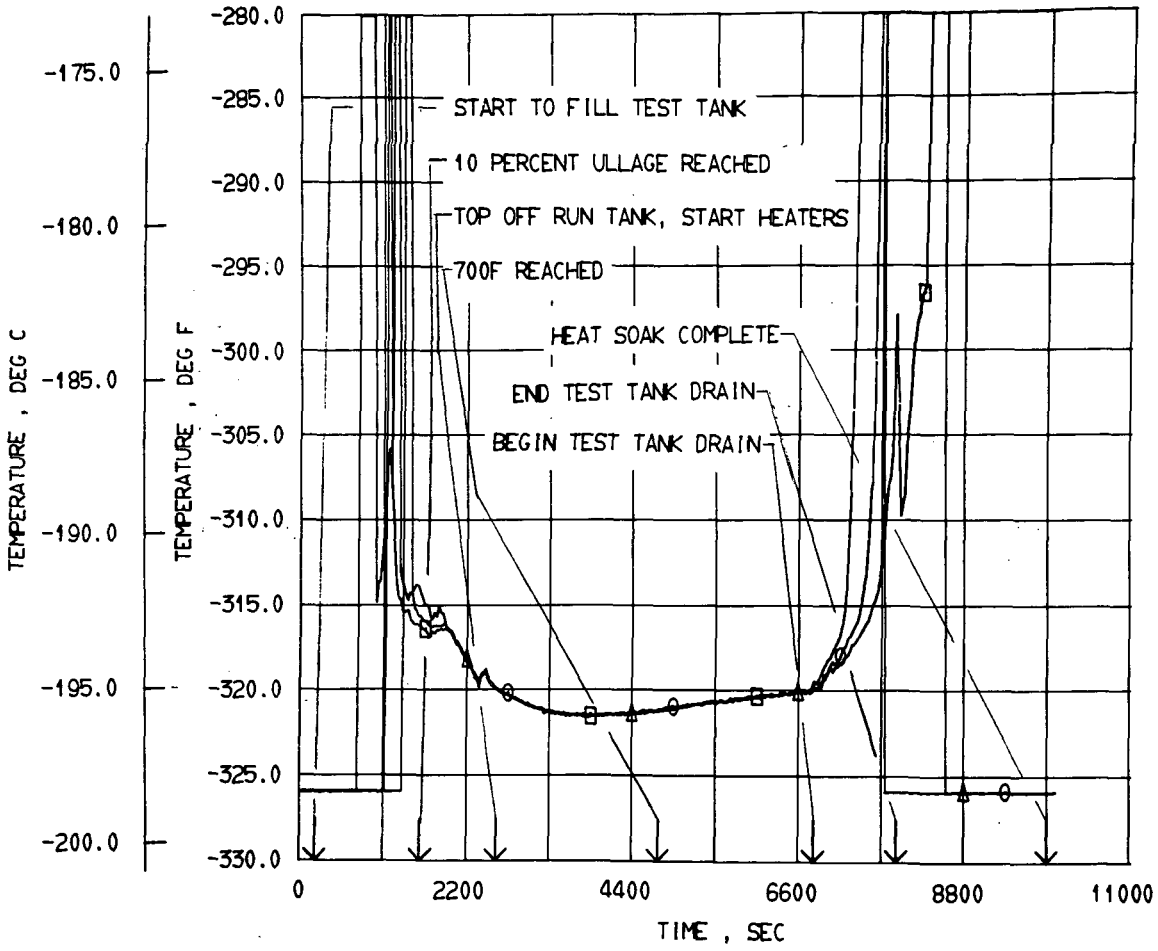

Figure 73. Square tank exterior insulation, temperature cycle 10, liquid temperatures at 5, 25 and 50% levels.

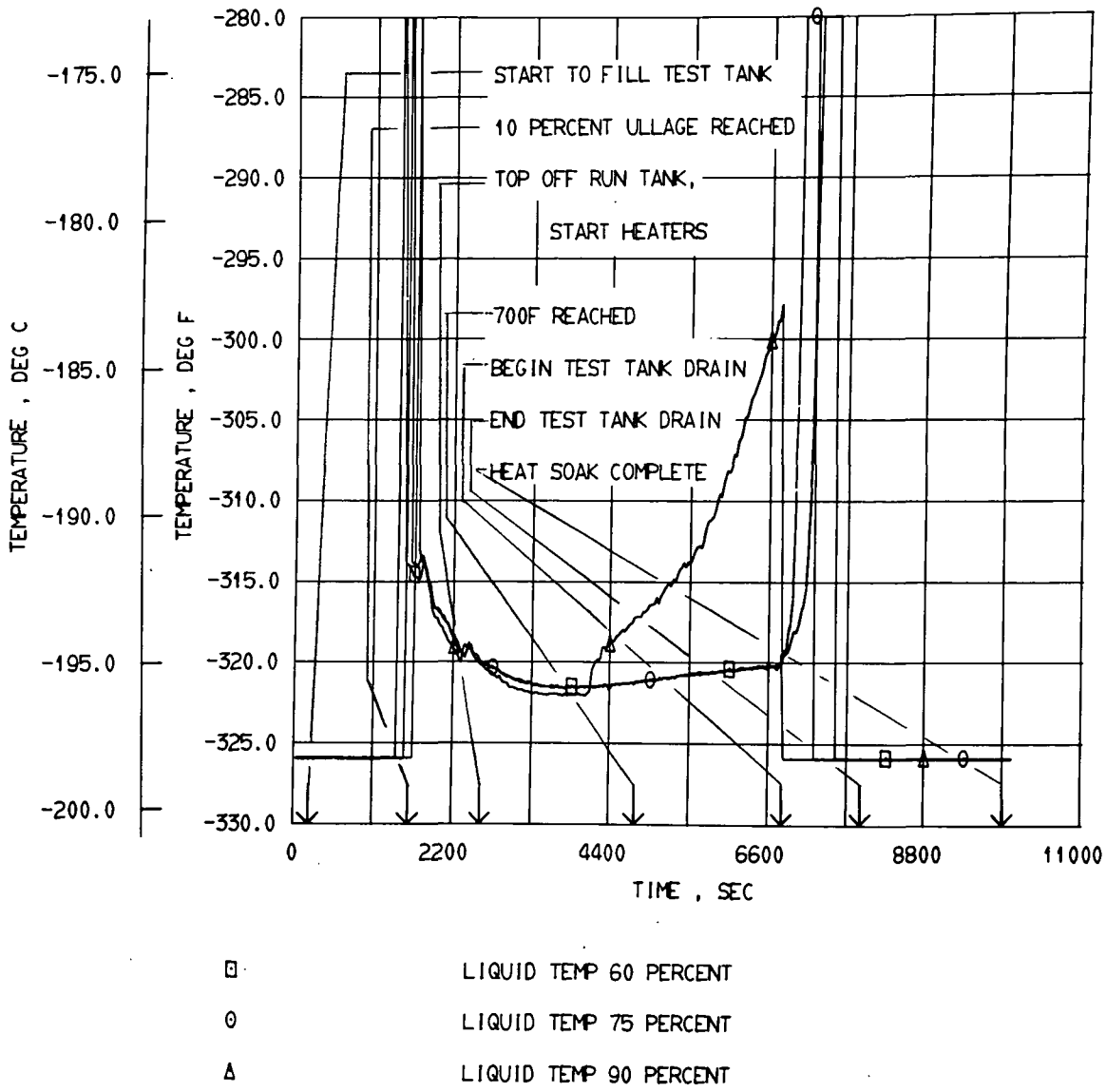

Figure 74. Square tank exterior insulation, temperature cycle 10, liquid temperatures at 60,75 and 90% levels.

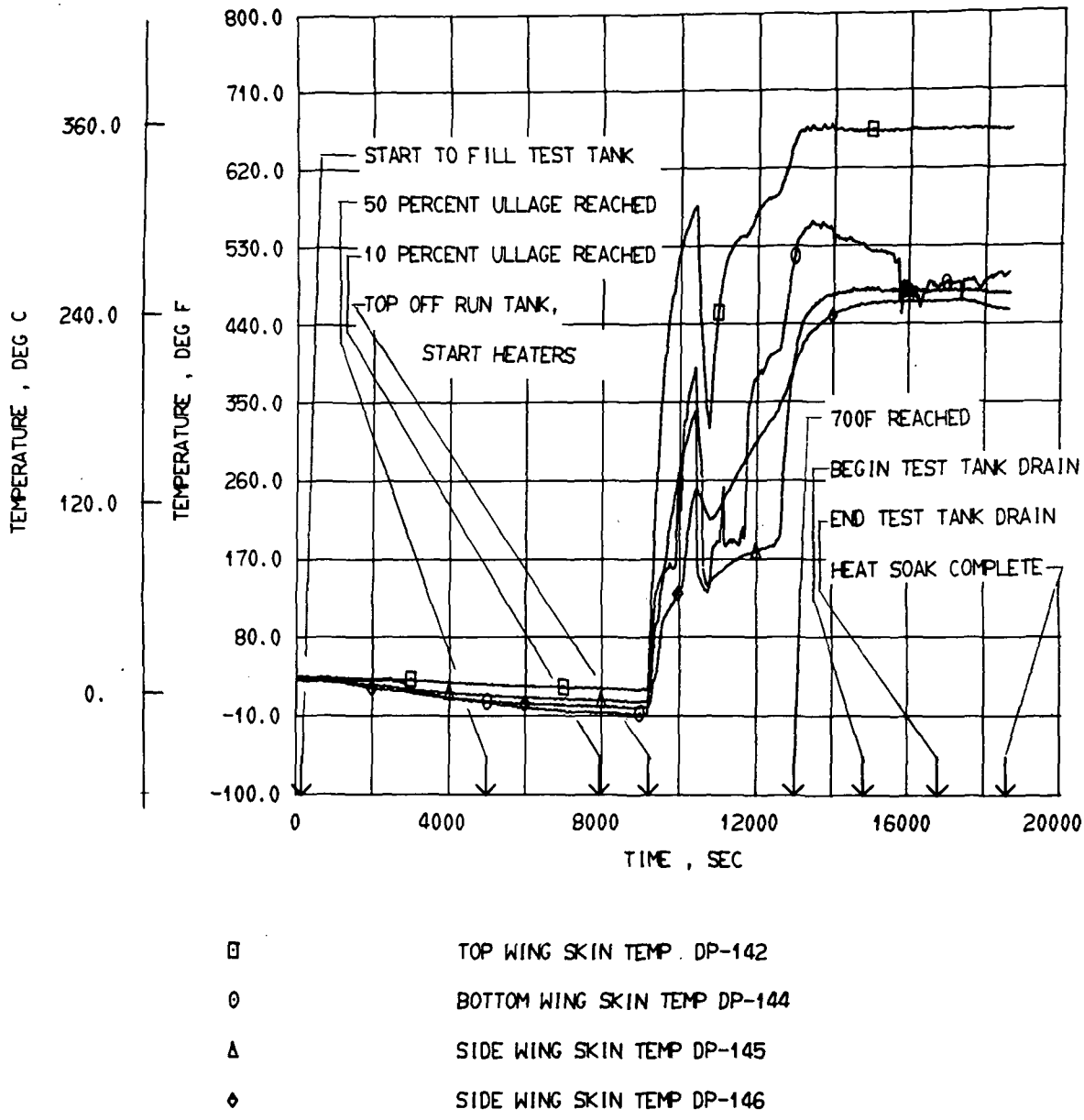

Figure 75. Square tank exterior insulation, temperature cycle 1, top, bottom and side wing skin temperatures.

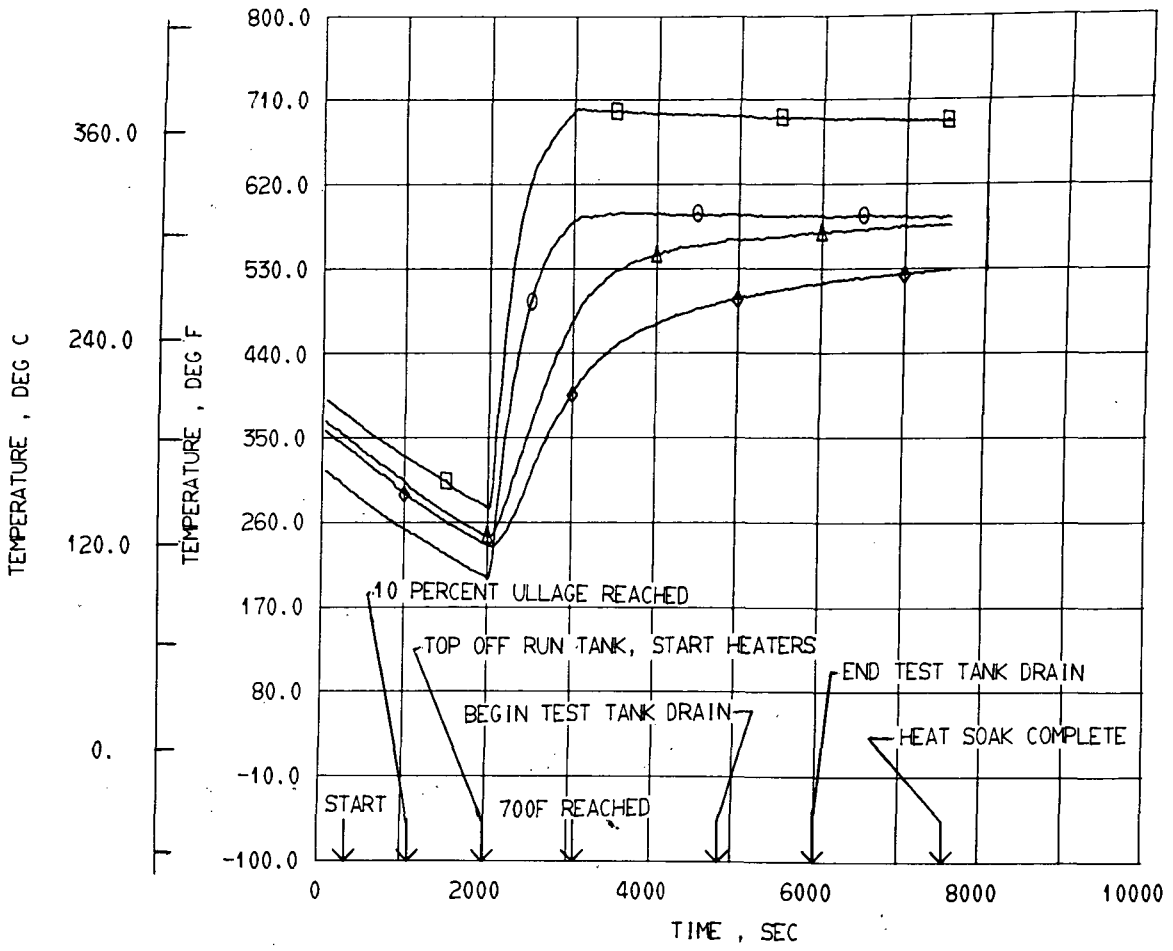

Figure 76. Square tank exterior insulation, temperature cycle 4, top, bottom and side wing skin temperatures.

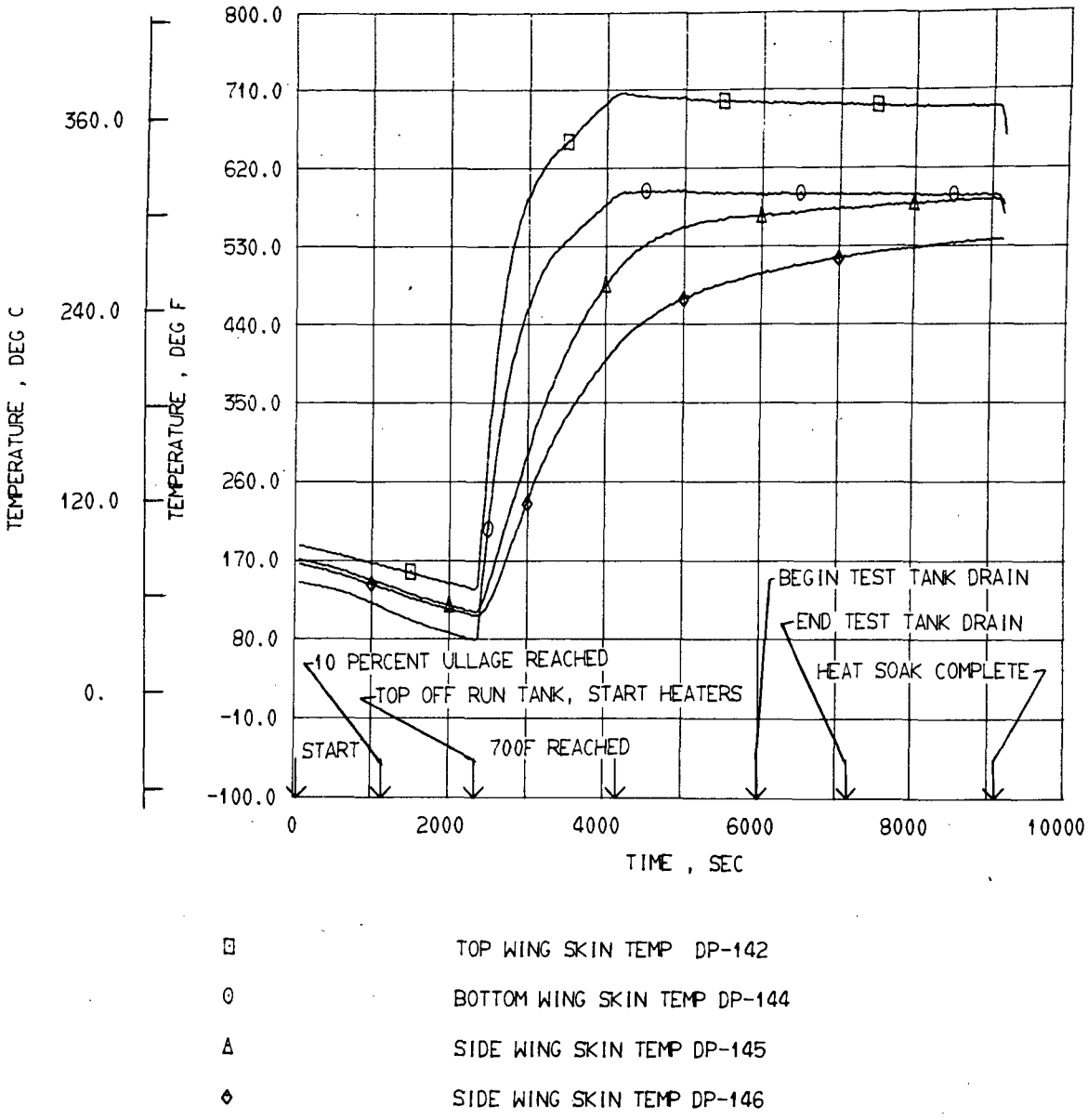

Figure 77. Squre tank exterior insulation, temperature cycle 7, top, bottom and side wing skin temperatures.

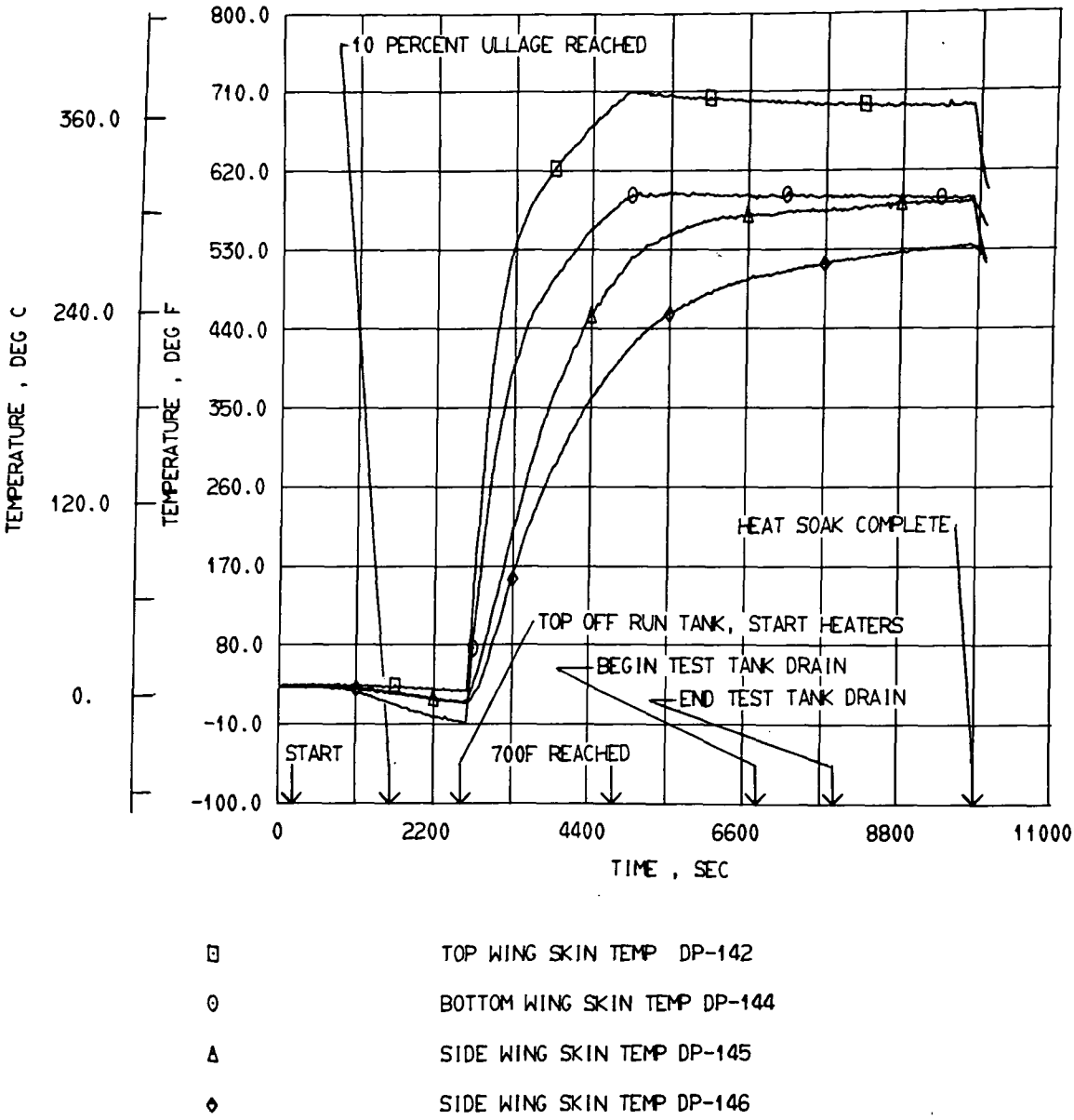

Figure 78. Square tank exterior insulation, temperature cycle 10, top, bottom and side wing skin temperatures.

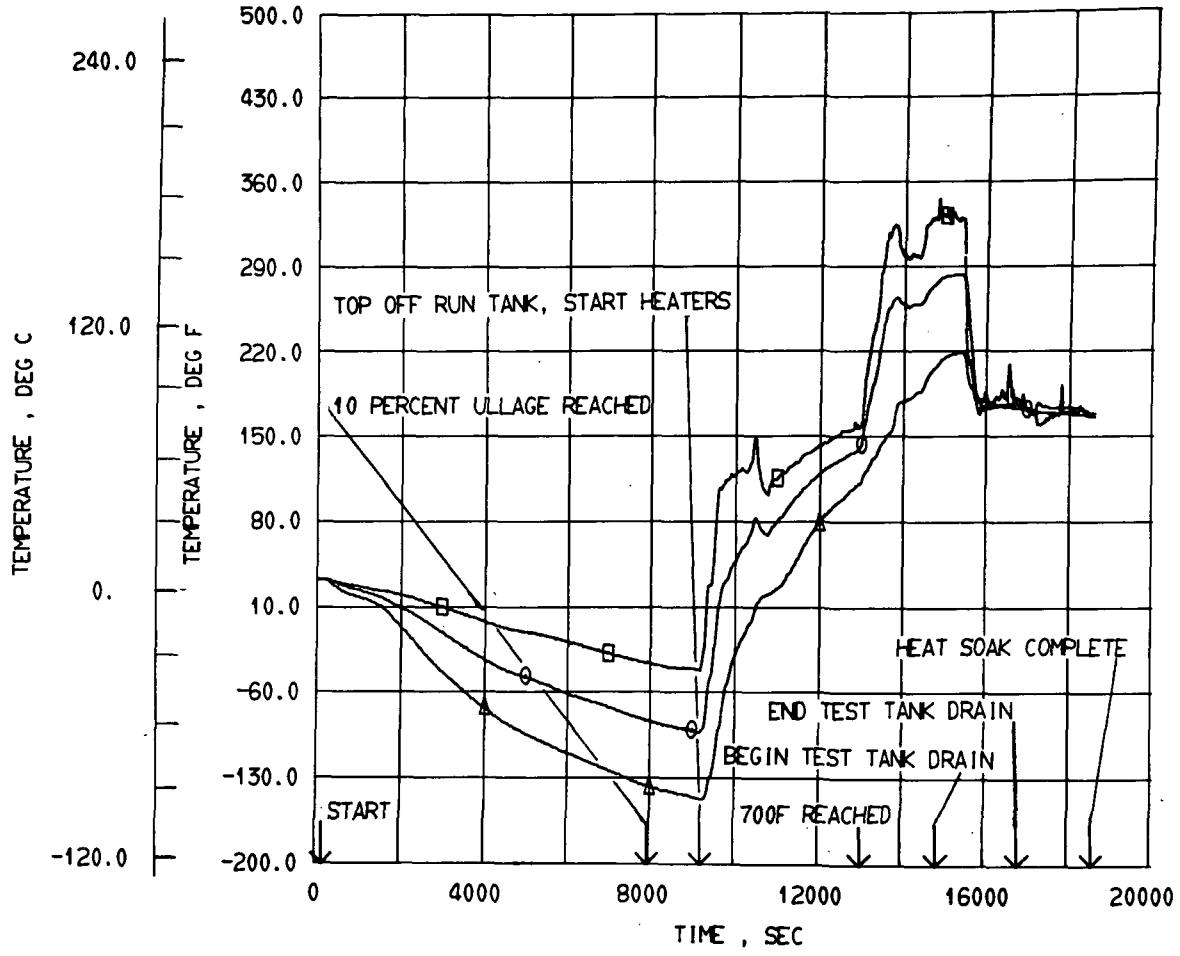

Figure 79. Square tank exterior insulation, temperature cycle 1, wing bottom insulation temperatures.

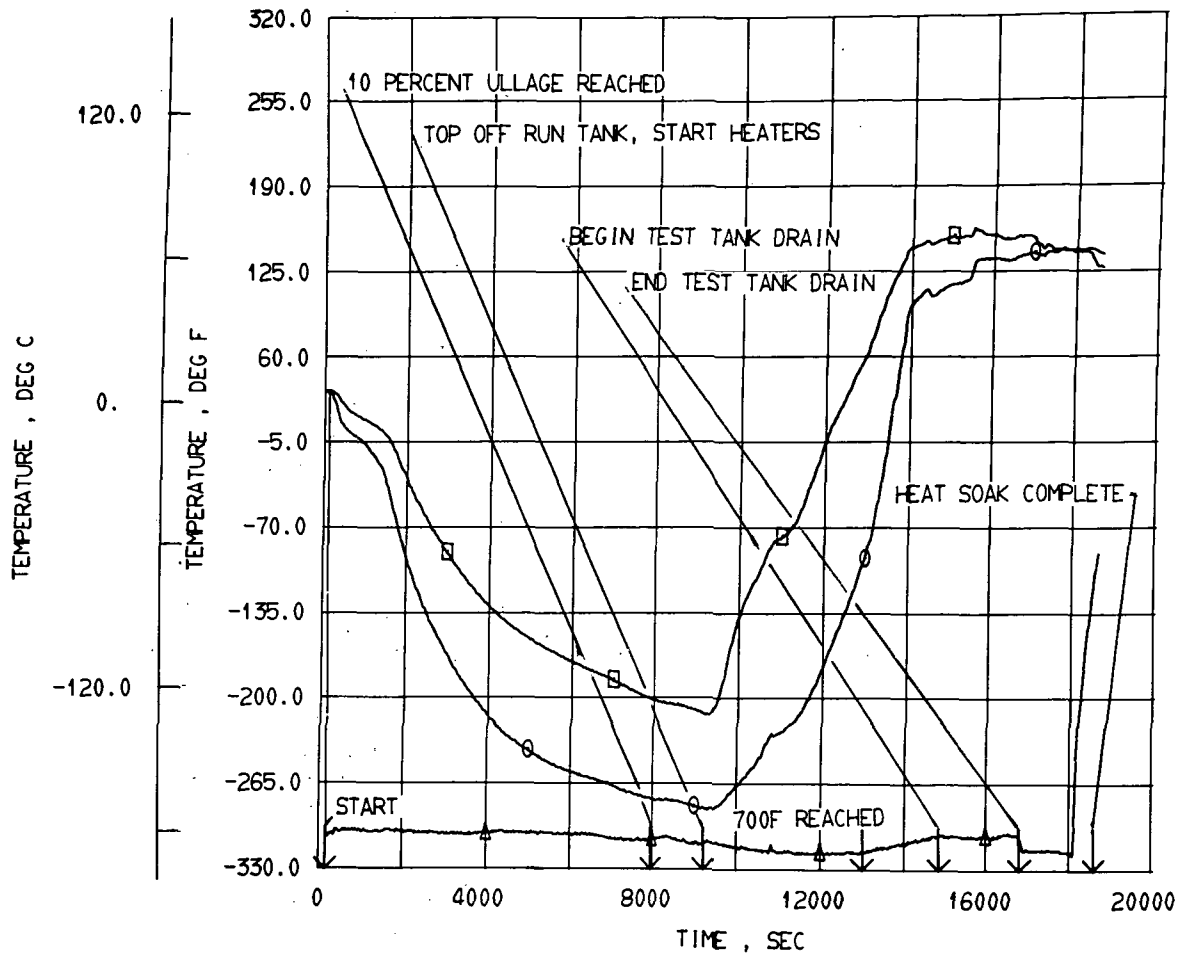

Figure 80. Square tank exterior insulation, temperature cycle 1, wing bottom insulation temperatures.

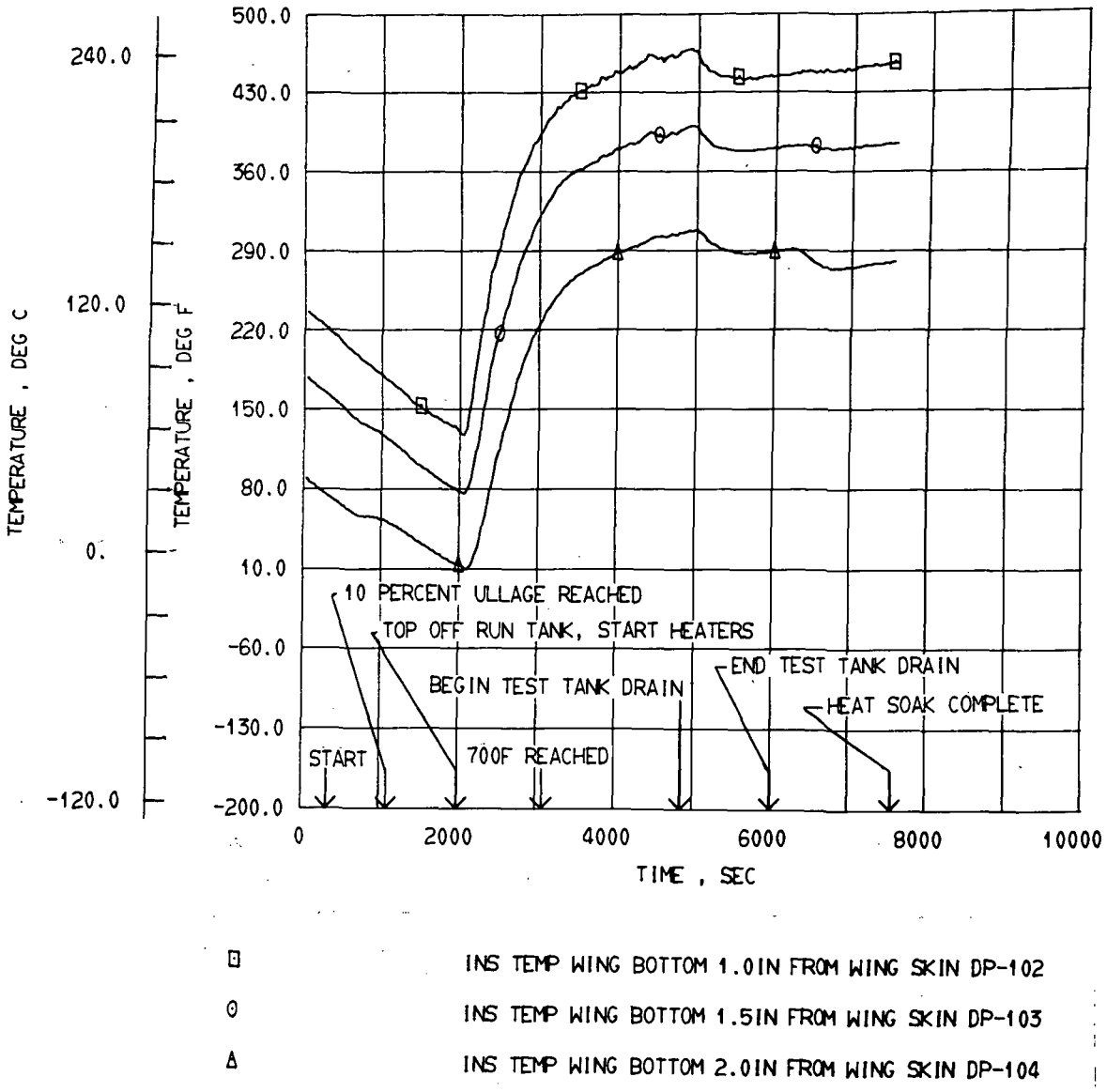

Figure 81. Square tank exterior insulation, temperature cycle 4, wing bottom insulation temperatures.

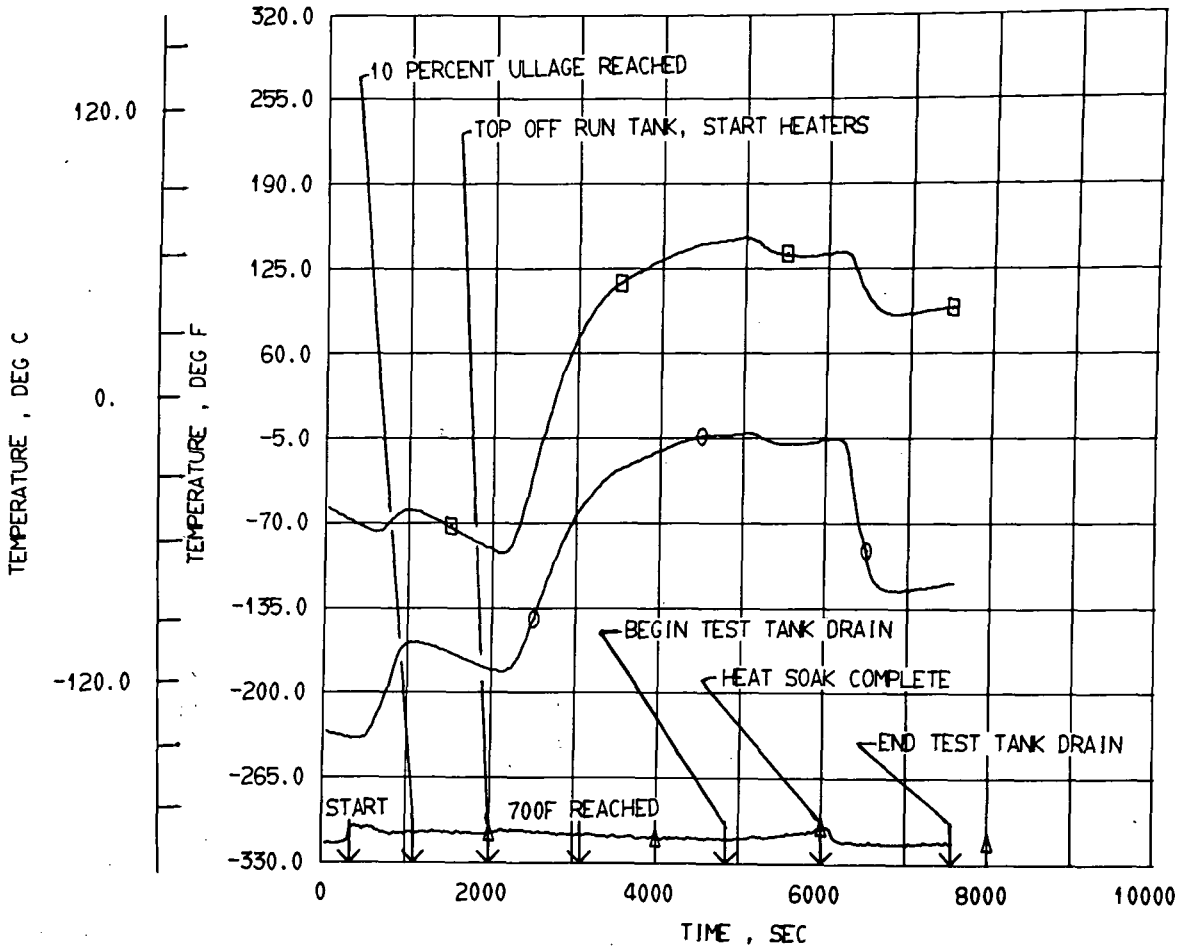

Figure 82. Square tank exterior insulation, temperature cycle 4, wing bottom insulation temperatures.

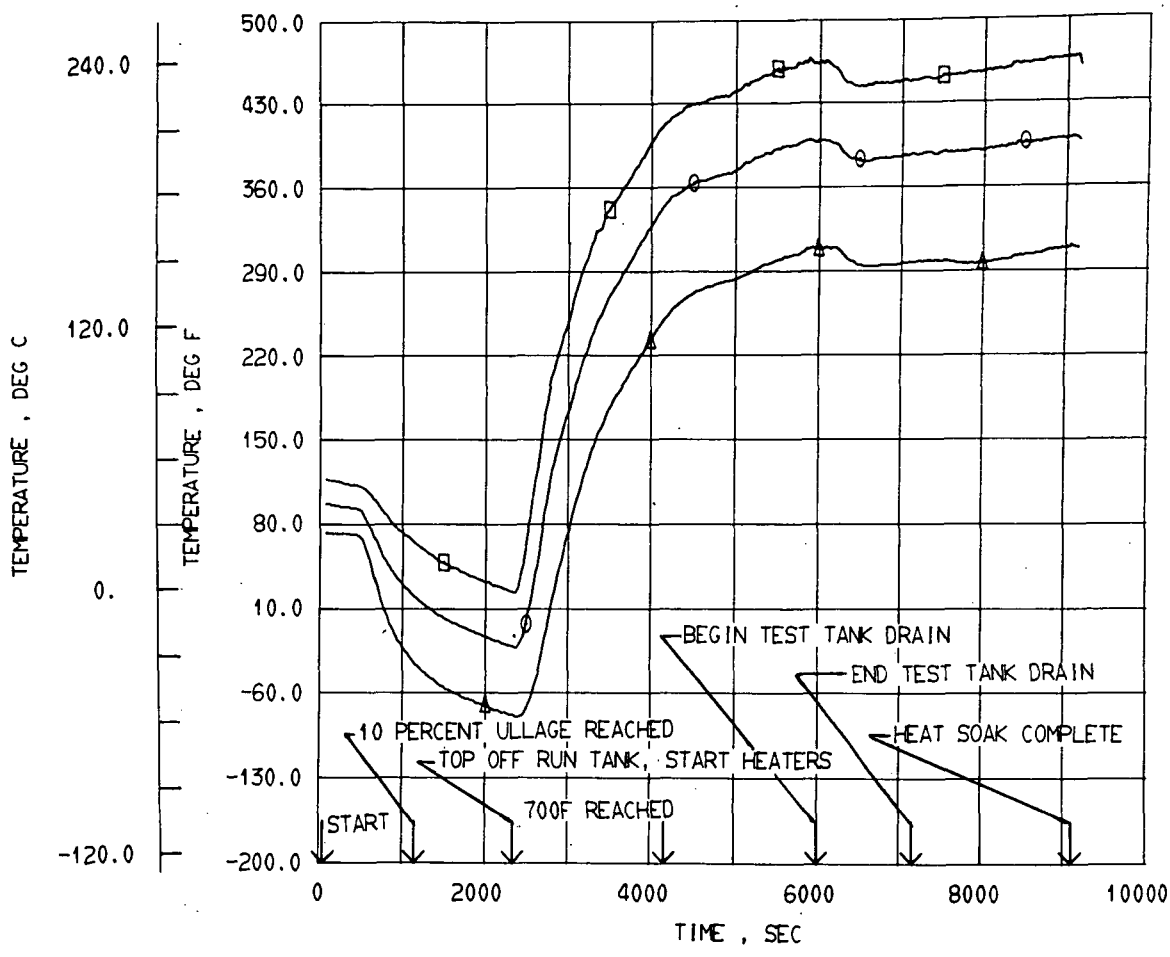

Figure 83. Square tank exterior insulation, temperature cycle 7, wing bottom insulation temperatures.

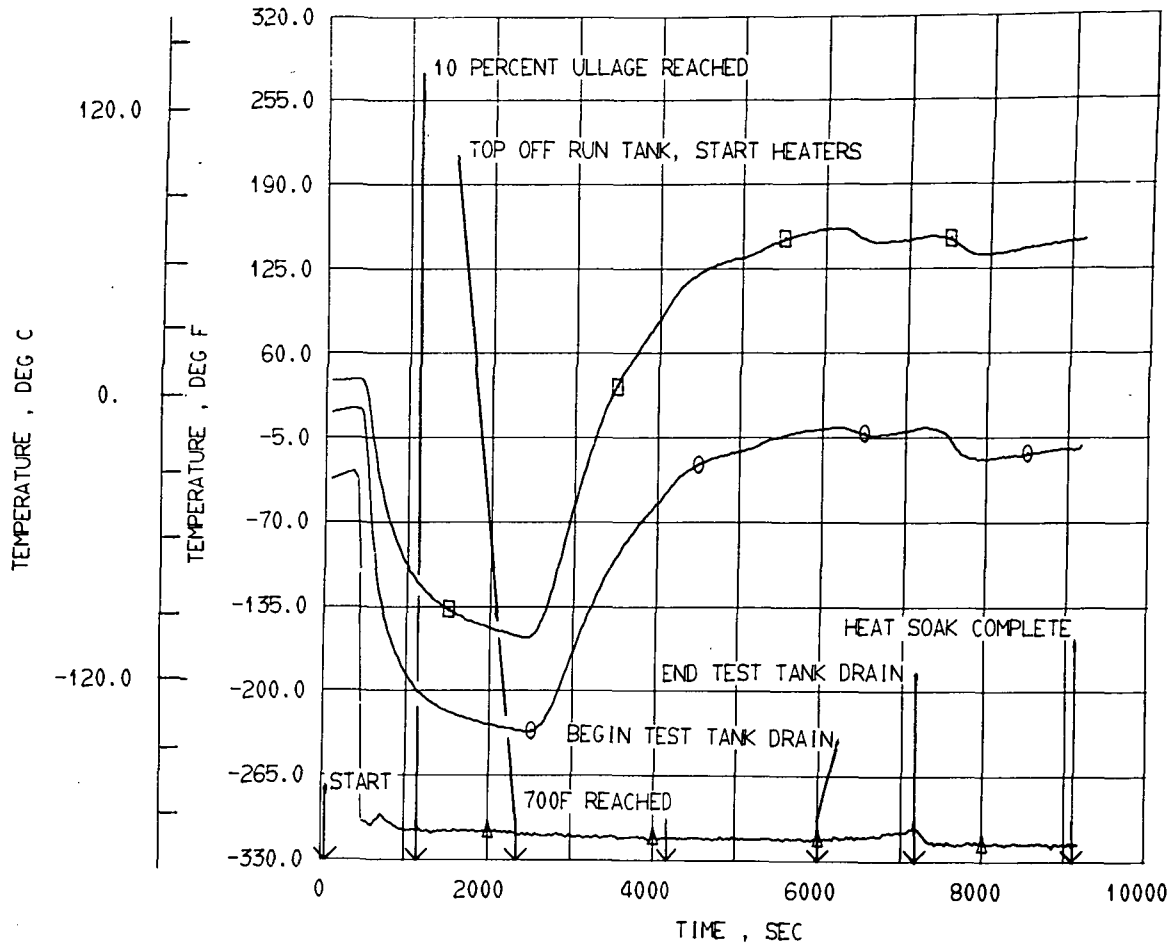

Figure 84. Square tank exterior insulation, temperature cycle 7, wing bottom insulation temperatures.

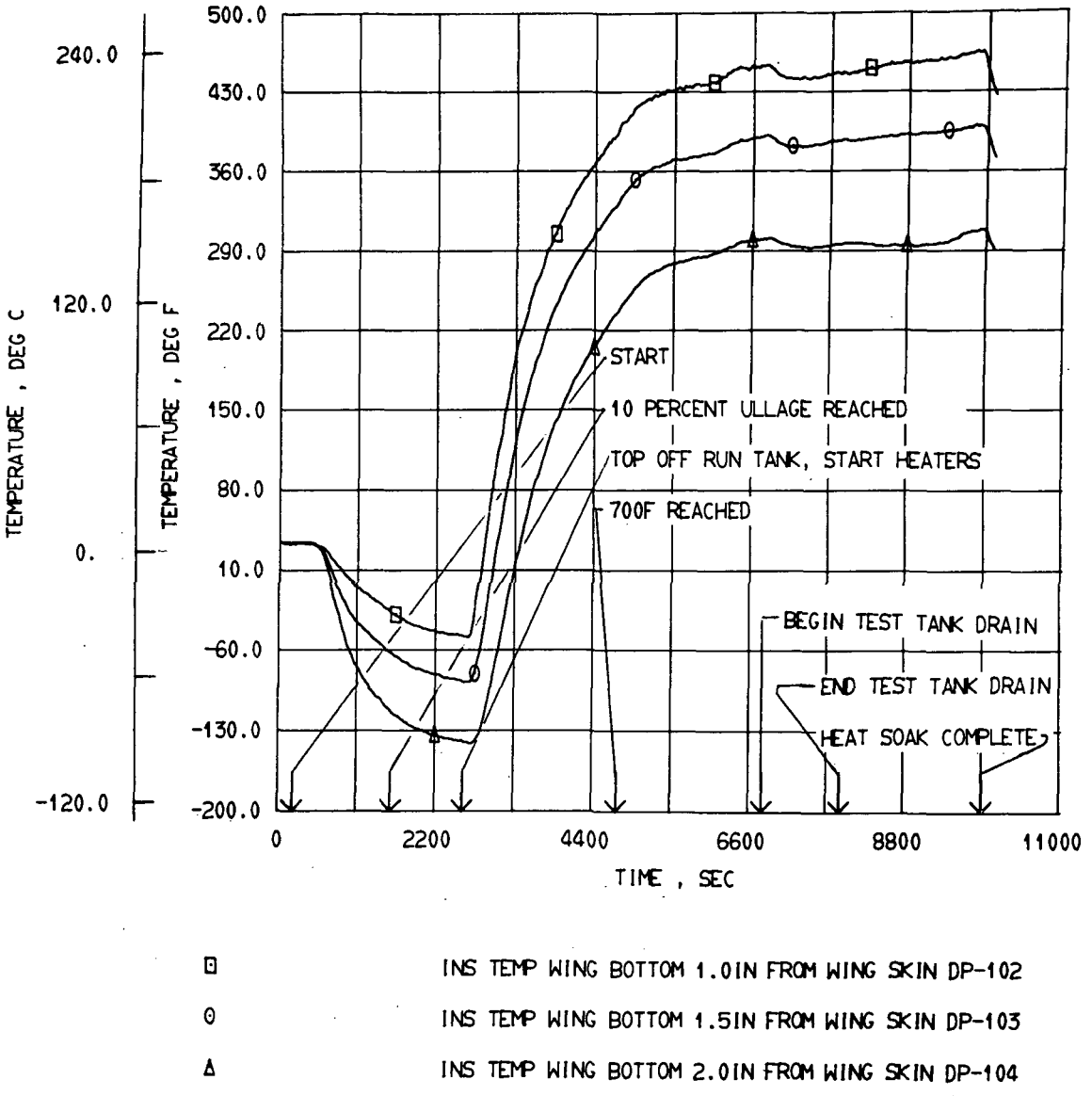

Figure 85. Square tank exterior insulation, temperature cycle 10, wing bottom insulation temperatures.

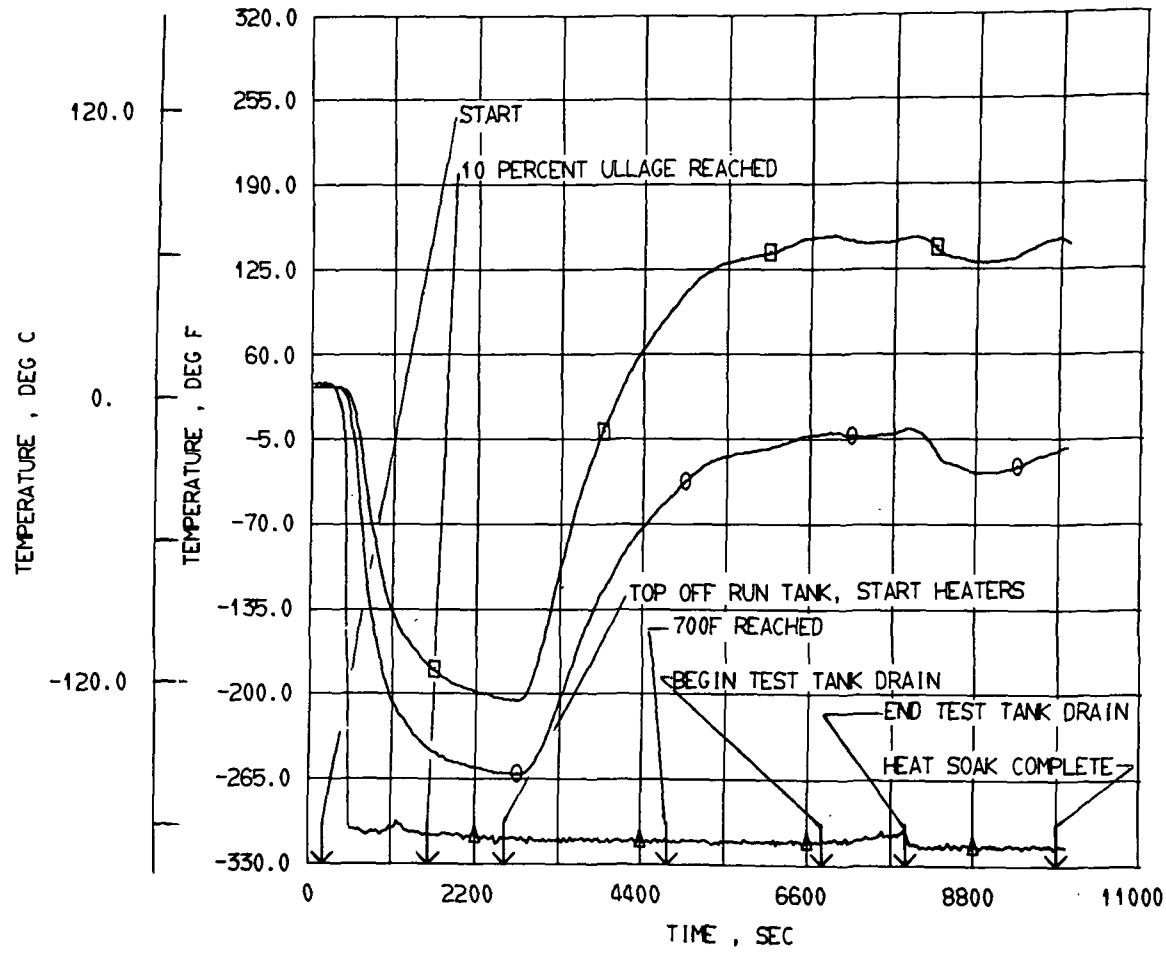

Figure 86. Square tank exterior insulation, temperature cycle 10, wing bottom insulation temperatures.

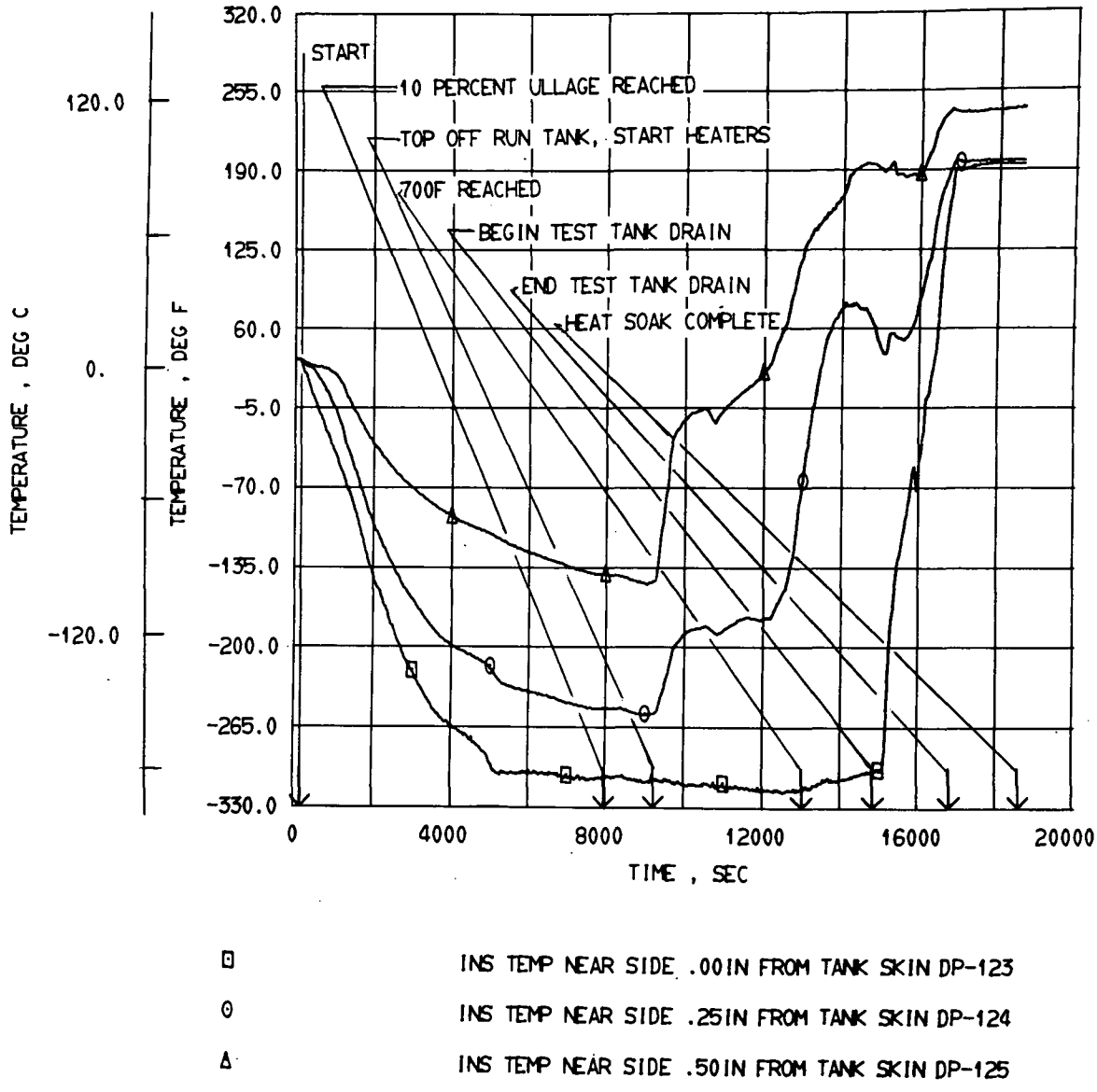

Figure 87. Square tank exterior insulation, temperature cycle 1, side insulation temperatures.

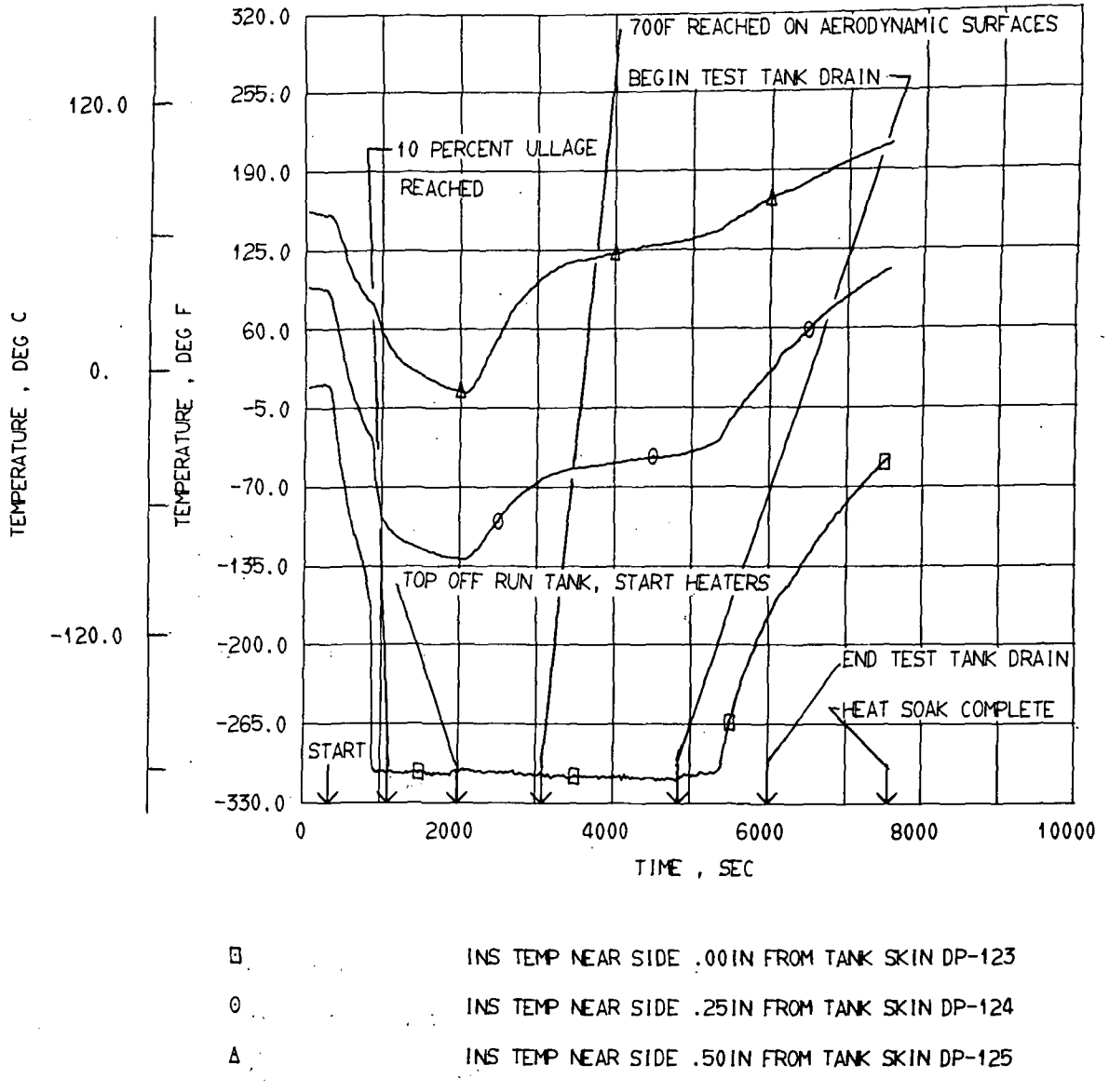

Figure 88. Square tank exterior insulation, temperature cycle 4, side insulation temperatures.

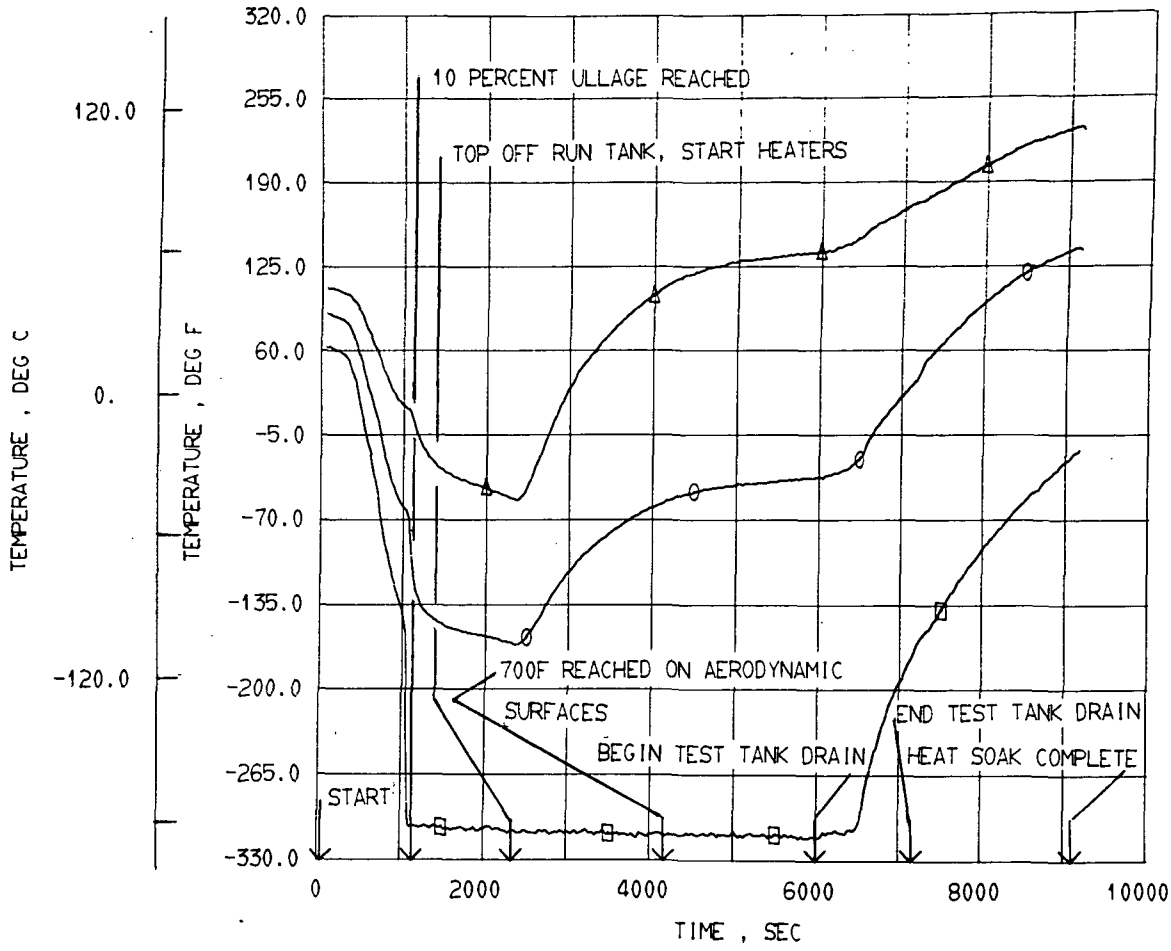

Figure 89. Square tank exterior insulation, temperature cycle 7, side insulation temperatures.

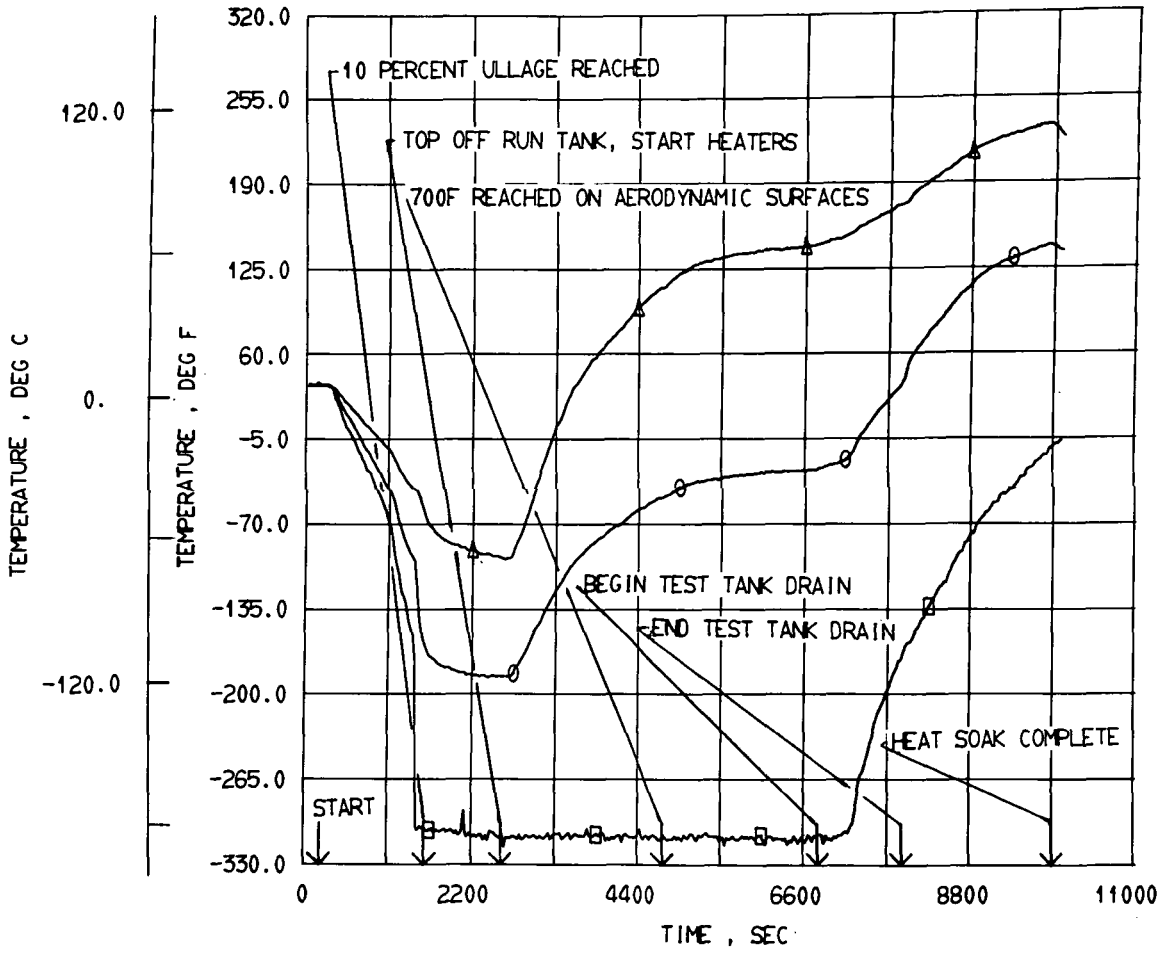

Figure 90 . Square tank exterior insulation, temperature cycle 10, side insulation temperatures.

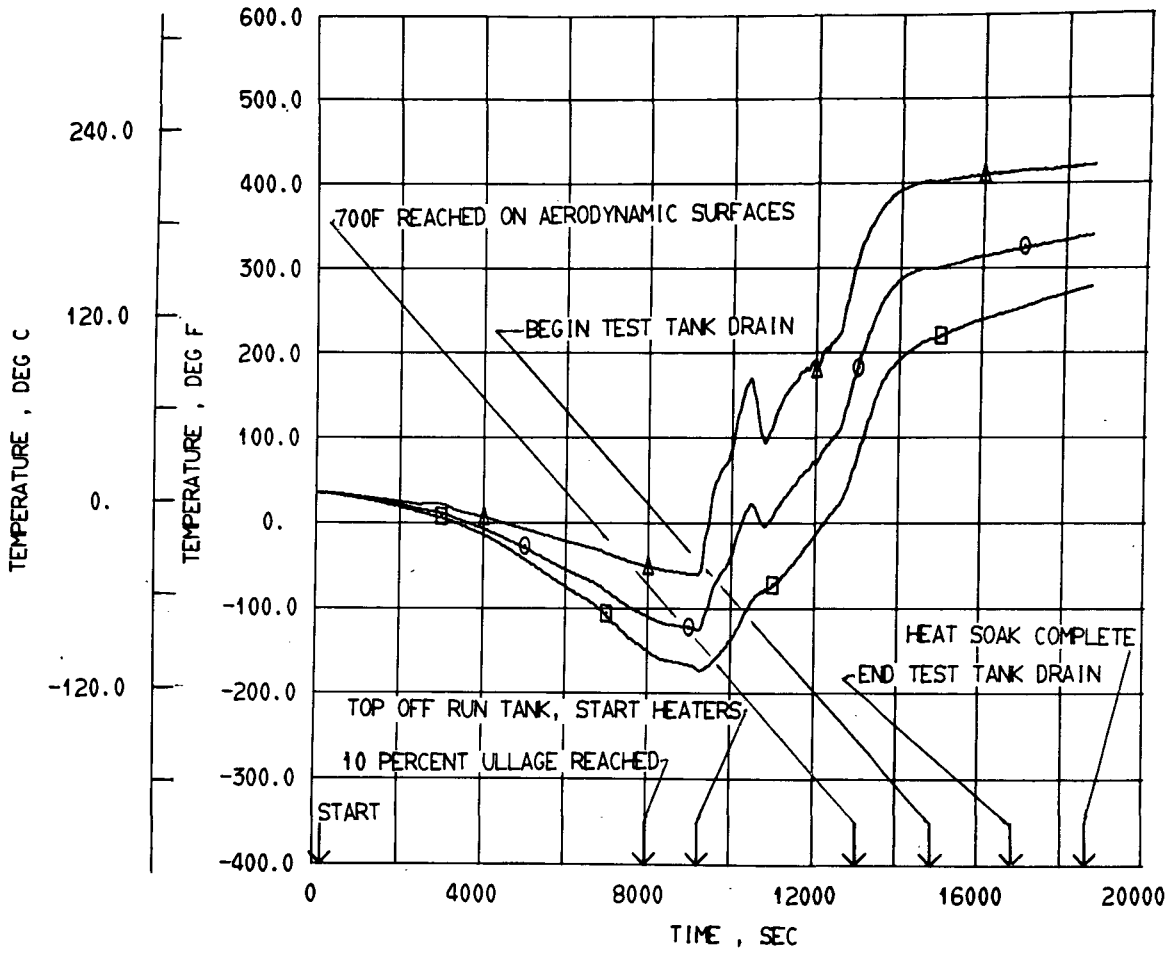

Figure 91. Square tank exterior insulation, temperature cycle 1, wing top insulation temperatures.

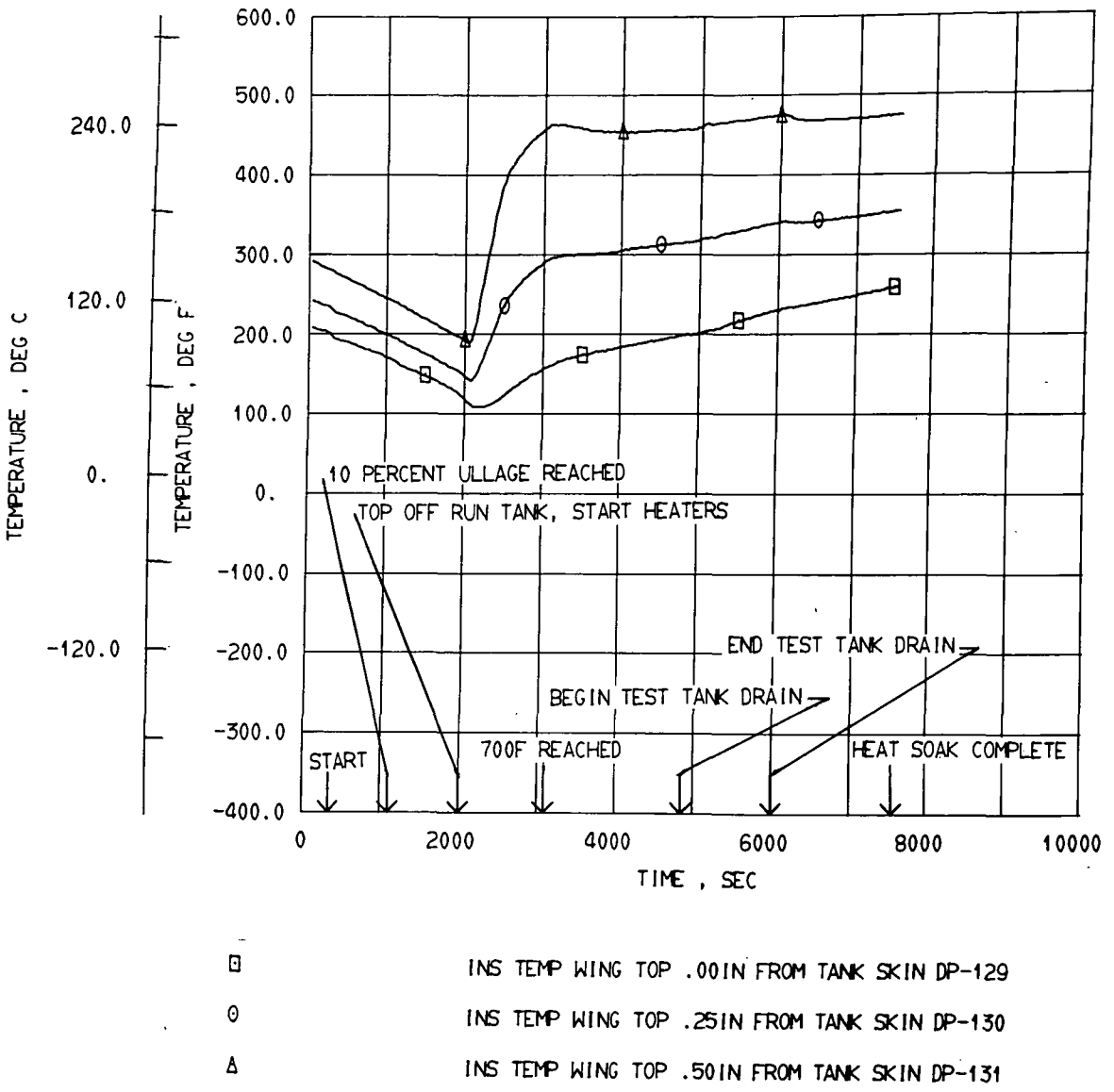

Figure 92. Square tank exterior insulation, temperature cycle 4, wing top insulation temperatures.

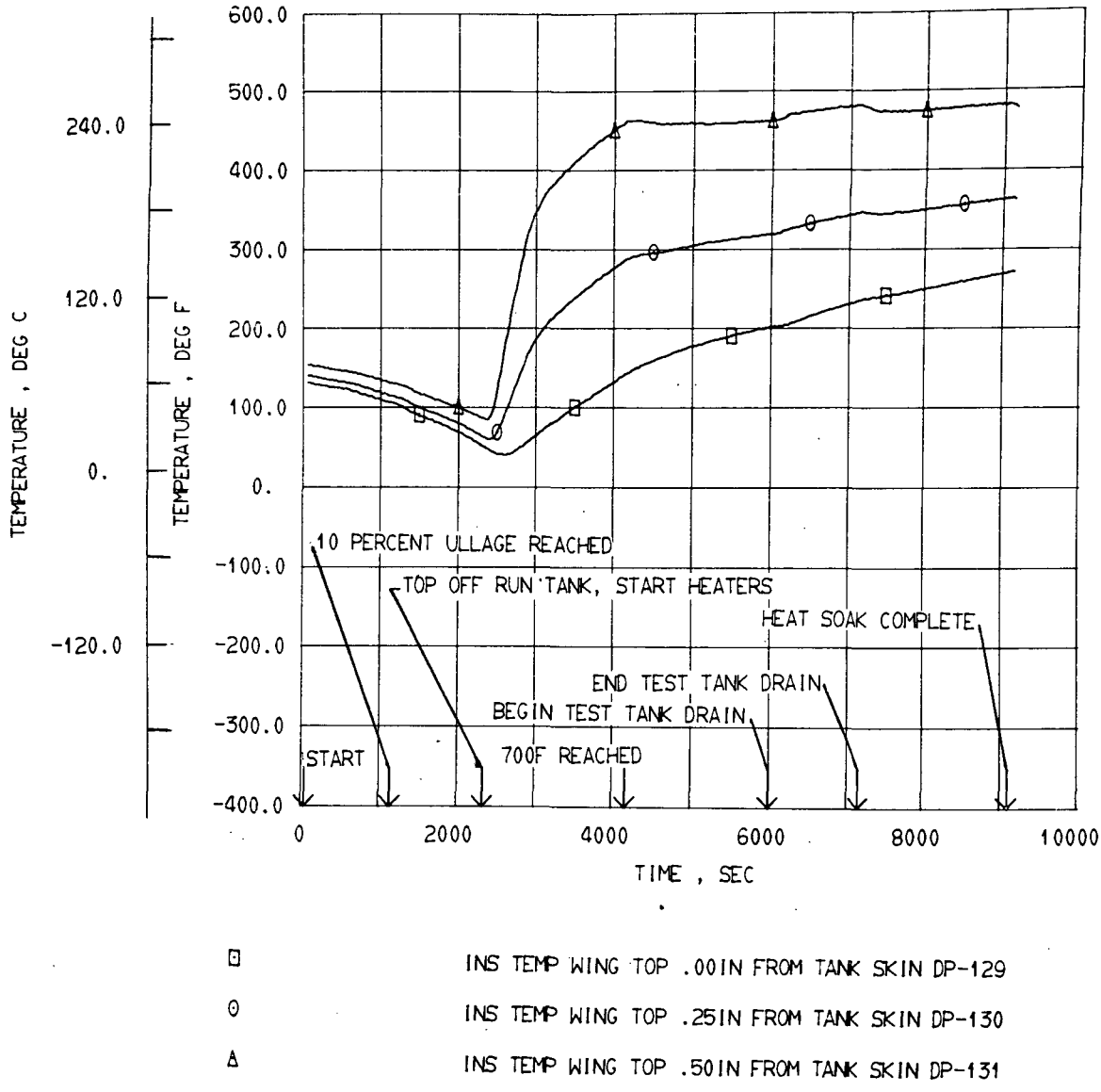

Figure 93. Square tank exterior insulation, temperature cycle 7, wing top insulation temperatures.

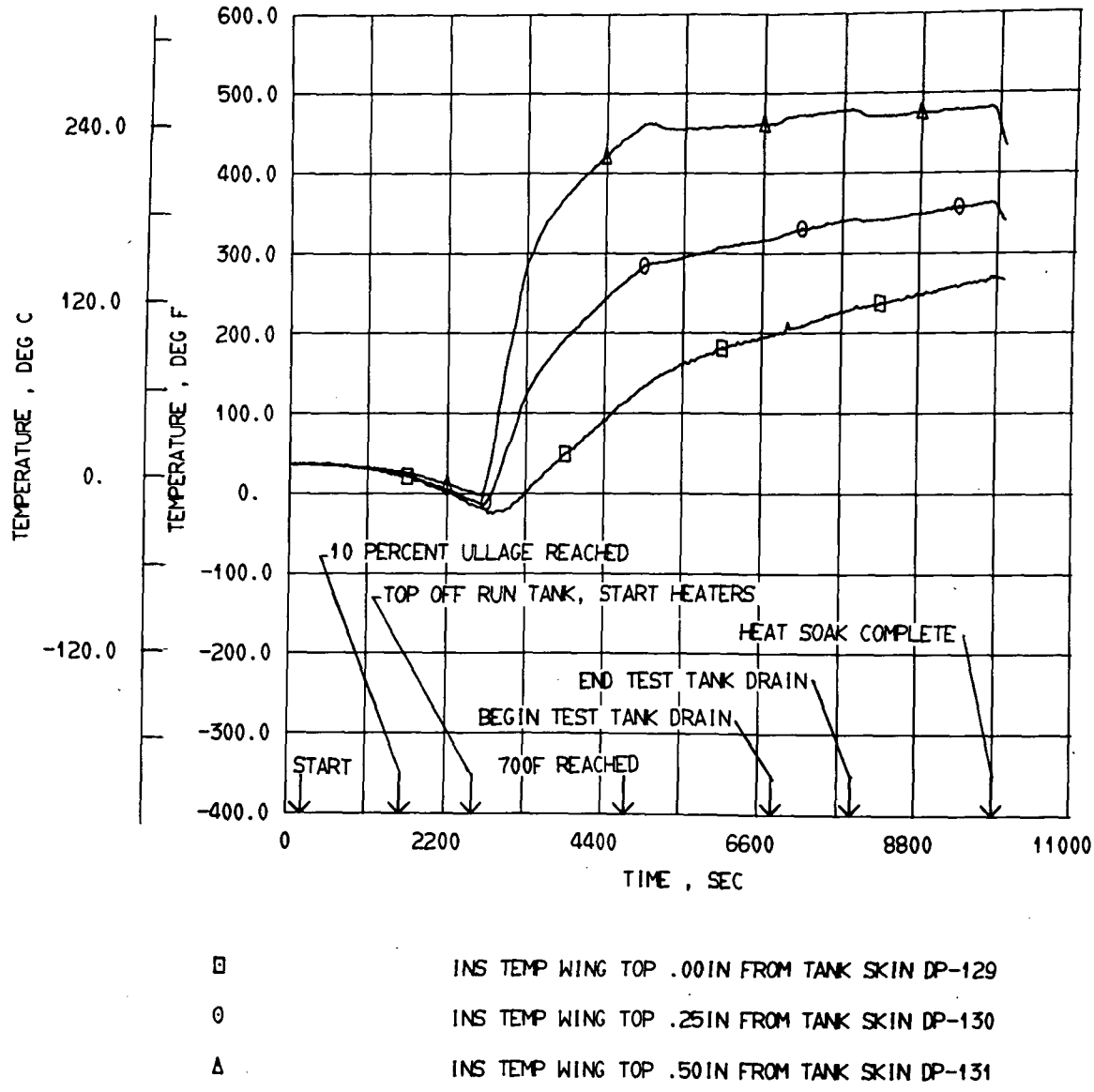

Figure 94. Square tank exterior insulation, temperature cycle 10, wing top insulation temperatures.

3. Pressurization Cycles

After the 10 temperature cycles were completed the tank and insulation was subjected to external pressure cycling while the wing surface was held at 700°F (371.5°C). The pressure oscillations were approximately 1/10 of a cycle per minute while the liquid level in the tank was maintained at 10% ullage. The test was scheduled for and did complete 20 cycles.

The testing sequence was completed on two successive test days because of the time required and data recording limitations. The first 10 cycles were between the pressures shown in Table X and, in general, required 10 minutes per cycle.

TABLE X. - PRESSURE CYCLES 1 THROUGH 10

Delta time	Event	Pressure on insulation
0 sec	Initiate cycle	11.72 psia (8.07 N/cm^2)
300 sec	Cycle at 50%	1.0 psia (0.69 N/cm^2)
600 sec	Cycle complete	11.72 psia (8.07 N/cm^2)

The second 10 cycles were completed on the following day and were between the pressures shown in Table XI. The average time per cycle during this sequence was closer to 9 min.

TABLE XI. - PRESSURE CYCLES 11 THROUGH 20

Delta time	Event	Pressure on insulation
0 sec	Initiate cycle	11.70 psia (8.06 N/cm^2)
270 sec	Cycle at 50%	1.0 psia (0.69 N/cm^2)
540 sec	Cycle complete	11.70 psia (8.06 N/cm^2)

The rate of liquid makeup as a function of time was determined from the vent venturi flowmeter data shown by figures 95 and 96 The integrated average flowrate for the first 10 cycles was 198.3 lb/hr (25 g/sec) and for the last 10 cycles 172.07 lb/hr (21.7 g/sec). These equate to the rate of liquid makeup during the two series pressure cycle tests.

Figure 97 and 98 show the temperature of the simulated wing structure during the pressure cycles. The temperature measurement on the wing bottom was very sensitive to pressure. As the figures show, it varied as much as 49°F (27.2°C) during the first 10 cycles and 42.6°F (23.6°C) during the last 10 cycles.

The insulation temperature (fig 99 through 106) also varies with pressure in a unique way. As the pressure decreased, the temperature thru the insulation on the lower half of the tank increased and the temperature thru the upper half decreased. See figures 102 and 99 and figure 107.

This phenomena is explained by considering gas convection effects outside of and within the insulation. The convection currents flow from the bottom of the tank toward the top, which accounts for the higher top wing structural temperature when the wing is at the highest pressure, (fig. 97 and 98). Therefore, when the gas pressure around the tank was decreased the mass of gas within the volume occupied by the insulation was also decreased. This causes the convective heat transfer coefficient to be decreased, resulting in a reduction of the rate of convective heat transfer from the bottom insulation, and a higher insulation temperature is noted (fig. 101 and 102).

The insulation on the sides and top shows the opposite effect; i.e., decreasing pressure the temperature also decreases. This confirms the convection theory because it shows that there was no heated gas passing through the insulation on the sides and top at the lower pressure.

A good example of this phenomena can be found at 6000 sec during pressure cycles 1 through 10. Table XII shows temperature data from this cycle.

TABLE XII. - CYCLE 6 PRESSURE AND TEMPERATURE DATA

Ambient pressure	11.72 psia (8.07 N/cm^2)	1.0 psia (0.69 N/cm^2)
Temperature of:		
Top insulation outside	451°F (233°C)	437°F (224°C)
Top insulation middle	300°F (149°C)	287°F (142°C)
Top insulation inside	173°F (78°C)	172°F (78°C)
Side insulation outside	182°F (83°C)	129.7°F (54.5°C)
Side insulation middle	60°F (15.5°C)	14°F (-10°C)
Side insulation inside	-307°F (-189°C)	-307°F (-189°C)
Bottom insulation outside	445°F (230°C)	398°F (204°C)
Bottom insulation 2 in. (5.1 cm) from skin	373°F (189°C)	336°F (169°C)
Bottom insulation 1½ in. (3.8 cm) from skin	290°F (143°C)	297°F (147.5°C)
Bottom insulation 1 in. (2.5 cm) from skin	100°F (37.8°C)	170°F (76.7°C)
Bottom insulation ½ in. (1.3 cm) from skin	-37°F (-38.4°C)	76.5°F (24.8°C)
Bottom insulation inside	-313°F (-192°C)	-313°F (-192°C)

The pressure on the insulation is shown in figures 107 and 108. The strange shape of the first six cycles at the 3.5 psia (2.42 N/cm^2) level was caused by an instrumentation system malfunction, and the smooth curves after 6000 sec resulted from the analysis and correction of this problem. The correction eliminated the step change in pressure, but caused the pressures to read approximately 1.5 psia (1.03 N/cm^2) too high when at ambient. This error is also present in cycles 11 through 20.

No damage or degradation to the insulation resulted from the pressure cycling.

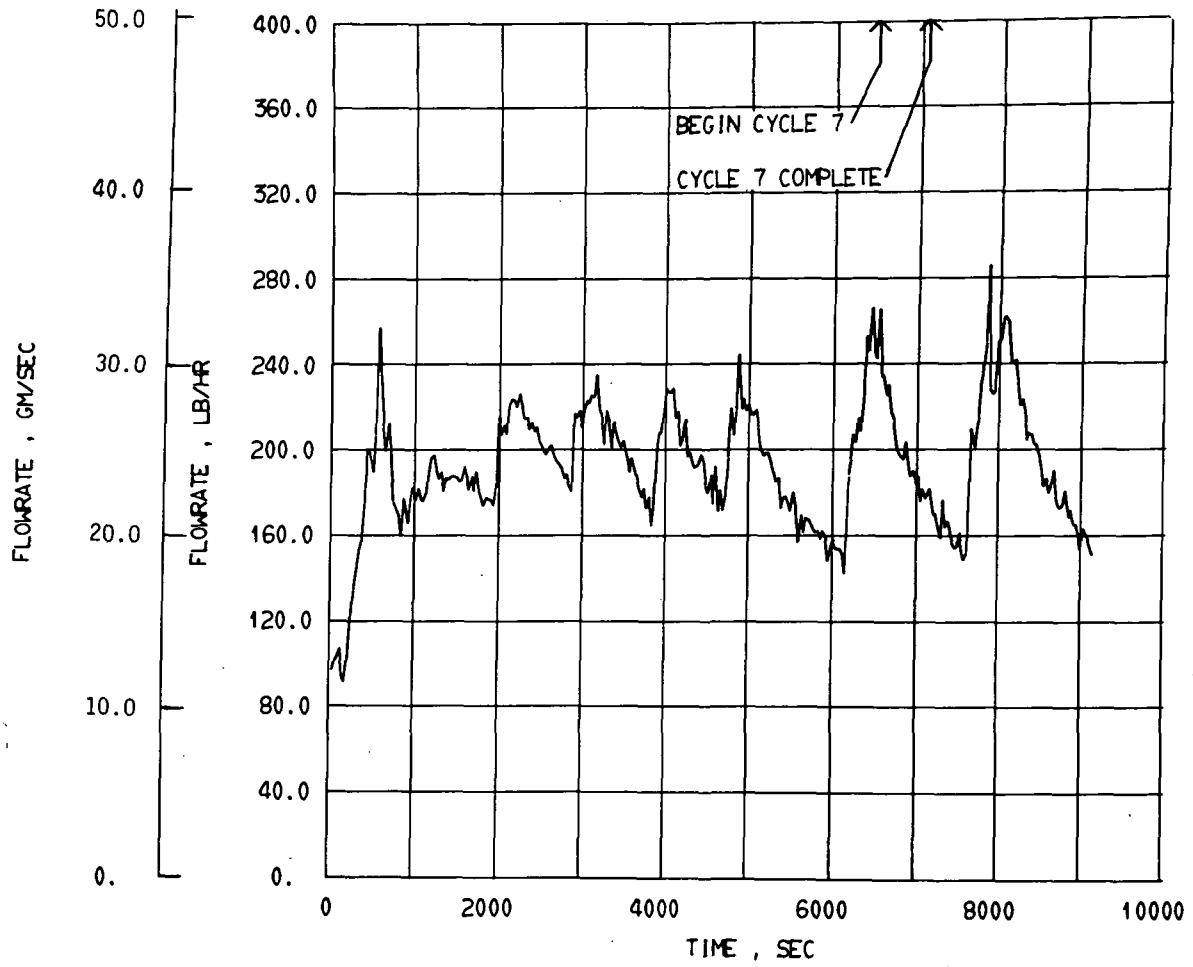

Figure 95. Square tank exterior insulation, pressure cycles 1 thru 10, Venturi flow rate.

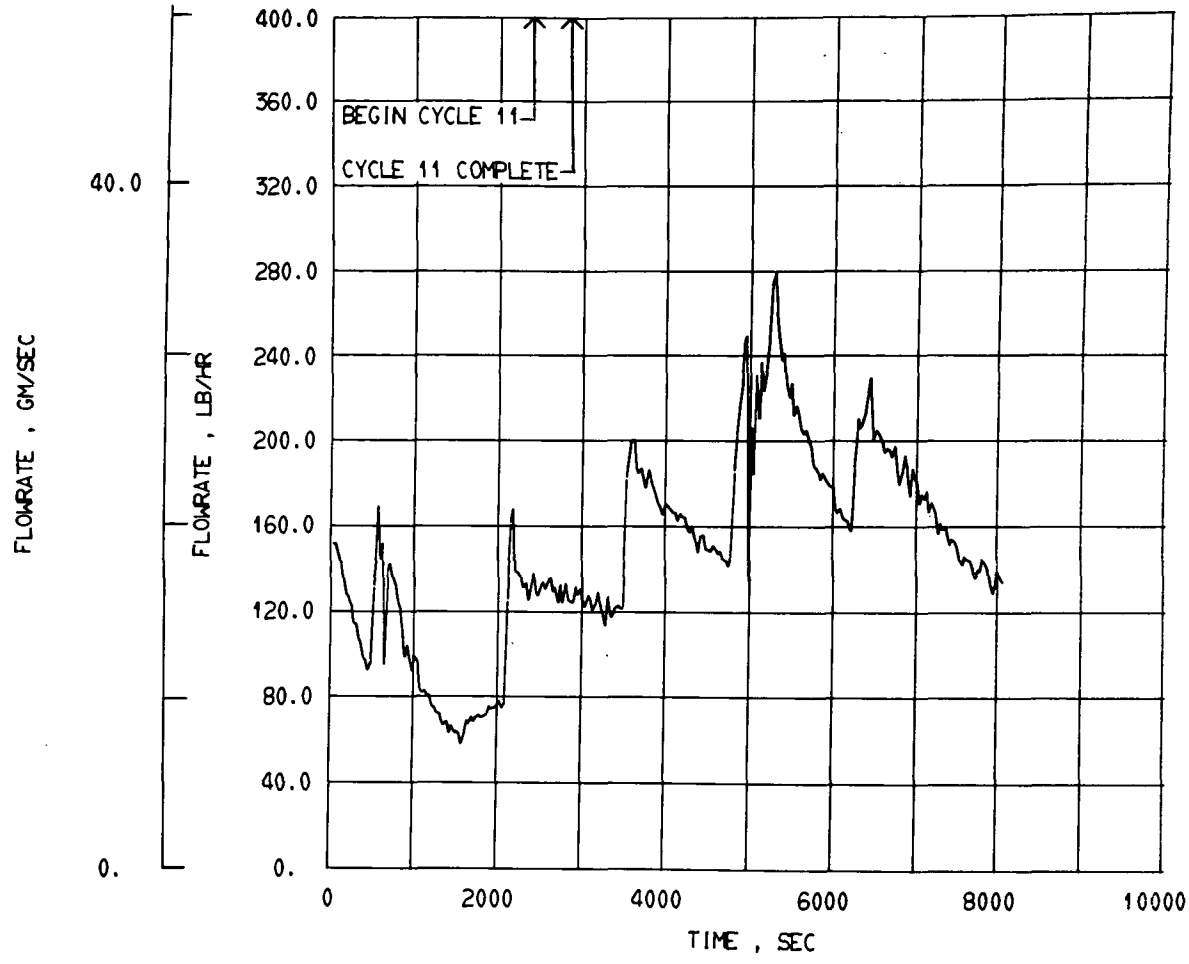

Figure 96. Square tank exterior insulation, pressure cycles 11 thru 20, Venturi flow rate.

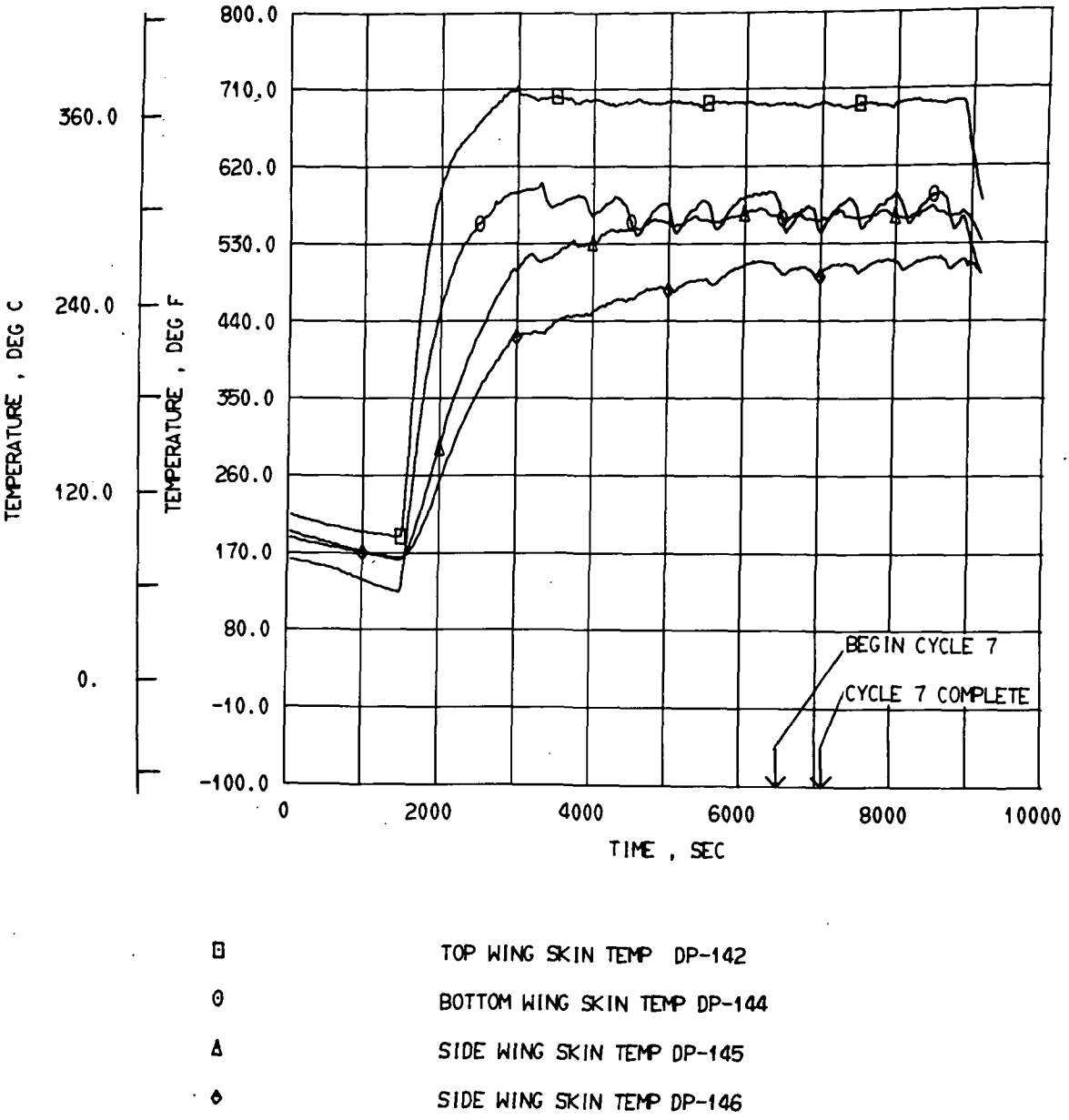

Figure 97. Square tank exterior insulation, pressure cycles 1 thru 10, top, bottom and side wing skin temperatures.

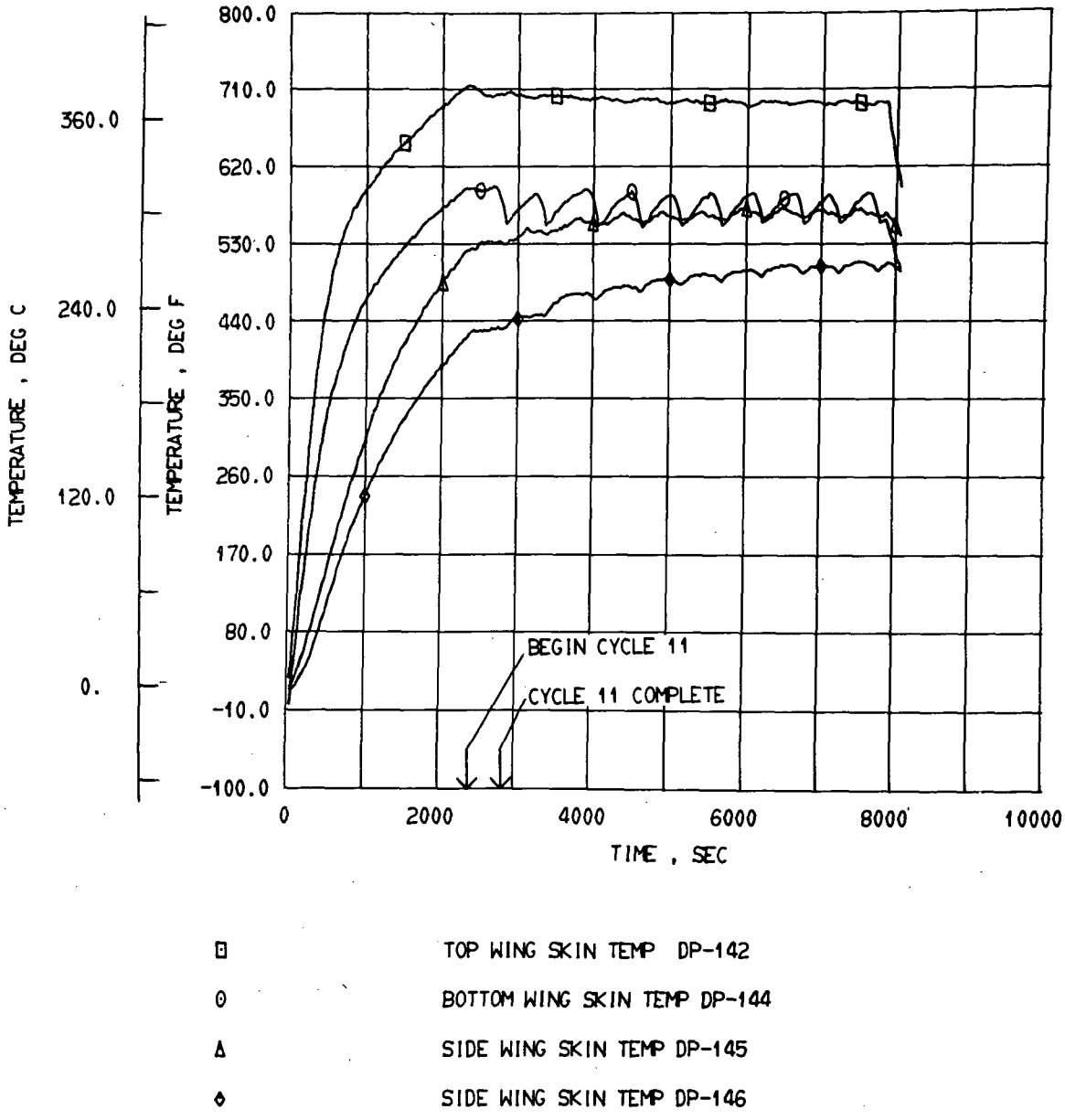

Figure 98. Square tank exterior insulation, pressure cycles 11 thru 20, top, bottom and side wing skin temperatures.

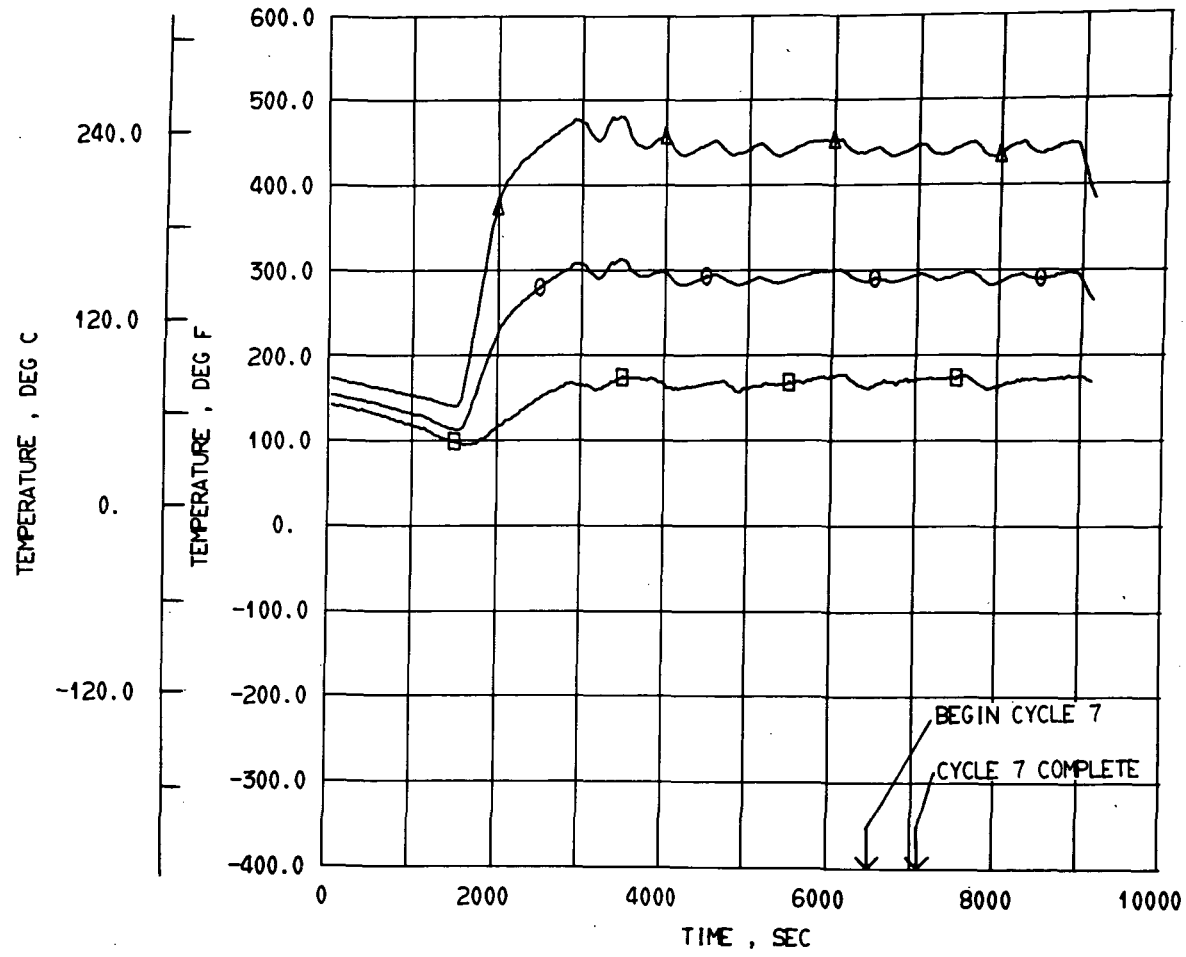

Figure 99. Square tank exterior insulation, pressure cycles 1 thru 10, wing top insulation temperatures.

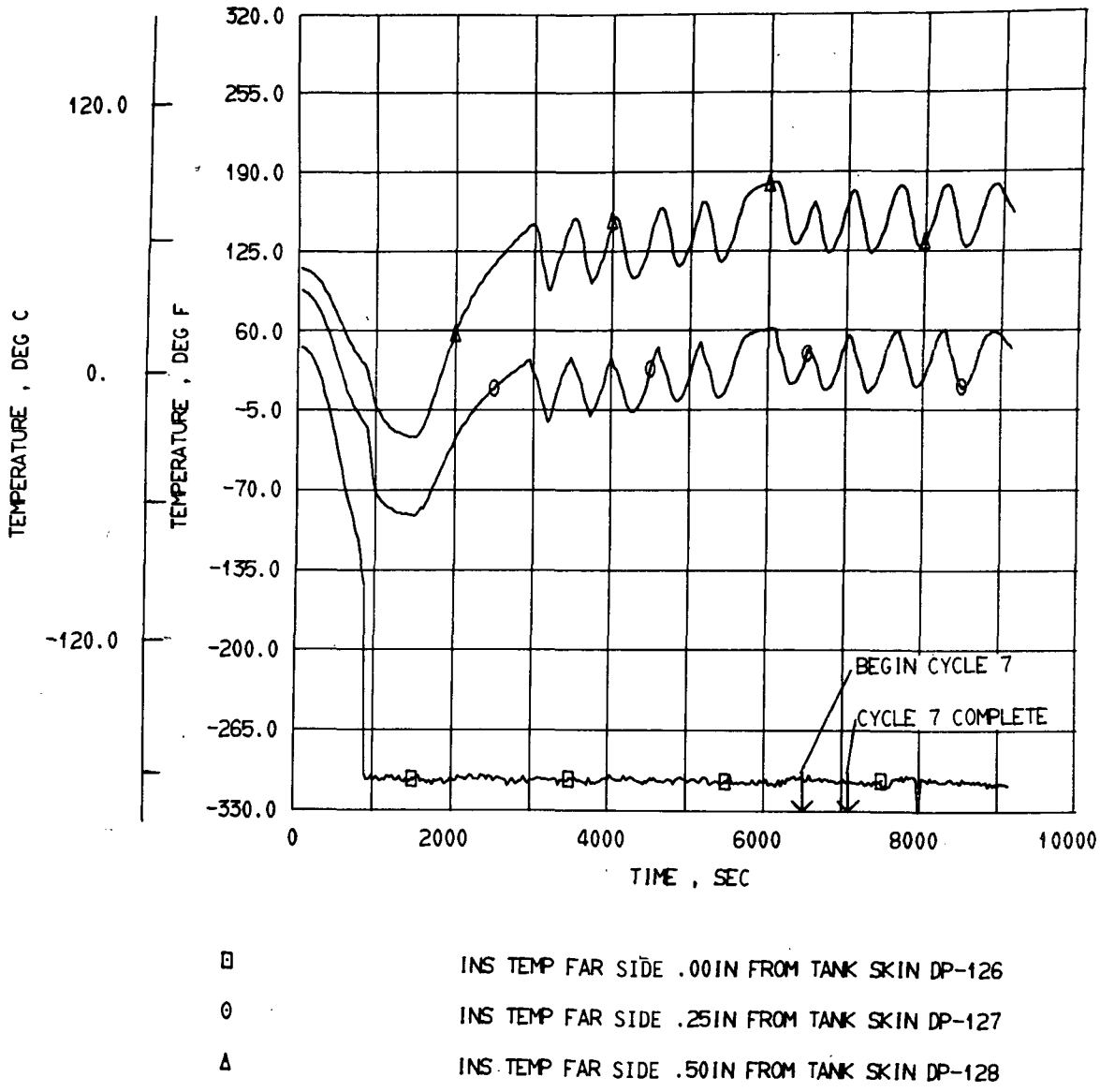

Figure 100. Square tank exterior insulation, pressure cycles 1 through 10, wing insulation temperatures.

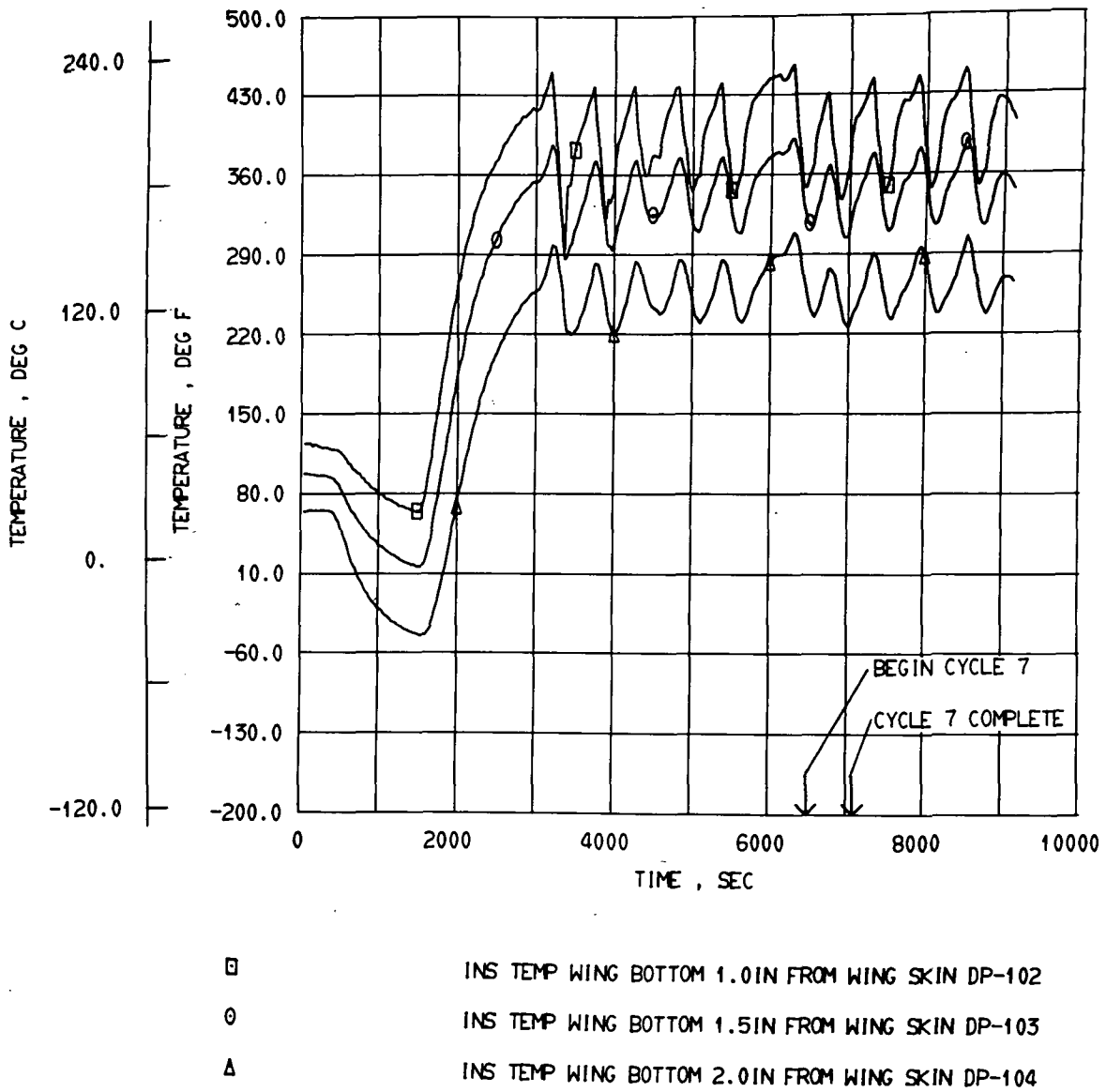

Figure 101. Square tank exterior insulation, pressure cycles 1 through 10, wing bottom insulation temperatures.

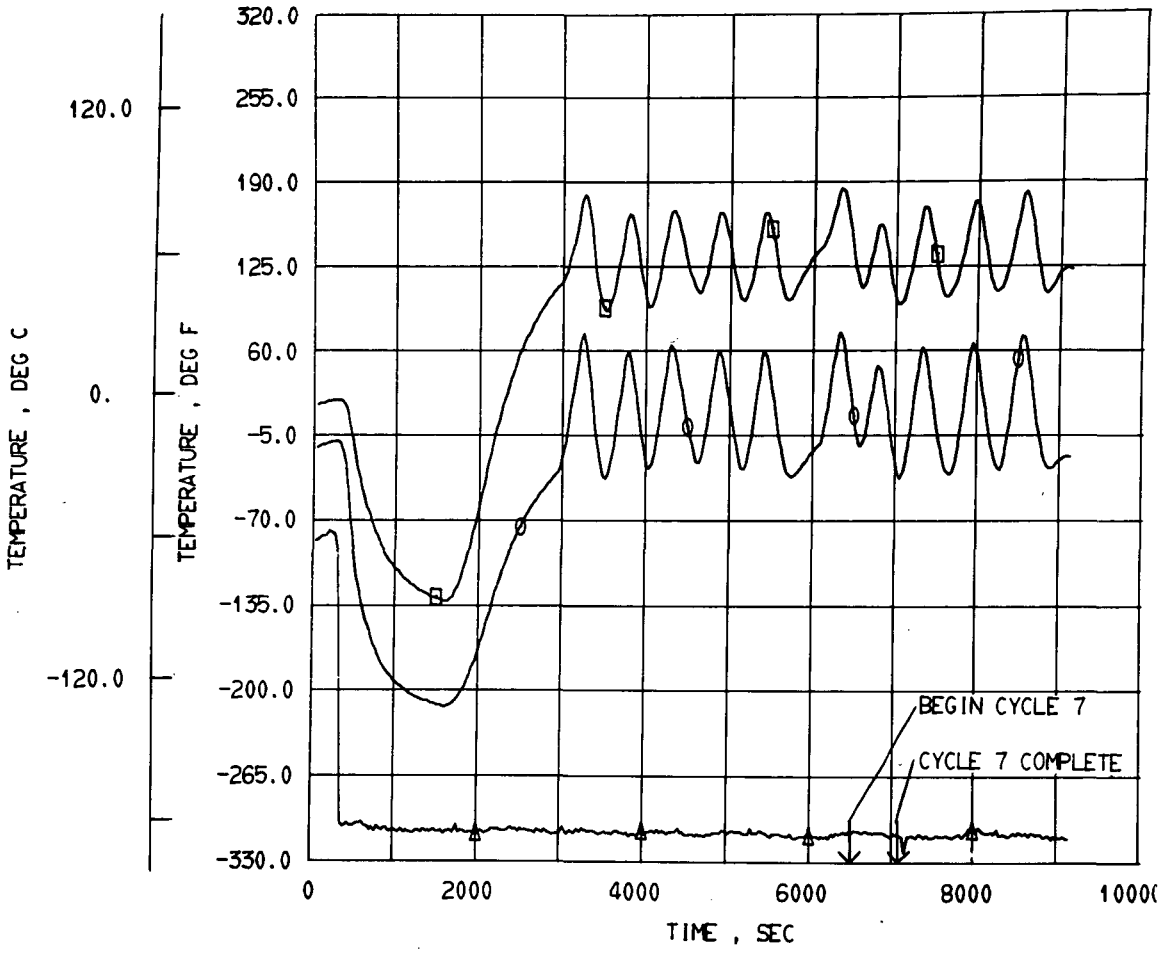

Figure 102. Square tank exterior insulation, pressure cycles 1 through 10, wing bottom insulation temperatures.

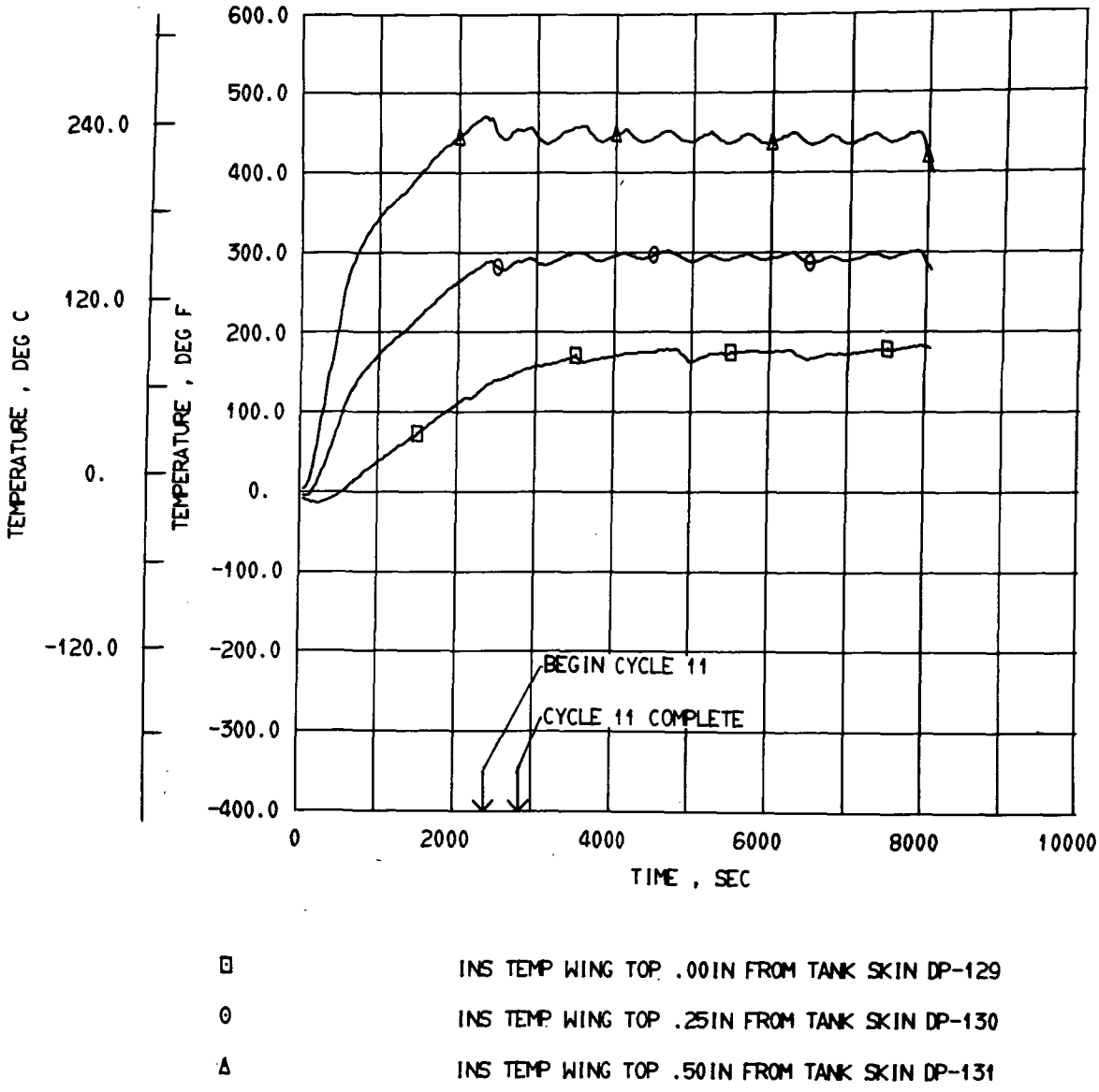

Figure 103. Square tank exterior insulation, pressure cycles 11 through 20, wing top insulation temperatures.

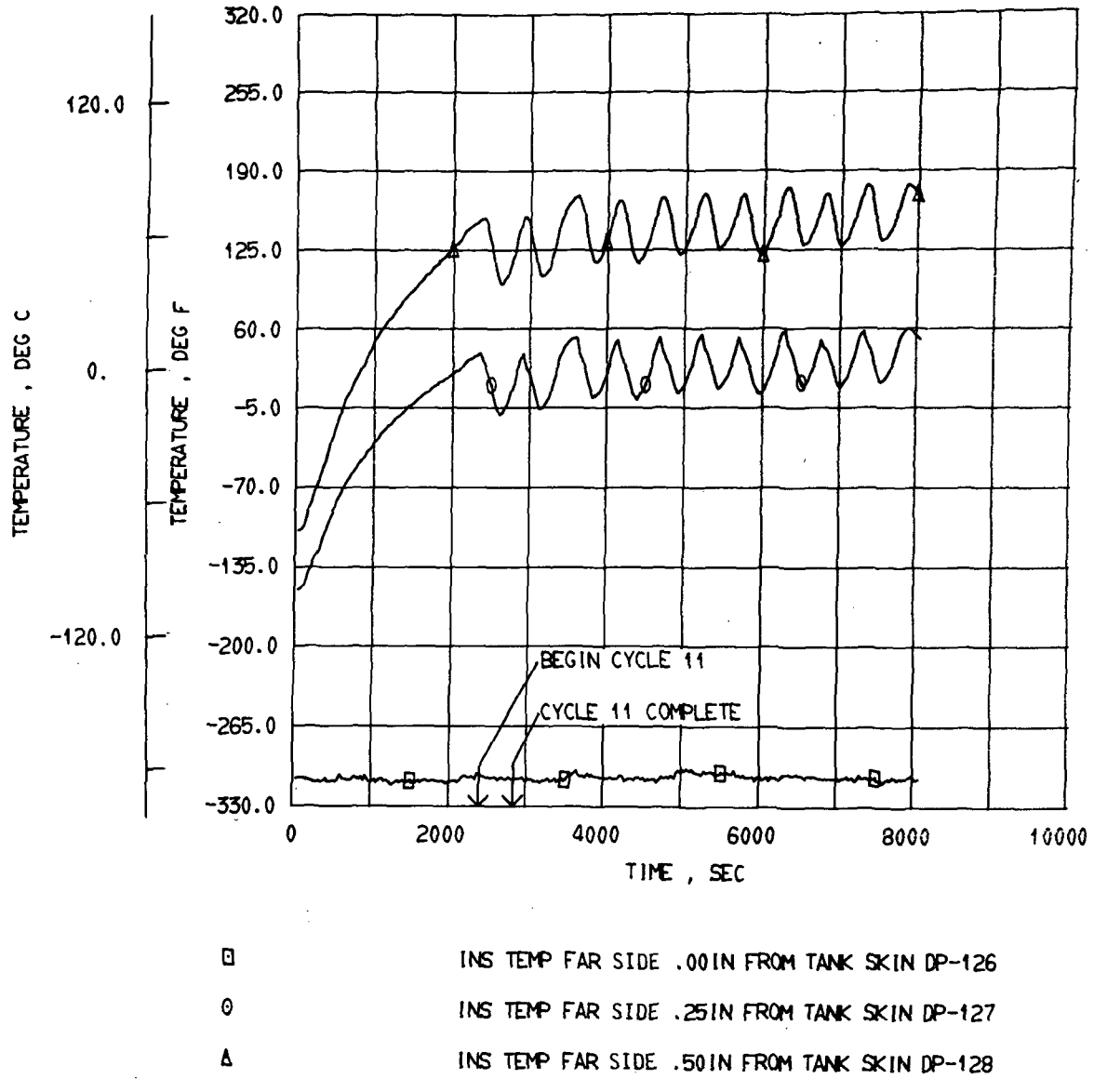

Figure 104. Square tank exterior insulation, pressure cycles 11 through 20, wing insulation temperatures.

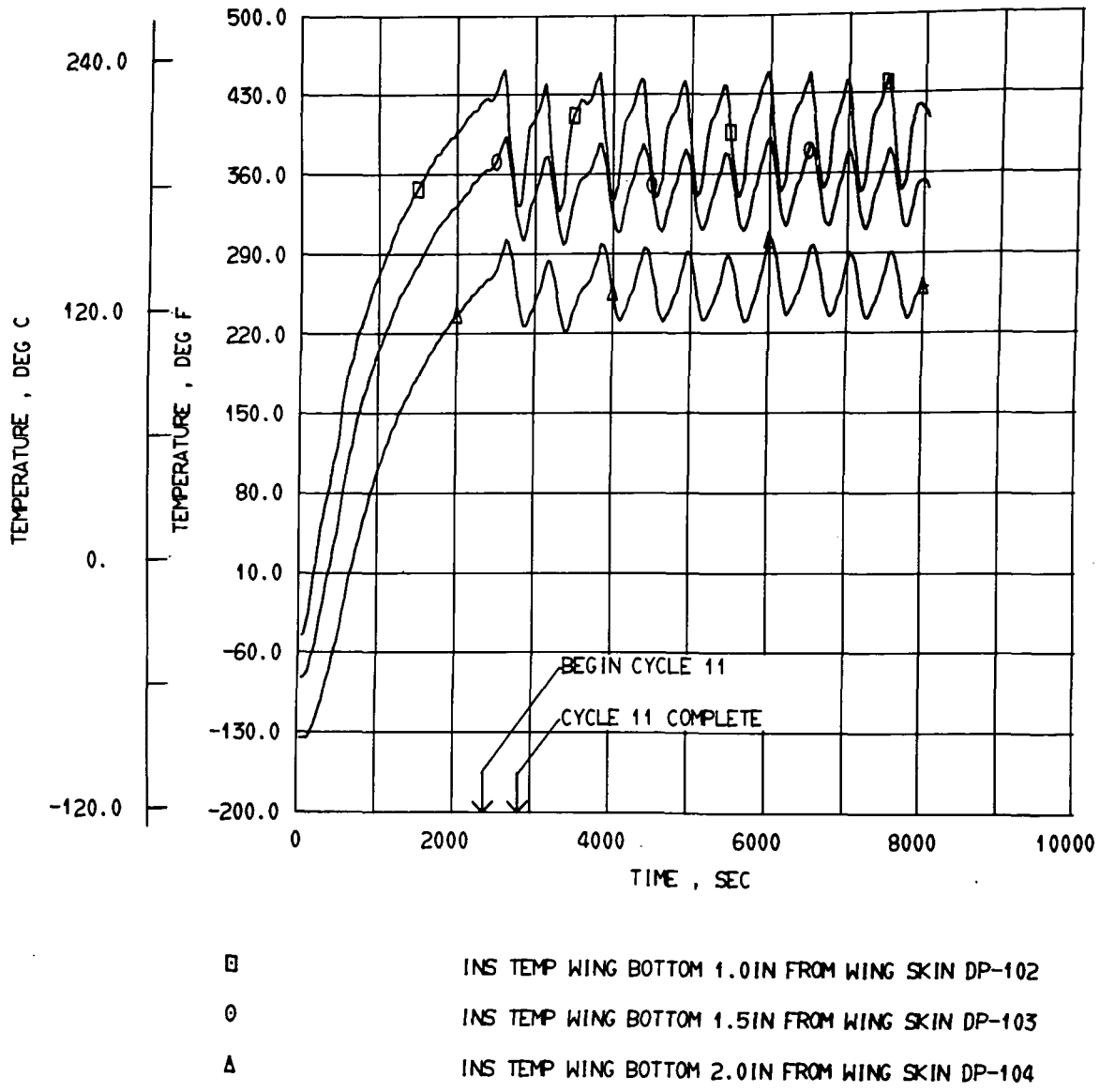

Figure 105. Square tank exterior insulation, pressure cycles 11 through 20, wing bottom insulation temperatures.

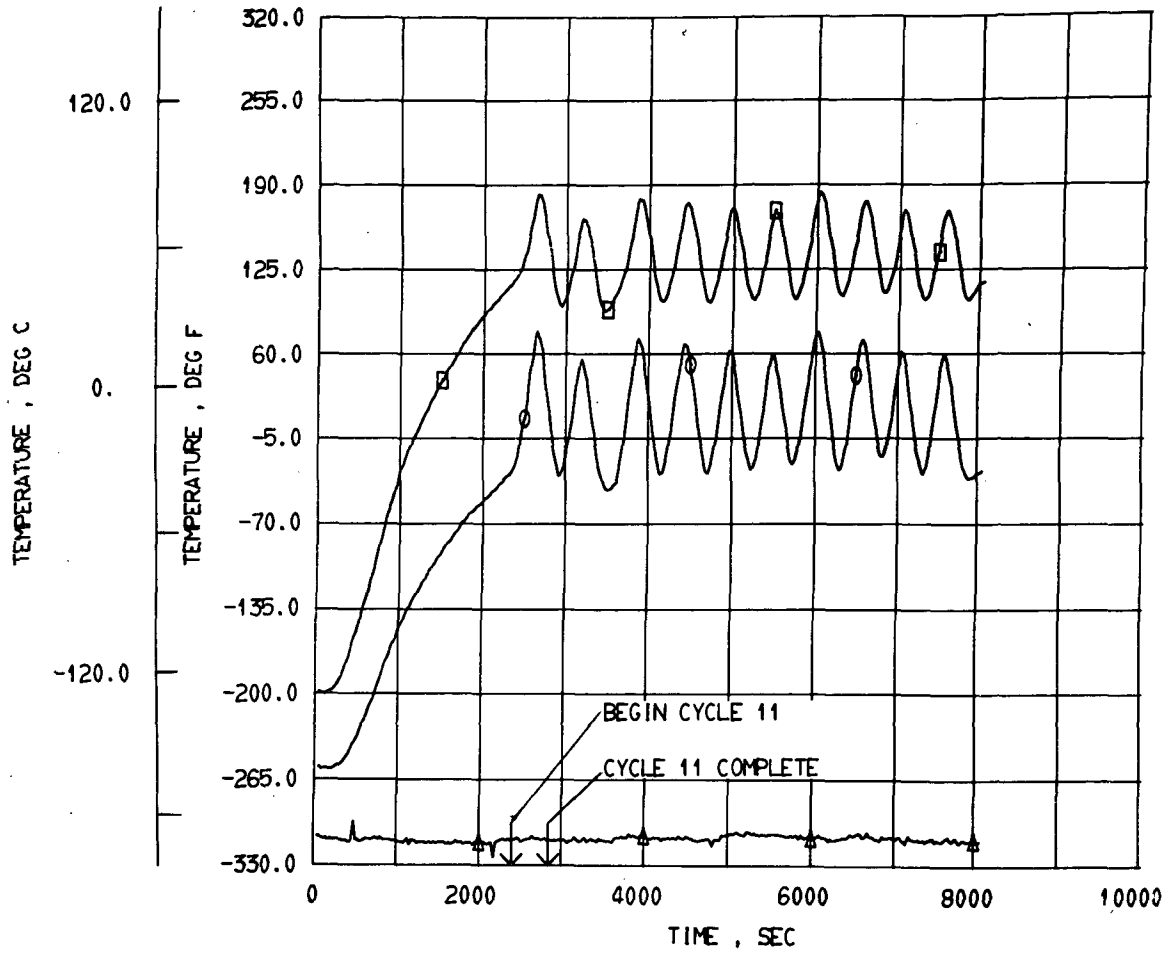

Figure 106. Square tank exterior insulation, pressure cycles 11 through 20, wing bottom insulation temperatures.

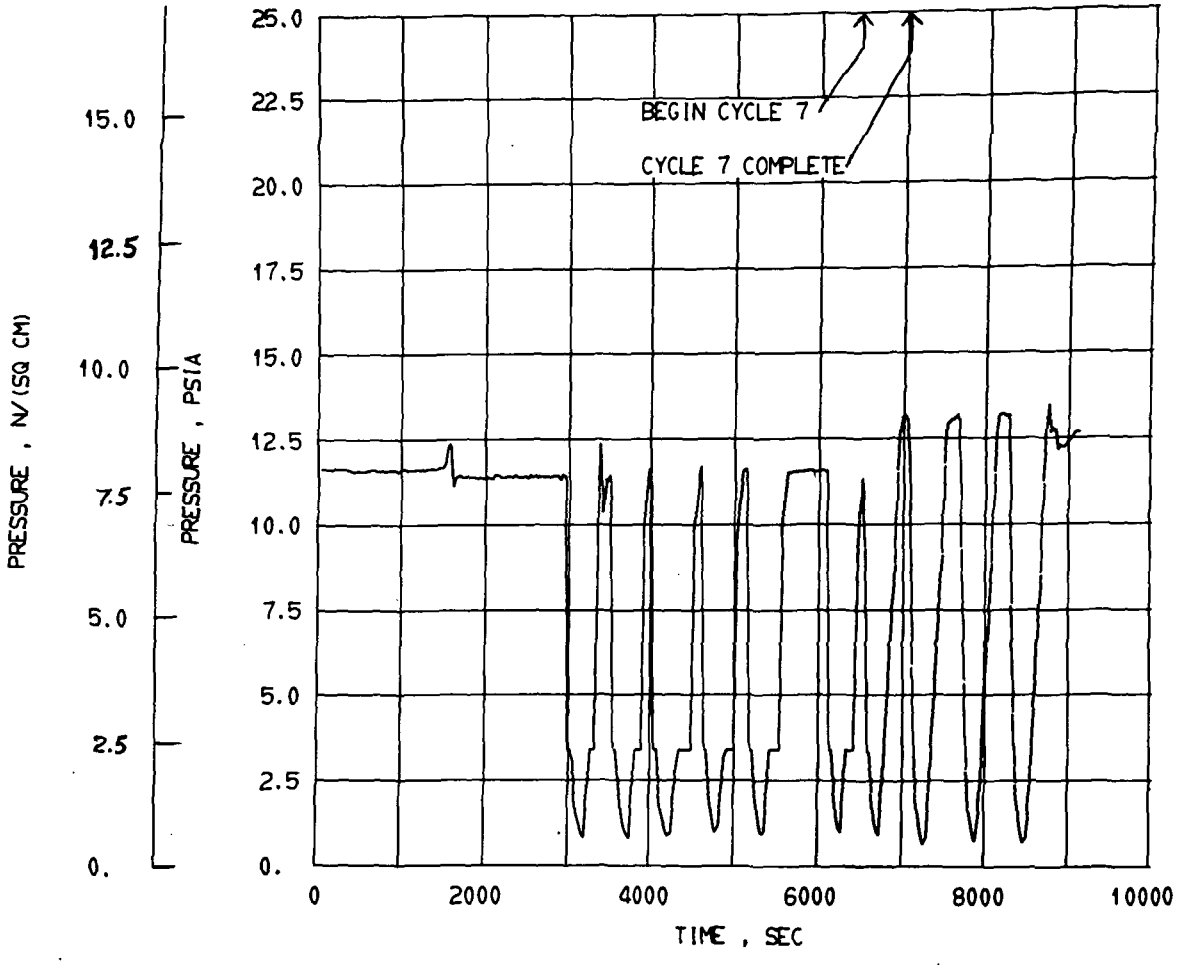

Figure 107. Square tank exterior insulation, pressure cycles 1 through 10, wing chamber pressure.

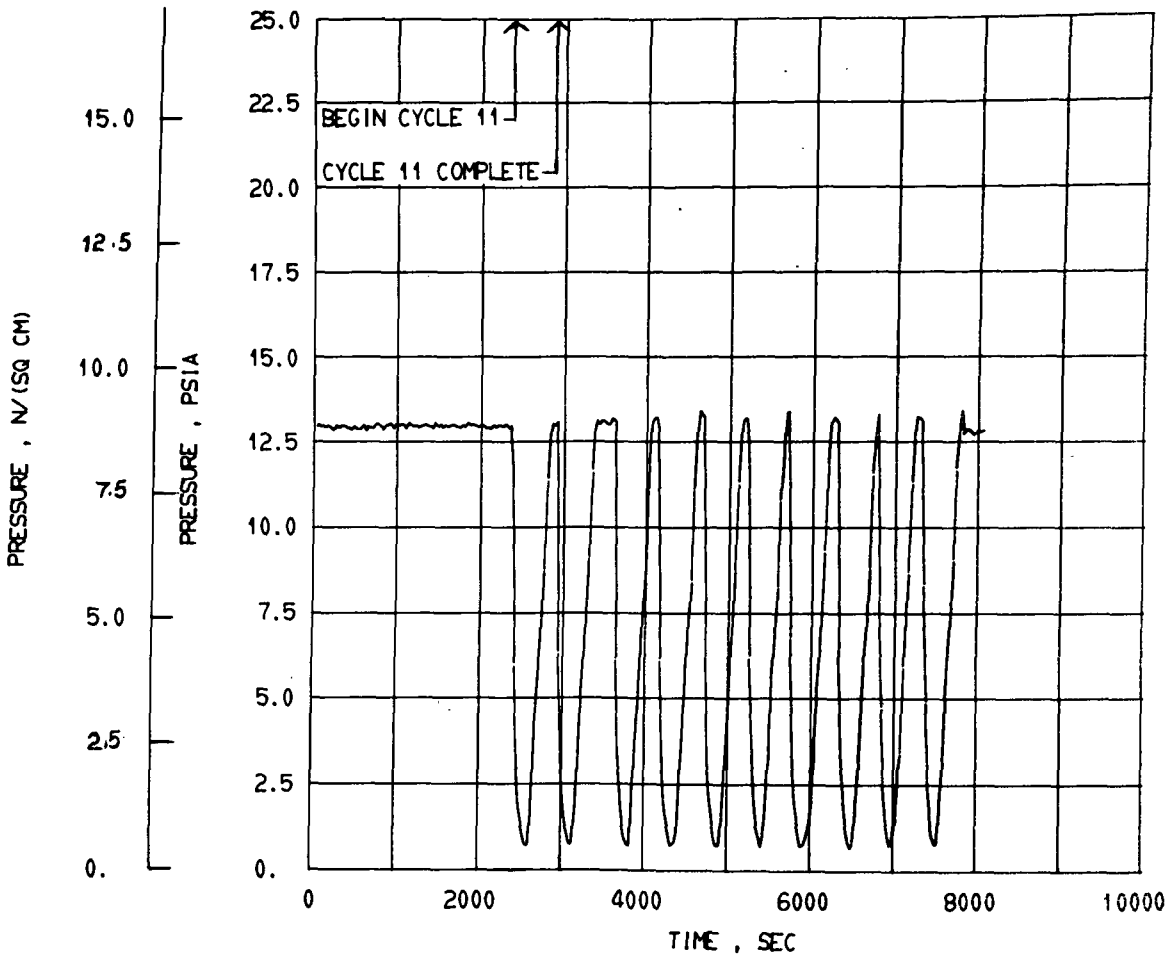

Figure 108. Square tank exterior insulation, pressure cycles 11 through 20, wing chamber pressure.

B. POSTTEST EXAMINATION

After completion of the second and final baseline tests, the tank was removed from the test rig for examination. Initial inspection indicated a change in the appearance of the aluminum foil insulation cover. As orginally installed, the cover had a mirror like finish, after test the surface had a dull gray texture indicating considerable oxidation. This was probably a result of exposure to wet nitrogen gas at 700°F (371°C) during the first baseline test. The wet gas originated from leakage in the lamp cooling system.

With the exception of the surface change noted, no other degradation was apparent. All fiberglass netting was in place and the insulation and cover shape had not changed.

Samples of the insulation were removed from the tank for detailed examination and weighing. Sections 1 ft^2 (0.093 m^2) from the ½-in. (1.27-cm) and 2½-in. (6.35-cm) thick insulation yielded densities of 1.20 lb/ft^3 (19.2 kg/m^3) and 0.73 lb/ft^3 (11.7 kg/m^3), respectively. No degradation of the fiberglass matt was noted.

VI. CONCLUSIONS AND RECOMMENDATIONS

A. CONCLUSIONS

As a result of the investigations conducted during this program the following conclusions have been drawn.

1) With the proper selection of available materials, insulation systems capable of meeting the severe environmental requirements of a supersonic cruise aircraft are feasible and within the state-of-the-art. These environmental requirements include temperature ranges of from -269°F (-167°C) to +700°F (371°C) and pressure variations of from ambient to 1 psia (0.69 N/cm^2).

2) Although not demonstrated during the program, the external insulation system should have an almost indefinite life. This system must, however, be provided with a dry gas purge to prevent moisture accumulation with attendant degradation of thermal conductivity.

3) The installed weight of the insulation can be quite low, which is a prime factor in aircraft equipment design considerations. Installed densities of the internal and external insulations developed during this program were 1.20 lb/ft^3 (19.2 kg/m^3) for the ½-in. (1.27-cm) and 0.72 lb/ft^3 (11.7 kg/m^2) for the 2½-in. (6.35-cm) external insulation, and 4.85 lb/ft^3 (77.7 kg/m^3) for the ½-in. (1.27-cm) and 3.38 lb/ft^3 (54.1 kg/m^3) for the 2½-in. (6.35-cm) internal insulation.

4) With some additional effort the internal insulation system can become a workable system. This effort lies in the areas of improved fabrication and installation techniques since feasibility and performance were proven in the calorimeter and materials test programs.

   Some specific improvements that should be made are:

   a) Piercing the face sheet with a hot needle in a manner that will melt the face sheet without tearing it. This operation should be automated to minimize variations from hole to hole.

b) Dimpling the face sheet at a temperature significantly above the maximum operating temperature of the system. In this case, with a system operating temperature of 650°F (343.3°C) the dimpling temperature should be 850 to 1000°F (454.5 to 537.8°C).

c) Using a larger cell size, which would make the core less rigid. In addition, the core material should be changed from an impregnated cloth to a pure film such as Kapton to minimize core wall leakage.

d) Improving the adhesive to provide a more flexible bond joint. The BR-34 material, when cured, provides an excellent bond but becomes quite rigid. Although no problems have occurred as a result of the rigid joints, more flexibility would lower the stress levels during flexing, providing a greater joint life.

B. RECOMMENDATIONS

During the program two basic insulation systems were developed and one system was demonstrated by a full-scale tank test under aircraft operating environmental conditions. One system, the external configuration, lends itself to installation on the external surfaces of individual metal tanks. The second system, the internal configuration, would be installed on the inside of the wing structure as a integral system.

The second system using the wing structure as the tank skin, would probably provide the lowest airborne weight penalty and, therefore, deserves further consideration. The development and full-scale test of this system should be continued following a plan which includes --

1) Refinement of the fabrication techniques with particular attention given to proper cell face sheet dimpling and piercing of the capillary holes;

2) Use of a core material having a larger cell size. The 35-cell-per-foot core is much more rigid than is required to provide the necessary structural integrity. Therefore, the solid fraction of the core material itself is higher than necessary resulting in considerably more solid conduction than needs to be achieved. The larger cell size would not only lower the stress levels by increasing flexibility, but would provide a lower effective thermal conductivity, which would more nearly approach the conductivity of nitrogen gas.

APPENDIX A

SPECIAL CALORIMETER TESTS

Page Intentionally Left Blank

APPENDIX A - SPECIAL CALORIMETER TESTS

Shortly before the insulation panels were installed in the tank it was discovered that the fiberglass-polyimide core cell walls were porous to an unexpected and significant degree. The honeycomb core material had earlier been discovered to be porous, although it had been originally inspected after receipt from the manufacturer and found to be acceptably leaktight. At the initial discovery of porosity, a number of months after the material was received, it was subjected to a multiple dipping operation with Ciba Geigy P13N polyimide varnish. Immediately after this treatment, it appeared from inspection of the core that the porosity had effectively been eliminated. Apparently in both cases the material deteriorated with age, handling, and possibly with thermal cycling in the assembly of panels.

A standardized test procedure was devised to measure cell leakage. Cells were pressurized to 2 psi (13.8 kN/m^2) (closeoff pressure corresponding to no leakage) with nitrogen and the flow rate of gas leaking from the cells was measured with a rotometer type flow indicator. Typically, the leakage in about 90% of the cells was in the range between 0.05 and 0.35 scfh (0.393 and 2.75 cm^3/s) at this flow condition. Approximately 2 to 4% of the cells leaked in excess of 1.0 scfh (7.86 cm^3/s). It can be predicted from a simple analysis that a degradation on the order of 10 to 50% of the gas conductivity should be expected from a leakage on the order of 0.1 to 0.3 scfh (0.79 to 2.36 cm^3/s) (under the test conditions). The effect of the higher leakage rates for a few cells is more difficult to predict.

To evaluate the resulting degradation, a series of calorimeter tests were conducted. The tests were performed with a simplified apparatus to minimize costs, but primarily to limit the use of core material, which was in short supply. A single heater plate, 9x12 in. (22.9x30.5-cm), was fabricated from 1/16-in. (1.6-mm) stainless steel, and the insulation specimen was bonded to this plate. The heater plate was guarded from the back, and to some extent on the sides with a second heater made of 1/8-in. (3.2-mm) aluminum. The primary heater was separated from the guard heater with about 1 in. (2.54 cm) of polyurethane foam. The primary heater was instrumented with 10 and the guard heater with two copper constantan thermocouples.

Tests 1 thru 4 and 7 were conducted without the guard heater and these results are more questionable than the others. Results for the guarded tests appear to be more consistent, and should be qualitatively useful. However, this test apparatus deviated sufficiently from accepted practices in thermal conductivity measurement to cast doubt on the absolute accuracy of the measurements obtained. In particular, the guard heater did not completely surround the primary heater. This defect could be expected to result in an indication of higher than actual thermal conductivity. In addition, the stainless steel heater plate did not provide sufficient thermal conduction to assure a uniform hot side temperature. The 1/16-in. (1.6-mm) stainless steel plate was selected to provide an indication of expected systematic temperature gradients from bottom to top, due to upward communication of nitrogen vapor through the cell walls. While temperature differences as great as 200°F (93.3°C) occurred across the plate, no systematic gradients were noted.

To evaluate the effect of the cell wall porosity, Specimens 4, 5, and 9 were sealed by coating the core (by a dip process) with diluted silicone adhesive (GE RTV560). This was found to be an effective way to seal the porosity, although long-term effectiveness was not evaluated, and about 98% of all cells were found to have no measurable porosity. The balance had a leakage rate of 0.05 scfh (0.39 cm^3/s) or less. Because the silicone coating increased the solid conduction path, a second method to eliminate the effects of porosity was used. This consisted of placing an 0.002-in. (0.05-mm) Teflon membrane between the insulation and the liquid nitrogen. This method was used on Specimens 4, 11, and 12.

Test results are presented in Table XIII and plotted in Figure 109. Of the 12 tests conducted, three were aborted due to leakage problems. Three of the remaining tests were conducted without benefit of a guard heater. The results of the remaining six tests, 5, 6, 8, 9, 10, and 12, indicate a range of thermal conductivity for the 1/2-in. (1.27-cm) specimens of 0.041 to 0.064 Btu/hr-ft-°F (0.71 to 1.11 W/m-°C). In addition to the elimination of the porosity for some specimens by use of a membrane or by coating the core walls, the pretreatment of the fiberglass filler material was varied. In Specimen 5, the filler was not dried prior to installation in the insulation panel. Specimen 5 was then dried in place by being subjected overnight to a temperature of approximately 200°F (93.3°C) and a rough vacuum of 1 mm Hg or less, and tested the same as Specimen 6. Examination of the test data indicates that both porosity and the condition of the filler material affect the thermal conductivity. Comparing the results of Tests

8 and 10, which had no reduction of porosity, with Tests 5, 6, 9, and 12, it would appear that the porosity accounted for an increase in thermal conductivity of 19 to 56%. Comparison of Tests 6 and 12 with Test 5 indicates a degradation of 12% when the filler material is not dryed prior to installation. This result shows much less effect from moisture than had previously been noted. However, no account had been taken of variations in relative humidity, and that factor could be responsible, in part, for the inconsistency.

The measured thermal conductivities for the four tests, 5, 6, 9, and 12, for which porosity had been effectively eliminated, are quite close considering the unsophisticated apparatus that was used. These results, with an average thermal conductivity of 0.043 Btu/hr-ft-°F (0.74 W/m-°C), are roughly 70% greater than those previously obtained with more adequate measuring equipment. It was concluded that most of the discrepancy was due to the apparatus used and that the actual thermal conductivity was in the results of Tests 8 and 10; it follows that the degradation due to porosity is in the range of 19 to 56% of the originally reported thermal conductivity, and agrees reasonably well with the analytical prediction. On the basis of these results and conclusions, it was decided to install the internal insulation in the tank without further treatment to minimize porosity.

TABLE XIII. - SUMMARY OF CALORIMETER TESTS TO EVALUATE EFFECT OF CORE POROSITY

Test No.	Specimen	Average hot side temperature, °F (°C)	Thermal conductivity, Btu/hr-ft-°F (W/m-°C)
1	½-in. (1.27-cm) Core; No Guard	64 (18)	0.107 (1.85)
2	2-in. (5.08) Core; No Guard	42 (6)	0.15 (2.59)
3	2-in. (5.08-cm) Core; No Guard	Abort Due to Seal Failure	
4	2-in. (5.08-cm) Core; No Guard; Teflon Membrane between Insulation and Liquid Nitrogen	118 (48)	0.055 (0.95)
5	½-in. (1.27-cm) Core; Silicone Coated; Filler Not Preconditioned	125 (52)	0.046 (0.80)
6	Same Specimen as 5, But with Filler Dried in Place	85 (29)	0.041 (0.71)
7	2-in. (5.08-cm) Core; Filler Dried in Place; No Guard	Abort Due to Seal Failure	
8	½-in. (1.27-cm) Core; Not Sealed; Filler Dried before Installation	64 (18)	0.049 (0.85)
9	½-in. (1.27-cm) Core; Silicone Coated; Filler Dried before Installation	120 (49)	0.043 (0.74)
10	½-in. (1.27-cm) Not Sealed; Filler Dried before Installation	79 (26)	0.064 (1.11)
11	Same as Specimen 11, But with Teflon Membrane between Insulation and Liquid Nitrogen	Aborted Due to Membrane Failure	
12	Same as Specimen 11, But with Teflon Membrane between Insulation and Liquid Nitrogen	121 (49)	0.041 (0.71)

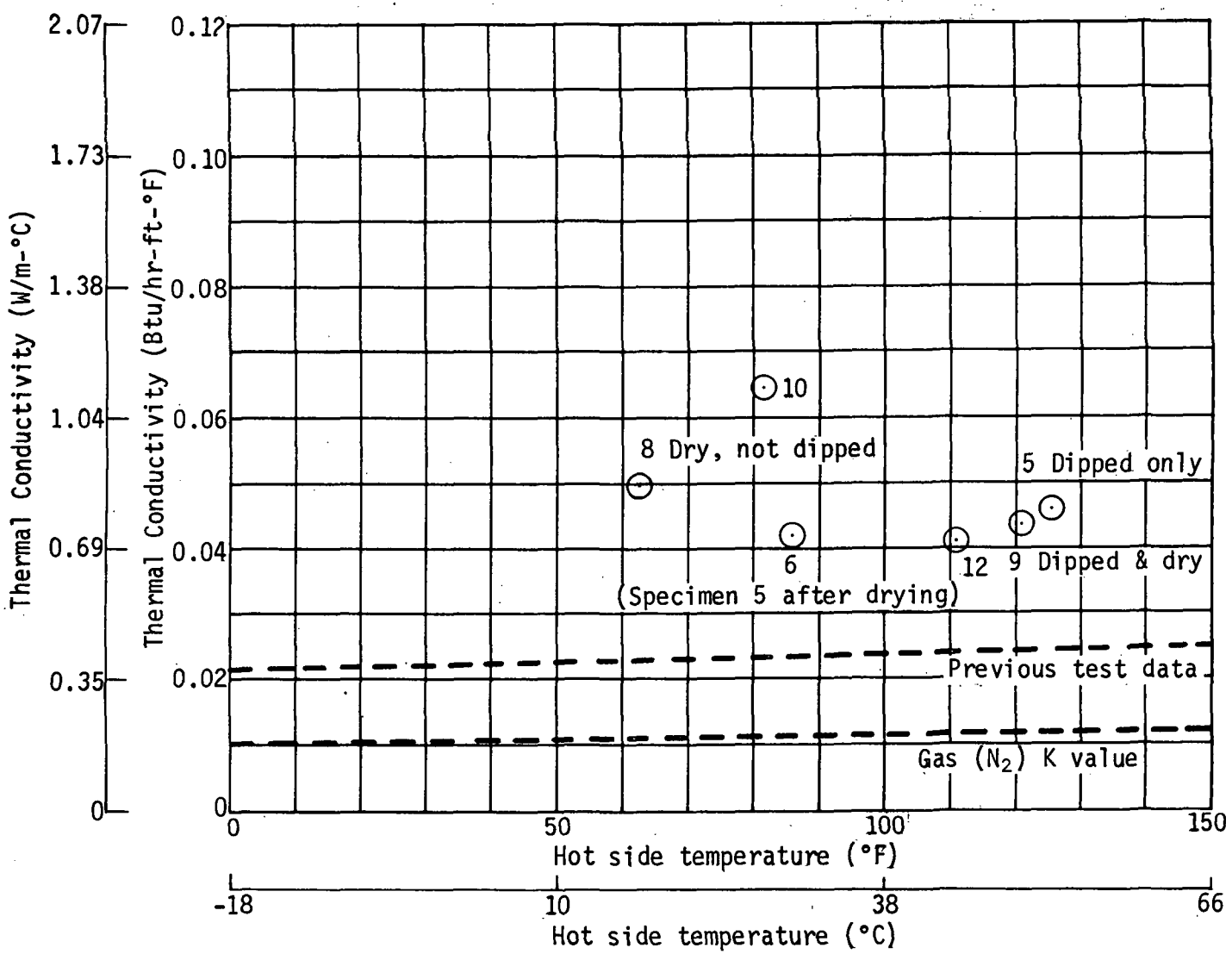

Figure 109. Special calorimeter test results 1/2 in. (1.27 cm) polyimide core cold side LN_2, -320°F (-196°C)

Page Intentionally Left Blank

APPENDIX B

INSULATION SYSTEMS FOR LIQUID METHANE FUEL TANKS FOR SUPERSONIC CRUISE AIRCRAFT

INSULATION INSTALLATION PROCESS PLAN

SEPTEMBER 1971
REVISED: FEBRUARY 1972

Page Intentionally Left Blank

APPENDIX B - INSULATION INSTALLATION PROCESS PLAN

Objective - The intent of this plan is to delineate, in detail, the procedures to be followed in preparing and reinstalling insulation in the internally insulated tanks.

1.0 TANK CLEANING

1.1 Remove the BR-34 prime coat and FM-34 film from the tank by:

1.1.1 Using a high-temperature oven, heat the tank from ambient to 775°F in 1 hr; hold for 3 hr at 775°F; cool from 775°F to ambient in minimum of 1 hr.

1.1.2 Remove the FM-34 by scraping with a knife and being careful not to nick or otherwise damage the surface of the thin skin.

1.1.3 Remove all BR-34 by buffing with green "scotch brite" scouring pads.

1.2 The tank shall be chemically cleaned per Martin Marietta process No. MP-50405-1 and MP-50042. See figure 110. Immediately after cleaning, the tank is to be sealed in a polyethylene bag.

2.0 TANK PREPARATION

2.1 With the tank cleaned and dry, apply the prime coat using BR-34 thinned to 60% solids by weight (Reference 1). Thinned BR-34 is not to be stored; i.e., it is to be used as soon as possible after thinning. Verify that the BR-34 is in date and has been properly stored.

The thinning formula is to be:

$$W_t = 0.35\ W_1$$

where

W_t = Weight of BR-34 thinner required,

W_1 = Weight of the unthinned BR-34 as received from the manufacturer.

CLEANING AND PASSIVATING STAINLESS STEEL				
STEP	PROCESS	SOLUTION	TIME (minutes)	REMARKS
1	Mechanically Clean	--	As Required	If scale or hard deposits exist, remove with a stainless steel wire brush (4.15).
1 2a 2	Solvent Degrease 70 to 100°F	3.1, 3.7, 3.8, 3.13, or 3.16	As Required	Hand wash, using a stiff bristle brush (4.13) or clean cheesecloth, or flush by fill and drain method. Drain dry or dry with nitrogen (3.3).
1 2b 2	Vapor Degrease	--	--	Vapor degrease in accordance with MP-50046.
3	Alkaline Clean	--	--	Alkaline clean in accordance with MP-50036.
1 4	Rinse	3.5 or 3.6	5 to 10	After rinsing, examine for water break. If this occurs, repeat steps 3 and 4.
→ 5a	Pickle & Passivate (Immersion)	Nitric-Hydrofluoric Acid	--	Pickle and passivate by immersion in accordance with applicable portions of MP-50402.*
5b	Pickle & Passivate (Manual Application)	3.12.2	--	Pickle and passivate by manual application in accordance with applicable portions of MP-50402.*
6	Rinse	3.5 or 3.6	5 to 7	
3 7	Remove Smut (Deoxidize)	Nitric-dichromate 3.12.8	4 to 6	Immerse in deoxidizer to remove smut.
8	Rinse	3.5 or 3.6	5 to 7	
9	Final Rinse (Flush)	3.5 or 3.6	5 to 7	After rinsing, pH of drippings shall be within 1 unit of influent.
10	Dry	Air	As Required	Blow nitrogen or air through all internal areas or dry in oven, 4.6 or 4.7, at a temperature compatible with the part.
11	Seal	--	--	Seal in accordance with MP-50405-2 or reassemble, whichever is applicable.

Figure 110 Cleaning and passivating stainless steel (Martin Marietta Corporation process sheet).

The thinned BR-34 is to be applied by brush, using as much care as practical to obtain a uniform thickness.

2.2 The cure cycle for the BR-34 primer is to be (Ref 1):

30-minute air dry
30-minute oven dry at 220°F
45-minute oven dry at 410°F.

A time vs temperature log of this cycle will be kept.

2.3 Remove the tank from the oven and allow it to return to ambient temperature. The tank shall then be covered with a polyethylene sheet and will remain sealed until the core insulation is installed.

3.0 INSULATION PREPARATION

3.1 Fiberglass packing material (aluminized PF-105 Owens Corning) is to be used in the core panels. This material is to be bulk dried according to the following procedure. This procedure might have to be repeated a number of times because of the available oven size and the large volume of the packing.

3.1.1 Place packing in metal box. The box is to be covered with a fiberglass cloth lid.

3.1.2 With the packing in the oven, heat to 600°F, hold for a minimum of 16 hr and then perform a dry gaseous nitrogen purge of the insulation during the cooldown cycle.

3.1.3 Maintain the GN_2 purge, cool the oven to 350°F and install a nylon film over the glass cover cloth. Install the GN_2 purge hose in the box and turn the oven heaters off. Allow the packing and box to return to ambient temperature.

3.1.4 Put the fiberglass packing in polyethylene bags and seal.

3.2 Face Sheet Holes. All core panels will have holes formed by using a 0.020-in. diameter needle and a pencil soldering iron. Panels that already have holes shall be checked visually. Face sheet holes will not be punched in the 2½-in. thick bottom core panels, along the seam areas, until after installation.

3.3 Panels shall be primed on the tank wall side of each panel. The priming procedure will be:

3.3.1 Clean the back side of the core with MEK. This can be done either with an appropriate paint roller or Kimwipes.

3.3.2 Apply BR-34 primer, thinned per paragraph 2.1 above, to the panels. A paint roller is to be used for this application.

3.3.3 Cure the primed panels in accordance with the cycle given in paragraph 2.2 above.

3.3.4 The eight side panels and the two lid panels are to be sprayed with BR-34 on the fiberglass insulation side to prevent the fiberglass packing from falling out during installation of the panels. The BR-34 is to be thinned with BR-34 thinner in the following proportions: 50 g of BR-34 to 100 g of BR-34 thinner. The quantity is that which is required to form a thin 'holding' skin.

3.3.5 Place the individual panels in polyethylene bags, purge with dry GN_2, and seal the bags.

3.4 Packing installation into the panels. Verify that paragraph 3.3 has been completed. The packing is to be done so that the individual cells are full and well packed. Voids in the packing material are not acceptable. The nominal quantity of packing to be used is 1.15 g/in.^{2} per ½-in. of core thickness. Table XIV is to be used as a guide.

TABLE XIV CORE PACKING REQUIREMENTS

CORE SIZE (in.)	Packing Required (g)
24x26x½ thick	720
19x24x2½ thick	2,600
19x24x2½ tapered to 2 thick	2,360

Note: A log sheet (fig. 111) will be used for each panel installed in the tank. This log is to include:

1) Weight of the panel both before and after installation of the packing.

PANEL LOG SHEET

Panel Number	Weight (grams)		Face Sheet Holes Verification	Dimensions after Trim	Remarks
	Before Packing	After Packing			
1					
2					
3					
4					
5					
6					
7					
8					
9					
10					
11					
12					
13					
14					
15					
16					
17					
18					

Figure 111 Panel log sheet.

2) Precise panel location and identification. See figure 112.

3) Verification of face sheet hole existence.

4) Dimensions of the panel after trimming.

5) Any other information peculiar to any one particular panel.

4.0 INSTALLING INSULATION PANELS IN TANK

4.1 Sequence of installation (see figure 112):

4.1.1 End panel 5. Spacer to be used between the end panel and the tank bottom to allow for the interfacing bottom panel (1). Perform inspection of this panel to verify the adequacy of the installation procedure.

4.1.2 All four bottom panels (1, 2, 3, 4).

4.1.3 End panel 6.

4.1.4 Side panels, 7 through 10.

4.1.5 Side panels, 11 through 14.

4.1.6 Lid panels, 15 through 18.

4.2 Panel installation procedure:

4.2.1 Prefit panels to their positions and trim as required.

4.2.2 Unthinned BR-34 and Style 120 fiberglass cloth will be used. Six-ounce glass cloth will be used as a bleeder cover.

4.2.3 Using a squeegee, wet-out the 120 glass cloth with BR-34. All excessive adhesive is to be removed from the cloth.

4.2.4 Using a squeegee, apply enough BR-34 to the tank wall to assure that it is completely wetted.

4.2.5 Apply the glass cloth to the tank wall and remove all discontinuities and wrinkles.

4.2.6 Apply approximately 100 g/ft^2 of BR-34 on top of the wetted glass cloth.

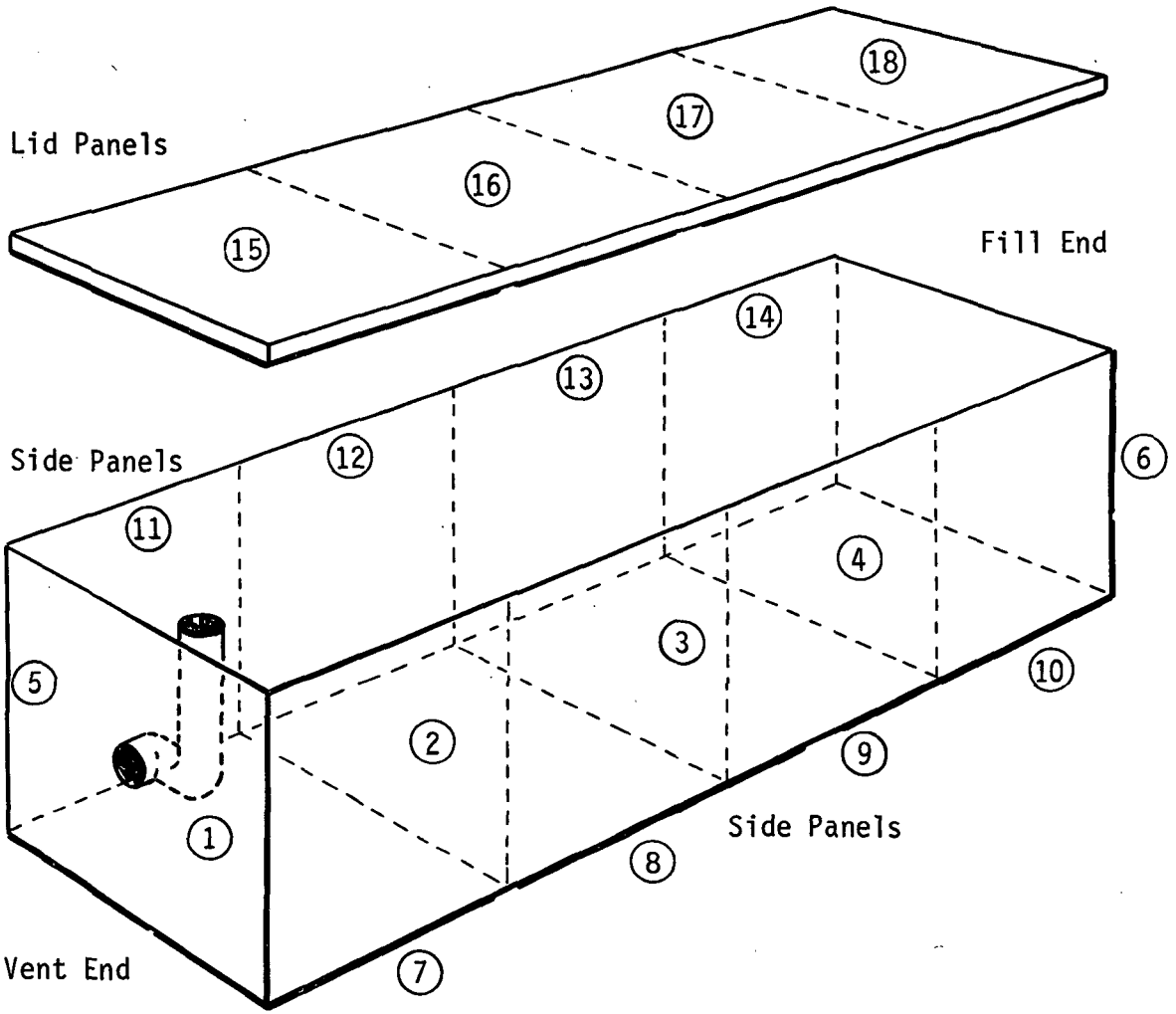

Figure 112 Panel Identification

4.2.7 Install the panel on the tank wall; install the bleeder cloth and the vacuum bag. Evacuate the bag and verify that the panel(s) have not shifted and the vacuum bag is adequately sealed.

CAUTION

Do not allow the vacuum sealing material to come into contact with the BR-34 prime.

4.2.8 Hold the panel(s) under vacuum (15 in. Hg minimum) approximately 30 min.

4.2.9 Apply radiant heat to the panel(s) and perform the following cure cycle while maintaining vacuum.

NOTE

A minimum of three thermocouples will be used for monitoring the tank wall temperature during the cure cycles. A printout (recorder) of the cycle temperatures will be available.

CURE CYCLE

Heat from ambient to 350°F in 60 min.
Hold at 350°F for 120 min.
Turn heat off and allow panel to return to ambient.

4.2.10 Remove the vacuum bag and perform a spot leak check of the individual cells to verify the integrity of the panel installation.

5.0 SEAM INSTALLATION PROCEDURE

5.1 Material Preparation

5.1.1 The seam joint material is to be 1-mil Kapton film. The eight corner seam pieces are formed on the aluminum angle tool prior to dimpling. The 18 longitudinal strips do not require preforming before dimpling.

5.1.2 A dimple pattern will be vacuum and heat formed into the Kapton seam strips. The dimples are ½-in. in diameter and spaced on 1-in. centers. The Kapton strips are 3-in. wide. The strips shall be vacuum formed at 36 in. Hg differential and at a temperature of 600°F.

5.1.3 Wipe both sides of all seam strips with MEK and Kimwipes.

5.1.4 Cut approximately 50 strips of ½-in. thick fiberglass packing (PF-105-700) to a width of ½-in.

5.2 Strip Installation

5.2.1 The adhesive to be used for applying the seam joints is Thermadite 17 by Whittaker Corporation. The adhesive is to be thinned with one part MEK to one part T-17 by weight.

5.2.2 Pack the fiberglass insulation into all joints until the insulation is flush with the face sheet surface.

5.2.3 Apply the thinned T-17 to one side only of the strips using a ½-in. acid brush and install the strips in the following sequence (refer to figure 112):

Joints between side panels:	11 and 12
	12 and 13
	13 and 14
Joints between side panels:	7 and 8
	8 and 9
	9 and 10
Joints between bottom panels:	1 and 2
	2 and 3
	3 and 4
Joints between bottom and side panels:	1 and 7
	2 and 8
	3 and 9
	4 and 10
	1 and 11
	2 and 12
	3 and 13
	4 and 14
Joints between bottom and end panels:	1 and 5
	4 and 6
Joints between end and side panels:	5 and 11
	5 and 7
	6 and 10
	6 and 14
Joints between lid panel joints:	as required

5.2.4 All strips must overlap the ends of other strips to preclude a large number of seam joints in a small area.

5.2.5 Weight the seam material with lead weights and allow the T-17 to cure at ambient temperature for a minimum of 18 hr.

5.3 Final Operations

5.3.1 The joints between the respective end panels and the fill and vent pipes are sealed as follows: Pack insulation into void. Wrap with 3-in. wide, 1-mil Kapton strips; go around each joint twice. Coat each end with approximately 1/16-in. of RTV-156 and allow to room cure for 24 hr.

5.3.2 Trim the unbonded Kapton film around all joints.

5.3.3 Using the 0.020-in. diameter hot needle, repuncture the holes in the face sheet that have been covered by the seam joint materials.

6.0 REFERENCE 1: "FM-34 ADHESIVE FILM" BY AMERICAN CYANAMID COMPANY.

APPENDIX C

AVERAGE APPARENT THERMAL CONDUCTIVITY OF THE INSULATION

Page Intentionally Left Blank

APPENDIX C - AVERAGE APPARENT THERMAL CONDUCTIVITY OF THE INSULATION

The total heat leak is composed of the heat leaks through the insulation, tank supports, and fill and vent lines.

1. Insulation

Calorimeter tests indicated that the insulation had a conductivity of 0.015 Btu/hr-ft-°F (0.26 W/m-°K) under the tank conditions. The total surface area of the tank was 51.96 ft^2 (4.83 m^2). This does not include the short sections of fill and vent line located at each end. For this tank one has to consider the sides, top, bottom, and ends. The heat through the insulation is

$$q_{(insulation)} = \frac{KA}{L} \Delta T$$

For the sides

$$q_{(side)} = \frac{KA}{L} \Delta T = \frac{(0.015)(11.02)(2)}{0.5/12} \Delta T$$

$$= 7.93 \Delta T$$

For an outside temperature of

T_{oi} = 141.5°F (334°K), initial

T_{of} = 160.5°F (344.4°K), final

and an inside temperature of

T_{ini} = -313.5°F (81.2°K), initial

T_{inf} = -313.5°F (81.2°K), final

$q_{(side)}$ = 7.93 [141.5 - (-313.5)] = 3610 Btu/hr (3806 kW), initial

$q_{(side)}$ = 7193 [160.5 - (-313.5)] = 3760 Btu/hr (3964 kW), final

For the ends

$$q_{(ends)} = \frac{KA}{L}\Delta T = \frac{(0.015)(2.31)(2)}{0.5/12}\Delta T$$

$$= 1.662\ \Delta T$$

Assume that ΔT (ends)

$q_{(ends)}$ = 1.66 [141.5 - (-313.5)] = 757 Btu/hr (798 kW), initial

$q_{(ends)}$ = 1.66 [160.5 - (-313.5)] = 787 Btu/hr (830 kW), final

For the top

$$q_{(top)} = \frac{KA}{L}\Delta T = \frac{(0.015)(12.65)}{0.5/12}\Delta T$$

$$= 4.56\ \Delta T$$

For an outside temperature of

T_{oi} = 400°F (478°K), initial

T_{of} = 496.4°F (531°K), final

and an inside temperature of

T_{ini} = 258°F (399°K), initial

T_{inf} = 276.3°F (409°K), final

$q_{(top)}$ = 4.56 (400 - 258) = 648 Btu/hr (683 kW), initial

$q_{(top)}$ = 4.56 (496.4 - 276.3) = 1005 Btu/hr (1059 kW), final.

For the bottom

$$q_{(bottom)} = \frac{KA}{L}\Delta T = \frac{(0.015)(12.65)}{2.5/12}\Delta T$$

$$= 0.912\ \Delta T$$

For an outside temperature of

T_{oi} = 472°F (517°K), initial

T_{of} = 473°F (518°K), final

and an inside temperature of

T_{ini} = -314.7°F (80°K), initial

T_{inf} = -314.7°F (80°K), final

$q_{(bottom)}$ = 0.912 [472 - (-314.7)] = 717.0 Btu/hr (756 kW), initial

$q_{(bottom)}$ = 0.912 [473 - (-314.7)] = 717.8 Btu/hr (757 kW), final.

2. Supports

The tank was supported by six stainless steel tubes with the following approximate geometry:

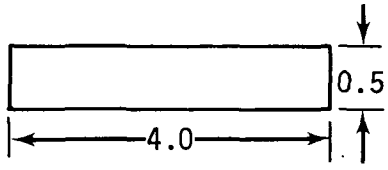

0.065 in. (0.165 cm) thickness

0.089 in.^{2} (0.57 cm^2) area

$$q_{(supports)} = \frac{KA}{L}\Delta T = \frac{(10)\left(\frac{0.089}{144}\right)}{4/12}\Delta T$$

$$= 0.01855\ \Delta T$$

and for six supports

$q_{(supports)}$ = 0.1112 ΔT

T_H = 700°F (644°K) for both initial and final

T_c = 258°F (399°K), initial

T_c = 276.3°F (409°K), final

$q_{(supports)}$ = (0.1112)(700 - 258) = 49.2 Btu/hr (51.9 kW), initial

$q_{(supports)}$ = (0.1112)(700 - 276.3) = 47.1 Btu/hr (49.7 kW), final.

3. Fill and Vent Lines

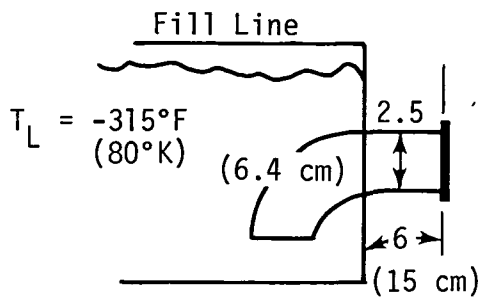

Note: 2½x0.035-in. 6.4x0.09-cm wall, cross sectional conductance

$$\text{area} = \frac{\pi}{4}\left[(2.5)^2 - (2.43)^2\right]$$

$$= 0.275 \text{ in.}^2 \ (1.77 \text{ cm}^2)$$

The insulated fill line has the dimensions shown in the sketch and the note to the right of the sketch. The inside temperature is shown and the temperature of the fill line reached approximately 350°F (449.9°K). This is based on the fact that the surroundings are at 700°F (644.7°K) and there is very little heat leak through the fill line.

$$q_{(\text{fill line})} = \frac{(10)\left(\frac{0.275}{144}\right)}{6/12}\left[350 - (-315)\right]$$

$$= 0.0382\ (765)$$

$$= 29.2 \text{ Btu/hr } (30.8 \text{ kW})$$

Heat leak by radiation was assumed to be blackbody

$$q_{(\text{fill line})} = \sigma A\left(T_1^4 - T_2^4\right)$$

$$= (0.1714 \times 10^{-8})\frac{\pi D^2}{4}\left[(700)^4 - (305)^4\right]$$

$$= 11.97 \text{ Btu/hr } (12.6 \text{ kW})$$

Vent line heat leak was assumed negligible because of its relative size to the fill line and its similar insulation.

4. Effective Thermal Conductance

The total heat leak is --

Initial baseline, Btu/hr (kW)			Final baseline, Btu/hr (kW)	
Sides	3610	(3806)	3760	(3964)
Ends	757	(798)	787	(830)
Top	648	(683)	1005	(1059)
Supports	49.2	(52)	47.1	(50)
Fill Line	41.2	(43)	41.2	(43)
Total	5105.4	(5382)	5640.3	(5946)
Bottom	717	(756)	717.8	(757)

$$q_{(total)} = \frac{K_{eff}\ A}{L}\ \Delta T$$

$$K_{eff} = \frac{q_{total}\ L}{A\ \Delta T}$$

Initial Baseline

$$K_{eff} = \frac{qL}{\Delta T\ A}$$

Top, sides, ends

$$K_{eff} = \frac{(5105.4)(0.0416)}{(347)(39.31)}$$

K_{eff} = 0.01555 Btu/hr-ft-°F (0.269 W/m-°K)

Bottom

$$K_{eff} = \frac{(717)(0.208)}{(12.65)(787)}$$

K_{eff} = 0.0149 Btu/hr-ft-°F (0.258 W/m-°K)

Final Baseline

$$K_{eff} = \frac{qL}{\Delta TA}$$

Top, sides, ends

$$K_{eff} = \frac{(5640.3)(0.0416)}{(386)(39.31)}$$

K_{eff} = 0.01545 Btu/hr-ft-°F (0.267 W/m-°K)

Bottom

$$K_{eff} = \frac{(717.8)(0.208)}{(12.65)(788)}$$

K_{eff} = 0.01495 Btu/hr-ft-°F (0.258 W/m-°K)

The thermal conductivity of the basic insulation (K) and the effective conductivity $\left(K_{eff}\right)$ indicate good thermal design by their close agreement.

APPENDIX D

EMPIRICAL THERMAL CONDUCTANCE

Page Intentionally Left Blank

APPENDIX D EMPIRICAL THERMAL CONDUCTANCE

An actual K_{eff} can be calculated from the actual test data by means of an energy balance. The test tank was vented throughout the baseline tests, resulting in a near constant tank pressure, and liquid and tank temperatures. Using this and the fact that the heat constant of the ullage gas is small and, therefore, may be neglected, the general energy equation is reduced to

$$Q_E + h_L \left(m_i - m_f\right)_L - m_{vent}\, h_{vent} = 0,$$

where

Q_E = external heat leak, Btu (cal);

m = mass, lb (kg);

h = enthalpy, Btu/lb (cal/g),

and the subscripts are as follows:

L = liquid

i = initial

f = final

vent = vented gas.

Since,

$$\left(m_i - m_f\right) = m_{vent} \text{ and } \left(h_{vent} - h_L\right) = H_V$$

where H_V is the heat of vaporization, we finally have,

$$Q_E = m_{vent}\, H_V = 0$$

or

$$q_E = \dot{m}_{vent}\, H_V$$

where

q_E = external heat leak, Btu/hr (cal/hr);

$\dot{m}$ = flowrate, lb/hr (kg/hr).

In solving for K_{eff}

$$q_E = \frac{K_{eff}}{L} A \Delta T = K_{eff} \left[\left(\frac{A \Delta T}{\ell} \right)_{\frac{1}{2}} + \left(\frac{A \Delta T}{\ell} \right)_{2\frac{1}{2}} \right]$$

where

A = surface area, ft^2 (m^2);

ΔT = temperature difference, °R (°K);

ℓ = insulation thickness, ft (m),

and the subscripts are as follows:

$\frac{1}{2}$ = ½-in. (1.27-cm) insulation;

$2\frac{1}{2}$ = 2½-in. (6.35-cm) insulation,

or

$$K_{eff} \left[\left(\frac{A \Delta T}{\ell} \right)_{\frac{1}{2}} + \left(\frac{A \Delta T}{\ell} \right)_{2\frac{1}{2}} \right] = \dot{m}_{vent} H_V.$$

During the initial baseline test, the steady-state vent flow rate was 121.2 lb/hr (55 kg/hr); during the final baseline test the steady-state flow rate was 96.7 lb/hr (43.9 kg/hr); and the outside insulation temperatures were as tabulated.

	Initial	Final
Top	396.0°F (475°K)	392.5°F (473°K)
Sides	146.7°F (337°K)	166°F (347°K)
Ends	146.7°F (337°K)	166°F (347°K)
Bottom	471.5°F (517°K)	497°F (531°K)

Hence

Initial K_{eff} -

$$K_{eff}\left\{\frac{(39.31)[229.7-(-315)]}{0.5/12}+\frac{(12.65)[471.5-(-315)]}{2.5/12}\right\}=(121.3)(85.5)$$

K_{eff} = 0.0184 Btu/hr-ft-°F (0.318 W/m-°K)

and Final K_{eff} -

$$K_{eff}\left\{\frac{(39.31)[241-(-315)]}{0.5/12}+\frac{(12.65)[497-(-315)]}{2.5/12}\right\}=(96.7)(85.5)$$

K_{eff} = 0.0144 Btu/hr-ft-°F (0.249 W/m-°K)

The flows were based upon the level sensor data from figures 113 and 114.

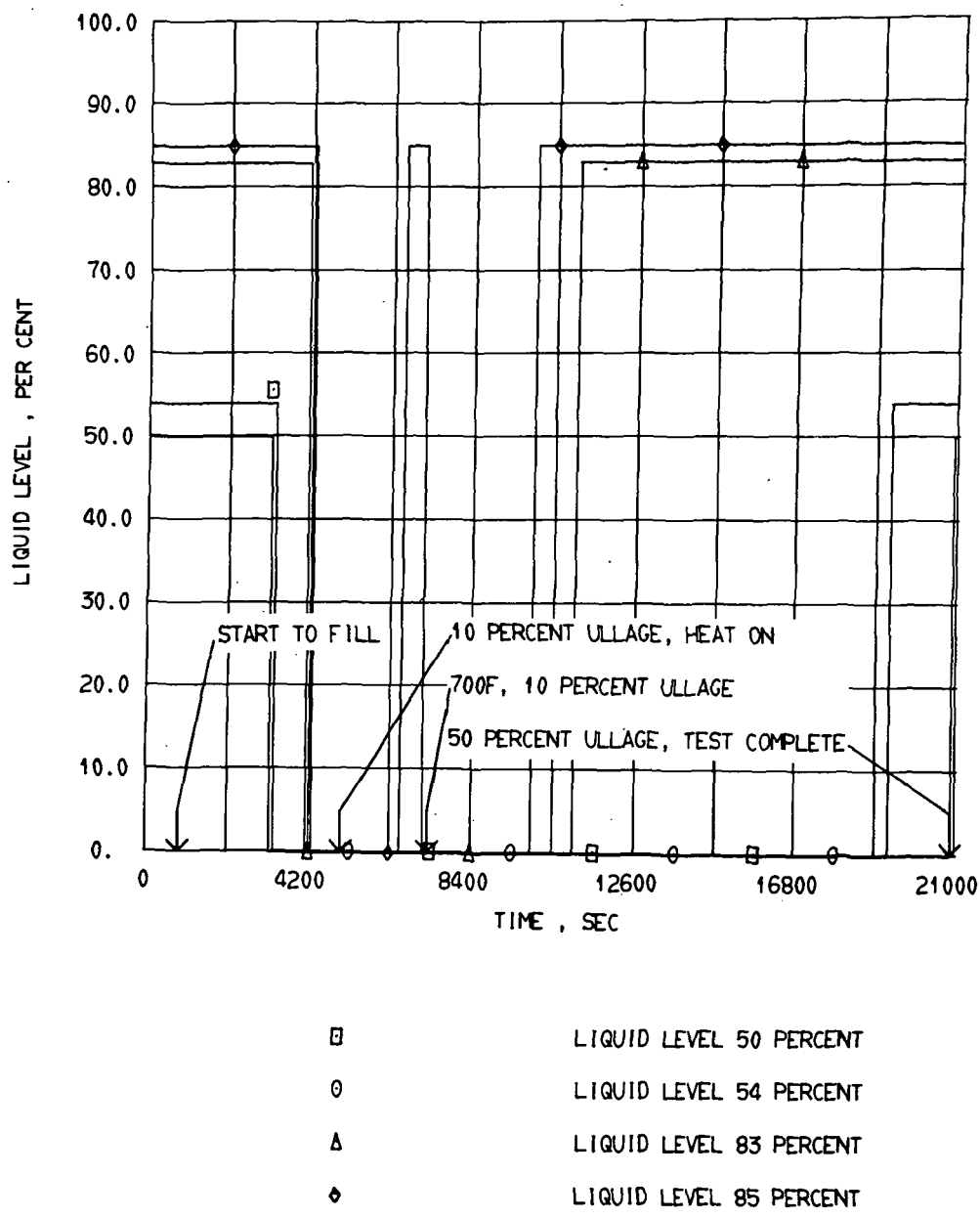

Figure 113 Square tank exterior insulation, initial baseline test, 50, 54, 83, and 85% liquid levels.

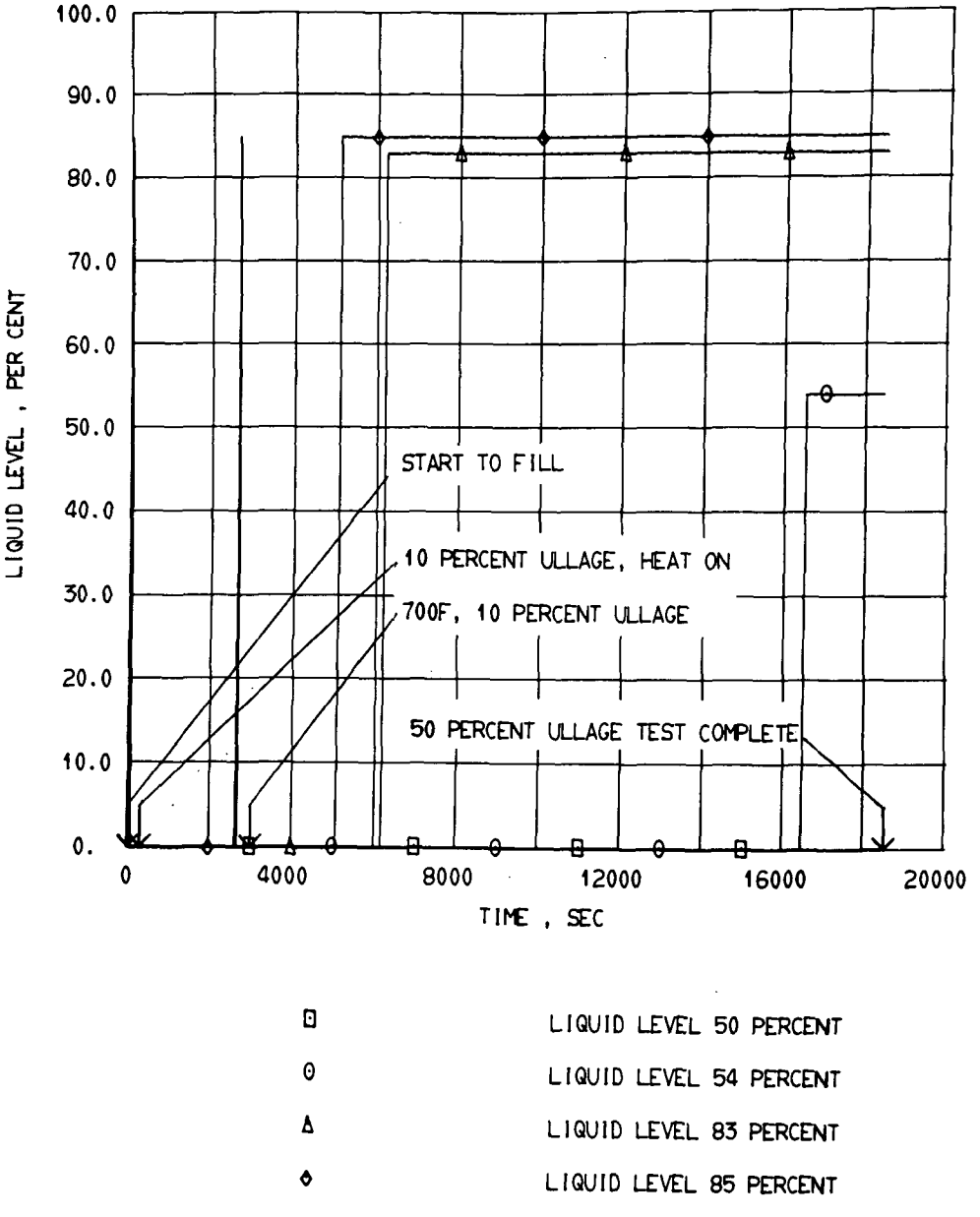

Figure 114 Square tank exterior insulation, final baseline test, 50, 54, 83, and 85% liquid levels.

Page Intentionally Left Blank

DISTRIBUTION LIST

ADDRESSEE			NO. OF COPIES
NASA-Lewis Research Center 21000 Brookpark Road Cleveland, Ohio 44135			
Attention:	Report Control Office	MS 5-5	1
	Technology Utilization Office	MS 3-19	1
	Library	MS 60-3	2
	Fluid System Components Div.	MS 5-3	1
	W. L. Stewart	MS 77-2	1
	Len Schopen	MS 77-3	1
	J. M. Ladd	MS 60-6	25
	J. B. Esgar	MS 60-4	1
	R. H. Kemp	MS 49-1	1
	R. R. Hibbard	MS 3-5	1
	F. S. Stepka	MS 60-6	1
	R. Chambellan	MS 60-4	2
	E. Pleban	MS 60-4	1
	S. Lieblein	MS 100-1	1
	J. Esterly	MS 60-4	1
NASA Scientific & Technical Information Facility P. O. Box 33 College Park, Maryland 20740			
Attention:	NASA Representative RQT-2448		10
NASA Headquarters 600 Independence Avenue, S.W. Washington, D. C. 20546			
Attention:	N. F. Rekos (RAP)		1
Department of the Army U. S. Army Aviation Material Laboratory Fort Eustis, Virginia 23604			
Attention:	John White		1
Wright-Patterson AFB, Ohio 45433			
Attention:	J. Richens AFAFL (AFIC)		1
	A. Wennerstrom (ARF)		1
	A. V. Churchill AFAPL (APFF)		1
	W. H. Goesch, Air Force Flight Dynamics Laboratory		1
	L. R. Phillips, Air Force Flight Dynamics Laboratory		1
Air Force Office of Scientific Research Propulsion Research Division USAF Washington, D. C. 20025			1

ADDRESSEE	NO. OF COPIES
Department of the Navy Bureau of Naval Weapons Washington, D. C. 20025 Attention: Robert Brown, RAPP14	1
Department of Navy Bureau of Ships Washington, D. C. 20360 Attention: G. L. Graves	1
NASA-Langley Research Center Langley Station Technical Library Hampton, Virginia 23365 Attention: Mark R. Nichols John V. Becker	1 1
Naval Air Propulsion Test Center (AE) Naval Base Philadelphia, Pennsylvania 19112 Attention: J. R. Pichtedberger	1
United Aircraft Corporation Pratt & Whitney Aircraft Division Florida Research & Development Center P. O. Box 2691 West Palm Beach, Florida 33402 Attention: R. A. Schmidtke F. H. Daley	1 1
United Aircraft Library UAC Research Bldg. 400 Main Street East Hartford, Connecticut 06108 Attention: G. Andreini John Goncar	2 2
Northern Research & Engineering Corporation 219 Vassar Street Cambridge, Massachusetts 02139 Attention: K. Ginwala	1
General Electric Company Aircraft Engines Group Cincinnati, Ohio 45215 Attention: E. N. Bumberger M-88 J. P. Smith, Jr.	1 1

ADDRESSEE	NO. OF COPIES
General Electric Company - Flight Propulsion Division 930-1000 Western Avenue West Lynn, Massachusetts 01905 Attention: Dr. C. W. Smith - Library Bldg. 2-40M	1
AiResearch Manufacturing Company Garrett Corporation 9851 Sepulveda Boulevard Los Angeles, California 90009 Attention: Mr. R. D. Meuller	1
AVCO Corporation Lycoming Division 550 South Main Street Stratford, Connecticut 06497 Attention: C. W. Bolton	1
Continental Aviation & Engineering Corporation 12700 Kercheval Avenue Detroit, Michigan 48215 Attention: Eli H. Benstein Howard C. Welch	1 1
International Harvester Company, Solar 2200 Pacific Highway San Diego, California 92112 Attention: P. A. Pitt Mrs. L. Walper	1 1
Phillips Petroleum Company Phillips Petroleum Center Bartlesville, Oklahoma 74003 Attention: H. E. Alquist	1
Goodyear Atomic Corporation Box 268 Piketon, Ohio 45861 Attention: Department No. 423 for: C. O. Longebrake	1
George Deriderian AIR 53622 B Department of Navy Bureau of Navy Washington, D. C. 20360	1
The Boeing Company Commercial Airplane Division P. O. Box 3707 Seattle, Washington 98124 Attention: G. J. Schott M. S. 80-66	1

ADDRESSEE	NO. OF COPIES
The Boeing Company Missile and Information Systems Division 224 N. Wilkinson Street Dayton, Ohio 45402 Attention: Warren K. Thorson	1
The Boeing Company P.O. Box 3733 Seattle, Washington 98124 Attention: George Hays	1
Lockheed California Company P. O. Box 551 Burbank, California 91503 Attention: E. F. Versaw	1
McDonnald Douglas Aircraft Company 3855 Lakewood Blvd. Long Beach, California 90801 Attention: Technical Information Center, CL-250 for J. E. Merriman W. B. King	 1 1
General Motors Corporation Allison Division P.O. Box 24013 Indianapolis, Indiana 46206 Attention: J. N. Barney G. E. Holbrook Library H. E. Helms	 1 1 1 1
Engineering Library TRW Inc. 23555 Euclid Avenue Cleveland, Ohio 44117 Attention: Elizabeth Barrett, Librarian J. Edward Taylor, Director Product Development Jet and Ordnance Division	 1 1
Esso Research and Engineering Center P. O. Box 61 Linden, New Jersey 07036 Attention: H. G. Hukek L. Goldstein	 1 1

ADDRESSEE	NO. OF COPIES
General Dynamics Fort Worth Division P. O. Box 748 For Worth, Texas 76101 Attention: P. R. deTonnancour ME-2246	1
Dynamic Science 1800 West Deer Valley Drive Phoenix, Arizona 85027 Attention: L. M. Shaw	1
Institute of Gas Technology 3424 S. State Street Chicago, Illinois 60616	1
The Gillette Company Prudential Tower Bldg. Boston, Massachusetts 02199 Attention: J. V. Rajunas	1
General Dynamics/Convair Division P.O. Box 1128 San Diego, California 92112 Attention: Glen Yates	1